

408 758

63-4-2

RADC-TDR-63-54

CATALOGED BY DDO

AS AD No. 408758



FINAL REPORT

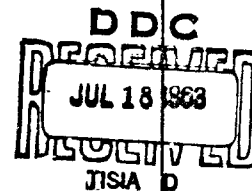
AN ENGINEERING STUDY OF A
POST-ATTACK ANTENNA SYSTEM

TECHNICAL DOCUMENTARY REPORT NO. RADC-TDR-63-64

May 1963

Applied Research Laboratory
Rome Air Development Center
Research and Technology Division
Air Force Systems Command
Griffiss Air Force Base, New York

Project No. 5579, Task No. 557901



(Prepared under Contract AF30(602)-2753 by Goodyear Aircraft
Corporation, Akron 15, Ohio. Authors: D.D. Cellins
and G.W. Congdon)

20050223 153

Best Available Copy

Qualified requesters may obtain copies from DDC, Arlington Hall Station, Arlington 12, Va. Orders will be expedited if placed through the librarian or other person designated to request documents from DDC.

When U.S. Government drawings, specifications, or other data are used for any purpose other than a definitely related government procurement operation, the government thereby incurs no responsibility nor any obligation whatsoever; and the fact that the government may have formulated, furnished, or in any way supplied the said drawings, specifications, or other data is not to be regarded by implication or otherwise, as in any manner licensing the holder or any other person or corporation, or conveying any rights or permission to manufacture, use, or sell any patented invention that may in any way be related thereto.

Do not return this copy. Retain or destroy.

FOREWORD

This report covers an engineering study and test program conducted by Goodyear Aircraft Corporation on a cost-sharing basis for the United States Air Force, Rome Air Development Center, under contract AF30(602)-2753 during the period from 4 May 1962 through 30 November 1962.

This report is designated as Goodyear Aircraft Corporation Engineering Report GER-10670.

ABSTRACT

This report describes the results of an engineering study program for a post-attack, survivable antenna installation. The purpose of the program was to determine the feasibility of an air supported, integrated, radome-antenna configuration that can be packaged in a small volume, stored underground in a hardened enclosure, and capable of being quickly and automatically erected. Performance characteristics are to be comparable to a conventional 25 by 18 foot parabolic reflector.

Theoretical computations were made to establish the aperture parameters, feed configuration, reflector shape, and reflector parallel conductor configuration. Tests were performed to confirm the theoretically established design configuration. Accuracy requirements were established for the reflector shape and parallel conductor arrangement.

A preliminary stress analysis was made to establish the strength requirements for the inflatable antenna structure under operational environmental conditions. A design configuration is presented for the inflatable antenna structure. Material selection considerations, tooling, and manufacturing techniques are discussed.

A preliminary design concept is presented for a hardened antenna stowage enclosure, which also includes feed erection and rotation mechanisms and inflation system.

A scale model of the inflatable antenna was designed, fabricated, and tested. Extensive far-field antenna pattern tests were performed, and results are shown.

The results of the study and test program show that an antenna system consisting of a rotatable feed inside a non-rotating inflatable structure that serves as both a radome and a reflector is feasible. An inflatable structure can be fabricated to a specified contour, surfaced with a reflector consisting of closely spaced parallel conductors, and after inflation maintain this contour such that it will successfully meet radiation and environmental requirements. Also an inflatable antenna of this type can be practically stowed in and deployed from a hardened enclosure designed to withstand nuclear attack.

PUBLICATION REVIEW

This report has been reviewed and is approved.

Approved:

David F. Barber
for DAVID F. BARBER
Chief, Applied Research Laboratory
Directorate of Engineering

Approved:

William S. Bethke
WILLIAM S. BETHKE
Director of Engineering

FOR THE COMMANDER:

Irving J. Gabelman
IRVING J. GABELMAN
Director of Advanced Studies

TABLE OF CONTENTS

Section	Page
1 INTRODUCTION	1
2 SUMMARY	1
3 ENGINEERING STUDY	2
A. General	2
B. RF Design	4
1. General	4
2. Aperture Parameters	4
3. Feed Design	5
4. Primary Feed Pattern Measurements	6
5. Reflector	10
6. Theory of Parallel Conductors	12
C. Inflatable Structure Design	31
1. General	31
2. Inflatable Structure Configuration	31
3. Inflatable Structure Fabrication	40
4. Structural Considerations	40
5. Material Test Program	47
D. Radoflector Hardened Antenna System Installation	48
1. General	48
2. Hardened Enclosure	54
3. Radoflector Pressurization System	55
4. Feed Horn Erection Mechanism	55
5. Feed Horn Azimuth Drive System	56
6. Concept Review by Hardened Enclosure Consultants	56
4 SCALE MODEL	57
A. General	57
B. RF Design	57
C. Inflatable Structure Design	57
1. Contour	57
2. Material Selection	59
3. Elongation Considerations	59
4. Configuration	59
5. Fabrication Techniques and Tooling	62
D. Base Platform and Guy System	71
E. Feed Support	71
F. Entrance Air Lock	71
G. Pressurization System	71
H. Testing	71
1. General	71
2. Standard Dish Tests	71
3. Scale Model Tests	78
4. Vertical Contour Evaluation	85
5. Analysis of Far Field Test Results	86
5 CONCLUSIONS AND RECOMMENDATIONS	90
Appendix	
A ANTENNA TEST PATTERNS	A-1
B REFERENCES	B-1
C ADDENDUM	C-1

LIST OF ILLUSTRATIONS

Figure	Page
1 Erected Radoflector and Hardened Enclosure Concept	3
2 Primary Feed Horn for Scale Model Radoflector	6
3 Primary Feed Azimuth Pattern at Center Frequency (Vertical Polarization)	7
4 Primary Feed Azimuth Pattern at Center Frequency (Horizontal Polarization)	8
5 Primary Feed Azimuth Pattern at Center Frequency (45-Degree Polarization)	9
6 Geometric Optics Relationships of Feed-Reflector Combination	11
7 Universal Dish	15
8 Antenna Test Site	16
9 Universal Dish Elevation Pattern at Center Frequency ($f = 9.08$ GC)	17
10 Universal Dish Elevation Pattern at High Frequency Limit ($f = 9.44$ GC)	18
11 Universal Dish Elevation Pattern at Low Frequency Limit ($f = 8.72$ GC)	19
12 Feed Position Parameters Determined from Universal Dish Tests	20
13 Reflector Contour and Feed Positioned on Radoflector (Determined from Universal Dish Tests)	22
14 Wave Guide Grid Test Pieces	26
15 Grid Panel Transmissivity Test Setup	28
16 Transmissivity Characteristics of Parallel Wire Grid Panel (Wire Diameter = 0.010 Inch, Wire Spacing = 0.13 Inch, $f = 9.08$ GC, Wires Parallel to E Field)	29
17 Transmissivity Characteristics of Parallel Wire Grid Panel (Wire Diameter = 0.010 Inch, Wire Spacing = 0.13 Inch, $f = 9.08$ GC, Wires Perpendicular to E Field)	30
18 Inflatable Antenna Assembly (Sheet 1 of 3)	33
18 Inflatable Antenna Assembly (Sheet 2 of 3)	35
18 Inflatable Antenna Assembly (Sheet 3 of 3)	37
19 Inflatable Structure Geometry and Contour	39
20 Radoflector Structural Geometry	41
21 Guy Wire Arrangement	45
22 Stress-Strain Curves (DuPont Yarn Tests)	49
23 Automatic Hardened Site Inflatable Radoflector Concept	51
24 Radoflector Hardened Antenna Installation (Stowed Configuration)	53
25 Radoflector Hardened Antenna Installation (Operating Configuration)	54
26 Tool Contour	60
27 Static Testing a Cylinder of Mylar-Dacron Material	61
28 Radoflector Scale Model Design (Sheet 1 of 2)	63
28 Radoflector Scale Model Design (Sheet 2 of 2)	65

LIST OF ILLUSTRATIONS (Continued)

Figure		Page
29	Radoflector Scale Model Tool during Fabrication	67
30	Radoflector Scale Model Tool Completed	68
31	Preform Tool with Partial Gore in Tool and under Vacuum	69
32	Preform Tool and Form Tool with Gores in Fabrication Process	70
33	Scale Model Base Assembly	72
34	Base Assembly with Feed and Feed Adjustment Mounted	73
35	Scale Model with Entrance Air Lock Attached	74
36	Standard Dish	76
37	Standard Dish Mounted on Radoflector Support Base on Test Range	77
38	Feed Position Parameters Determined for Standard Dish Tests	78
39	Standard Dish Elevation Pattern at Center Frequency	79
40	Standard Dish Azimuth Pattern at Center Frequency (Elevation Angle = 9 degrees) ..	80
41	Scale Model Radoflector on Test Site	81
42	Feed Position Parameters Determined from Scale Model Radoflector Tests	82
43	Scale Model Radoflector Elevation Pattern at Center Frequency	83
44	Scale Model Radoflector Azimuth Pattern at Center Frequency (Elevation Angle = 9 Degrees)	84
45	Scale Model Contour Template Mounting	87
46	Scale Model Contour Measurement Locations	90

LIST OF TABLES

Table		Page
1	Antenna Performance Parameters	2
2	Feed Horn Characteristics	10
3	Full-Scale Vertical Reflector Contour Coordinates	13
4	Scale Model Vertical Reflector Contour Coordinates	14
5	Renormalized Scale Model Vertical Reflector Contour Coordinates (Feed Horn Axis Corresponds to X Axis)	21
6	Membrane Stresses	34
7	Test Program	50
8	Parameter Comparison (Scale Model versus Full-Scale Radoflector)	58
9	Standard Dish Test Results	75
10	Scale Model Radoflector Test Results	85
11	Variation of Electrical Characteristics of Scale Model Radoflector as Feed Position Is Varied in Azimuth ($f = 9.08$ GC)	85
12	Scale Model Radoflector Contour Measurements	88

AN ENGINEERING STUDY OF A POST-ATTACK ANTENNA SYSTEM

1. INTRODUCTION

On 4 May 1962 Goodyear Aircraft Corporation (GAC) initiated an engineering study under contract with Rome Air Development Center (RADC) of the United States Air Force to determine the feasibility of an air-supported, integrated, radome-antenna configuration and at the same time determine its adaptability to a post-attack, hardened posture.

In addition to the contract funds from RADC, GAC approximately matched these funds from company development monies to allow for expanded effort in certain phases of the program. The composite results of both efforts are presented in this technical documentary report.

The basic concept, which uses a parallel conductor grid made of a metallic material as a reflector, is not original with GAC; however, GAC has adapted this concept to an inflatable structure suitable for storage and erection from a hardened posture. The need for practical antenna systems that can be utilized following a nuclear blast is very real. With increasing warhead yields it has become very difficult to design an above-ground system that can survive both the fireball or the over-pressure levels. At the same time there is a practical size and economic limit to which hardened installations can be built to house fully erected antennas.

With this aim in mind a program was initiated which utilized the hardened concept but at the same time was capable of packaging the antenna in a relatively small volume when not operational. During the following six months (May through October 1962) GAC studied the problems, conceived a design, and tested a scale model of such a system. The results of this program are contained in this technical documentary report.

2. SUMMARY

The results of the engineering study to determine the feasibility of a post-attack survivable antenna installation are that such an antenna system is not only feasible but also very practical. Two basic conclusions were reached:

- (1) An inflatable structure can be fabricated to a specified contour, surfaced with a reflector consisting of a grid of closely spaced parallel conductors or dipoles, and after inflation hold its contour such that it will successfully meet its specified radiation and environmental requirements.
- (2) Based on preliminary design data and the adaption of standard methods used in the hardening of missile silos, a practical, unsophisticated, hardened enclosure can be designed to meet the storage and erection requirements of a post-attack antenna system. The level of protection provided is related directly to the capability of the enclosure.

Table 1 outlines the antenna performance parameters established by the contract as design goals. It also compares these goals with those parameters achieved during the rf far field tests at the center frequency of 9080 mcs of a 0.1377 scale model of the radome-antenna configuration (Radoflector^{*}). All goals were achieved by the scale model tests except for the -15 db side lobe level achieved versus the -25 db side lobe desired. However, after an examination of program test results, it is believed that a minimum of -19 db side lobe level can be achieved in a full-scale unit by optimizing the reflector shape, improving contour accuracy, minimizing aperture blockage, and further refining the feed design.

^{*}An antenna consisting of a rotatable fixed feed inside a non-rotating inflatable structure that serves as both a radome and a parabolic antenna.

TABLE 1.
Antenna Performance Parameters

PARAMETERS	FULL-SCALE DESIGN GOALS	0.1377 SCALE MODEL RESULTS	REMARKS
Size	18 x 25 ft parabolic reflector	Horizontal - 3.25 ft (spherical shape) Vertical - 3.35 ft (shaped parabolic)	Not a design goal as such, but an information parameter.
Frequency	1.2 - 1.3 gc (kmc)	8.720 - 9.440 gc	Operating frequency is an inverse function of the scale factor.
Gain	30 db	30.9 db	At the center frequency 9.08 gc.
Side Lobe Levels	-25 db	-15 db	At the center frequency of 9.08 gc.
Azimuth Beamwidth	2.5 degrees	2.1 degrees	At the center frequency of 9.08 gc.
Elevation Beamwidth	$\csc^2 \theta$, from 9 to 30 degrees	$\csc^2 \theta$, from 9 to 30 degrees (± 1.5 db)	At the center frequency of 9.08 gc.

It is important to realize that the scale model Radoflector achieved the results of Table 1 on its initial try. The scale model could have been optimized to improve the side lobe level by some figure; however, inasmuch as only feasibility was being proven, it was determined that the expenditure of additional time and money would not be worthwhile in this phase of the program.

Installed as a ground control intercept or return to base communications antenna, in the environs of a missile silo complex as an emergency communications (troposcatter or microwave) system, or as an emergency search radar system in the aircraft air defense environment, the post-attack antenna system will be capable of erection and operation without external resources immediately following a devastating nuclear blast.

It is recommended that the Air Force proceed with the design and fabrication of an engineering service test model of the post-attack antenna system described herein and also included in the prototype design data. Particularly, it is recommended that immediate effort be applied to the materials test program outlined in Section 3 to select the best combination of high-strength, lightweight, inflatable materials.

3. ENGINEERING STUDY

A. General

The post-attack antenna system described herein (Figure 1) employs an inflatable truncated oblate spherical radome-type structure 69 feet in diameter. Parallel metallic conductors are bonded to the surface at precise intervals and inclined to cross all lines that are parallel to the base at 45 degrees for the top half of the reflecting surface. The bottom portion of the reflecting surface is metallized. The metallic conductors and metallized section are employed over 360 degrees of the Radoflector in the horizontal plane and their combined vertical height is 25.4 feet. The bottom edge of the illuminated aperture will be 5 feet above ground level. The desired beam shaping is accomplished by contouring the reflector surface.

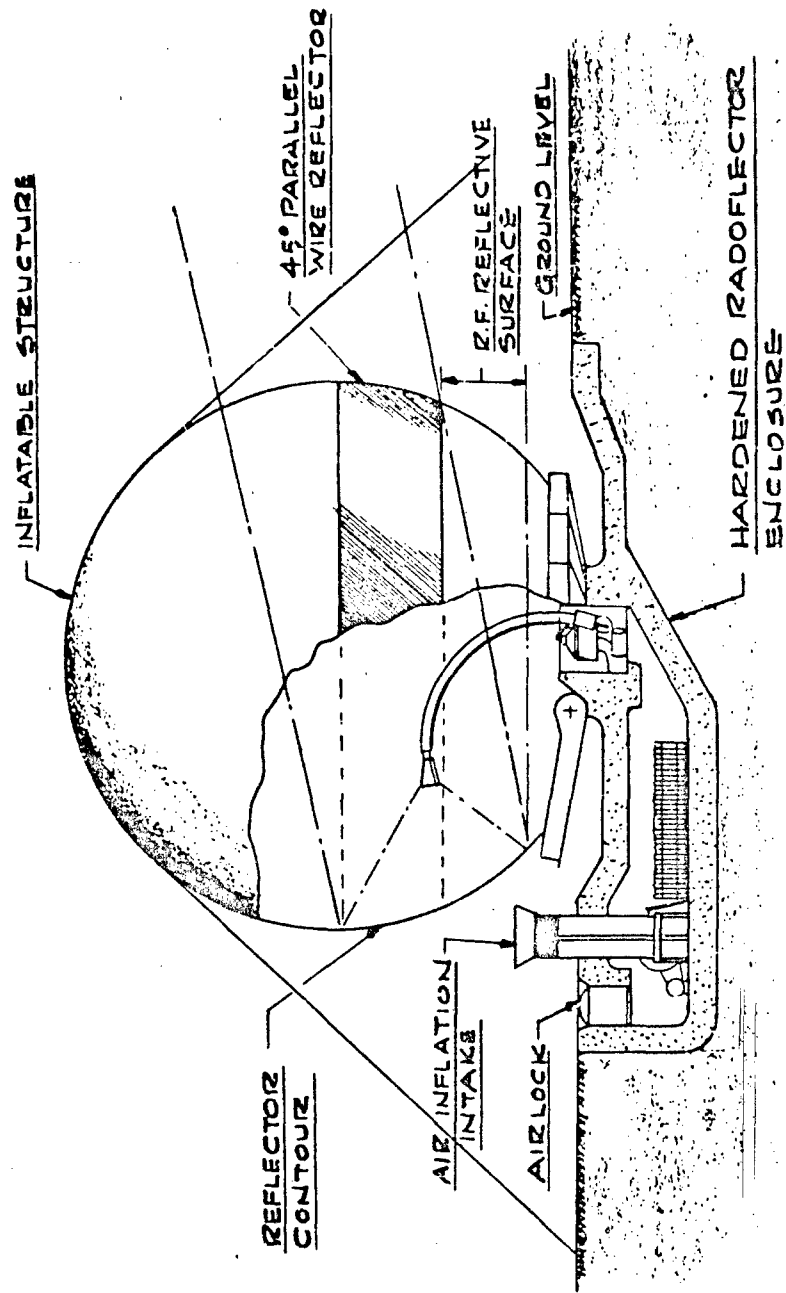


Figure 1. Erected Radreflector and Hardened Enclosure Concept

The feed, located within the expanded structure at the focal point, radiates energy with 45 degree polarization parallel to the metallic conductors which reflect the energy. The reflected collimated energy is then transmitted through the opposite side of the oblate spheroid since the conductors are oriented 90 degrees from their counterparts on the reflecting side. By proper choice of conductor size and spacing, the reflected beam will not be appreciably affected by the conductors or the metallized surface. The feed horn is rotated to generate the scanning.

To determine the feasibility of such a system the engineering study was approached as follows:

- (1) With the full-scale parameters (Table 1) firmly in mind, the initial effort was applied to the determination of the vertical contour and a proper scale factor for a scale model.
 - (2) The design of the scale model was determined, and fabrication was completed.
 - (3) As fabrication and testing of the scale model were proceeding the design of the full-scale system was also being carried forward with the intended purpose of applying to the full-scale design that which was learned from the scale model design, fabrication, and test.
- The engineering study was divided into three major areas:
- (1) *RF Design.* The rf design established the reflector aperture and contour requirements, scale factor for the scale model, the feed design, the size and spacing of the reflective material, transmission line characteristics, etc.
 - (2) *Inflatable Structure Design.* The inflatable structure design established the inflatable structure configuration and fabrication requirements for both the scale model and full-size post-attack antenna system.
 - (3) *Mechanical Design.* The mechanical design established the configuration of the mounting base, guying system, inflation and regulation, hardened enclosure requirement, etc., for both the scale model and the full-scale system.

B. Rf Design

1. General

An antenna system that consists of a reflector surface and a source of primary illumination will exhibit a secondary pattern which is dependent upon two independent parameters:

- (1) Reflector contour.
- (2) Distribution of primary illumination across the reflector aperture.

The following concepts can be used to obtain a shaped secondary radiation pattern:

- (1) *Complex feed concept.* A shaped secondary radiation pattern can be produced by using a parabolic reflector and a feed system that exhibits a shaped primary pattern with more than one focal center. The required complex feed system can be made up of an array of feeds or a lens and feed combination. The feed array would exhibit more than one discrete focal center. The principle of superposition can be used in determining the distribution of focal centers and the radiation characteristics of the feed array.
- (2) *Shaped reflector concept.* A shaped secondary radiation pattern can be produced by using a simple primary feed and a contoured reflector surface. A portion of the reflector would be paraboloidal, and a portion will be contoured according to geometric optics and conservation of energy principles.

The shaped reflector concept was chosen in preference to the complex feed approach for the initial design effort. The shaped reflector concept lends itself easily to the inflatable structure (Radoflector) design and reduces the complexity of the feed design.

2. Aperture Parameters

The aperture requirements of the proposed full-scale antenna are dependent on the gain, side lobe, and azimuth beamwidth requirements:

Gain = 30 db.

Side lobe level = -25 db (maximum).

Azimuth beamwidth = 2.5 degrees (maximum).

By applying these requirements to the relations that determine gain, side lobe level, and beamwidth of a paraboloid antenna, the required aperture diameter (D) can be determined. It should be noted that the required gain figure must be increased to compensate for losses due to:

- (1) Shaping of the elevation pattern.
- (2) Non-perfect reflecting surface (metallic conductors parallel to E field).
- (3) Reflection from non-perfect radome material (metallic conductors perpendicular to E field).

The center frequency (f_0) of the full-scale antenna is 1.25 gc (kmc). At this frequency the corresponding free-space wavelength (λ) is 9.45 inches.

By assuming the elevation beamwidth β , (before shaping) to be equal to the required azimuth beamwidth α , a gain figure for a paraboloid antenna can be determined by the following experimentally determined relations (Reference 1):

$$G \text{ (power gain)} = 27,000/\alpha\beta. \quad (1)$$

When $\alpha = \beta = 2.5$ degrees, $G = 4330$.

The gain figure expressed in db is $G(\text{db}) = 36.3$ db.

In determining a net gain figure, a reduction of 2 db from this gain figure due to shaping of the elevation pattern was assumed (Reference 2), and an additional loss of 2 db due to non-perfect reflective and transmittant surfaces was estimated from cursory wire grid studies. The net gain figure of 32.3 db is 2.3 db greater than the requirement for the proposed antenna system.

The required aperture diameter (D) is determined from the azimuth beamwidth requirement from the following relation (Reference 3):

$$\text{Half-power beamwidth, } \alpha = (69.5 \text{ degrees}) (\lambda/D). \quad (2)$$

Letting $\alpha = 2.5$ and solving for D,

$$D = 262.0 \text{ inches or } 22.0 \text{ feet.}$$

An optimum spherical surface which will approximate the required parabolic surface of aperture diameter (D) and the corresponding optimum focal point (F_{op}) can be determined from the following relations (Reference 3):

$$(a/R)^4 = 14.7 (\Delta/\lambda) / (R/\lambda) \quad (3)$$

and

$$F_{op} = 1/4 (R + \sqrt{R^2 - a^2}) \quad (4)$$

where

a = aperture radius = $D/2$

R = radius of required spherical surface and

Δ/λ = maximum allowable phase deviation in wavelengths = $1/16$.

Using the above relations, the required radius is

$$R = 27.2 \text{ feet (minimum).}$$

To compensate for contour tolerances and a desired lowedge illumination (in the order of -12 to -14 db) a radius of $R = 34.5$ feet was chosen. The purpose of decreasing edge illumination is to decrease side lobe levels and the phasing effects of the shaped pattern. From Equation 3, the corresponding value for parabolic aperture diameter is $D = 25.4$ feet.

From Equation 4, the optimum focal point (F_{op}) corresponding to $R = 34.5$ feet is $F_{op} = 16.65$ feet.

3. Feed Design

The simplest antenna feed for the proposed antenna is an ordinary rectangular aperture waveguide horn. The H-plane axis of the horn is positioned at an angle of 45 degrees with respect to

the horizontal. The horn is required to exhibit equal E-plane and H-plane radiation patterns in order to achieve horizontal and vertical illumination symmetry. The aperture and focal point requirements of the proposed antenna require a horn that exhibits a -10 db taper at ± 41 degrees in both principal planes. From design and experimental considerations, a suitable primary feed horn will have an H-plane aperture (A) of 15.35 inches and an E-plane aperture (B) of 11.0 inches.

A more efficient primary feed is one that exhibits an elliptical illumination pattern with the horizontal beamwidth of the pattern broader than the vertical beamwidth. In this manner the gain and side lobe levels should be improved by the more efficient illumination of the available aperture. However, since the proposed antenna requires an E-field polarization of 45 degrees, a complex feed horn design would be necessary. Such a horn would utilize a section of square or circular guide and a phase shifting card. The basic principles are similar to those used in the design of circular polarized horns.

From the standpoint of simplicity and economy, the rectangular aperture waveguide horn is used.

4. Primary Feed Pattern Measurements

Primary pattern measurements were obtained from a feed horn scaled down for the scale model Radoflector. Figure 2 shows the scale model feed horn. The aperture dimensions for the scale model horn are A = 2.12 inches and B = 1.51 inches.

Radiation patterns were taken in an anechoic chamber at frequencies of 8.67, 9.08, and 9.45 gc. H-plane (0-degree) and E-plane (90-degree) patterns were obtained as well as a 45-degree polarization pattern. The resultant symmetry of illumination was adequate for the requirements of the proposed antenna system. Figures 3, 4, and 5 show the respective radiation patterns.

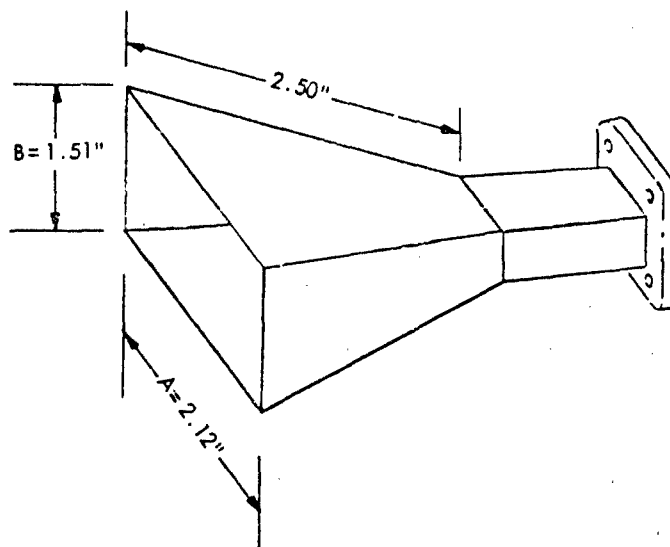


Figure 2. Primary Feed Horn for Scale Model Radoflector

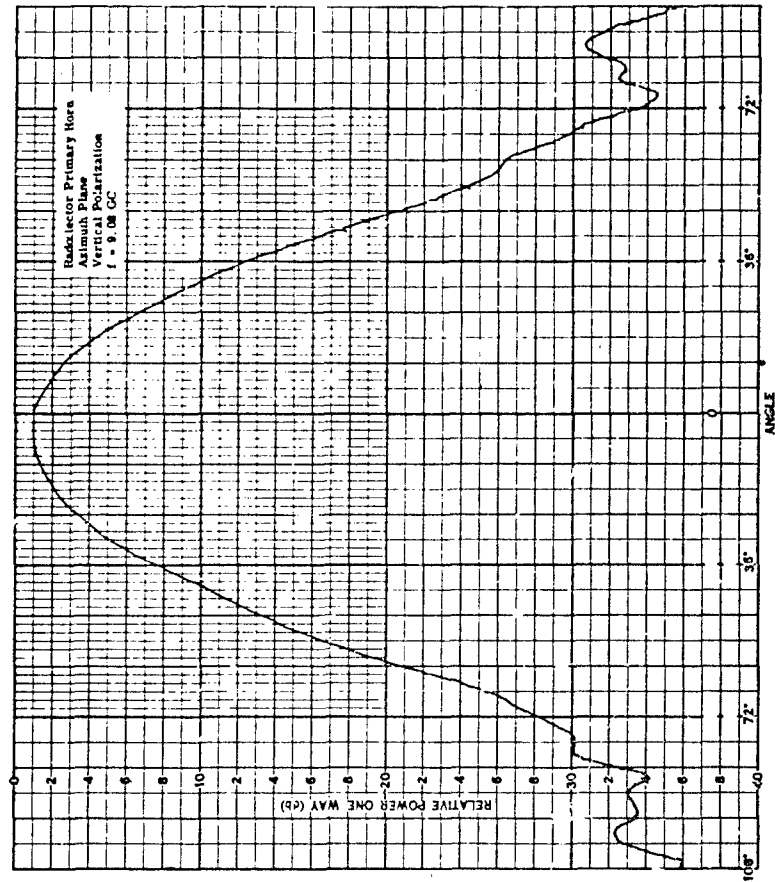


Figure 3. Primary Feed Azimuth Pattern at Center Frequency (Vertical Polarization)

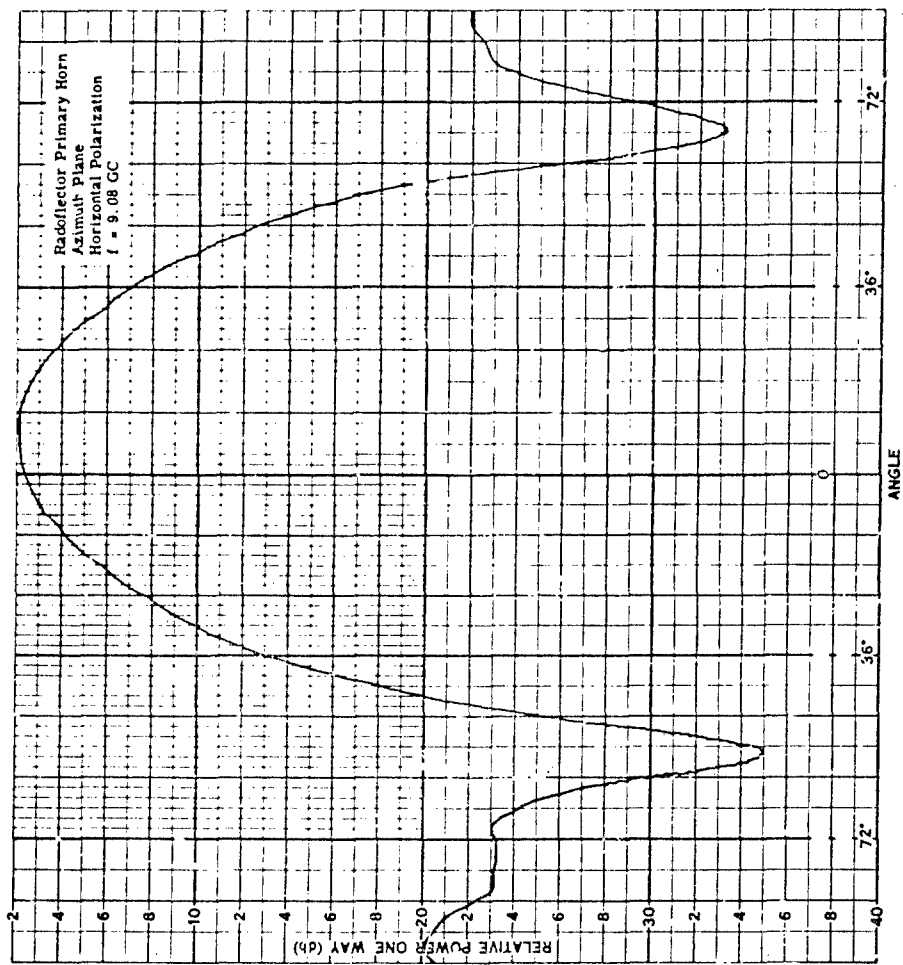


Figure 4. Primary Feed Azimuth Pattern at Center Frequency (Horizontal Polarization)

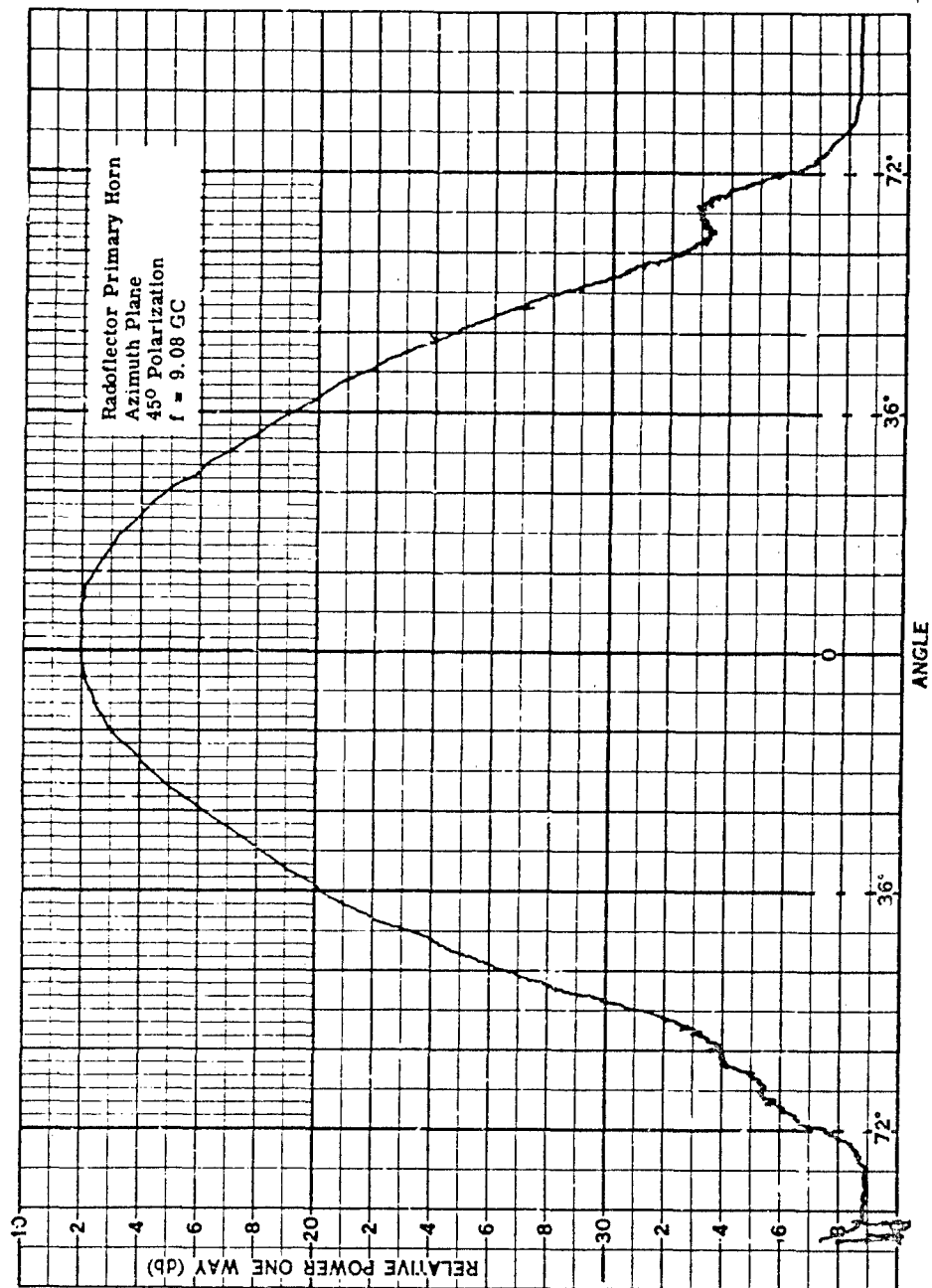


Figure 5. Primary Feed Azimuth Pattern at Center Frequency (45-Degree Polarization)

Since the horn will be used in a 45-degree polarization orientation, the azimuth side lobe level for this condition must be kept at a minimum. Figure 5 shows the side lobe level to be less than -23 db. The 10 db beamwidths for all cases were 85 degrees or less throughout the effective frequency range (refer to Table 2).

TABLE 2.
Feed Horn Characteristics

FREQUENCY (GC)	POLARIZATION	10-DB TAPER AZIMUTH ANGLES (Degrees)	10-DB BEAMWIDTH (Degrees)
9.08	Horizontal	+41.0, -39.0	80
9.08	Vertical	+38.2, -37.0	75.2
9.08	45 degrees	+41.0, -41.0	82.0
8.72	Horizontal	+42.0, -43.0	85
8.72	Vertical	+40.8, -40.0	80.8
8.72	45 degrees	+42.8, -42.0	84.8
9.44	Horizontal	+37.0, -37.0	74.0
9.44	Vertical	+36.8, -36.8	73.6
9.44	45 degrees	+38.0, -38.0	76.0

VSWR < 1.3 at f = 9.08, 8.72, and 9.44 gc.

5. Reflector

a. *Contour Design.* Considering an antenna system that consists of a singly curved feed-reflector combination, the primary radiation pattern and reflector surface contour are related by the following equation (see Figure 6):

$$\frac{\int_{\theta_1}^{\theta_2} P(\theta) d\theta}{\int_{\theta_1}^{\theta_2} P(\theta) d\theta} = \frac{\int_{\phi_1}^{\phi_2} I(\phi) d\phi}{\int_{\phi_1}^{\phi_2} I(\phi) d\phi} \quad (5)$$

$$\ln \rho / \rho_1 = \int_{\phi_1}^{\phi} \tan \left[\frac{\phi - \theta(\phi)}{2} \right] d\phi \quad (6)$$

where

- $I(\phi)$ = primary radiation pattern
- $P(\theta)$ = secondary radiation pattern
- $\rho(\phi)$ = reflector surface contour
- ϕ = primary pattern angle
- θ = secondary pattern angle
- ϕ_1 and ϕ_2 = reflector limits
- θ_1 and θ_2 = secondary pattern limits and
- ρ_1 = contour point at ϕ_1 .

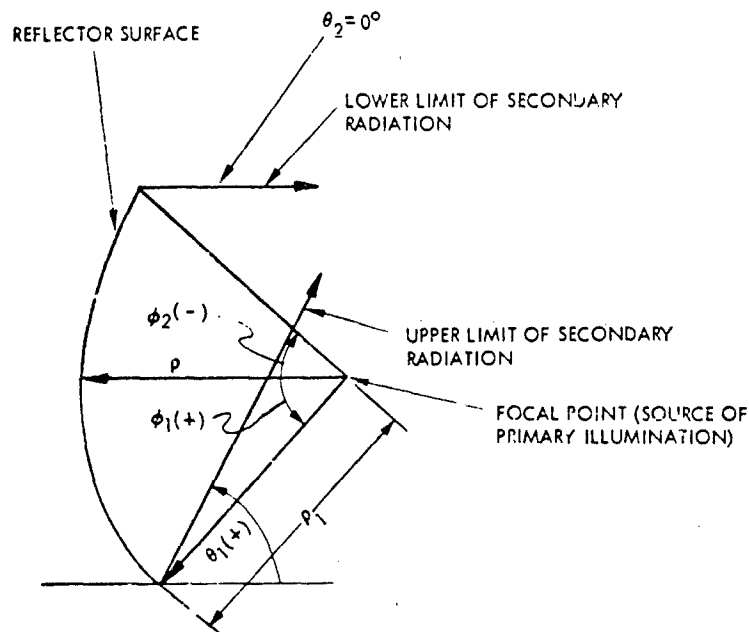


Figure 6. Geometric Optics Relationships of Feed-Reflector Combination

The above relations are derived from geometric optic theory and conservation of energy principles.

For the specific case of the proposed antenna,

$$P(\theta) = K \csc^2 (\theta + \alpha)$$

$$\theta_1 = 0 \text{ degrees}$$

$$\theta_2 = 21 \text{ degrees}$$

where

$$K = 1/\csc^2 (9^\circ).$$

It should be noted that when the vertical contour is positioned on the radome structure at a depression angle of 9 degrees, the effective secondary pattern will be $P'(\theta) = K \csc^2 \theta$ from 9 to 30 degrees.

$I(\phi)$ is dependent upon the gain, side lobe level, and azimuth beamwidth requirements of the proposed antenna. For the shaped reflector concept the pattern would normally be a simple cosine function between limits ϕ_1 and ϕ_2 .

Once the primary and secondary patterns have been established, Equations 5 and 6 can be evaluated either by mathematical or graphical integration techniques. The values of θ corresponding to the variable parameter (ϕ) can be determined as a function of ϕ , and the function $\tan [\phi - \theta(\phi)]/2$ versus ϕ can be plotted. By using a graphical integration technique, Equation 6 can be evaluated, and $\ln p/p_1$ as a function of ϕ can be determined. Using antilog conversion methods, the required contour $p/p_1(\phi)$ can be determined. The center of the coordinate system corresponds to the focal point of the antenna.

It should be noted that the above analysis considers singly curved reflectors only. However, past experience has indicated that this method produces results which closely approximate the results obtained with the more complex analysis of doubly curved surfaces.

The reflector contour is in terms of ρ/ρ_1 ; the scale factor (magnitude of ρ_1) is dependent on the aperture and focal distance dimensions which are in turn dependent upon gain, side lobe, and azimuth beamwidth requirements. Table 3 is a tabulation of the X and Y coordinates which describe the vertical reflector contour for the proposed antenna system. The point ($x = 0, y = 0$) corresponds to ρ/ρ_1 at $\phi = 0$ degrees.

In order to achieve the desired csc^2 pattern from 9 to 30 degrees, the contour must be properly positioned on the radome structure. The desired pattern should be achieved when the horizontal axis of the contour is rotated downward 9 degrees at a pivot point corresponding to the center of the original 69-foot diameter sphere. The center of the feed horn will be 20 feet above ground level.

The horizontal reflector contour is obtained by rotating the properly positioned elevation contour 360 degrees about a vertical axis through the center of the spheroid.

b. *Vertical Contour Evaluation.* A scaled down (0.1377 scale, same as the scale model) vertical contour, defined by Table 4 coordinates, was simulated on a universal dish (Figure 7). The universal dish consists of a support base containing parallel blades which are adjustable in a direction normal to the plane of the blades. Using a micrometer, the blades were adjusted to the respective coordinant points. The spacing used between blade edges was 0.385 inch.

The space between the blades was filled in with modeling clay. An aluminum foil covering was used as the reflecting surface. The top and bottom edges of the dish were extended using aluminum sheeting formed to the desired contours. The vertical height of the dish was 40.25 inches; the width was 18 inches.

The pattern measurements of the universal dish were obtained using a 400-foot antenna test range with the dish mounted on a "mast" support tower (See Figure 8).

The secondary antenna patterns were obtained using the scale model primary feed previously described. Initially, the feed was placed at the theoretical focal point ($f = 27.60$ inches). The feed position was adjusted iteratively to obtain the best approximation to the desired secondary pattern. Figures 9, 10, and 11 show the final patterns at the center frequency, upper frequency limit, and lower frequency limit respectively. The patterns deviate less than ± 1.5 db from the theoretical curve. The finalized feed position parameters are as follows (see Figure 12):

X = 28.0 inches (focal distance)
Y = 1.8 inches
 $\phi = 0$ degrees.

It should be noted that the above tests were performed on a singly curved reflector surface; however, the results should be valid for a doubly curved contour where the azimuth curve is parabolic. For the case of the Radoflector that portion of the spheroid that is within $\lambda/16$ of a parabola is used in azimuth.

Table 5 shows the scale model contour coordinants, renormalized with respect to the new focal point. In this coordinant system the coordinants of the focal point are

X = 28.0 inch
Y = 0 inch.

The antenna patterns obtained from the universal dish tests showed the peak of the curve to occur at $\theta = +2$ degrees with respect to an optically boresighted reference. For this reason the X axis of the contour must be rotated downward an additional 2 degrees from the 9 degree reference that was previously determined. With this configuration (as shown in Figure 13) the peak of the $\text{csc}^2 \theta$ pattern should occur at $\theta = 9$ degrees with respect to the horizontal.

6. Theory of Parallel Conductors

a. *General.* A surface that consists of parallel conductors exhibits a reflection coefficient (Γ) which is a function of the angle of the conductor axis with respect to polarization angle of the incident electromagnetic wave which is normal to the surface.

TABLE 3.
Full-Scale Vertical Reflector Contour Coordinants

Y COORDINANT (Inches)	X COORDINANT (Inches)	Y COORDINANT (Inches)	X COORDINANT (Inches)
0	+0.400	+154.38	+31.045
+2.20	+0.348	+158.00	+32.625
+5.75	+0.218	+161.63	+34.215
+9.37	+0.145	+165.00	+35.815
+13.00	0	0	+0.400
+16.63	+0.109	-1.50	+0.471
+20.25	+0.181	-5.13	+0.689
+23.88	+0.304	-7.75	+1.015
+27.50	+0.450	-12.38	+1.341
+31.13	+0.638	-16.00	+1.668
+34.75	+0.830	-19.63	+2.066
+38.38	+1.050	-23.25	+2.465
+42.00	+1.340	-26.88	+2.987
+45.63	+1.691	-30.50	+3.553
+49.25	+2.062	-34.13	+4.169
+52.88	+2.429	-37.75	+4.872
+56.50	+2.922	-41.38	+5.604
+60.13	+3.368	-45.00	+6.395
+63.75	+3.980	-48.25	+7.337
+67.38	+4.600	-52.25	+8.120
+71.00	+5.202	-55.88	+9.034
+74.25	+5.960	-57.25	+9.947
+78.25	+6.740	-63.13	+11.035
+81.88	+7.576	-66.75	+12.216
+83.25	+8.483	-70.38	+13.340
+89.13	+9.461	-74.00	+14.631
+92.75	+10.440	-77.63	+15.950
+96.38	+11.419	-81.25	+17.306
+100.00	+12.398	-84.88	+18.814
+103.63	+13.340	-88.50	+20.336
+107.25	+14.319	-92.13	+21.917
+110.88	+15.312	-95.75	+23.526
+114.50	+16.276	-99.38	+25.172
+118.13	+17.364	-103.00	+26.825
+121.75	+18.415	-106.63	+28.580
+125.38	+19.611	-110.25	+30.559
+129.00	+20.808	-113.88	+32.444
+132.63	+22.076	-117.50	+34.401
+136.25	+23.454	-121.13	+36.518
+139.88	+24.853	-124.75	+38.498
+143.50	+26.318	-128.38	+40.709
+147.13	+27.876	-132.00	+43.210
+150.75	+29.471	-135.63	+45.748
		-139.00	+48.908

TABLE 4.
Scale Model Vertical Reflector Contour Coordinants

Y COORDINANT (Inches)	X COORDINANT (Inches)	Y COORDINANT (Inches)	X COORDINANT (Inches)
0	+0.055	+20.3	+4.282
+0.3	+0.048	+21.8	+4.480
+0.8	+0.030	+21.3	+4.720
+1.3	+0.020	+22.8	+4.940
+1.8	0	0	+0.055
+2.3	+0.015	-0.2	+0.065
+2.8	+0.025	-0.7	+0.095
+3.3	+0.042	-1.2	+0.140
+3.8	+0.062	-1.7	+0.185
+4.3	+0.088	-2.2	+0.230
+4.8	+0.115	-2.7	+0.285
+5.3	+0.145	-3.2	+0.340
+5.8	+0.185	-3.7	+0.417
+6.3	+0.233	-4.2	+0.470
+6.8	+0.285	-4.7	+0.575
+7.3	+0.335	-5.2	+0.672
+7.8	+0.390	-5.7	+0.773
+8.3	+0.465	-6.2	+0.882
+8.8	+0.550	-6.7	+1.012
+9.3	+0.635	-7.2	+1.120
+9.8	+0.725	-7.7	+1.246
+10.3	+0.823	-8.2	+1.372
+10.8	+0.930	-8.7	+1.522
+11.3	+1.045	-9.2	+1.685
+11.8	+1.170	-9.7	+1.840
+12.3	+1.305	-10.2	+2.018
+12.8	+1.440	-10.7	+2.200
+13.3	+1.575	-11.2	+2.387
+13.8	+1.710	-11.7	+2.595
+14.3	+1.840	-12.2	+2.805
+14.8	+1.975	-12.7	+3.023
+15.3	+2.112	-13.2	+3.245
+15.8	+2.245	-13.7	+3.472
+16.3	+2.395	-14.2	+3.700
+16.8	+2.540	-14.7	+3.942
+17.3	+2.705	-15.2	+4.215
+17.8	+2.870	-15.7	+4.475
+18.3	+3.045	-16.2	+4.745
+18.8	+3.235	-16.7	+5.037
+19.3	+3.428	-17.2	+5.310
+19.8	+3.630	-17.7	+5.615
+20.3	+3.845	-18.2	+5.960
+20.8	+4.065	-18.89	+6.342
+21.36	+4.283		

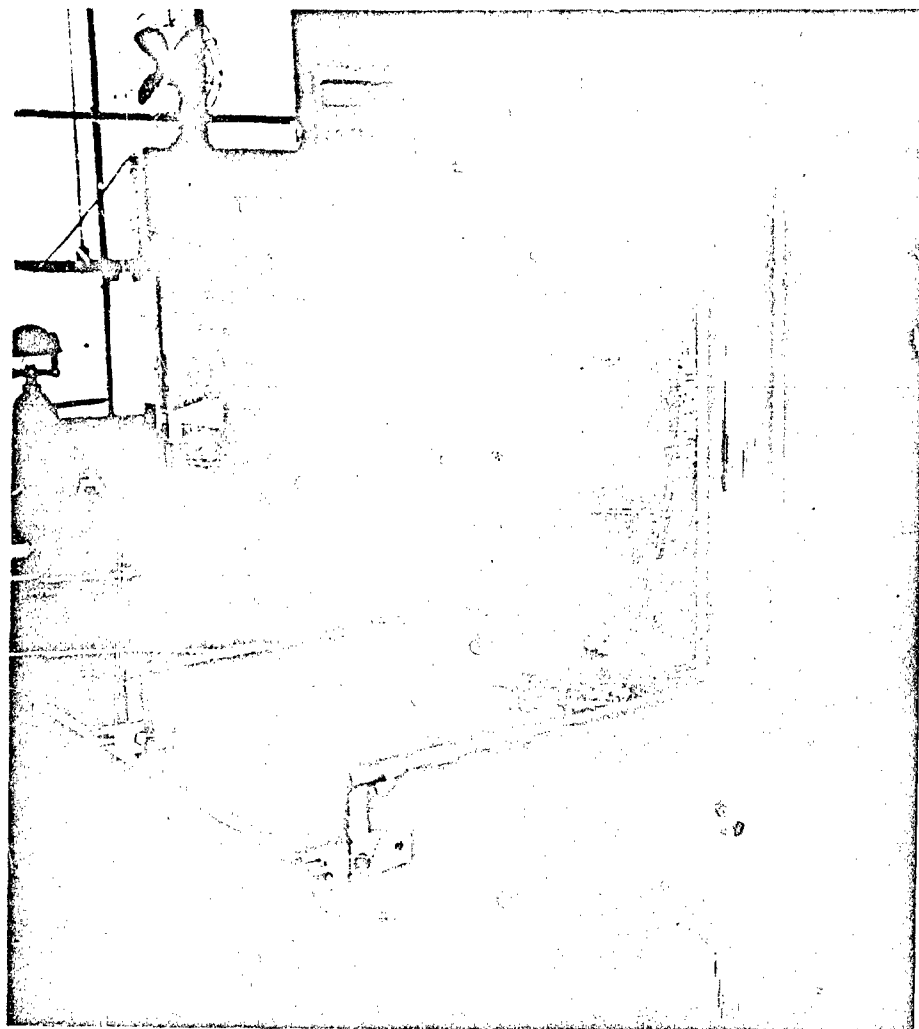


Figure 7. Universal Dish

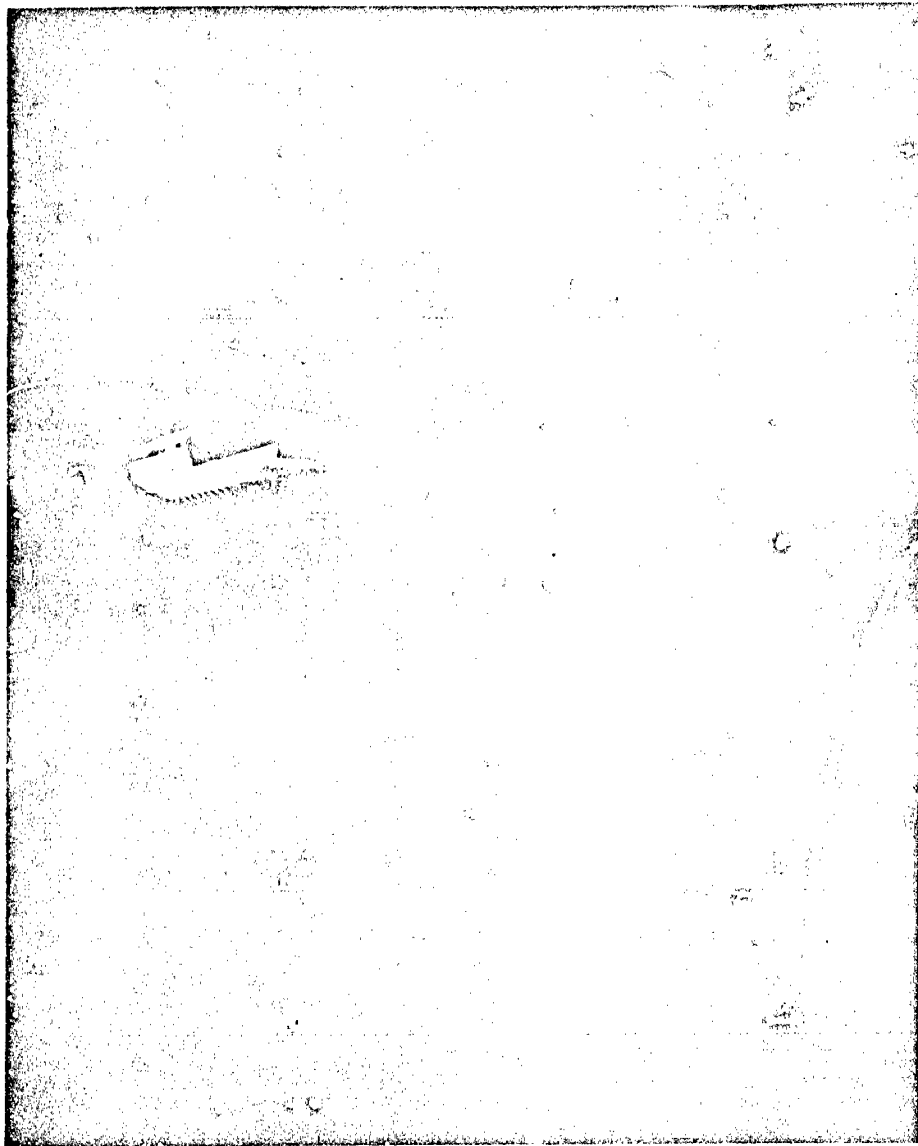


Figure 8. Antenna Test Site

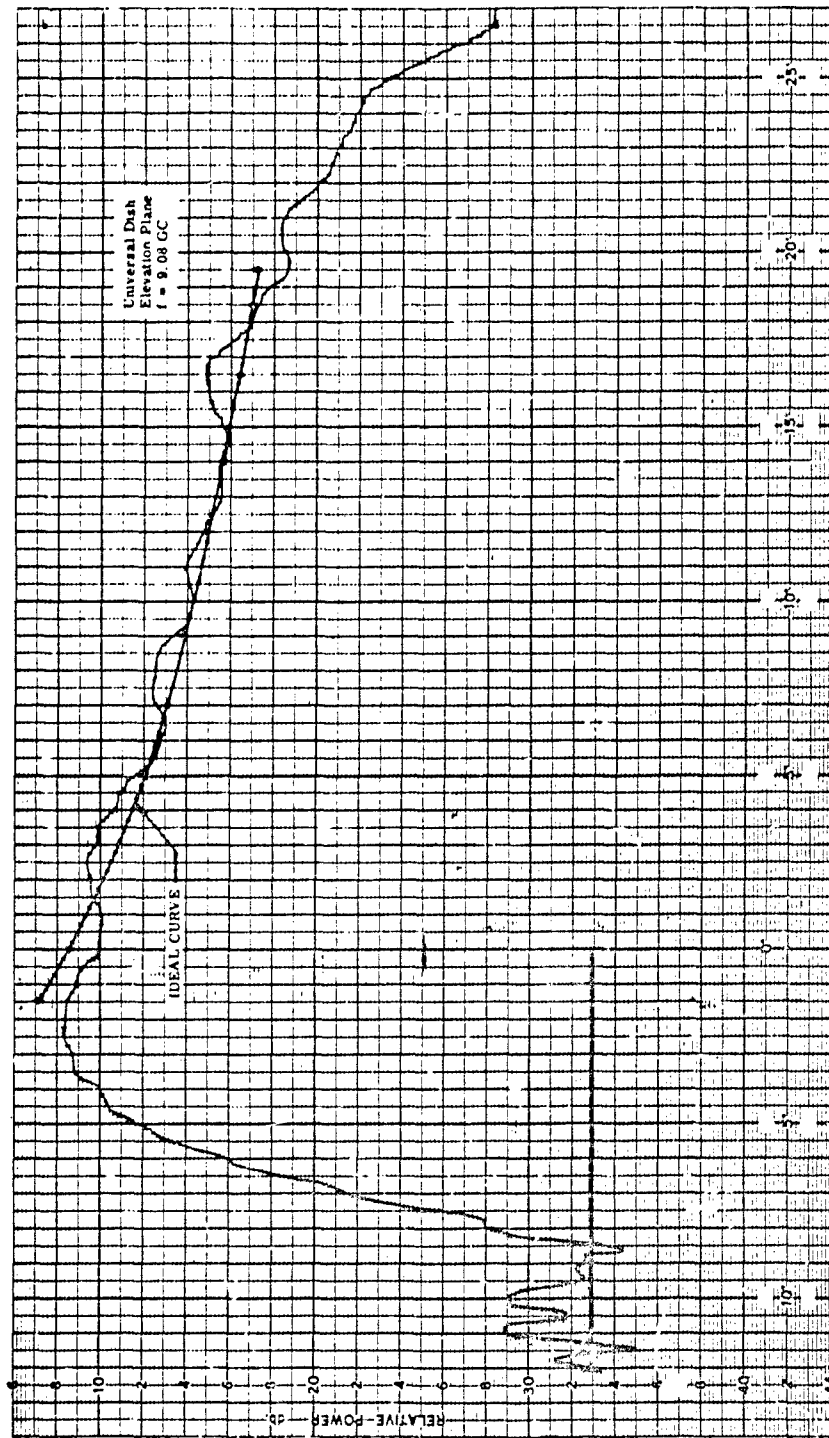


Figure 9. Universal Dish Elevation Pattern at Center Frequency ($f = 9.08 \text{ GC}$)

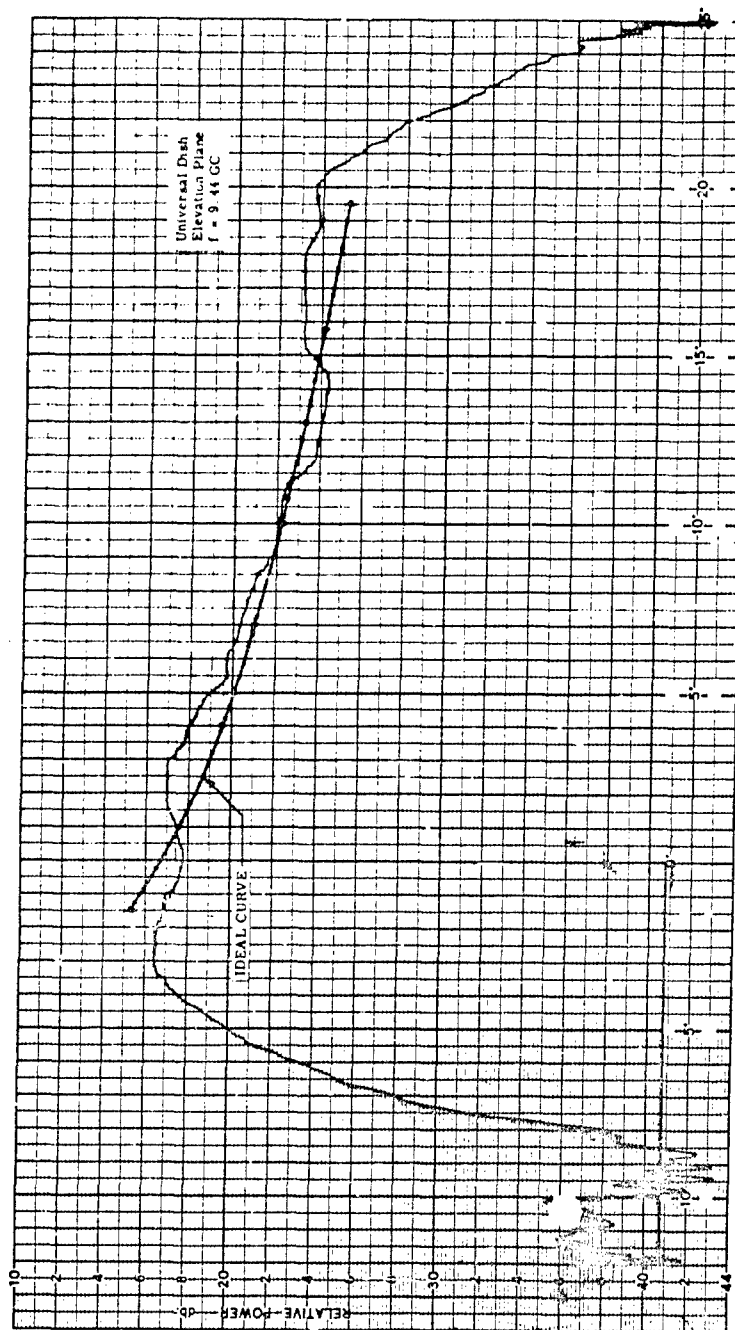


Figure 10. Universal Dish Elevation Pattern at High Frequency Limit ($f = 9.44$ GC)

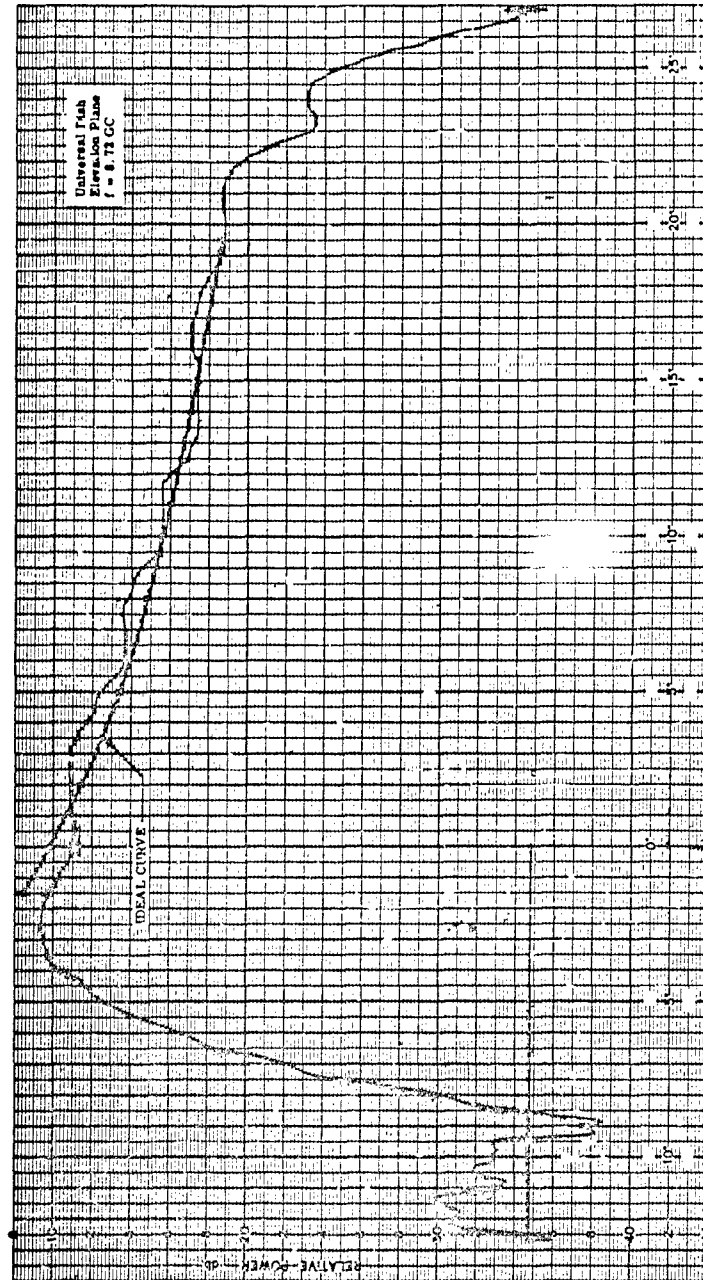


Figure 11. Universal Dish Elevation Pattern at Low Frequency Limit ($f = 8.72$ GC)

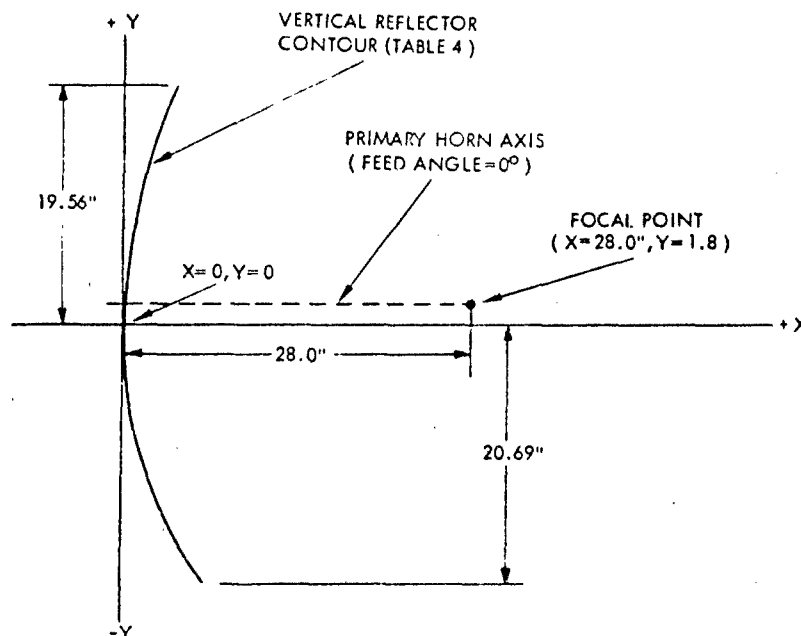


Figure 12. Feed Position Parameters Determined from Universal Dish Tests

When the conductors are parallel to the E field, the reflection coefficient of the array will be maximum (Γ_{\max}). When the conductors are perpendicular to the E field, the resultant reflection coefficient will be minimum (Γ_{\min}). The magnitudes of Γ_{\max} and Γ_{\min} are dependent upon the conductor configuration, spacing, and wavelength.

The following conductor configurations were considered as possible reflective surfaces and can be utilized in achieving a surface that exhibits suitable Γ_{\max} and Γ_{\min} characteristics:

- (1) Parallel wires of finite diameter
- (2) Parallel, flat, metallic conductors of negligible depth and finite width
- (3) Parallel metallic conductors of negligible width and finite depth.

A final decision as to the exact configuration of the parallel conductors for the full-scale design will require further study and material adherence tests. At the present time the parallel, flat, metallic conductors of negligible depth and finite width seem the most practical. The parallel wires at lower frequencies can become large in diameter, difficult to fabricate and attach to the inflatable structure, and difficult to fold. The same basic reasoning is also true for the case of the parallel metallic conductors of negligible width and finite depth.

b. *Parallel Wires of Finite Diameter.* A single perfectly conducting wire of diameter (d) has a finite value of normalized susceptance jB/Y_0 (where Y_0 = admittance of free space). The value is dependent upon the wavelength of the incident signal (λ) and the orientation of wire axis with respect to polarization angle (E vector). When two or more parallel wires are considered, the center-to-center spacing (s) becomes a critical parameter in determining a resultant susceptance value. Investigations have furnished susceptance characteristics of parallel wire grids as a function of diameter, spacing, and wavelength. From these sources, susceptance characteristics of

TABLE 5.
Renormalized Scale Model Vertical Reflector Contour Coordinates
(Feed Horn Axis Corresponds to X Axis)

Y COORDINANT (Inches)	X COORDINANT (Inches)	Y COORDINANT (Inches)	X COORDINANT (Inches)
0	0	0	0
+0.5	+0.015	-0.5	+0.020
+1.0	+0.025	-1.0	+0.030
+1.5	+0.042	-1.5	+0.048
+2.0	+0.062	-2.0	+0.065
+2.5	+0.088	-2.5	+0.095
+3.0	+0.115	-3.0	+0.140
+3.5	+0.145	-3.5	+0.185
+4.0	+0.185	-4.0	+0.230
+4.5	+0.233	-4.5	+0.285
+5.0	+0.285	-5.0	+0.340
+5.5	+0.335	-5.5	+0.412
+6.0	+0.390	-6.0	+0.490
+6.5	+0.465	-6.5	+0.575
+7.0	+0.550	-7.0	+0.672
+7.5	+0.635	-7.5	+0.773
+8.0	+0.725	-8.0	+0.882
+8.5	+0.823	-8.5	+1.012
+9.0	+0.930	-9.0	+1.120
+9.5	+1.045	-9.5	+1.248
+10.0	+1.170	-10.0	+1.372
+10.5	+1.305	-10.5	+1.522
+11.0	+1.440	-11.0	+1.685
+11.5	+1.575	-11.5	+1.840
+12.0	+1.710	-12.0	+2.018
+12.5	+1.840	-12.5	+2.200
+13.0	+1.975	-13.0	+2.387
+13.5	+2.112	-13.5	+2.595
+14.0	+2.245	-14.0	+2.805
+14.5	+2.395	-14.5	+3.023
+15.0	+2.540	-15.0	+3.245
+15.5	+2.705	-15.5	+3.472
+16.0	+2.870	-16.0	+3.700
+16.5	+3.045	-16.5	+3.942
+17.0	+3.235	-17.0	+4.215
+17.5	+3.428	-17.5	+4.475
+18.0	+3.630	-18.0	+4.745
+18.5	+3.845	-18.5	+5.037
+19.0	+4.065	-19.0	+5.310
+19.56	+4.283	-19.5	+5.615
		-20.0	+5.960
		-20.69	+6.342

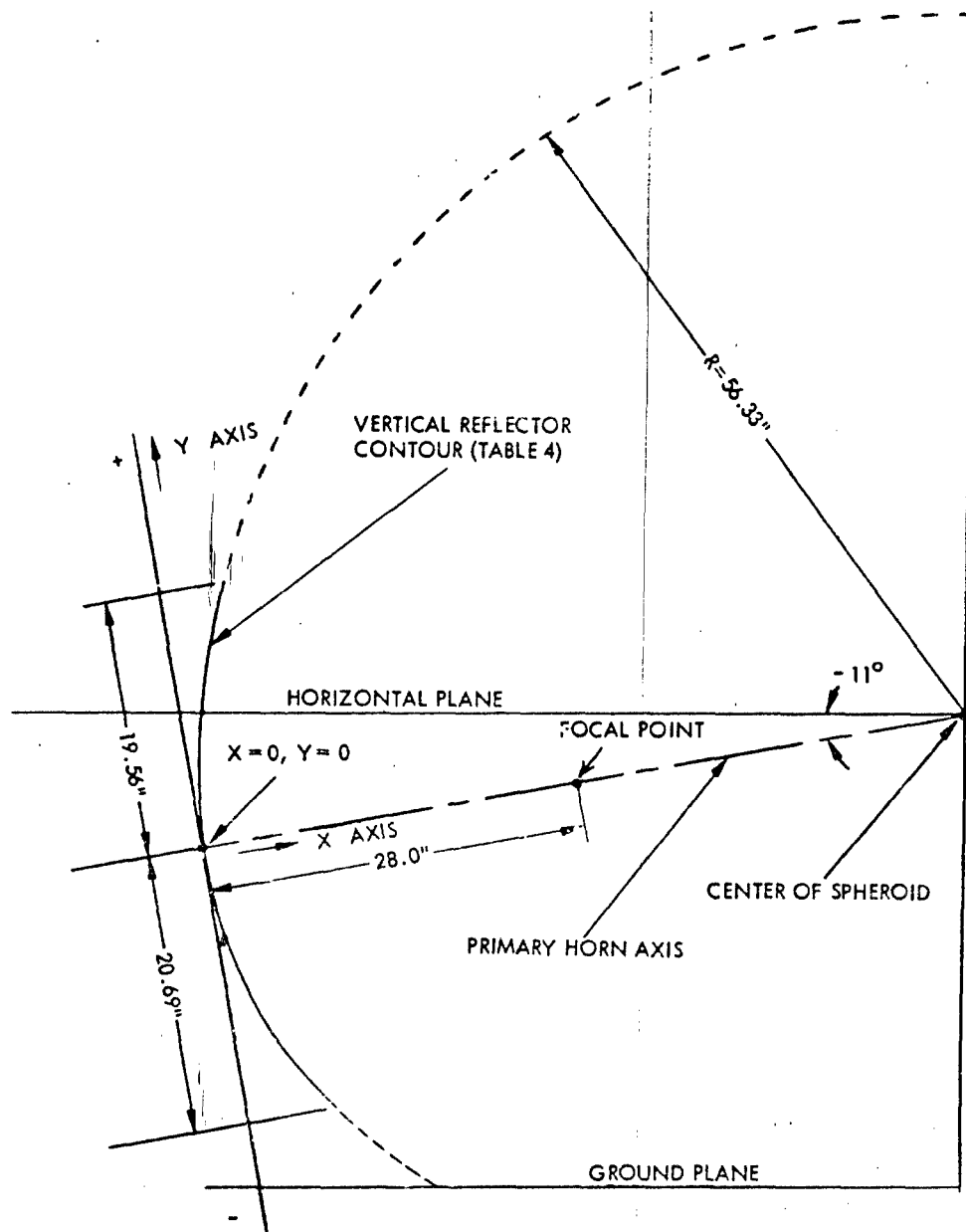


Figure 13. Reflector Contour and Feed Positioned on Radeflector
(Determined from Universal Dish Tests)

parallel wires were determined for both parallel E field and perpendicular E field conditions, as the diameter and spacing parameters were varied.

The susceptance values were transformed into corresponding reflection coefficients (Γ), using the following relations:

$$|\Gamma| = \left| \frac{1 - Y_R/Y_0}{1 + Y_R/Y_0} \right| \quad (7)$$

where Y_R/Y_0 is the normalized input admittance of the grid in free space. From an equivalent circuit analogy, $Y_R/Y_0 = 1 + jB/Y_0$.

By substitution, Equation 7 reduces to

$$\Gamma = \left| \frac{-jB/Y_0}{2 + jB/Y_0} \right| \quad (8)$$

The characteristics of Γ as a function of d/λ and s/λ can be determined by solving Equation 8, using the corresponding value of jB/Y_0 (obtained from Reference 4). The optimum parameters were determined by first arbitrarily choosing a value for wire diameter (d). The spacing parameter (s/λ) was then determined as that value which would produce a susceptance value (jB/Y_0) in the order of 5.0 when the wires are parallel to the E field. This value was determined from iterative Smith Chart technique which determined the Γ_{\max} and Γ_{\min} characteristics as a function of wire size and spacing. When this value of susceptance is achieved, the total loss can be maintained below 1 db. If the initial choice of d cannot produce the required susceptance value, a new wire diameter is chosen, and the required spacing is determined.

The major factors which contribute to the total loss are:

- (1) A reflection of the incident signal at the non-perfect transparent surface (α_R).
- (2) Transmission loss at the non-perfect reflecting surface (α_T).

The total loss can be expressed as

$$\begin{aligned} \alpha(\text{db}) &= \alpha_R + \alpha_T \\ \alpha(\text{db}) &= 10 \log (\Gamma_{\min}^2) + 10 \log (1 - \Gamma_{\min}^2) (1 - \Gamma_{\max}^2) \\ &= 10 \log [\Gamma_{\min}^2 (1 - \Gamma_{\min}^2) (1 - \Gamma_{\max}^2)]. \end{aligned} \quad (9)$$

An approximate solution can be expressed as

$$\alpha(\text{db}) = 10 \log [\Gamma_{\min}^2 (1 - \Gamma_{\max}^2)] \quad (10)$$

where Γ_{\max} = reflection coefficient when wires are parallel to E field and

Γ_{\min} = reflection coefficient when wires are perpendicular to E field.

It should be noted that the above relations are valid when the nonperfect transparent surface shadows the entire reflector aperture. If the percentage shadowed aperture is reduced, a slight reduction in reflection loss (α_R) will be realized. In the same manner, if a portion of the reflection aperture is made to be a perfect reflector, the transmission loss (α_T) will decrease proportionally.

The parallel wires of finite diameter were selected for the design of the scale model grid since they are essentially equivalent to scaled down parallel flat strips.

c. Parallel Flat Metallic Conductors

(1) *Negligible Depth and Finite Width.* The procedure for determining optimum width (w) and spacing (s) parameters of parallel flat strip grids differs from that of the wire grid case in that an initial dimensional value is not chosen. The parameters w and s are expressed in terms of wavelengths.

Using the information of Reference 4, which relates jB/Y_0 to the parameters w/λ and s/λ , and Equation 8, the corresponding reflection coefficient characteristics can be determined.

The optimum combination of w and s was determined as the minimum w/s ratio that produces a parallel E field susceptance value (jB/Y_0) in the order of 5.0.

The corresponding values of Γ_{\max} and Γ_{\min} were determined and the total loss calculated. If the total loss exceeded 1 db, variations of the w/s ratio were taken until the loss requirements were satisfied.

Using the above criteria, the following optimum grid parameters were determined for an array of parallel flat strips:

Strip width (w) = 0.05λ

Center-to-center spacing (s) = 0.15λ .

At the design frequency of the full-scale Radoflector ($f_0 = 1.25$ gc), the corresponding wavelength (λ) is 9.45 inches and the dimensional parameters are

Strip width (w) = 0.47 inch

Center-to-center spacing (s) = 1.42 inches.

The corresponding losses are

Transmission loss at reflecting surface (α_T) = 0.70 db

Reflection loss at transparent surface (α_R) = 0.15 db

Total loss (α) = 0.85 db.

(2) *Negligible Width and Finite Depth.* Using the technique outlined in the prior discussion the following grid parameters were determined for a normal array of parallel fins of negligible width and finite depth:

Depth of conductor (d) = 0.25λ

Center-to-center spacing (s) = 0.38λ

Thickness of conductor (t) < 0.01λ .

At the design frequency of the full-scale Radoflector ($f_0 = 1.25$ gc), the dimensional parameters are

Depth of conductor (d) = 2.36 inches

Center-to-center spacing (s) = 3.6 inches

Width of conductor (w) < 0.10 inch.

The corresponding losses are

Transmission loss at reflecting surface (α_T) = 0.6 db

Reflection loss at transparent surface (α_R) < 0.1 db

Total loss (α) < 0.7 db.

d. *Tolerance Considerations.* The results of scale-model Radoflector tests have shown that the reflector surface tolerance is the most critical factor that affects side lobe levels. The following tolerance limits have been established:

(1) Reflector Surface Contour Accuracy

$$\Delta p = \pm \lambda/16$$

$$\Delta p = \pm 0.60 \text{ inch at } f_0 = 1.25 \text{ gc.}$$

NOTE: References 5 and 6 indicated that the surface contour accuracy should be $\lambda/32$ or ± 0.30 inch at 1.25 gc. After further consideration and analysis it is now believed that the specified radiation requirements can be achieved with this lower tolerance limit of $\lambda/16$.

(2) Feed Positioning Tolerance

$$\Delta F = \pm \lambda/16$$

$$\Delta F = \pm 0.60 \text{ inch at } f_0 = 1.25 \text{ gc.}$$

A theoretical analysis was performed considering the tolerance effects of a parallel flat strip configuration. The analysis has shown that variations of strip width (w) and spacing (s) are more critical under parallel E field conditions (reflecting grid) than under perpendicular E field conditions (non-reflecting grid). When optimum w and s parameters are chosen, positive width tolerances

($+\Delta w$) and negative spacing tolerances ($-\Delta s$) are not critical. Conversely, the negative width tolerance ($-\Delta w$) and positive spacing tolerance ($+\Delta s$) are critical.

When $-\Delta w = -0.005\lambda$, the transmission loss (α_T) will be increased by 0.25 db. When $+\Delta s = 0.01\lambda$, the transmission loss (α_T) will increase by 0.15 db.

The following tolerances on flat strip width and spacing parameters were determined as adequate:

$$\begin{aligned}\Delta w &= +0.01\lambda \\ &\quad -0.005\lambda \\ \Delta s &= +0.01\lambda \\ &\quad -0.02\lambda\end{aligned}$$

A theoretical tolerance analysis for the parallel wire grid case determined the following tolerance limitations:

$$\begin{aligned}\Delta d &= \pm 0.01\lambda \\ \Delta s &= +0.02\lambda \\ &\quad -0.04\lambda\end{aligned}$$

c. *Wave Guide Tests (Parallel Wires).* The reflectivity and transmissivity characteristics of parallel wire grids were experimentally determined for conditions of parallel E field and perpendicular E field orientations. Two X band waveguide test pieces were fabricated to verify the theoretically determined reflection characteristics of parallel wire grids. Using wire grid parameters ($d = 0.01$ inch, $s = 0.13$ inch) determined for the scale model Radoflector surface (refer to Section 4, paragraph B), parallel E field and perpendicular E field test samples were fabricated (see Figure 14). Using a slotted line VSWR measurement technique, the sample was inserted between the slotted line and a matched load. At the design frequency ($f_0 = 9.08$ gc), corresponding VSWR measurements were taken and transformed into equivalent reflection coefficients:

$$\Gamma = (\text{VSWR} - 1)/(\text{VSWR} + 1). \quad (11)$$

The following test results were obtained:

Case 1. Wires Parallel to E Field

VSWR = 35

$$\Gamma = 0.944$$

$$\text{Power reflected} = \Gamma^2 (100) = 89 \text{ percent} \quad (12)$$

$$\text{Power transmitted} = (1 - \Gamma^2) (100) = 11 \text{ percent} \quad (13)$$

$$\begin{aligned}\text{Transmission loss at reflecting surface } (\alpha_T) &= 10 \log (1 - \Gamma^2) \\ &= 0.5 \text{ db}\end{aligned} \quad (14)$$

Case 2. Wires Perpendicular to E Field

VSWR = 1.85

$$\Gamma = 0.298$$

$$\text{Power reflected} = \Gamma^2 (100) = 8.9 \text{ percent}$$

$$\text{Power transmitted} = (1 - \Gamma^2) (100) = 91.1 \text{ percent}$$

$$\text{Reflection loss at transparent surface } (\alpha_R) = 10 \log \Gamma^2 = 0.4 \text{ db} \quad (15)$$

The experimentally determined reflection loss value (α_R) was found to be slightly greater than the theoretical value. The discrepancy can be attributed to the fact that the guide wavelength (λ_g) at the design frequency is greater than the corresponding free space wavelength (λ). The ratio $\lambda_g/\lambda = 1.4$ at $f_0 = 9.08$ gc. The effective wire spacing in wavelength in the waveguide is less than the corresponding value (s/λ) in free space, resulting in a greater reflection coefficient in the former case. The result is an increased value of α_R .

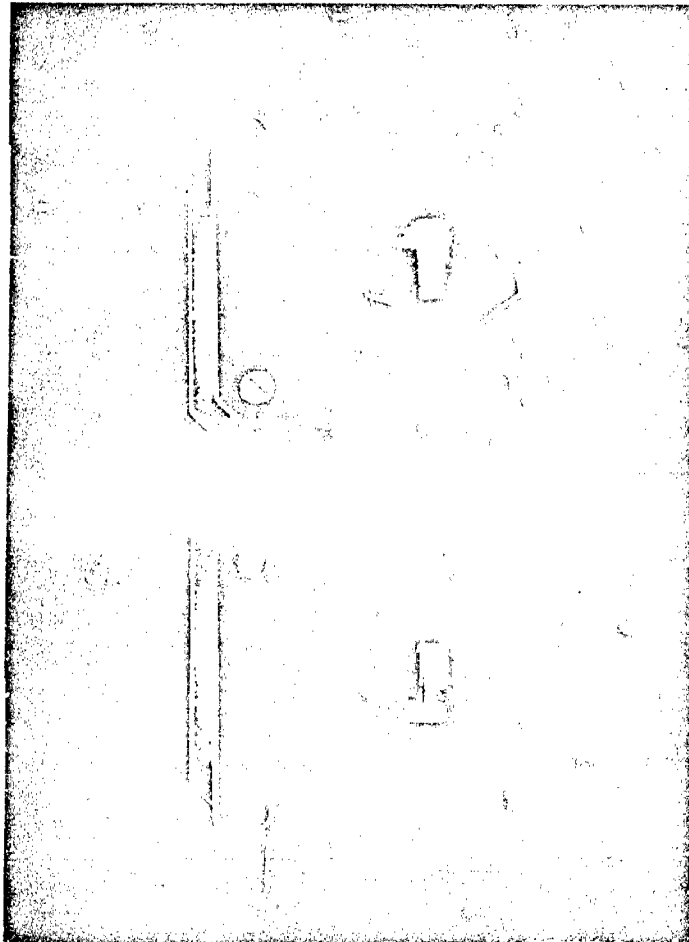


Figure 14. Wave Guide Grid Test Pieces

1. *Free Space Transmissivity Test (Parallel Wires).* To determine the effect of the grid support material efficiency and to further investigate the reflectivity characteristics of a parallel wire grid in free space, a transmissivity test was performed.

The parallel wire grid parameters for the scale model (Refer to Section 4, paragraph B) were used in fabricating a test panel of the following description:

- (1) Size - 31 x 38 inches.
- (2) Material - Dacron-Mylar laminate, the same material that was used on the scale model Radoflector structure (refer to Section 4, paragraph C-2).
- (3) Wire Size - 0.010 (+0.002) inch.
- (4) Wire Spacing (center-to-center) - 0.12 (+0.025, -0.050) inch.

The grid was mounted on a turntable, 18 inches in front of an X band horn. A similar test setup with a smaller panel is shown in Figure 15. A stationary pickup horn, placed approximately 8 feet away in the anechoic chamber, was used to measure the horizontal radiation pattern under the following conditions:

- (1) Grid wire parallel to E field.
- (2) Grid wire perpendicular to E field.

The grid panel was removed, and the radiation pattern of the horn alone was determined (see Figures 16 and 17).

The average power level between the limits ϕ_1 and ϕ_2 can be determined for each case by graphically integrating the corresponding power pattern between the respective limits. Since the power level of the transmitter was equal for each power pattern, the following relation determines the amount of power transmitted through the parallel wire grid test panel:

$$a_{TG} = 10 \log \frac{P_T}{P_0} = \frac{\int_{\phi_1}^{\phi_2} P_H (db) d\phi}{\phi_2 - \phi_1} - \frac{\int_{\phi_1}^{\phi_2} P_G (db) d\phi}{\phi_2 - \phi_1} \quad (16)$$

where

a_{TG} = transmission loss of grid

$\frac{P_T}{P_0} (100)$ = percentage of transmitted power

$P_H(db)$ = radiation pattern of transmitting horn as a function of ϕ (azimuth angle determined by transmitter horn axis and receiver horn axis)

$P_G(db)$ = radiation pattern of horn transmitting through the wire grid in proper orientation and

ϕ_1 and ϕ_2 = limits of integration.

The percentage of reflection power can be expressed as

$$\frac{P_R}{P_0} (\%) = \left(1 - \frac{P_T}{P_0} \right) (100). \quad (17)$$

The corresponding reflection loss of the grid can be expressed as

$$a_{RG} = 10 \log \left(1 - \frac{P_T}{P_0} \right). \quad (18)$$

This method of determining grid transmissivity was necessary since the defraction effect of the test panel could have been significant when the wires were parallel to the E field.

The free space tests showed the parallel wire grid to exhibit the following characteristics:

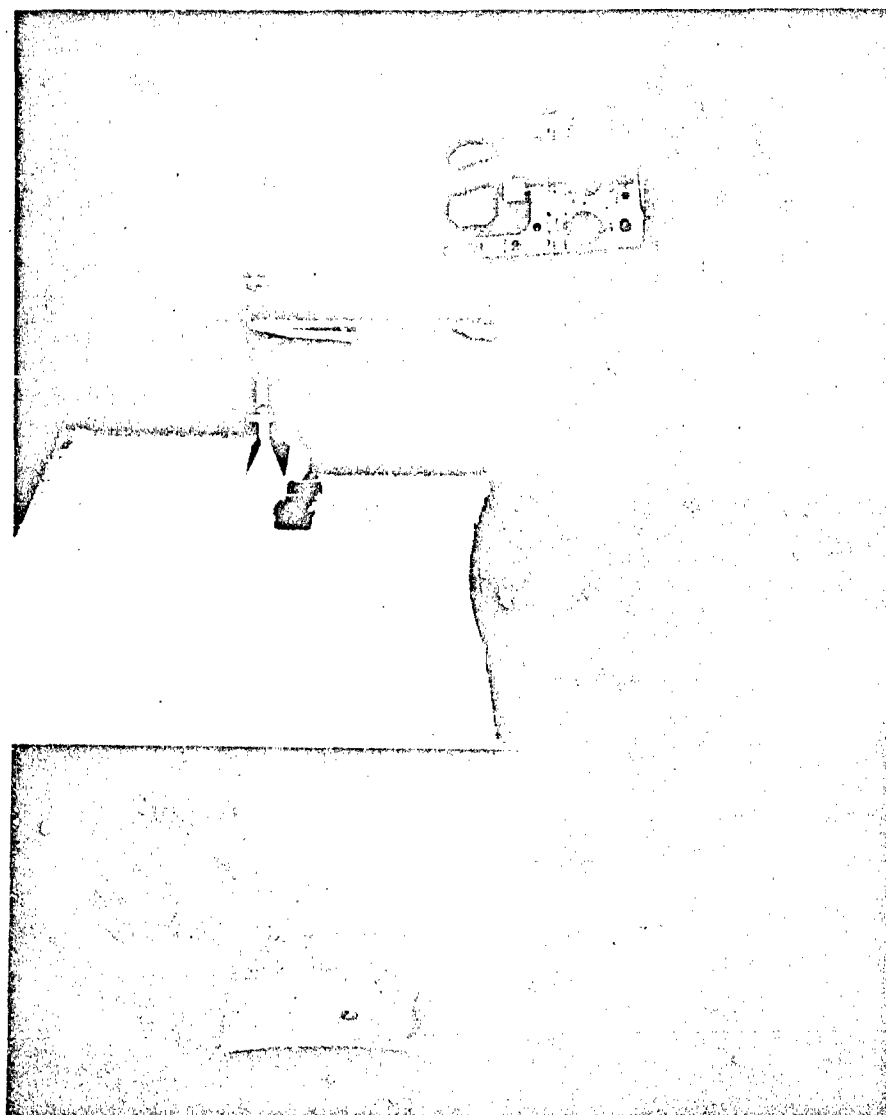


Figure 15. Grid Panel Transmissivity Test Setup

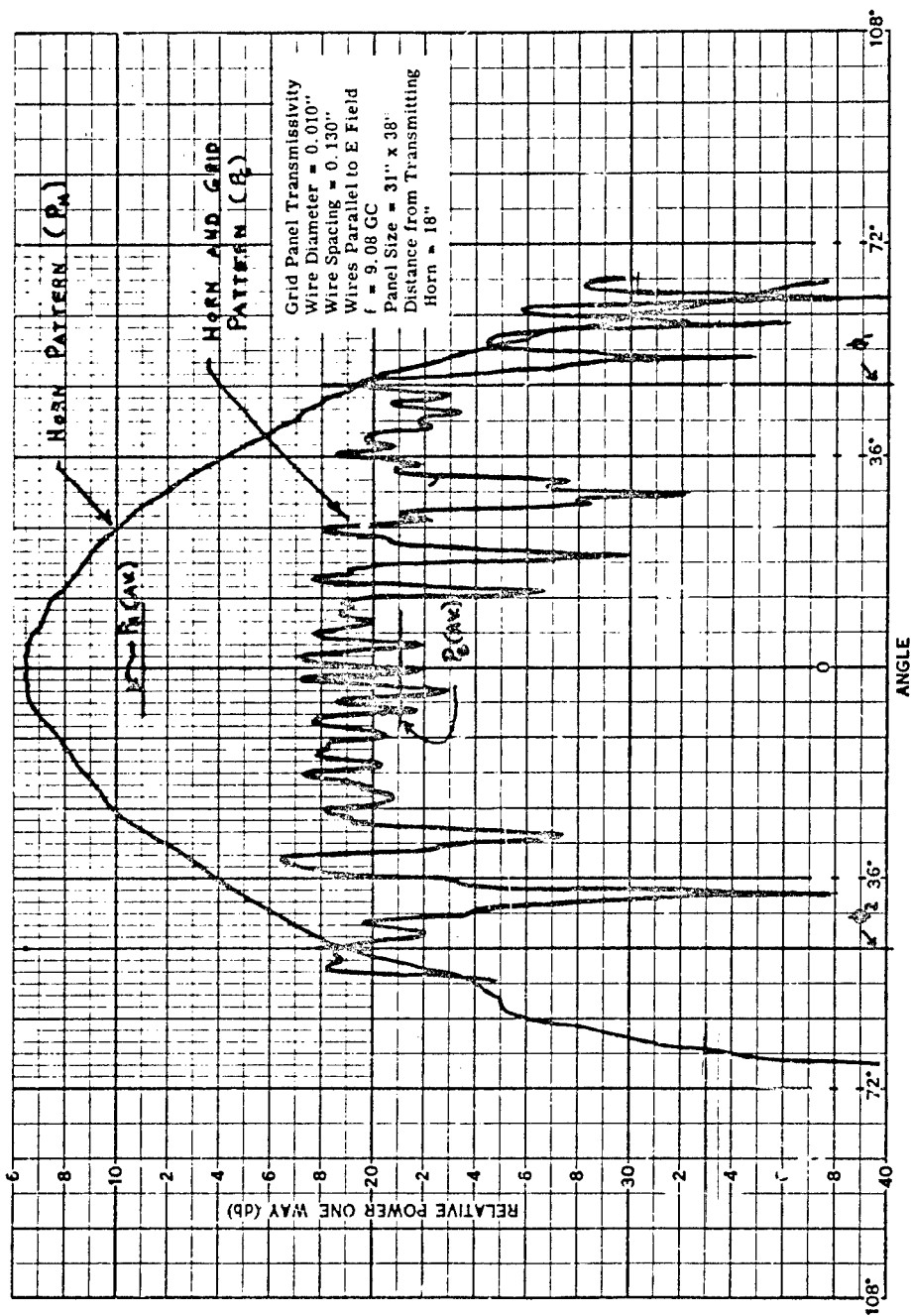


Figure 16. Transmissivity Characteristics of Parallel Wire Grid Panel
 (Wire Diameter = 0.010 Inch, Wire Spacing = 0.13 Inch,
 $f = 9.08$ GC, Wires Parallel to E Field)

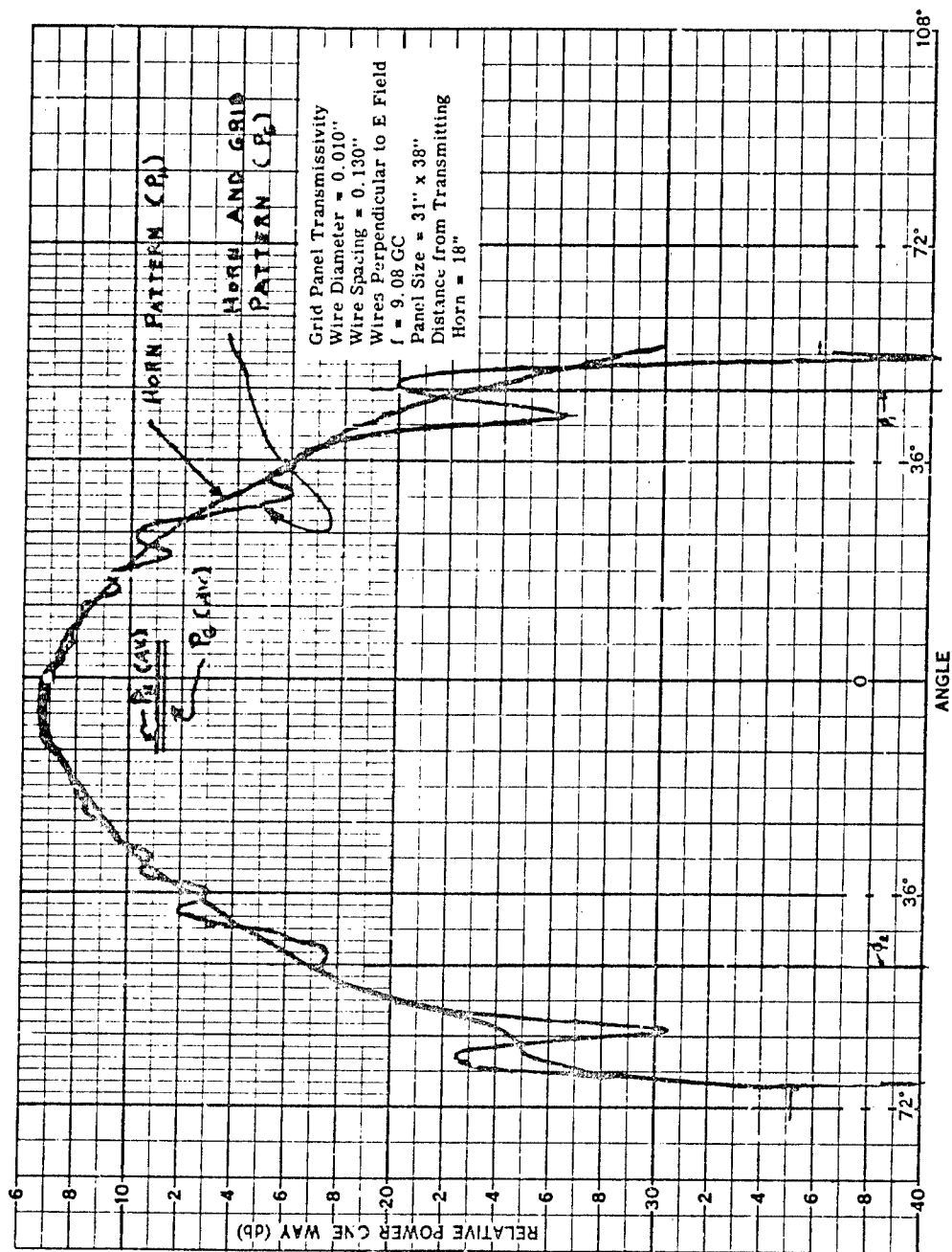


Figure 17. Transmissivity Characteristics of Parallel Wire Grid Panel
 (Wire Diameter = 0.010 Inch, Wire Spacing = 0.13 Inch,
 $f = 9.08 \text{ GC}$, Wires Perpendicular to E Field)

Case 1. Grid Wires Parallel to E Field

Reflected power = 90.0 percent

Transmitted power = 10.0 percent

Transmission loss at reflecting surface (a_T) = 0.45 db

Case 2. Grid Wires Perpendicular to E Field

Transmitted power = 96 percent

Reflected power = 4 percent

Reflection loss at transparent surface (a_R) = 0.2 db

The experimental results are in good agreement with the corresponding theoretically determined values for the scale model (refer to Section 4, paragraph B). The results showed that the effect of the Dacron-Mylar support material was negligible.

g. *Finalized (Full-Scale) Parameters.* The finalized parameters and tolerances for the full-scale Radoflector are as follows:

- (1) Center frequency = 1.25 gc
- (2) Frequency band = 1.20 to 1.30 gc
- (3) Horizontal radius of revolution = 34.35 feet (diameter = 68.70 feet)
- (4) Focal distance = 16.65 feet
- (5) Focal radius = 17.52 feet
- (6) Equivalent parabolic reflector diameter = 25.4 feet
- (7) F/D of parabolic reflector = 0.656
- (8) Bottom edge of parabola from ground level (min) = 3.0 feet
- (9) Center of feed from ground (min) = 20.0 feet
- (10) Tolerance control of surface accuracy = ± 0.60 inch
- (11) Feed positioning tolerances = ± 0.60 inch
- (12) Parallel flat strip grid center-to-center spacing = 1.42 (+0.10, -0.20) inches
- (13) Parallel flat conducting strip width = 0.47 (+0.10, -0.05) inch
- (14) Horn aperture (A) = 16.80 inches
Horn aperture (B) = 12.75 inches
- (15) Illuminated reflector aperture (horizontal) = 25.4 inches
Illuminated reflector aperture (vertical) = 25.4 inches

C. Inflatable Structure Design

1. General

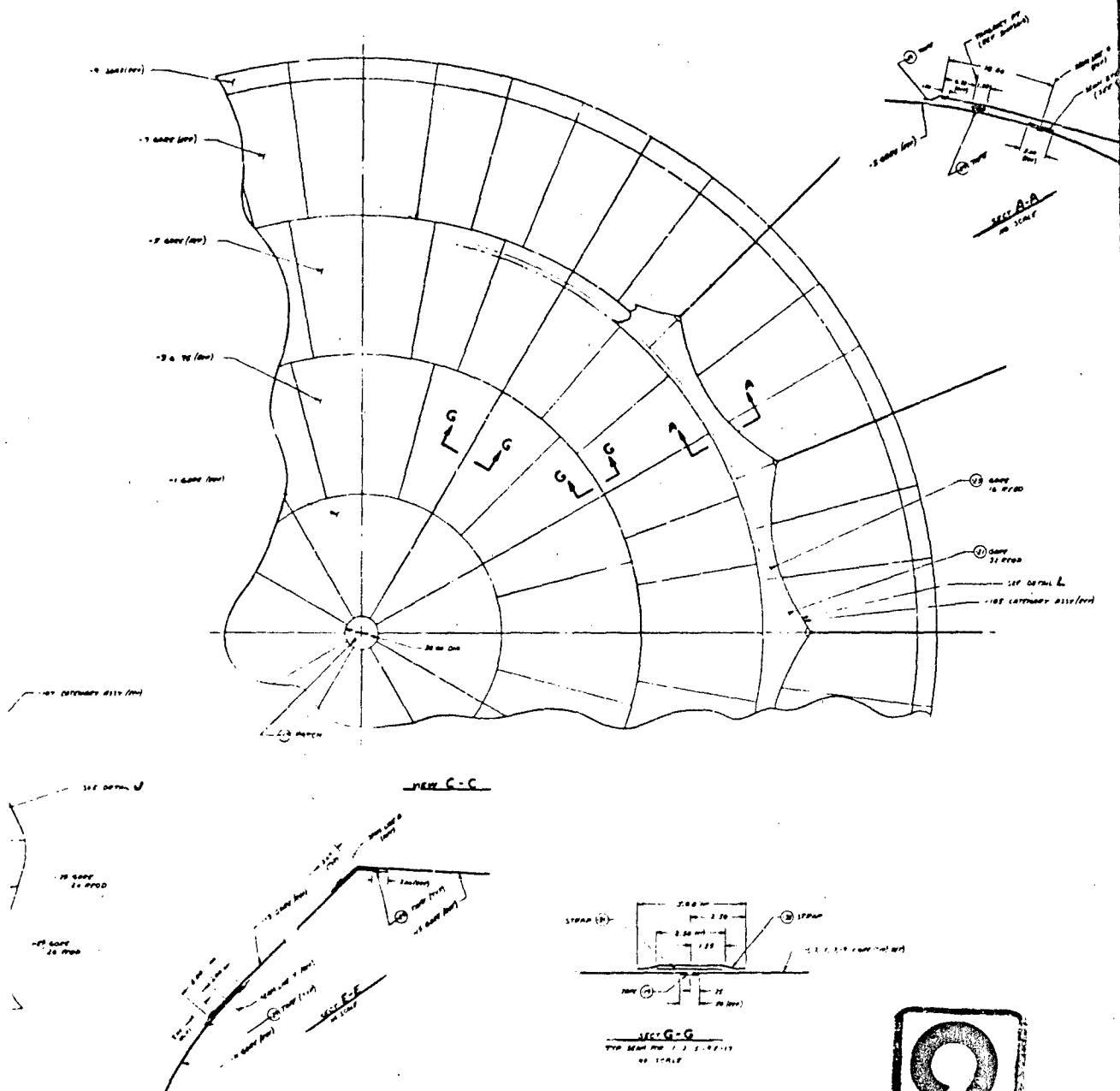
The principle of the post-attack antenna system is based on using the surface of a radome as an antenna reflector that can be packaged and stowed in a hardened installation. Therefore, to meet these requirements the Radoflector utilizes an inflatable structure as the radome-reflector. When inflated, the structure must expand to a shape which contains both the azimuth and elevation reflector contour over part of its surface. Figure 18 is an engineering drawing that shows in detail the inflatable structure design. Figure 19 shows the inflatable structure geometry and contour.

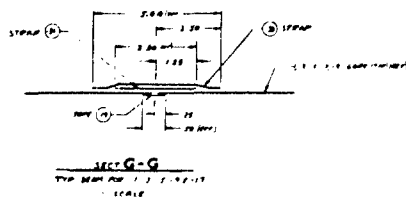
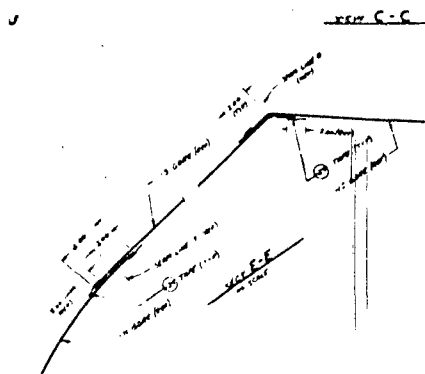
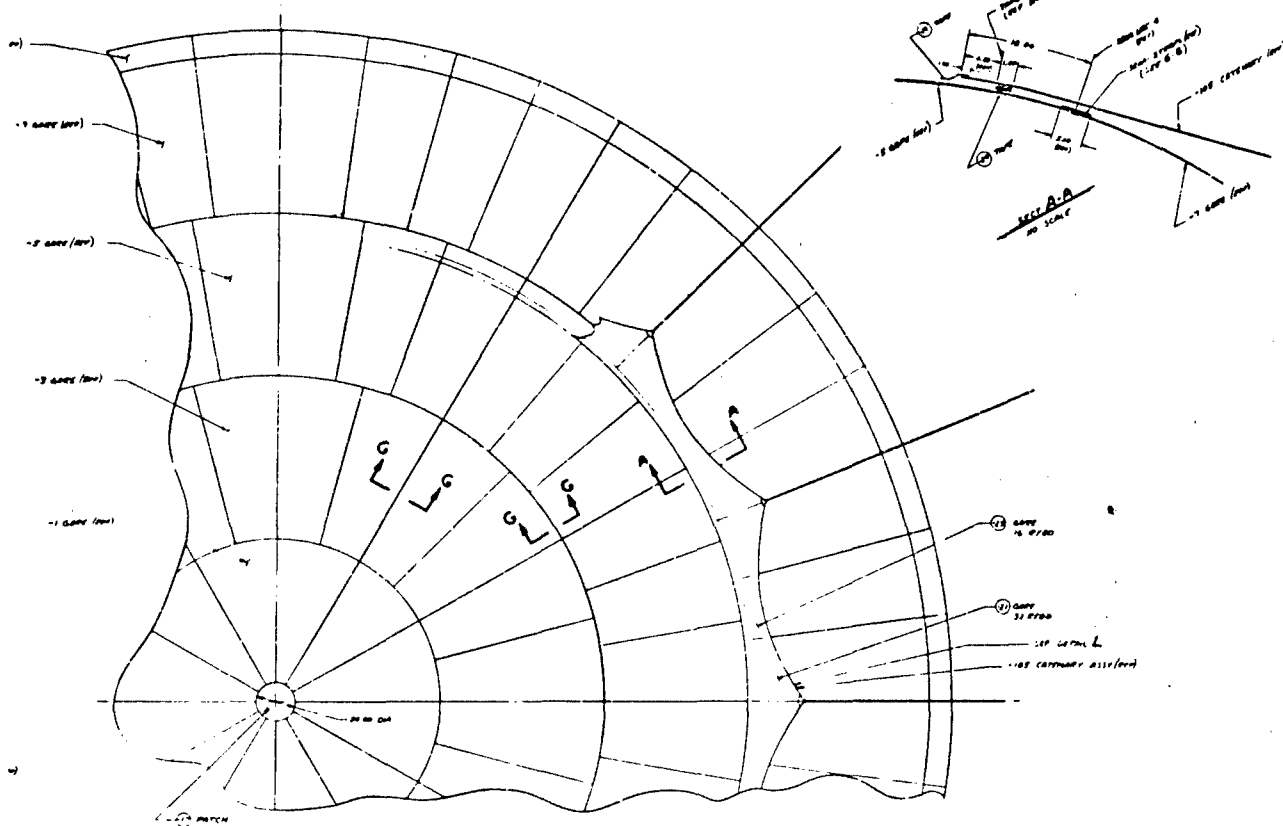
2. Inflatable Structure Configuration

The antenna reflector is formed by the walls of the inflatable structure which in turn are made up of two functions generated about the vertical centerline. The upper part of the reflector is a parabola, and the lower part is a fourth degree equation that is a tangent to the parabola.

The material used for the inflatable structure must finally be selected as a result of a materials test program and a detailed stress analysis, taking into account extreme operating and environmental conditions. The design shown in Figure 18 utilizes a Dacron-Mylar laminate selected on the basis of a preliminary material investigation.

A Dacron-Mylar laminate has the advantage of providing shear resistance in the plane of the fabric with a single ply of fabric. If a Dacron cloth with a neoprene or other elastomer were to be used, two plies of fabric would be needed to provide shear resistance. The Dacron-Neoprene

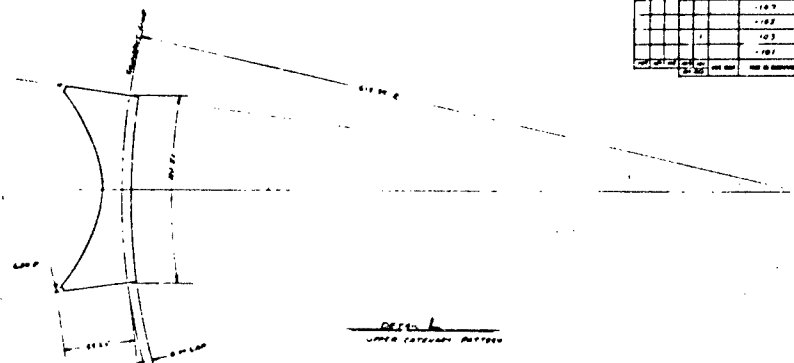


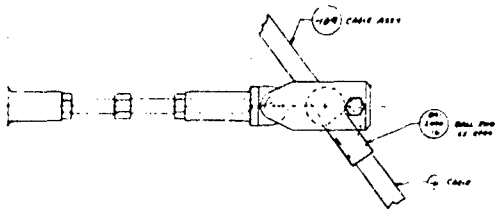


3

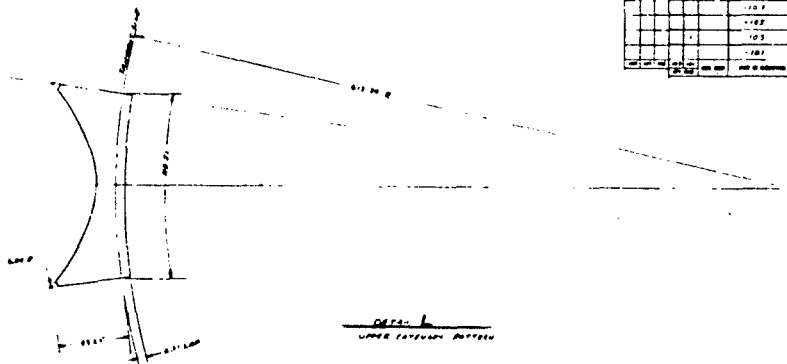


REF	DATE	TIME	TO	FROM	REMARKS
1	12/12/40	10:00	TO	FROM	REMARKS
2	12/12/40	10:00	TO	FROM	REMARKS
3	12/12/40	10:00	TO	FROM	REMARKS
4	12/12/40	10:00	TO	FROM	REMARKS
5	12/12/40	10:00	TO	FROM	REMARKS
6	12/12/40	10:00	TO	FROM	REMARKS
7	12/12/40	10:00	TO	FROM	REMARKS
8	12/12/40	10:00	TO	FROM	REMARKS
9	12/12/40	10:00	TO	FROM	REMARKS
10	12/12/40	10:00	TO	FROM	REMARKS
11	12/12/40	10:00	TO	FROM	REMARKS
12	12/12/40	10:00	TO	FROM	REMARKS
13	12/12/40	10:00	TO	FROM	REMARKS
14	12/12/40	10:00	TO	FROM	REMARKS
15	12/12/40	10:00	TO	FROM	REMARKS
16	12/12/40	10:00	TO	FROM	REMARKS
17	12/12/40	10:00	TO	FROM	REMARKS
18	12/12/40	10:00	TO	FROM	REMARKS
19	12/12/40	10:00	TO	FROM	REMARKS
20	12/12/40	10:00	TO	FROM	REMARKS
21	12/12/40	10:00	TO	FROM	REMARKS
22	12/12/40	10:00	TO	FROM	REMARKS
23	12/12/40	10:00	TO	FROM	REMARKS
24	12/12/40	10:00	TO	FROM	REMARKS
25	12/12/40	10:00	TO	FROM	REMARKS
26	12/12/40	10:00	TO	FROM	REMARKS
27	12/12/40	10:00	TO	FROM	REMARKS
28	12/12/40	10:00	TO	FROM	REMARKS
29	12/12/40	10:00	TO	FROM	REMARKS
30	12/12/40	10:00	TO	FROM	REMARKS
31	12/12/40	10:00	TO	FROM	REMARKS
32	12/12/40	10:00	TO	FROM	REMARKS
33	12/12/40	10:00	TO	FROM	REMARKS
34	12/12/40	10:00	TO	FROM	REMARKS
35	12/12/40	10:00	TO	FROM	REMARKS
36	12/12/40	10:00	TO	FROM	REMARKS
37	12/12/40	10:00	TO	FROM	REMARKS
38	12/12/40	10:00	TO	FROM	REMARKS
39	12/12/40	10:00	TO	FROM	REMARKS
40	12/12/40	10:00	TO	FROM	REMARKS
41	12/12/40	10:00	TO	FROM	REMARKS
42	12/12/40	10:00	TO	FROM	REMARKS
43	12/12/40	10:00	TO	FROM	REMARKS
44	12/12/40	10:00	TO	FROM	REMARKS
45	12/12/40	10:00	TO	FROM	REMARKS
46	12/12/40	10:00	TO	FROM	REMARKS
47	12/12/40	10:00	TO	FROM	REMARKS
48	12/12/40	10:00	TO	FROM	REMARKS
49	12/12/40	10:00	TO	FROM	REMARKS
50	12/12/40	10:00	TO	FROM	REMARKS
51	12/12/40	10:00	TO	FROM	REMARKS
52	12/12/40	10:00	TO	FROM	REMARKS
53	12/12/40	10:00	TO	FROM	REMARKS
54	12/12/40	10:00	TO	FROM	REMARKS
55	12/12/40	10:00	TO	FROM	REMARKS
56	12/12/40	10:00	TO	FROM	REMARKS
57	12/12/40	10:00	TO	FROM	REMARKS
58	12/12/40	10:00	TO	FROM	REMARKS
59	12/12/40	10:00	TO	FROM	REMARKS
60	12/12/40	10:00	TO	FROM	REMARKS
61	12/12/40	10:00	TO	FROM	REMARKS
62	12/12/40	10:00	TO	FROM	REMARKS
63	12/12/40	10:00	TO	FROM	REMARKS
64	12/12/40	10:00	TO	FROM	REMARKS
65	12/12/40	10:00	TO	FROM	REMARKS
66	12/12/40	10:00	TO	FROM	REMARKS
67	12/12/40	10:00	TO	FROM	REMARKS
68	12/12/40	10:00	TO	FROM	REMARKS
69	12/12/40	10:00	TO	FROM	REMARKS
70	12/12/40	10:00	TO	FROM	REMARKS
71	12/12/40	10:00	TO	FROM	REMARKS
72	12/12/40	10:00	TO	FROM	REMARKS
73	12/12/40	10:00	TO	FROM	REMARKS
74	12/12/40	10:00	TO	FROM	REMARKS
75	12/12/40	10:00	TO	FROM	REMARKS
76	12/12/40	10:00	TO	FROM	REMARKS
77	12/12/40	10:00	TO	FROM	REMARKS
78	12/12/40	10:00	TO	FROM	REMARKS
79	12/12/40	10:00	TO	FROM	REMARKS
80	12/12/40	10:00	TO	FROM	REMARKS
81	12/12/40	10:00	TO	FROM	REMARKS
82	12/12/40	10:00	TO	FROM	REMARKS
83	12/12/40	10:00	TO	FROM	REMARKS
84	12/12/40	10:00	TO	FROM	REMARKS
85	12/12/40	10:00	TO	FROM	REMARKS
86	12/12/40	10:00	TO	FROM	REMARKS
87	12/12/40	10:00	TO	FROM	REMARKS
88	12/12/40	10:00	TO	FROM	REMARKS
89	12/12/40	10:00	TO	FROM	REMARKS
90	12/12/40	10:00	TO	FROM	REMARKS
91	12/12/40	10:00	TO	FROM	REMARKS
92	12/12/40	10:00	TO	FROM	REMARKS
93	12/12/40	10:00	TO	FROM	REMARKS
94	12/12/40	10:00	TO	FROM	REMARKS
95	12/12/40	10:00	TO	FROM	REMARKS
96	12/12/40	10:00	TO	FROM	REMARKS
97	12/12/40	10:00	TO	FROM	REMARKS
98	12/12/40	10:00	TO	FROM	REMARKS
99	12/12/40	10:00	TO	FROM	REMARKS
100	12/12/40	10:00	TO	FROM	REMARKS

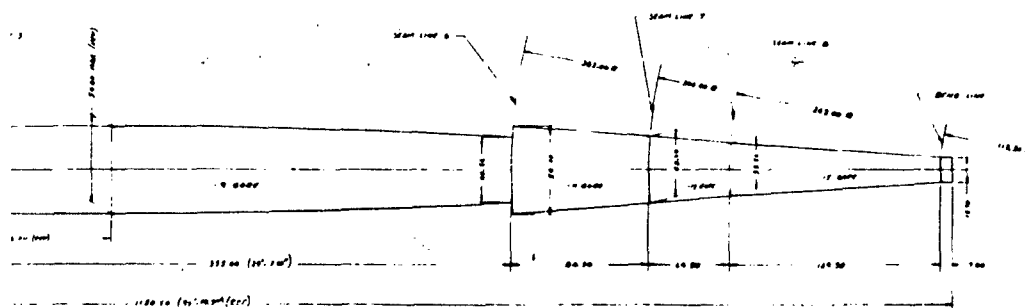




DETAIL K
FULL SCALE



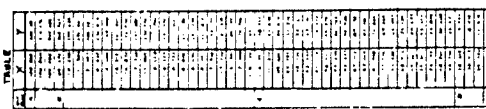
DETAIL L
UPPER CABLE ASSEMBLY



Antenna Assembly (Show: 3 of 3)

NO.	DESCRIPTION	QTY.	UNIT	REMARKS
1	1/2" DIA. ALUM. ROD	1	PC	
2	1/4" DIA. ALUM. ROD	1	PC	
3	1/8" DIA. ALUM. ROD	1	PC	
4	1/4" DIA. ALUM. ROD	1	PC	
5	1/8" DIA. ALUM. ROD	1	PC	
6	1/4" DIA. ALUM. ROD	1	PC	
7	1/8" DIA. ALUM. ROD	1	PC	
8	1/4" DIA. ALUM. ROD	1	PC	
9	1/8" DIA. ALUM. ROD	1	PC	
10	1/4" DIA. ALUM. ROD	1	PC	
11	1/8" DIA. ALUM. ROD	1	PC	
12	1/4" DIA. ALUM. ROD	1	PC	
13	1/8" DIA. ALUM. ROD	1	PC	
14	1/4" DIA. ALUM. ROD	1	PC	
15	1/8" DIA. ALUM. ROD	1	PC	
16	1/4" DIA. ALUM. ROD	1	PC	
17	1/8" DIA. ALUM. ROD	1	PC	
18	1/4" DIA. ALUM. ROD	1	PC	
19	1/8" DIA. ALUM. ROD	1	PC	
20	1/4" DIA. ALUM. ROD	1	PC	
21	1/8" DIA. ALUM. ROD	1	PC	
22	1/4" DIA. ALUM. ROD	1	PC	
23	1/8" DIA. ALUM. ROD	1	PC	
24	1/4" DIA. ALUM. ROD	1	PC	
25	1/8" DIA. ALUM. ROD	1	PC	
26	1/4" DIA. ALUM. ROD	1	PC	
27	1/8" DIA. ALUM. ROD	1	PC	
28	1/4" DIA. ALUM. ROD	1	PC	
29	1/8" DIA. ALUM. ROD	1	PC	
30	1/4" DIA. ALUM. ROD	1	PC	
31	1/8" DIA. ALUM. ROD	1	PC	
32	1/4" DIA. ALUM. ROD	1	PC	
33	1/8" DIA. ALUM. ROD	1	PC	
34	1/4" DIA. ALUM. ROD	1	PC	
35	1/8" DIA. ALUM. ROD	1	PC	
36	1/4" DIA. ALUM. ROD	1	PC	
37	1/8" DIA. ALUM. ROD	1	PC	
38	1/4" DIA. ALUM. ROD	1	PC	
39	1/8" DIA. ALUM. ROD	1	PC	
40	1/4" DIA. ALUM. ROD	1	PC	
41	1/8" DIA. ALUM. ROD	1	PC	
42	1/4" DIA. ALUM. ROD	1	PC	
43	1/8" DIA. ALUM. ROD	1	PC	
44	1/4" DIA. ALUM. ROD	1	PC	
45	1/8" DIA. ALUM. ROD	1	PC	
46	1/4" DIA. ALUM. ROD	1	PC	
47	1/8" DIA. ALUM. ROD	1	PC	
48	1/4" DIA. ALUM. ROD	1	PC	
49	1/8" DIA. ALUM. ROD	1	PC	
50	1/4" DIA. ALUM. ROD	1	PC	
51	1/8" DIA. ALUM. ROD	1	PC	
52	1/4" DIA. ALUM. ROD	1	PC	
53	1/8" DIA. ALUM. ROD	1	PC	
54	1/4" DIA. ALUM. ROD	1	PC	
55	1/8" DIA. ALUM. ROD	1	PC	
56	1/4" DIA. ALUM. ROD	1	PC	
57	1/8" DIA. ALUM. ROD	1	PC	
58	1/4" DIA. ALUM. ROD	1	PC	
59	1/8" DIA. ALUM. ROD	1	PC	
60	1/4" DIA. ALUM. ROD	1	PC	
61	1/8" DIA. ALUM. ROD	1	PC	
62	1/4" DIA. ALUM. ROD	1	PC	
63	1/8" DIA. ALUM. ROD	1	PC	
64	1/4" DIA. ALUM. ROD	1	PC	
65	1/8" DIA. ALUM. ROD	1	PC	
66	1/4" DIA. ALUM. ROD	1	PC	
67	1/8" DIA. ALUM. ROD	1	PC	
68	1/4" DIA. ALUM. ROD	1	PC	
69	1/8" DIA. ALUM. ROD	1	PC	
70	1/4" DIA. ALUM. ROD	1	PC	
71	1/8" DIA. ALUM. ROD	1	PC	
72	1/4" DIA. ALUM. ROD	1	PC	
73	1/8" DIA. ALUM. ROD	1	PC	
74	1/4" DIA. ALUM. ROD	1	PC	
75	1/8" DIA. ALUM. ROD	1	PC	
76	1/4" DIA. ALUM. ROD	1	PC	
77	1/8" DIA. ALUM. ROD	1	PC	
78	1/4" DIA. ALUM. ROD	1	PC	
79	1/8" DIA. ALUM. ROD	1	PC	
80	1/4" DIA. ALUM. ROD	1	PC	
81	1/8" DIA. ALUM. ROD	1	PC	
82	1/4" DIA. ALUM. ROD	1	PC	
83	1/8" DIA. ALUM. ROD	1	PC	
84	1/4" DIA. ALUM. ROD	1	PC	
85	1/8" DIA. ALUM. ROD	1	PC	
86	1/4" DIA. ALUM. ROD	1	PC	
87	1/8" DIA. ALUM. ROD	1	PC	
88	1/4" DIA. ALUM. ROD	1	PC	
89	1/8" DIA. ALUM. ROD	1	PC	
90	1/4" DIA. ALUM. ROD	1	PC	
91	1/8" DIA. ALUM. ROD	1	PC	
92	1/4" DIA. ALUM. ROD	1	PC	
93	1/8" DIA. ALUM. ROD	1	PC	
94	1/4" DIA. ALUM. ROD	1	PC	
95	1/8" DIA. ALUM. ROD	1	PC	
96	1/4" DIA. ALUM. ROD	1	PC	
97	1/8" DIA. ALUM. ROD	1	PC	
98	1/4" DIA. ALUM. ROD	1	PC	
99	1/8" DIA. ALUM. ROD	1	PC	
100	1/4" DIA. ALUM. ROD	1	PC	

3



39

fabric is easier to seam; however, it presently appears that recent improvements in Dacron-Mylar laminate seaming techniques offer this material as a good potential candidate which may show better dimensional stability characteristics.

A material that looks very promising for use as the antenna reflector is an rf reflective paint that reflects better than 95 percent of the incident rf energy while still maintaining very good flexibility and folding characteristics. The reflective paint would be put either on the inflatable surface directly or onto a separate entity. Aluminum foil-Mylar laminate as well as braided wire metal impregnated cloth and metalized film-cloths will also be investigated further as candidate materials for the optimum reflective surface.

Since the reflected beam of rf energy only passes through the upper portion of the opposite side of the antenna and since a solid reflector is more easily fabricated than the strip reflector, the lower part of the reflector is designed to utilize solid reflective material.

The inflatable structure is supported at the base by a catenary curtain that is attached to the open doors of the hardened site concrete enclosure. The diameter of the base support catenary system has been determined by the rf requirement of maintaining the antenna reflector at least five feet above the support base. This support catenary must hold the inflatable structure accurately; for this reason some adjustment of the support catenary will be provided. The catenary adjustment will be made only during the initial installation of the antenna on site and will not require adjustment as part of the erection operation.

A system of guy wires attached to the upper portion of the inflatable structure and extending downward at a 45-degree angle to the ground is utilized for support. This guy system is utilized to maintain dimensional tolerance of the inflatable structure during normal operating conditions and to provide additional support under the maximum survival environmental condition of a 125-mph wind loading or a combination condition of 75-mph plus two inches of ice. A catenary curtain is utilized to distribute the guy cable loads evenly into the inflatable structure.

In the stowed position, the guy cables are located in trenches that are lined with ablative material and sealed against water accumulation. The guy cables are deployed automatically by the inflatable structure, which pulls the cables into position as it is inflated. The guy cables and their protection during the stowed condition are discussed in paragraph D-2 of this section.

The inflatable structure pressurization system consists of a high capacity blower system used to initially fill the antenna to a pressure of about four inches of water and a high-pressure bottle system for rapidly "topping off" to a pressure of approximately 12 inches of water. This pressure system will also be discussed in paragraph D-2 of this section.

3. Inflatable Structure Fabrication

The inflatable structure is formed by a number of preformed gores that are seamed together to fabricate the oblate spheroid. In the design shown in Figure 18, 48 gores make up the structure.

In order to simplify the tooling that is used for preforming the gores, each gore will be preformed in two segments. One segment will cover the antenna reflector area, and the second will be the upper one closing off the top of the inflatable structure. This selection of gore segments will allow the circumferential seam to be in the area above the antenna reflector and will therefore preclude any rf pattern degradations that could occur due to the seam.

To preform the Dacron-Mylar laminate, the fabric will be placed on and clamped to a preforming tool. Then by evacuating the air pressure between the tool and the fabric, the fabric is formed to the contour of the tool. The tool and the fabric are then heated in an oven and cured. During this heat cycle, the Mylar and Dacron laminate is permanently formed to the contour of the mold.

The gores are seamed together with a heat sealing tape. The two adjacent edges of the gores are pretensioned on the mold prior to heat sealing. The fabric is held in this position, and with the use of preformed butt splice tapes the seam is tack-welded to help hold its position, bonded tightly with a warm iron, and finally bonded with a hot iron. This procedure has been utilized to develop a good seam without wrinkling or local deformation.

4. Structural Considerations

a. Radioreflexor Structural Analysis. For the purpose of a preliminary analysis, the inflatable structure is considered to be a truncated spherical shell as shown in Figure 20.

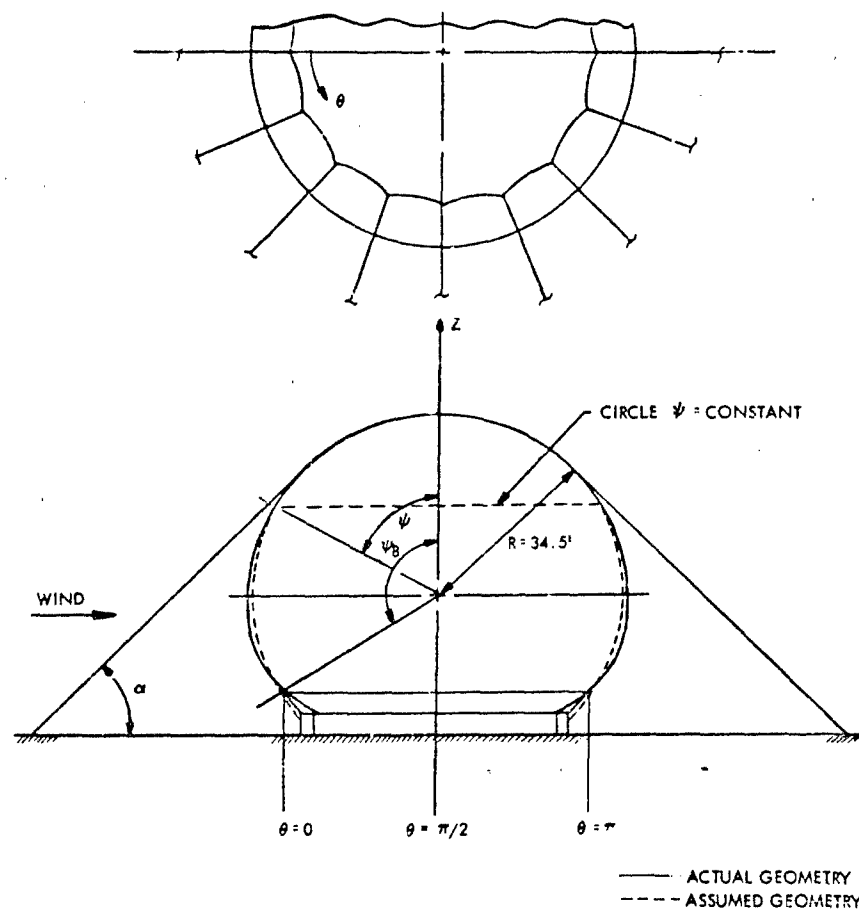


Figure 20. Radreflector Structural Geometry

(1) *Loading.* The loadings that the Radoflector will be subjected to are

1. Survival
 - (a) Maximum wind velocity of 125 mph
 - (b) Wind velocity of 75 mph plus 2 inches of ice
2. Operating
 - (a) Wind velocity of 50 mph, full performance
 - (b) Wind velocity of 75 mph, reduced performance

The Radoflector structural geometry is shown in Figure 20. The lift, drag, and overturning moment may be written in the following form:

$$\begin{aligned} L &= c_L \pi q R^2 \\ D &= c_D \pi q R^2 \\ M &= 2c_M \pi q R^3 \end{aligned}$$

where

c_L , c_D , and c_M are lift, drag, and moment coefficients
 q = stagnation pressure

and

R = radius of the sphere.

For the given geometry of the Radoflector and at supercritical Reynold's numbers, the coefficients are approximately

$$\left. \begin{aligned} c_L &= 0.53 \\ c_D &= 0.48 \\ c_M &= 0.18 \end{aligned} \right\} \text{(Reference 7)}$$

The impact pressures for velocities to be considered are as follows at sea level and standard atmosphere conditions:

at 50 mph, $q = 6.4$ psf
 at 75 mph, $q = 14.4$ psf
 at 125 mph, $q = 40.0$ psf

(2) *Wind Load Distribution.* The pressure distribution over the Radoflector surface usually can be approximated with sufficient accuracy by the following function of the "longitude" θ and the complementary angle ψ of the latitude (see Figure 20).

$$P/q = A + B \sin \psi \cos \theta - C(1 - 2 \sin^2 \psi \cos^2 \theta). \quad (19)$$

Integration of the pressure in X and Z direction yields the pressure drag and the lift in the form of

$$L = -A\pi q R^2 \sin^2 \psi_B + C\pi q R^2 \sin^2 \psi_B (1 - 0.5 \sin^2 \psi_B) \quad (20)$$

$$D_p = B \frac{\pi}{3} q R^2 [\cos \psi_B (\cos^2 \psi_B - 3) + 2]. \quad (21)$$

A third equation for determination of the unknown coefficients A, B, and C is

$$A + B + C = 1.0. \quad (22)$$

Equation 22 follows from the fact that $p = q$ at the stagnation point ($\theta = 0$, $\psi = \pi/2$). Solving Equations simultaneously for a truncation angle $\psi_B = 125$ degrees yields

$$\begin{aligned} A &= -0.222 \\ B &= 0.367 \\ C &= 0.855. \end{aligned}$$

(3) *Stress Distribution due to Wind Loads.* The membrane stresses N_ψ (in meridional direction), N_θ (in direction of the horizontal parallel circles), and $N_{\theta\psi}$ (associated shear stresses) are determined by solving the three differential equations that express equilibrium of any shell element in the radial, meridional, and circumferential direction for each of the three components of the wind load function, Equation 19 (References 8 and 9). However, the comparatively rigid restraint of the shell at the lower edge produces additional redundant reactions whose effect upon the stress distribution also is taken into account.

Table 6 gives a résumé of the stresses at any point of the Radoflector in general form. Table 6 also includes the stress relations for inflation pressure, weight proper, and ice load.

The principal stresses at any point of the shell now can be determined for any combination of wind load, weight proper, and ice load, using Mohr's equations. The inflation pressure is selected so that the inflation stresses $P(R/2)$ are greater than the absolute value of the minimum principal stress (compression stress) at any point of the shell to prevent wrinkling.

There are three areas in which maxima and minima of the membrane stresses may occur: (1) at and near the apex, (2) at and below forward and rear stagnation point, and (3) along the base ring. These areas are investigated to obtain maximum and minimum membrane stresses.

(4) *Effect of Guy Wires.* In Reference 8, a deflection analysis is presented which yields three components of the deflection at any point of the free Radoflector for all pertinent load conditions (wind load, weight proper, ice load, and inflation pressure) to be analyzed. The effect of the redundant reactions of the guy wires is taken into account by utilizing this theory. The cables are attached tangentially to the Radoflector by means of catenary curtains in order that concentrated loads on the fabric are avoided. For determining the redundant cable loads due to wind loading, it is convenient to treat the three wind components A, B, and C separately.

The A component poses no problem since n cables take equal loads. Thus, in effect, only one redundant magnitude is involved. The B component, integrated over the entire Radoflector surface, gives the pressure drag D_p (see Equation 21). Assuming the cables take a portion, D_c , of the total drag out of the Radoflector, while the balance still must be transmitted through the Radoflector itself to the base support, it can be shown that the load in the cable facing the wind direction due to drag D_c alone is

$$T_0 = (2D_c)/(\pi \cos \alpha) \text{ (see Figure 21)} \quad (40)$$

and the load in any of the other cables is

$$T_\theta = T_0 \cos \theta \quad (41)$$

provided that all cables are sufficiently pretensioned and none slackens. The function of the catenary curtain is to transform the concentrated cable loads into a continuous loading that acts tangentially to the Radoflector around the parallel circle of radius $r = R \cos \alpha$ and very closely follows the law

$$N_{\psi_c} = \left[-\frac{2D_c}{R \sin(2\alpha)} \right] (\cos \theta) \quad (42)$$

where N_{ψ_c} = the loading in the fabric due to cable tension.

The stresses at any point (ψ, θ) of the Radoflector due to the loading N_{ψ_c} are in the meridional direction

$$N_\psi = \left(-\frac{D_c}{\pi R} \right) \left(\frac{1 + \cos \alpha \cos \psi}{\cos \alpha \sin^3 \psi} \right) (\cos \theta). \quad (43)$$

In the direction of the parallel circle $\psi = \text{constant}$

$$N_\theta = -N_\psi. \quad (44)$$

TABLE 6.
Membrane Stresses

LOADING	STRESSES (lb/ft)	EQUATION
(1) Wind Load		
A Component	$N_{\psi} = N_{\theta} = -0.5 A q R$	(23)
	$N_{\theta\psi} = 0$	(24)
B Component*	$N_{\psi} = -\frac{B q R}{3} \frac{\cos \theta \cos \psi}{\sin^3 \psi} (2 - 3 \cos \psi + \cos^3 \psi)$	(25)
	$N_{\theta} = \frac{B q R}{3} \frac{\cos \theta}{\sin^3 \psi} (2 \cos \psi - 3 \sin^2 \psi - 2 \cos^4 \psi)$	(26)
	$N_{\theta\psi} = -\frac{B q R}{3} \frac{\sin \theta}{\sin^3 \psi} (2 - 3 \cos \psi + \cos^3 \psi)$	(27)
C Component	$N_{\psi} = C \frac{q R}{2} [2 - (\cos^2 \theta) (2 + \sin^2 \psi)]$	(28)
	$N_{\theta} = C \frac{q R}{2} (3 \cos^2 \psi - 1) \cos^2 \theta$	(29)
	$N_{\theta\psi} = C \frac{q R}{2} (\cos \psi \sin 2 \theta)$	(30)
From Redundant Reactions at Base	$N_{\psi} = a \cos 2 \theta \left(\frac{1 + \cos \psi_B}{1 + \cos \psi} \right)^2$	(31)
	$N_{\theta} = -N_{\psi}$	(32)
	$N_{\theta\psi} = -a \sin 2 \theta \left(\frac{1 + \cos \psi_B}{1 + \cos \psi} \right)^2$	(33)
	where $a = 3 C q R \left(\frac{\sin^2 \psi_B}{8 - (1 + \cos \psi_B)^3} \right)$	(34)
(2) Inflation Pressure (P_g)	$N_{\psi} = N_{\theta} = 0.5 P_g R$	(35)
	$N_{\psi\theta} = 0$	(36)
(3) Weight Proper (w , lb/ft ²) and Uniform Ice Load (w_i)	$N_{\psi} = -\frac{R(w + w_i)}{1 + \cos \psi}$	(37)
	$N_{\theta} = R(w + w_i) \left(\frac{1}{1 + \cos \psi} - \cos \psi \right)$	(38)
	$N_{\theta\psi} = 0$	(39)

NOTE: Effect of guy wires not included.

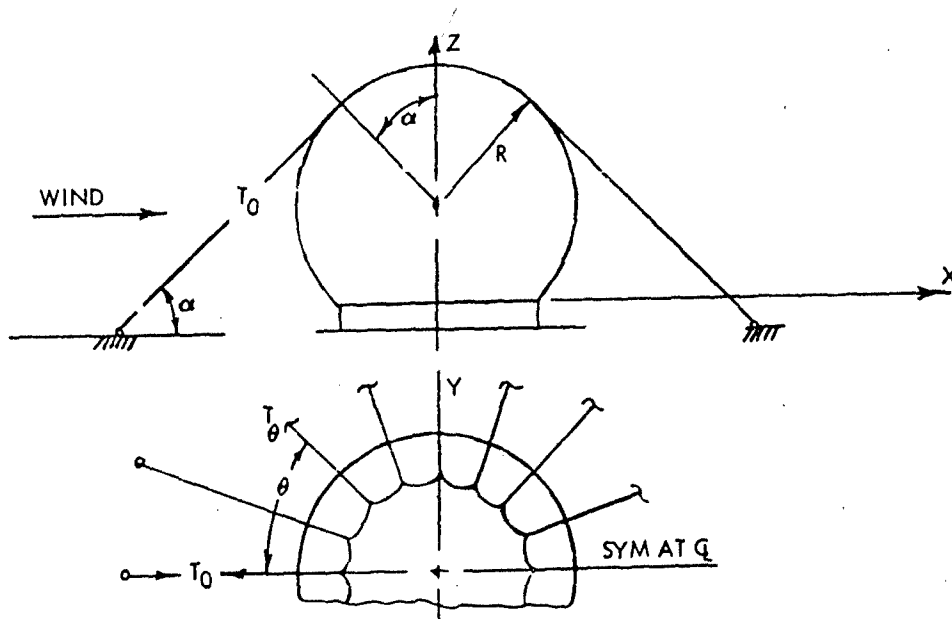


Figure 21. Guy Wire Arrangement

The shear stresses are

$$N_{\theta\psi} = \left(\frac{D_c}{\pi R} \right) \left(\frac{\cos \alpha - \cos \psi}{\cos \alpha \sin^3 \psi} \right) (\sin \theta). \quad (45)$$

Considering D_c the statically redundant magnitude, its actual value will be determined by establishing compatibility between the Radoflector deflections in X and Z direction at point $(\psi = \alpha, \theta = 0)$, with the strain of the cable that faces the wind direction. The reduction of the n-fold redundancy (from n cables) to but one redundant magnitude (D_c) is made possible by Equations 40 and 41. These in turn follow from the following facts:

- (1) When the Radoflector is loaded either by D component of the wind load or by the $N_{\psi c}$ forces defined by Equation 42, or both simultaneously, the attachment circle $\psi = \alpha$ as well as any other parallel circle $\psi = \text{constant}$ remains plane and circular.
- (2) The radius of any parallel circle remains unchanged.
- (3) All points of the meridian $\theta = \pm \pi/2$ experience deflections in X direction only.
- (4) All points of any parallel circle experience equal deflections in X direction.
- (5) The plane of each parallel circle rotates about an axis that is parallel to the Y axis and is situated in the plane of the parallel (Reference 8).

The C component of the wind loading can be treated in a similar fashion. It can be shown that the cable loads due to the C component of the wind must be in the form of

$$T = T' + T'' \cos 2\theta. \quad (46)$$

By means of this relationship, the n-fold redundancy is in effect reduced to a two-fold redundancy, represented by the two unknown constants T' and T'' in Equation 46. These unknowns can be found from two equations of compatibility of cable strains and Radoflector deflections at the two attachment points $(\psi = \alpha, \theta = 0)$ and

$$(\psi = \alpha, \theta = \pi/2).$$

(5) *Preliminary Numerical Results*

(a) *Wind Load of 125 mph.* The maximum principal tensile stress occurs at the base ring and is equal to approximately

$$N_{\max}(\text{wind}) = 1430 \text{ lb/ft.}^*$$

The minimum principal stress is a compressive stress and is equal to approximately

$$N_{\min}(\text{wind}) = -1080 \text{ lb/ft.}^*$$

If incipient wrinkling is permitted for the 125-mph survival condition, the minimum inflation pressure, P_g , is defined by

$$\frac{P_g R}{2} + N_{\min} = 0, \quad (47)$$

resulting in

$$P_g = 63 \text{ psf}$$

$$P_g = 12.1 \text{ in. of H}_2\text{O}.$$

The maximum principal tensile stress then is approximately

$$N_{\max} = N_{\max}(\text{wind}) + \frac{P_g R}{2}$$

$$N_{\max} = 2510 \text{ lb/ft.}$$

(b) *Wind Load of 75 MPH Plus Ice Load (2 Inches) Plus Weight Proper.* The maximum principal tensile stress occurs at the base ring and is equal to approximately

$$N_{\max}(\text{wind}) = 1415 \text{ lb/ft.}^*$$

The minimum principal stress is a compressive stress and is equal to approximately

$$N_{\min}(\text{wind}) = -990 \text{ lb/ft.}^*$$

The required gage pressure to prevent wrinkling is

$$P_g = 57.5 \text{ psf}$$

$$P_g = 11.1 \text{ in. H}_2\text{O}.$$

The maximum total principal stress is approximately

$$N_{\max} = 2405 \text{ lb/ft.}$$

(c) *Tension in the Guy Cable.* To determine the effect of the guy wire system upon the membrane stresses, a compatibility condition which involves the strain in the cable and the deflection of the radome was utilized. It was assumed that a radial deflection of the Radoflector has no effect on the tension in the cable. The compatibility condition determines the tension in the cable, and for a survival wind loading of 125 mph, the maximum tension in the cable is approximately $T_c(\max) = 12,000$ pounds.

This tension is a result of a fabric stiffness (E_f) of 2,000 lb/in. and a cable stiffness (EA_c) of 3.2×10^6 lb. The cable stiffness corresponds to approximately a 1/2-inch diameter steel cable.

(d) *Strength of Material and Factors of Safety.* In selecting a fabric of proper strength, it should be remembered that the term "safety factor" does not apply to fabric structures in the same sense as to conventional metal structures. All fabrics of organic (natural or synthetic)

*For both $N_{\max}(\text{wind})$ and $N_{\min}(\text{wind})$ the guy cable effect is included but inflation stresses are not.

origin are subjected to creep when under load. They will fail in creep rupture if the stress is above a certain critical level. The relation between creep rupture stress (F_{CR}), quick-breaking strength (F_Q), and time-to-fail is given by an approximate empirical equation of the form

$$\frac{F_{CR}}{F_Q} = K_1 - K_2 \log^{10} \frac{t}{r} \quad (48)$$

where

K_1 and K_2 are constants that depend on the material, kind of weave, etc.

t (days) is the time to failure

r is the unit of time (1 day).

For example, load-time tests conducted at room temperature on a two-ply Dacron-Neoprene fabric with $F_Q = 237$ lb/in. yielded

$$K_1 = 0.8498$$

$$K_2 = 0.0322.$$

Other factors to be considered are deterioration of the fabric material due to weathering, radiation, and heat. Based on past experience with fabric structures of many kinds, a "safety factor" of approximately 3 is considered sufficient for survival conditions.

Using a fabric with $F_Q = 650$ lb/in. = 7800 lb/ft results in the following safety factors:

$$\text{at 125-mph wind, SF} = \frac{7800}{2510} = 3.11$$

$$\text{at 75-mph wind plus 2 inches of ice and weight proper, SF} = \frac{7800}{2405} = 3.24.$$

b. *Preliminary Deflection Analysis.* In the analysis to determine the effect of the guy wire system on the Radoflector, expressions for the deflections of the combined system were developed for $\psi = \alpha$ and $\theta = 0, \pi/2$ (see Figure 20). These expressions are evaluated at $\psi = \alpha$ and $\theta = 0$. The magnitude of the radial and tangential deflections at this point for a fabric stiffness of 2000 lb/in. and 4000 lb/in. have been investigated on a preliminary basis and have been considered in the design. A thorough deflection analysis, however, must be conducted to determine the maximum deflection in the reflector area for the operating loads stated in Reference 8.

The inflatable structure was given the major consideration in the hardened emergency antenna system; however, some structural design emphasis was also given to the feed horn support since it was indicated that the design may have deflection problems.

The loads that the feed support structure is subjected to are the gravitational force plus the centrifugal force due to an angular velocity of 6.1 rpm. The acceleration deflections were considered negligible since the system need not be operating during the feed horn acceleration.

For the deflection analysis, the structure was considered to be a curved beam. A strain-energy solution was utilized, and for the loading condition defined above, the maximum radial and tangential deflections at the focal point are approximately

$$\delta_r = 0.2 \text{ in.}$$

$$\delta_t = 0.4 \text{ in.}$$

These magnitudes are within the allowable deflections.

5. Material Test Program

a. *General.* This section presents a material development and qualification test program directed toward the selection and qualification of a material and seam construction for the full-scale inflatable structure.

The base material must be selected primarily according to the external loads acting upon the Radoflector. The selection of the most practical method of attaching the reflecting elements on the inflatable structure is a secondary consideration.

Based on the preliminary stress analysis of the proposed Radoflector, a material breaking strength of approximately 600 to 650 lb/in. is indicated to prevent structure deformation due to external loads.

Environmental testing will be conducted on the basic material. Samples of the material will be subjected to the temperature and humidity conditions specified in the general requirements of Reference 6. Past experience in utilizing coated fabrics in airship envelope construction has demonstrated very little deterioration in a salt atmosphere.

In consideration of the environmental and functional requirements of the full-scale antenna system, Dacron-Mylar or Dacron-Tedlar laminates have been tentatively selected as materials best meeting the requirements for a structural material that is flexible, packageable, inflatable, and dimensionally stable. However, a material selection test program was beyond the scope of this contract, and it should be pointed out that these laminate materials and seam construction with these materials have not been tested at stress levels of the magnitude required for the full-scale design. Testing and further evaluation will be required to select the most suitable material. Such testing may show that other materials such as two-ply Dacron cloth with Neoprene or Hypalon elastomers are more desirable from a standpoint of meeting the uniaxial and biaxial strength and seam strength requirements.

b. *Contour Stability.* Due to the requirement for a high degree of dimensional stability in the Radoflector, a flexible material exhibiting high initial modulus (resistance to initial stretch) is required. To provide an indication of efficiencies of finished woven cloths, yarn data has been plotted to show stress-strain relationship of nylon, Dacron, and cotton yarn (see Figure 22). These plots indicate that the initial modulus of Dacron yarn is high when compared with that of other textile fibers.

As a result of past experience and the yarn survey, Dacron was selected as the most promising basic fiber for cloth in the inflatable structure construction. As to the cloth weave, the system of interlacing lengthwise warp yarns with crosswise filling yarns, a 2 x 2 basket weave (two yarns in both warp and filling woven as one) with low-twist filament yarns has been found to give the best adhesion and tear resistance.

c. *Material Development.* During the past two years, GAC has developed a new lightweight polyester film cloth laminate. This material is currently being used on a dynamic lift balloon program. The laminate consists of one ply of Dacron cloth laminated to Mylar film with an adhesive. In addition, the laminate has a polyurethane coating applied to the cloth side. Work on this particular laminate material has provided useful data and experience; however, this particular material is not adequate from a strength standpoint for the Radoflector. A test and evaluation program will be required to select a suitable material. This program will include a selection of the best candidate materials based on an evaluation of current material data. These materials will then be evaluated by typical developmental tests to determine their capability of meeting basic strength and elongation requirements. Seam techniques will be developed and tested to assure strength compatibility with the basic material. Final material selection will be made based on the above tests.

d. *Qualification Test Program.* Qualification type material testing will be conducted on the selected material in accordance with ASTM, Federal or Goodyear specifications, which outline standard textile test methods for evaluating the effects of stress-strain under the application of both uniaxial and biaxial loads, permeability, flexing, weathering, and temperature extremes on the material properties. A method using slotted waveguide techniques will be used to measure rf reflectivity and transmissivity. The type and quantity of material tests are summarized in Table 7.

D. Radoflector Hardened Antenna System Installation

1. General

A preliminary approach to a Radoflector hardened installation is shown in Figure 23. This is one type of hardened site that can be designed to withstand the overpressurization and thermal radiation of large-yield nuclear weapons at various distances from ground zero, depending on the specific requirements of a particular hardened system. The design approach taken here is to

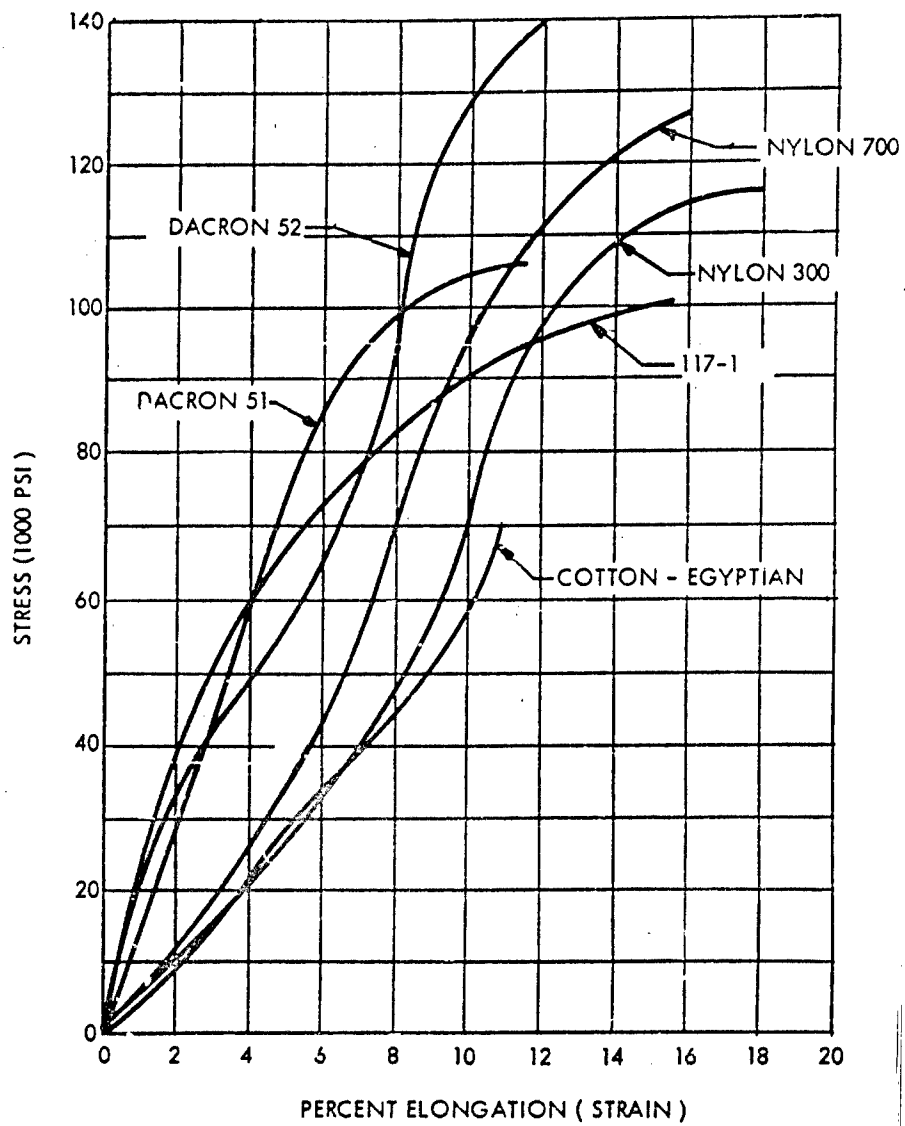



Figure 22. Stress-Strain Curves (DuPont Yarn Tests)

TABLE 7.
Test Program

TEST	SPECIMEN TYPE (MATERIAL) [†] ‡Base ‡Seamed	EXPOSURE TREATMENT*				TOTAL NO. OF TESTS
		Temperature			500-hr Weather- ometer aging	
		-30°F	Room			
			-140°F			
Weight and Thickness	x		x			10
Breaking Strength and Elongation						
Strip Tensile Method						
Original	x	x	x	x	x	90
After Crease	x	x	x	x		60
After Rotoflex	x	x	x	x		60
Cylinder Burst Method	x		x	x		20
Adhesion						
Ply	x	x	x	x		20
Coat	x	x	x	x		5
Blocking	x		x	x		5
Permeability (Air)						
Original	x		x			10
After Rotoflex	x		x			10
Cylinder Elongation (20 Percent Load)			x			4
Tear (Center )	x	x	x	x	x	60
Torsion (cylinder; (Shear Modulus)			x			2
Rf Reflectivity and Transmissivity	x		x			5
Total						361

*Specimens tested for -30°F and -140°F exposure resistance will be aged for 96 hours at test temperature.

†Five test specimens will be used to establish test value averages.

‡Two different specimens will be tested.



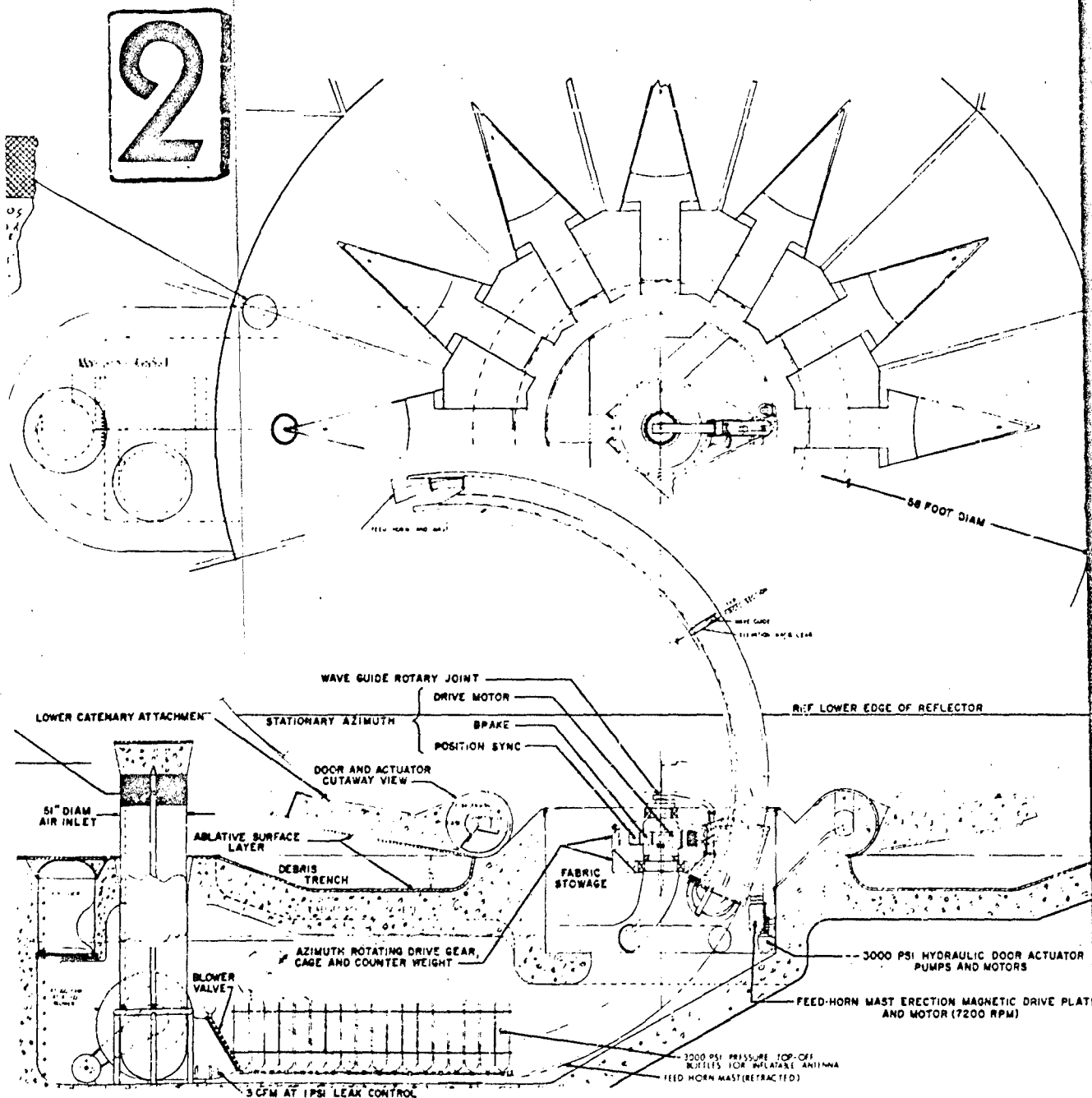


Figure 23. Automatic Hardened Site Inflatable Radoflector Concept

51



indicate a feasible engineering concept with the understanding that a considerable amount of additional effort is required to produce a desirable operating system.

The Radoflector hardened installation consists of a reinforced concrete enclosure that contains the Radoflector, an air pressurization system, a retractable feed horn, and an azimuth drive assembly.

The particular antenna hardened system is best described with reference to an artist's sketch. Figure 24 shows the antenna system in the stowed position. The pie-shaped door configuration used in this particular concept is shown together with the debris trench that encircles the closed doors. Also shown are the guy cable trenches, which are sealed to preclude any water or ice accumulation. In this stowed position, the exposed surfaces are coated with ablative material for protection against the thermal radiation that would be emitted from a nuclear explosion.

Figure 25 shows the antenna system in the operating position. The antenna system can be erected into the operating position in no more than 15 minutes and possibly as little as 5 minutes. Upon initiation of the system, hydraulic actuators open the concrete enclosure doors and raise the air pressure intake. As the doors unfold, they pull out some of the inflatable structure to allow the initial air pressure to be evenly distributed into the deflated envelope. A high capacity air blower then pressurizes the inflatable structure to about 4 inches of water and a high pressure bottle system will "top-off" the pressure to about 12 inches of water. As the inflatable structure is inflated, it automatically pulls the guy cables out of their trenches and into their erected position. Once the Radoflector takes its shape, the feed horn and its support are rotated into the operating position. The antenna is then ready for operation.

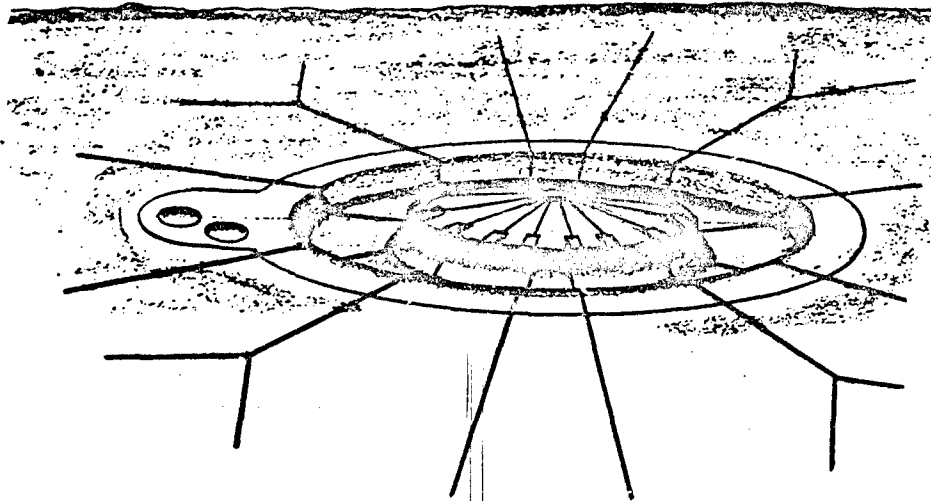


Figure 24. Radoflector Hardened Antenna Installation (Stowed Configuration)

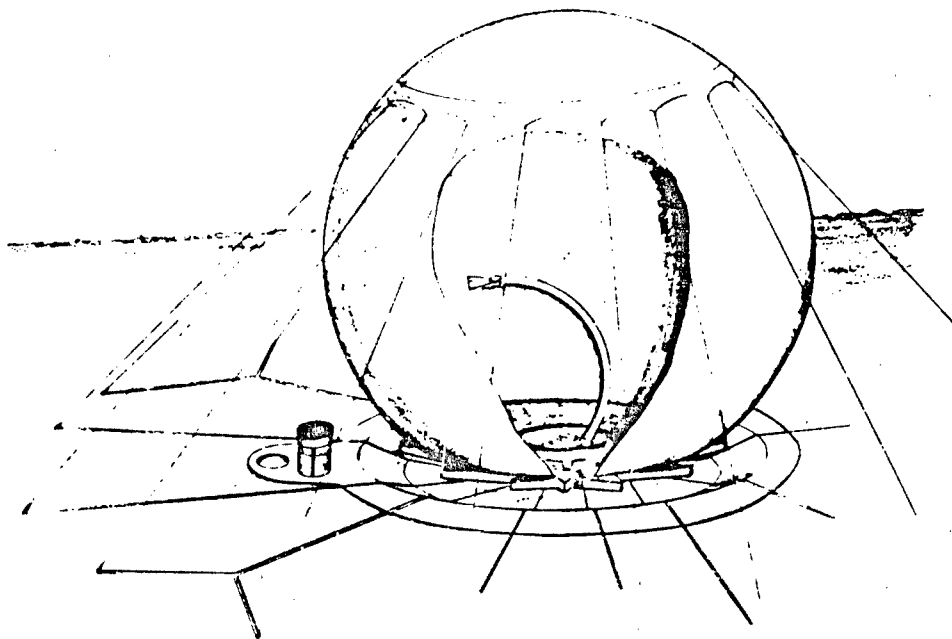


Figure 25. Radoflector Hardened Antenna Installation (Operating Configuration)

2. Hardened Enclosure

The deflated Radoflector is enclosed in a reinforced concrete enclosure. Included as integral parts of the enclosure are the enclosure doors, debris pit, inflatable structure container, azimuth drive support structure, air lock compartment, and the entrance apron.

The enclosure itself is constructed of reinforced concrete so that it may withstand the shock of a nuclear blast. A linear displacement due to this shock will not affect the performance of the antenna system unless power connections are severed. A rotational displacement of the system will alter operating performance.

As a final design objective the hardened antenna system will be designed to withstand an incident overpressure of approximately 300 psi. At these overpressure conditions, the thermal and initial radiation effects can be tolerated. Also, at the distances associated with the 300-psi overpressure, ground displacement would not present a serious problem. Some shock mounting of equipment would be required to protect the equipment from ground shock accelerations.

The enclosure doors provide three functions. When closed, the doors protect the contents of the enclosure cavity from being damaged by external forces. Additionally, as the doors open, they move any debris deposited by an explosion into the debris pit. When fully opened, an eyelet on each door innerface could provide an anchor point for cables attached to the inflatable structure catenary curtain.

Over-all, each enclosure door is approximately 14.75 feet long, 5.25 feet wide, 2 feet thick, and is estimated to weigh between 15,000 and 20,000 pounds. Eleven of the doors are identical, as described above. The twelfth door, located adjacently to the entrance apron, is different only in that it has an elliptical cap at the pointed end which closes the opening at the center of the doors. This causes the twelfth door to be approximately one foot longer than the remaining 11 doors.

The actuators used to operate the doors are an oversized version of a conventional rotary hydraulic actuator. Hydraulic fluid supply and return lines are connected to fittings on one end of the fixed shaft. Drilled openings in the shaft direct hydraulic fluid into and away from the two faces of the piston. The lines serve alternately as supply and return lines. As a door is raised (opening or closing), rate of motion is governed by the supply of fluid from the constant-speed, gear-type pump. Similarly, after the door passes over center and is free-falling, movement is still governed by the constant-speed pump because the fluid flow from the return side of the piston is restricted by the pump. Thus the enclosure doors move at essentially the same rate when raising or lowering. The door containing the elliptical cap (twelfth door) is controlled to always open first and close last.

A debris trench encircles the enclosure doors when closed and is used to prevent debris from jamming the doors when opening.

The inflatable structure storage area as indicated in Figure 23 is located around the feed horn rotary platform and the center platform support. A packaging factor of 10:1 volume ratio has been utilized as a first approximation for three reasons:

- (1) An inflatable spheroid is difficult to package in a minimum volume.
- (2) The available packaging volume is obstructed by the feed horn rotary platform.
- (3) A minimum amount of reflector folding is desirable to prevent any degradation of the antenna reflector surface.

The detailed procedure for folding the inflatable structure and placing it in the receptacle must still be determined. A procedure must be generated that will assure that the inflatable structure will unfold quickly and easily as it is inflated, keeping the guy system, catenary support system, and air seal intact and properly orientated.

An air lock compartment provides ingress and egress to the concrete enclosure. The compartment is shown to be approximately 3.75 feet in diameter and 6 feet high at the highest point (center), and facilitates entering the enclosure when the Radoflector is inflated.

3. Radoflector Pressurization System

The Radoflector pressurization system in this particular design concept is composed of a high-capacity blower system, high-pressure storage bottles, and a pressure maintenance unit.

The high-capacity blower system that has been selected has a capacity of approximately 45,000 cfm against a static pressure of 4 inches of water. This blower capacity will inflate the antenna in less than four minutes.

To top off the pressure, storage bottles pressurized to 3000 psi will be used to bring the antenna system up to its operating pressure of 12.1 inches of water. This increase in pressure will take place in approximately one minute, which makes the total antenna erection time approximately a five-minute operation with the assumption that the door opening and feed horn erection can be accomplished during the pressurization cycle.

The specific design concept includes a small compressor unit and associated controls for maintaining constant pressure during operation. This system will include a telescoping inlet tube to raise it above debris.

4. Feed Horn Erection Mechanism

The feed horn is erected by a unique actuating system. This system includes a drive motor, magnetic clutch, gear box, shaft, and drive gear.

The feed horn with its waveguide and support structure form an arc approximately 43 feet long, 1.5 feet wide, and 10 inches thick. This feed horn arc has a radius of 19 feet. The feed horn support structure has a row of gear-like teeth running nearly the full length of the unit; the teeth are mounted on one side of the unit. The teeth mate with a drive gear, which is in turn driven by the feed horn drive motor.

The drive gear, when actuated, rotates the feed horn and its support structure on a system of rollers from its stowed position in the concrete enclosure to its operating position. The feed horn structure at the end of its travel is fixed into position by wedge-like blocks that are mounted on the feed horn and engage the rollers at the fully extended position.

A waveguide disconnecting joint is located at the base of the feed horn structure. This joint is connected and disconnected from the rotary joint waveguide automatically as part of the feed horn erection. The two waveguide mating surfaces are flanged, having alignment pins to assure proper mating. The drive mechanism is designed so that the flanges are held together with sufficient pressure to prevent rf energy leakage. In addition, the ends of the waveguides are sealed with a thin film of plastic to keep out dirt and moisture when the feed horn is retracted.

The feed horn actuating system drive motor is mounted on the enclosure cavity wall. The motor is situated so that the clutch plate, mounted on the motor shaft, is opposite the clutch plate on the feed horn gear box assembly.

A magnetic clutch couples the feed horn actuator drive motor to the feed horn actuator gear box. The magnetic clutch, after actuating the feed horn, slips when the feed horn is fully extended. This feature assures that the feed horn will be run against the stops. The gear box is designed to hold the feed horn in this fully extended position.

5. Feed Horn Azimuth Drive System

A rotary platform is utilized to provide azimuth drive for the antenna feed horn. The feed structure is mounted on the rotary platform, and the rotary platform is supported by a center support shaft.

The waveguide rotary joint is a conventional-type mounted on the center shaft and interconnecting the stationary rf lines in the center shaft to the rotating feed horn. It should be noted that only one rotary joint is required because of the unique design of this antenna system.

An electric motor is mounted on the center shaft and serves as the feed horn azimuth drive motor. A dual helical gear mounted on the motor shaft engages a mating set of gears mounted on the inner surface of the rotating assembly, mechanically linking the drive motor to the rotating assembly. Use of dual helical gears assures smooth operation with a minimum of gear backlash.

6. Concept Review by Hardened Enclosure Consultants

A preliminary review of the GAC hardened enclosure design has been made by Parsons-Jurden Corporation, 26 Broadway, New York 4, N. Y. Parsons-Jurden Corporation and its parent organization, The Ralph M. Parsons Company, have had extensive experience in the development and the detailed design of hardened facilities to withstand the full range of nuclear weapons effects. Concept development, final design, and construction have been performed by them on such projects as Minuteman, Titan, and Nike-Zeus, as well as on other classified projects. Special areas of investigation included ground shock response characteristics of various sites, conceptual studies for communications and weapons facilities located in a variety of soil environments, analysis and design of linear and non-linear shock isolation devices to attenuate high accelerations to tolerable levels, and the development of test programs to prove the suitability of facility components. Based on this experience the review by Parsons-Jurden Corporation is in agreement with GAC's opinion that a hardened Radoflector installation can be designed to withstand a nuclear blast environment of 300-psi overpressure.

The following preliminary recommendations have already been made by Parsons-Jurden Corporation after a cursory review of the hardened concept described in this report:

- (1) Certain basic equipments require shock mounting against the devastating effects of the ground shock. Rattle space up to approximately one foot around shock-mounted equipment must be incorporated.
- (2) Consideration must be given to the protection of internal components against the electromagnetic pulse generated by the nuclear blast.
- (3) A single-slab-type door which would roll in or out on tracks might be more feasible than the "orange peel"-type doors presently shown in GAC's concept (Figure 23). With the single-slab door the door thickness could be reduced and pressure sealing would be simplified. To satisfy the need of a base support for the Radoflector, various designs such as an additional internal set of doors or an internal concrete collar for the Radoflector base support could be considered.

4. SCALE MODEL

A. General

A scale model of the Radoflector was designed, fabricated, and tested for the purpose of comparing the antenna pattern characteristics at scaled frequencies with the specified design goal performance parameters. The scale model was designed to duplicate, as closely as possible, the full-scale Radoflector inflatable structure configuration and shape, reflective surface, and feed system since these items are of prime importance in determining the electrical performance. The guy wire arrangement was duplicated to simulate their effect on antenna patterns. It was not intended that the scale model should demonstrate other mechanical features such as hardened site storage or operational deployment; therefore, no attempt was made to duplicate these features. The balance of the mechanical and structural design was limited to that sufficient to support the Radoflector for pattern test purposes. The original intent was to utilize a one-tenth scale model; however, in the interest of economy it was decided to utilize an existing eight-foot diameter hemispherical wood form block as the base on which to build up a contour tool for fabricating the inflatable structure. To utilize this existing form block, the size of the model was increased to a scale factor of $1/7.254$ or 0.1377 .

B. Rf Design

The full-scale contour was established as explained in Section 3, paragraph B-5-a. The scale model reflector shape was scaled down by the 0.1377 scale factor from the shape initially established for the full-scale Radoflector. The parameters of the scale model Radoflector compared with the full-scale parameters, adjusted as a result of the universal dish tests, are given in Table 8.

A change in focal distance from 27.6 to 28.0 inches resulted from the universal dish tests (refer to Section 3, paragraph B-5-b). The new focal distance determined a new optimum spherical radius (R) for minimum phase deviation. From the equations of Section 3, paragraph B-2, the corrected value for the scale model is $R = 4.9$ feet.

The original radius value ($R = 4.75$ feet), however, when used with the new focal dimension ($f = 28.0$ inches), results in a phase deviation factor which still remains less than $\lambda/16$. For this reason, the original radius value of 4.75 feet was not changed.

A selection of parallel wires of finite diameter for the reflective surface was made for the scale model. Wires were selected as the parallel conductors to facilitate fabrication so that a filament winding technique of applying the wires to the inflatable material could be used.

From the theoretical considerations of Section 3, paragraph B-6-b, the corresponding losses with a wire diameter of $0.010 (\pm 0.002)$ inch and a wire spacing of $0.13 (+0.025, -0.050)$ inch are as follows:

Transmission loss at reflecting surface (α_T) = 0.6 db.

Reflection loss at transparent surface (α_R) < 0.1 db.

Total loss (α) < 0.7 db.

The theoretical losses are in good agreement with the experimentally determined losses of Section 3, paragraph B-6-f.

To determine the tolerance of the wire diameter and spacing, utilization of the relationships given in Section 3, paragraph B-6-d yields the following:

Δd (wire diameter tolerance) = ± 0.002 inch.

Δs (wire spacing tolerance) = $+0.025$ inch, -0.050 inch.

C. Inflatable Structure Design

1. Contour

The shape of the inflatable Radoflector was developed as a body of revolution utilizing the renormalized coordinates shown in Table 5 with the X axis depressed 11 degrees. This contour is extended for 6 inches at the top and bottom of the reflector section with the same curvature to preclude any distortion due to change of the radius of curvature. The top is closed off by a radius tangent to the parabola extension. The tangent radius at the bottom is continued to the base

TABLE 8.
Parameter Comparison Scale Model versus Full-Scale Radoflector

DESIGN PARAMETER	SCALE MODEL	FULL SCALE
Center Frequency	9.09 gc	1.25 gc
Frequency Range	8.72 to 9.44 gc	1.20 to 1.30 gc
Horizontal Radius of Revolution (at Maximum Diameter)	56.7 inches	34.35 feet
Focal Distance	28 inches	16.65 feet
Focal Radius	28.4 inches	17.52 feet
Equivalent Parabolic Reflector Diameter	42 inches	25.4 feet
F/D Ratio	0.656	0.656
Distance from Bottom Edge of Reflector to Ground Plane	6 inches	5 feet (minimum)
Distance from Center of Feed to Ground Plane	28.8 inches	20 feet (minimum)
10-DB Beamwidth of Primary Feed Horn	82 degrees	73 degrees
Feed Horn Aperture	A = 2.12 inches B = 1.51 inches	A = 16.80 inches B = 12.75 inches
Illuminated Reflector Aperture	Horizontal - 42 inches Vertical - 40.25 inches	Horizontal - 25.4 feet Vertical - 25.4 feet
Conductor Size	Diameter = 0.010(± 0.002) inch	Width = 0.47 (+0.10, -0.05) inch
Conductor Spacing (Center-to-Center)	0.130(+0.025, -0.05) inch	1.42(+0.10, -0.20) inches
Tolerance Control of Surface	± 0.081 inch	± 0.60 inch
Angle of Depression of Electrical Axis of Vertical Reflector Contour (with Respect to Center of Revolution)	9 degrees	9 degrees

attachment point. The vertical axis of revolution is established to provide the horizontal curvature required to obtain the proper horizontal aperture. Figure 26 shows the contour geometry for the Radoflector fabrication tool. All ordinates and dimensions shown are reduced by one percent from the desired Radoflector inflated shape to allow for elongation at operating pressure.

2. Material Selection

The material selected for the model inflatable structure is a film-cloth laminate consisting of

Dacron cloth, Type 481	4.5 oz/yd ²
1-mil weatherable Mylar film	1.0 oz/yd ²
Clear adhesive	0.5 oz/yd ²

The total weight of the laminate material is 6.0 oz/yd². This material was manufactured by the Schjeldahl Company.

The Type 481 Dacron cloth is a 2 x 2 basket weave cloth made from Type 51 Dacron fiber. This cloth has a warp strength of 225 lb/in. and a fill strength of 205 lb/in. This laminate material is considerably stronger than required for the pressure and wind loading anticipated for the model. This material was selected because of the desirability of developing manufacturing techniques with a heavier material more closely representing the characteristics of a material that would be suitable for a full-scale Radoflector and because of the immediate availability of the Type 481 Dacron cloth.

3. Elongation Considerations

A cylinder 12 inches in diameter and 36 inches long was fabricated and pressure tested as shown in Figure 27 to determine elongation characteristics of the laminate material. Circumferential and longitudinal growth were measured under pressure with additional axial load applied to provide longitudinal stress level equal to the circumferential stress level since the near spherical shape of the Radoflector model would have near equal stress levels in all directions. Allowing a five-minute creep time interval for each reading, measurements were made over a pressure range of 0.5 to 5 psi which provided fabric stresses within the operating stress levels expected during field testing of the model. Elongation data was not conclusive; however, results indicated a growth in the order of 0.5 percent at the stress levels anticipated for the model.

A 22-inch diameter sphere was fabricated from the same Dacron-Mylar laminate material to be used for the scale model to further evaluate elongation and to check the preforming and splicing techniques. Each hemisphere of the sphere consists of five gores which were vacuum-formed and then assembled on a steel mold, using a Schjeldbond GT-100 as the bonding agent. The unit was then pressurized in one-psi increments from 1 to 5 psi. Measurements from the center of each gore on the opposite side were taken at each pressure increment as a further check on growth characteristics. Measurements showed an approximate average diametric growth of 0.64 percent with a short creep time increment of similar duration to that used on the cylinder elongation test.

Experience has shown that elongation will increase with time under load conditions; since the test measurements were taken after a rather short time period (5 minutes), an elongation allowance of 1 percent was selected. The contour dimensions used for initial fabrication of the model were decreased by this amount to allow for growth after pressurization.

4. Configuration

The model inflatable structure design shown in Figure 28 consists of 12 equal sized (30-degree segment) vertical gore panels bonded together at thin edges with a butt splice. A small circular section is inserted at the crown for termination of the gore panels. The Mylar face of the laminate is on the outside surface, and all joints are bonded on the inside (Dacron to Dacron) utilizing a butt strap. Eight straps crossing at the crown of the structure and extending down just below the 45-degree tangent point provide attachment for 16 guy cables.

The bottom edge of the inflatable structure is reinforced and flanged inward to provide for attachment to the base platform.

The upper half of the reflector surface consists of parallel 0.010-diameter stainless steel wires oriented at 45 degrees. The reflector elements were laid out by drawing methods and were checked by calculations.

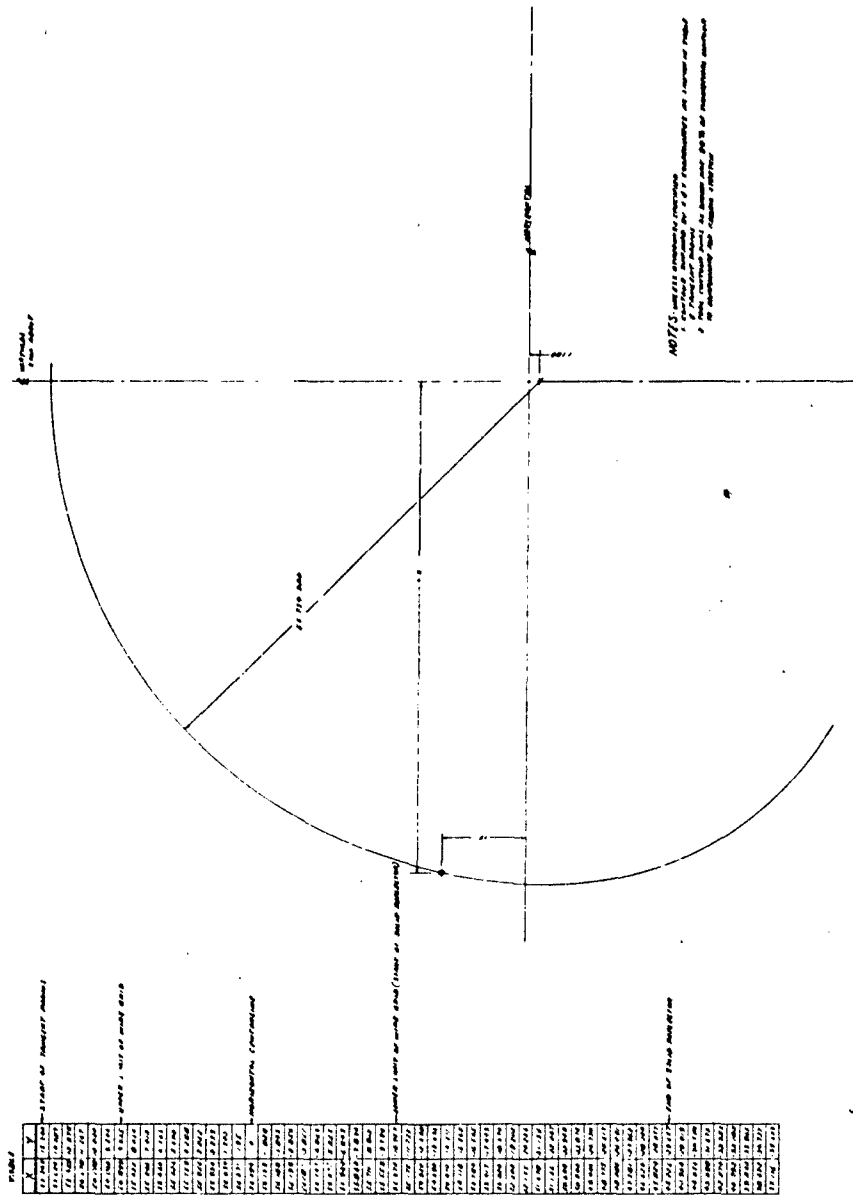


Figure 26. Tool Contour

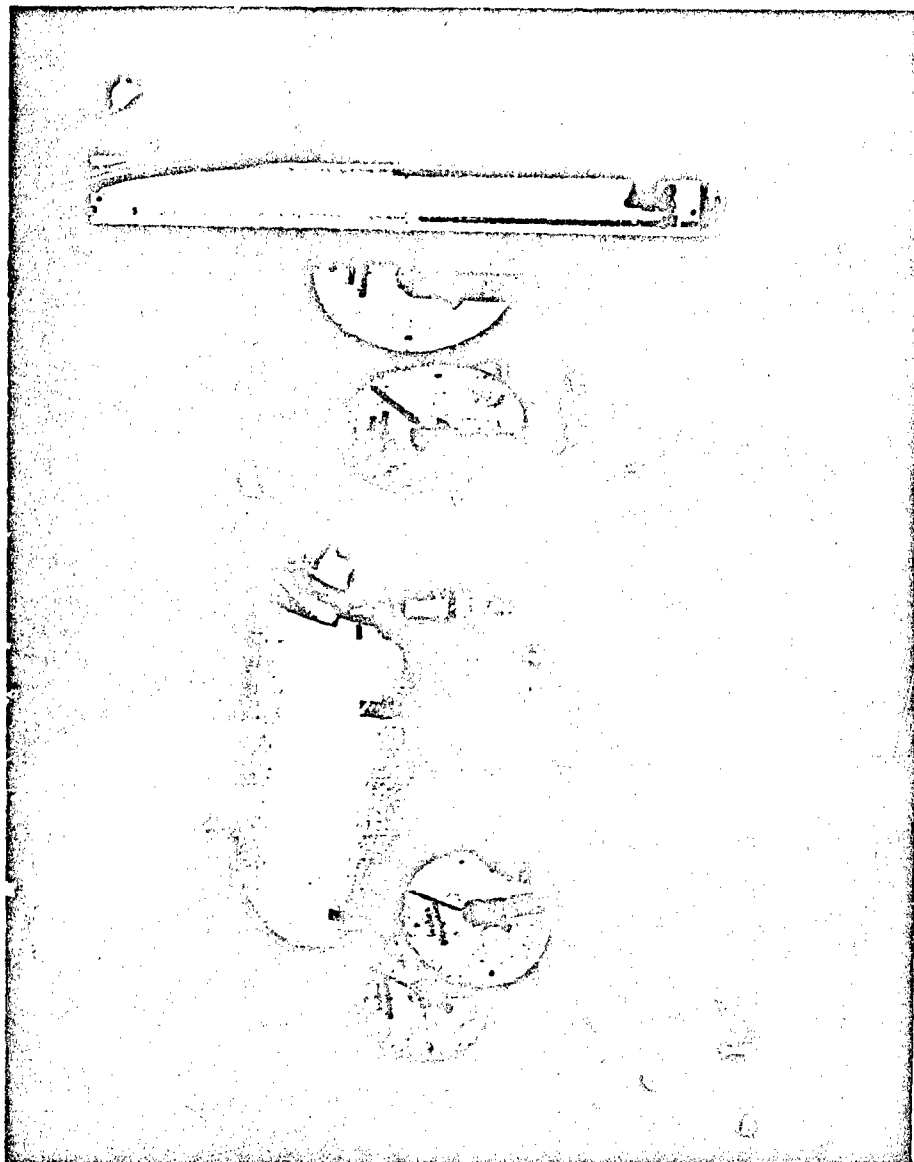


Figure 27. Static Testing a Cylinder of Mylar-Decron Material

A difficulty encountered with the wire layout evolved basically from the two different curvature functions that form the reflector surface contour. The wires are spaced at $0.13(+0.025, -0.050)$ inch and cross at a 45-degree angle to all lines that are parallel to the base at all heights of the Radoflector. This configuration was selected to obtain maximum efficiency of the reflector. The objective is to place the wires so that the projections of the reflector surface grid and the transparent grid surface (the opposite surface) onto a common plane should result in nearly a 90-degree included angle between the two lines at the intersection point. Also, this 90-degree pattern should be maintained over as large a portion of the aperture as possible. For the scale model layout, the exact 90-degree included angle is centered vertically in the middle of the wire pattern (upper half of the reflector) to optimize the included angle and spacing. The table in Figure 28 shows the geometric ordinates for the parallel wire locations on the surface of the reflector. It was found for the relatively short over-all height of the parallel wire reflector section located near the center of the near spherical structure that wires spaced at a constant spacing at a 45-degree angle on flat Mylar film, when formed to the reflector contour, would satisfy the geometric requirements within satisfactory limits.

The lower half of the reflector surface is a solid reflective material utilizing vacuum deposited aluminum 2000 angstroms thick on Mylar film. The two reflective materials are bonded to the outside surface of the inflatable structure.

5. Fabrication Techniques and Tooling

A hemispherical male form block was fabricated for laying up and bonding the gored structure and for use as a master for fabricating a female preforming mold. This tool design is based on adding a build-up to an existing eight-foot diameter hemispherical form block to achieve the desired contour. The existing form block was built up as shown in Figure 29 by adding wood ribs and expanded metal screen. Epoxy resin was applied to approach the desired contour. Final accurate contour was achieved by sweeping thin coats of resin on the surface with an accurate contour template which is hinged at the two vertical poles of the form block. The completed male tool is shown in Figure 30. From this male form block a fiberglass female preforming mold was fabricated. This female section was utilized as a preforming mold for the Dacron-Mylar gore sections. A fiberglass female trim template was also made from the male block for use in trimming the preformed gores to exact size.

Upon completion of the preform and the trim tools, the development of a fabrication process technique was undertaken. This development was very important in that a number of different materials, adhesives, and steps are involved in the manufacture of a gore. The following techniques were developed and utilized for fabricating the model:

The first step was to bond the aluminum wires at a 0.12 spacing to a Mylar film using a filament winding concept. The wire-Mylar film was then trimmed and oriented to a 45-degree angle. Using a heat sensitive tape, aluminized Mylar is then bonded to both ends of the wire film. Although the aluminized Mylar is not attached above the wires in the completed inflatable structure, it must be attached at this point to enable the applying of a vacuum in the preform tool and trimmed off later. This assembly, slightly larger than a gore, was then placed in the preform tool, a vacuum was applied, and the assembly was allowed to cure in the oven (see Figure 31). This assembly was then removed from the preform tool.

The second step was to cut a section of the Mylar-Dacron cloth to a size slightly larger than a gore. This section was then placed in the preform tool, a vacuum applied, and the material cured in an oven.

The third step was to bring the two preformed sections together in the preform tool, apply a bonding agent between them, connect a vacuum, and cure the complete assembly in an oven. This completed section then is one of 12 gores laminated of wire-Mylar, aluminized Mylar, and Mylar-Dacron cloth.

The fourth step was to accurately trim the completed section to the gore size, using the trim tool. At this time the aluminized Mylar material lying above the wires was trimmed off.

Six preformed gores were then bonded together on the inside surface (Dacron side), using a butt splice joint to form each half of the inflatable structure (see Figure 32). Schjelbend GT-100

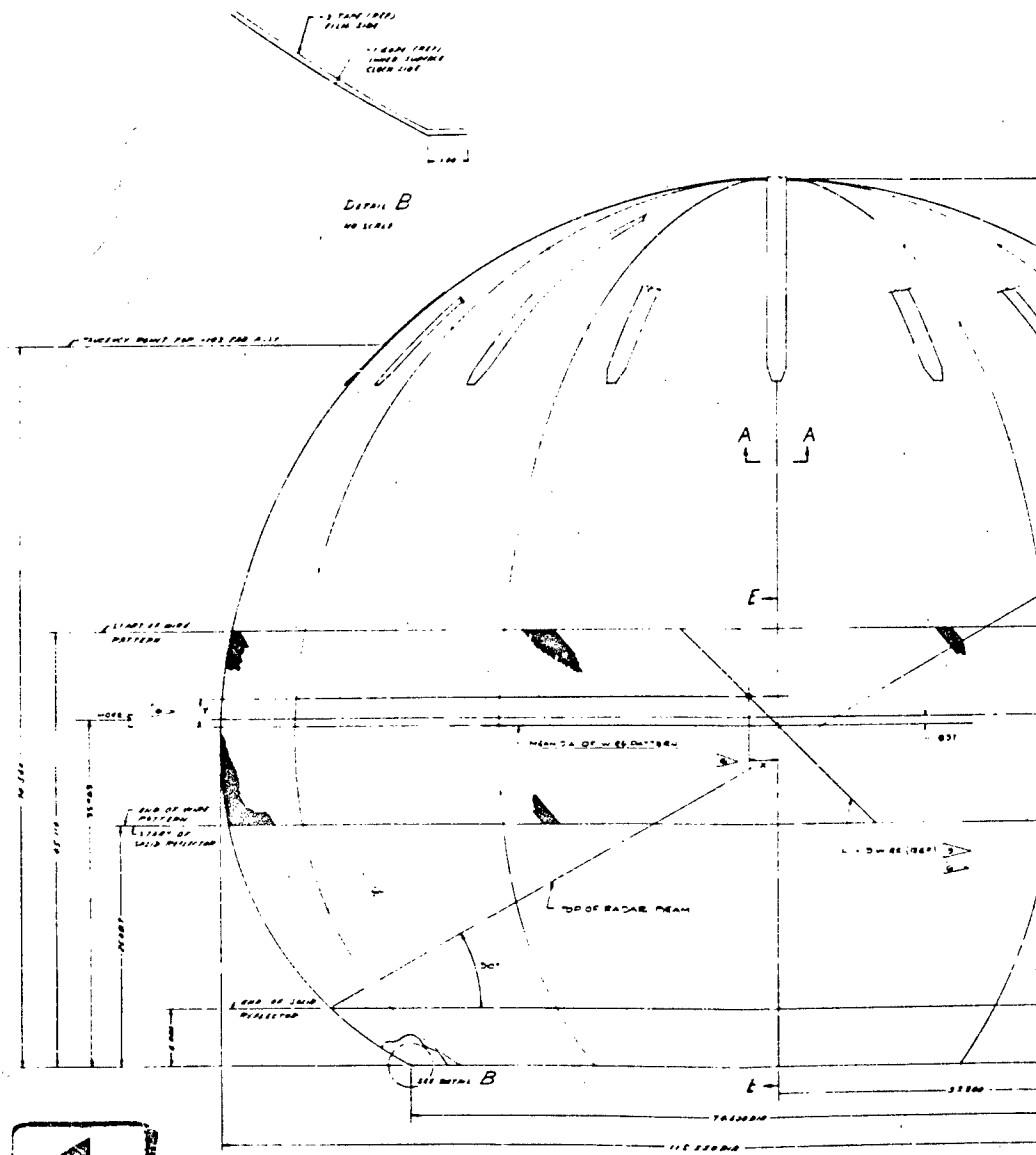
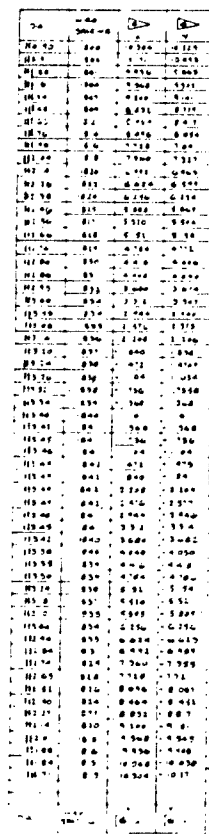
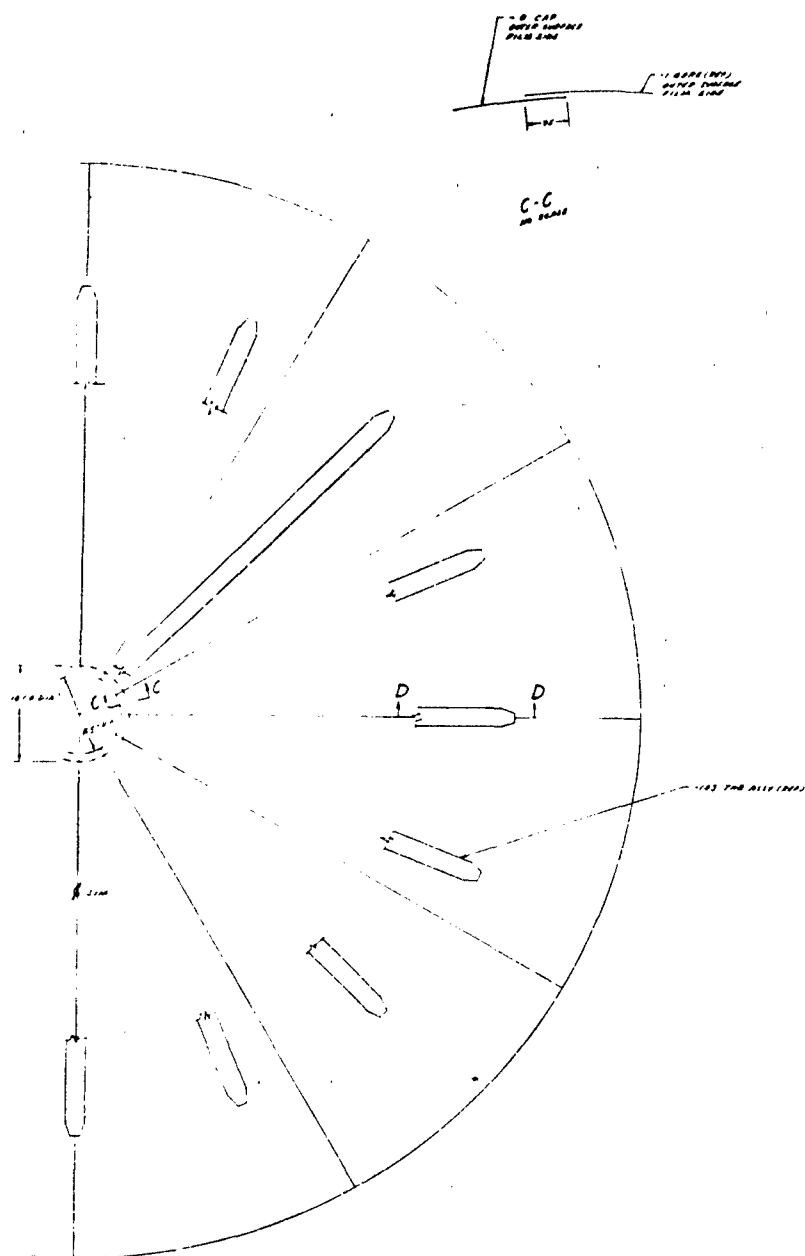


Figure 28. Radotlector Scale Model Design (Sheet 1 of 2)



1



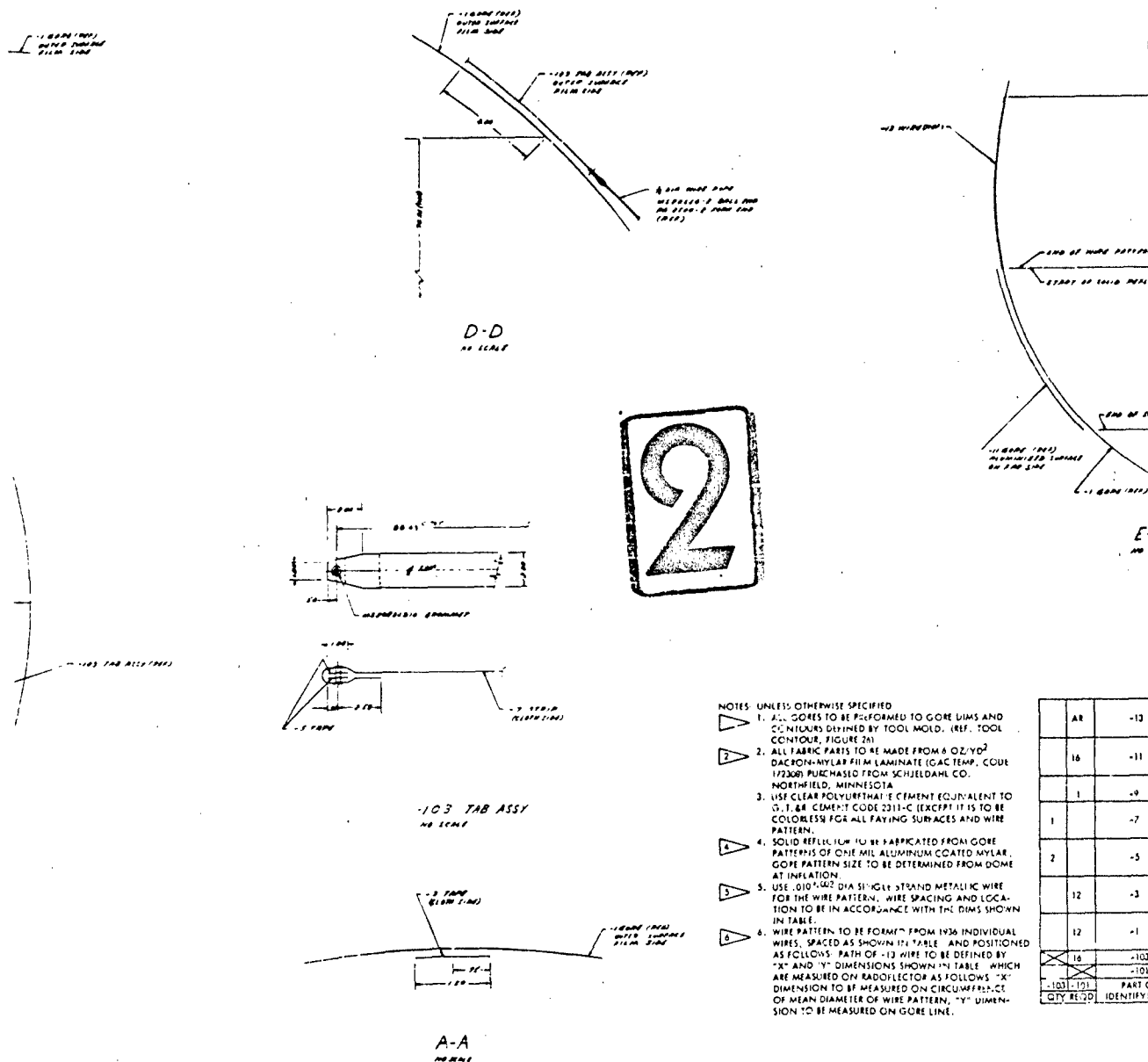
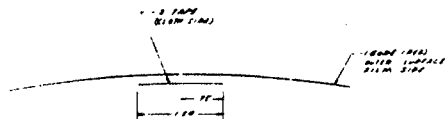
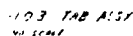
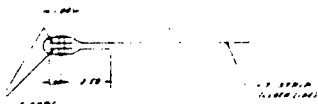
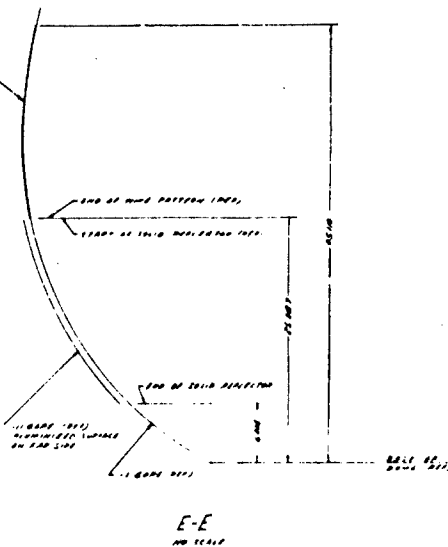


Figure 28. Red-Reflector Scale Model Design (Sheet 2 of 2)



A-A



NOTES UNLESS OTHERWISE SPECIFIED

- ▲ ALL CORES TO BE PREPARED TO CORE DIMENSIONS CONTIGUOUS DEFINED BY TOOL MOULD. IF TOOL MOULDING FIGURE 10-1 IS USED.
- ▲ ALL FABRIC PATTERNS TO BE MADE FROM A OF 70% DACRON-MYLAR FIBRE LAMINATE (FACETEMP, COOF 175000 PURCHASED FROM SCHJELDAD & SONS) CORNIFIED, MINIMUM THICKNESS .006".
- ▲ USE CLEAR POLYURETHANE CEMENT EQUIVALENT TO 7 T.A.R. FEMTAP COE 2311-C (EXCEPT IT IS TO BE COLORLESS FOR ALL SAYTING SURFACES AND WIRE PATTERN).
- ▲ SOLID REFLECTOR TO BE FABRICATED FROM GYPER FIBERGLASS CINT MIL ALUMINIUM COATED MYLAR. CORE PATTERN SIZE TO BE DETERMINED FROM DUNE ATTEMULATION.
- ▲ USE .010" DIA DIA SINGLE STRAND METALLIC WIRE FOR THE WIRE PATTERN, WIRE SPACING AND LOCATION TO BE IN ACCORDANCE WITH THE DIMS SHOWN IN TABLE.
- ▲ WIRE PATTERN TO BE FORMED FROM 1936 INSULATED WIRES, SPACED AS SHOWN IN TABLE AND POSITIONED ACCORDINGLY. PAPER OR CARBON COPY OF "X" AND "Y" DIMENSIONS SHOWN IN TABLE WHICH ARE MEASURED ON RADIOFLUORO AS FOLLOWS: "X" DIMENSION TO BE MEASURED ON CURCUMFERENCE OF MAIN DIAMETER OF CORE, "Y" DIMENSION TO BE MEASURED ON CORE LINE.

AR	WIRE		QTY DIA X 8000 FEET
16	-11	GORE	25.00 X 30.00
1	-9	CAP	FABRIC 10.00 DIA
1	-7	STRIP	FABRIC 2.00 X W/4
2	-5	TAPE	FABRIC 1.00 X 2.00
12	3	TAPE	FABRIC 1.50 W/4
12	-1	GORE	FABRIC 47.50 X 125/4
16	10	148 ASSY	
16	10	FABRIC DOME	
16 - 10 QTY REQD	PART OR IDENTIFYING NO.	NOMINCLATURE OR DESCRIPTION	MATERIAL AND SIZE

LIST OF MATERIALS



Figure 29. Reflector Scale Model Tool during Fabrication

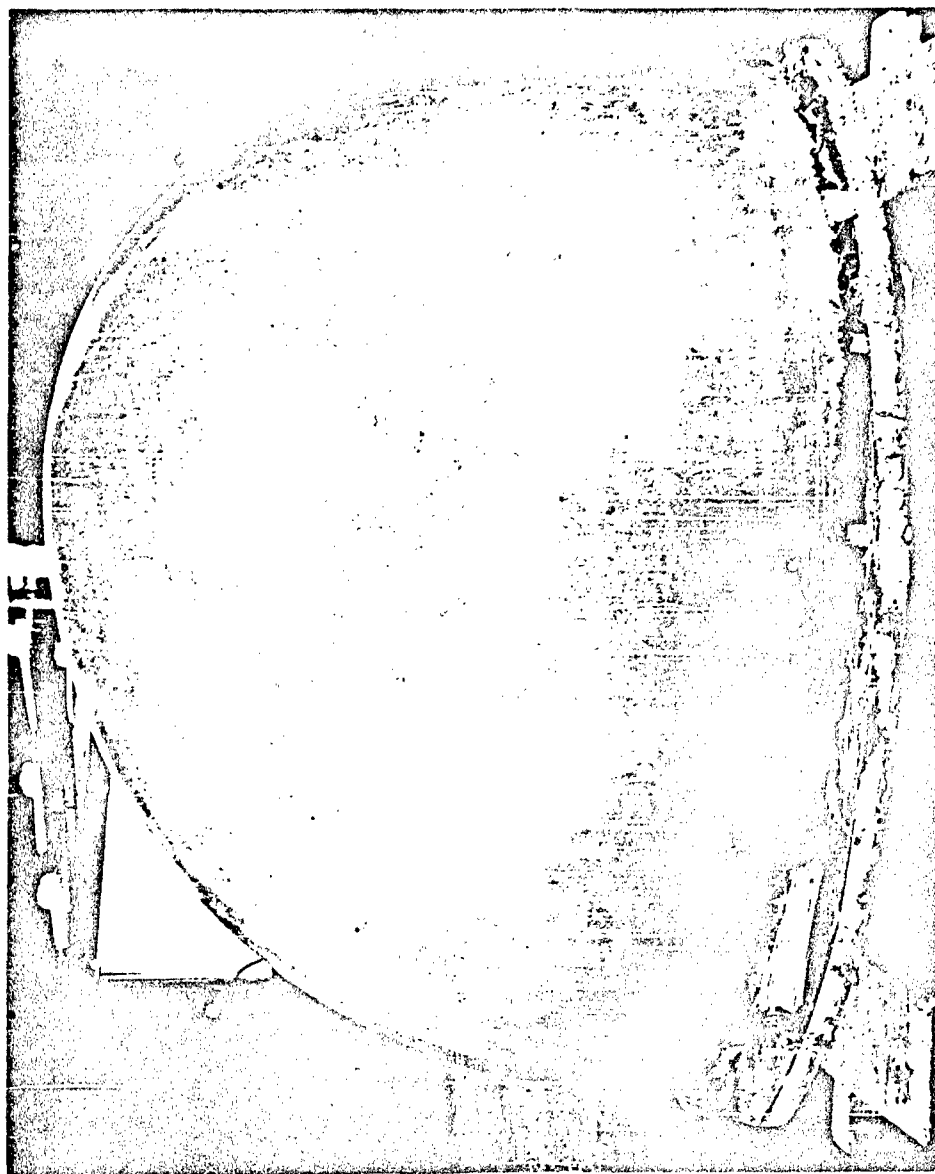


Figure 30. Radoflector Scale Model Tool Completed

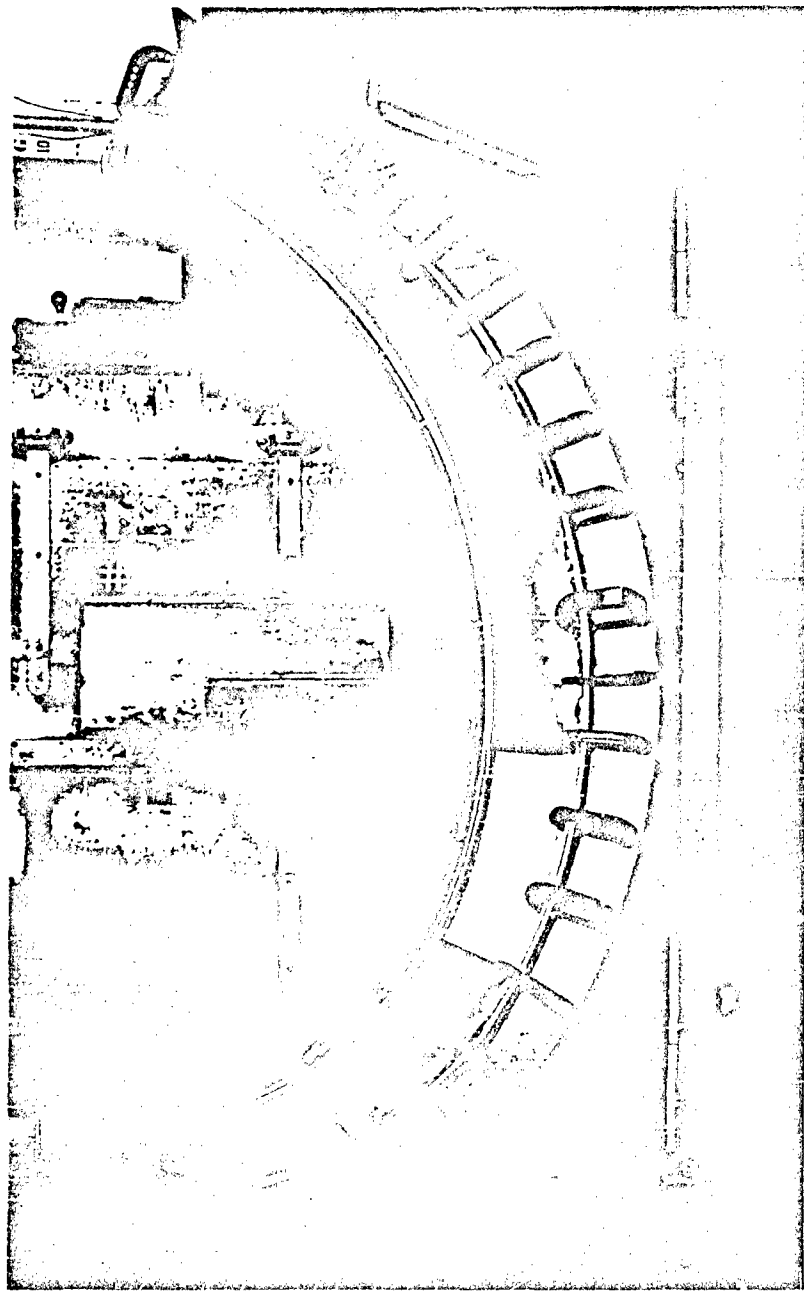


Figure 31. Preform Tool with Partial Core in Tool and Under Vacuum

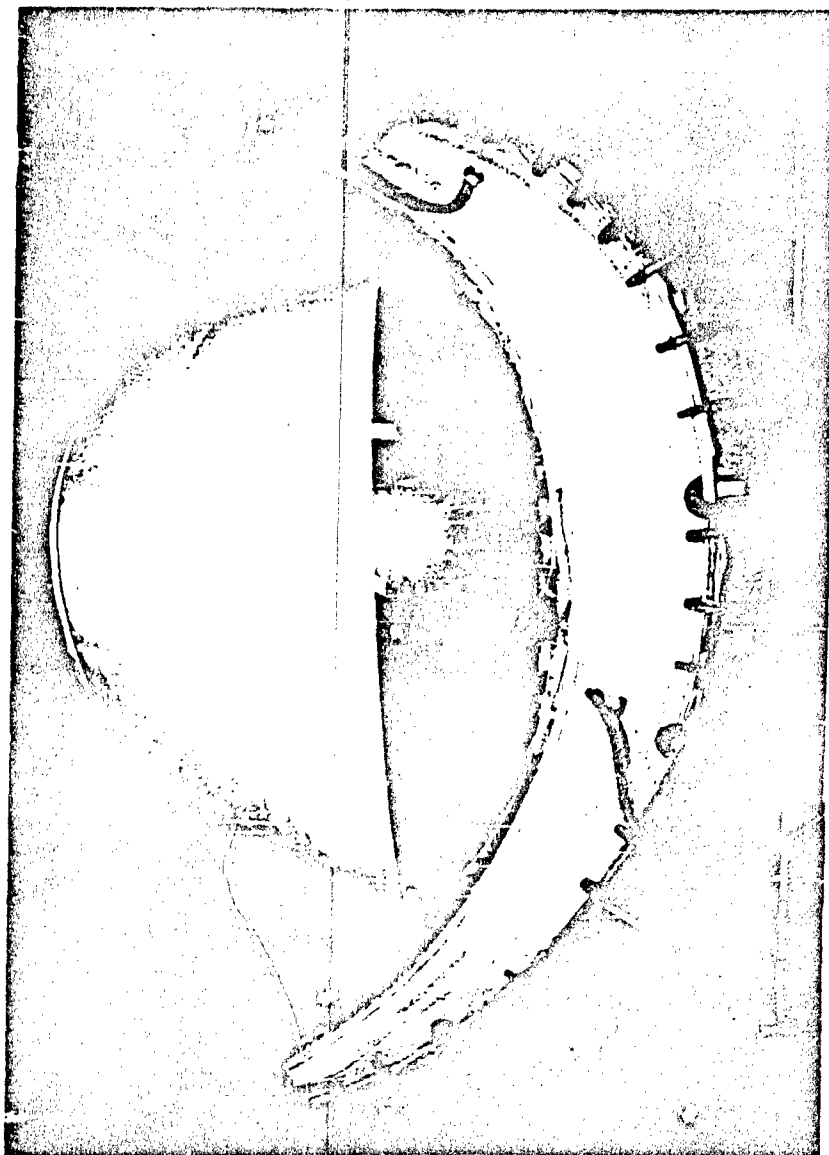


Figure 32. Preform Tool and Form Tool with Gores in Fabrication Process

heat sealing adhesive was used as the bonding agent. The two halves were then bonded together to make the complete Radoflector structure.

The seam construction presented the major problem in the assembly of the inflatable model. During fabrication, the heat sealing of the seams shrinks the laminate material in the seam area. This shrinkage causes a scalloping effect at the gore seams and wrinkling of the adjacent antenna fabric-film since the seams are shorter than the adjacent material because of shrinkage. After initial inflation, the wrinkling of material adjacent to the gore seams was still evident, indicating a near zero stress condition in this area with the majority of the load being in the seams.

In an attempt to improve this condition, the material next to the seams was shrunk with a hot iron of the same type used for making the original seams. This was done at all seams with the model inflated and was successful in eliminating practically all the wrinkles. Continued application of inflation pressure, after the above hot iron shrinking process, was successful in effecting a considerable improvement in the scalloping or indentation at the seams.

Subsequent to the assembly of the inflatable structure, the seaming technique was investigated further in an effort to eliminate the shrinkage problem and the resulting wrinkling and scalloping in the seam area. Seam samples have been made using butt splice strips made from pre-formed laminate material and a modified technique for applying the heat sealed adhesive. Very good results were obtained on sample seams made in this manner, indicating satisfactory elimination of the shrinkage characteristic encountered on the model.

D. Base Platform and Guy System

The base platform design is octagonal in shape, consisting of two 3/4-inch thick plywood skins spaced approximately four inches apart by eight radially spaced 2×4 's. Sixteen cantilevered outriggers are bolted to this main platform. Sixteen guy wires, to simulate full-scale configuration during model pattern tests, will be attached from the outriggers on the base to tabs on a support cap that fits over the top of the Radoflector model (see Figure 33).

E. Feed Support

The feed support is a cantilevered welded tubular strut with a sliding joint at the base to provide hand screw actuated vertical adjustment of the feed horn. The feed support is in turn mounted on a machine tool universal vice which provides precision two-axis lateral position adjustment. In addition, the tilt angle of the feed horn can be adjusted (see Figure 34). The above adjustments are provided so that the feed horn can be located in the optimum position with respect to the Radoflector surface during rf radiation pattern testing.

F. Entrance Air Lock

The entrance airlock consists of a fabric cylindrical sleeve that is attached to the base platform, a base plate, a pressure-sealed zipper entrance into the air lock, and a pressure-sealed entrance door in the base platform (see Figure 35).

G. Pressurization System

An existing portable electrically driven compressor system was utilized with suitable reducer valves to pressurize the Radoflector model. A liquid manometer was used to permit manual monitoring of the pressure during the pattern testing. Inflation pressure range was established to be between seven and nine inches of water. A pressure relief valve was provided in the base platform to protect the Radoflector from overpressure.

H. Testing

1. General

The scale model was analyzed both electrically and mechanically. To make a proper analysis, however, a comparison basis had to be established. This was accomplished electrically by fabricating a standard dish to the theoretical horizontal and vertical contours and mechanically by fabricating a vertical contour template to the theoretical vertical contour.

2. Standard Dish Tests

As stated previously, the feasibility of the Radoflector concept was established by comparing the test results of the scale model with the test results of an equivalent solid reflector in place of

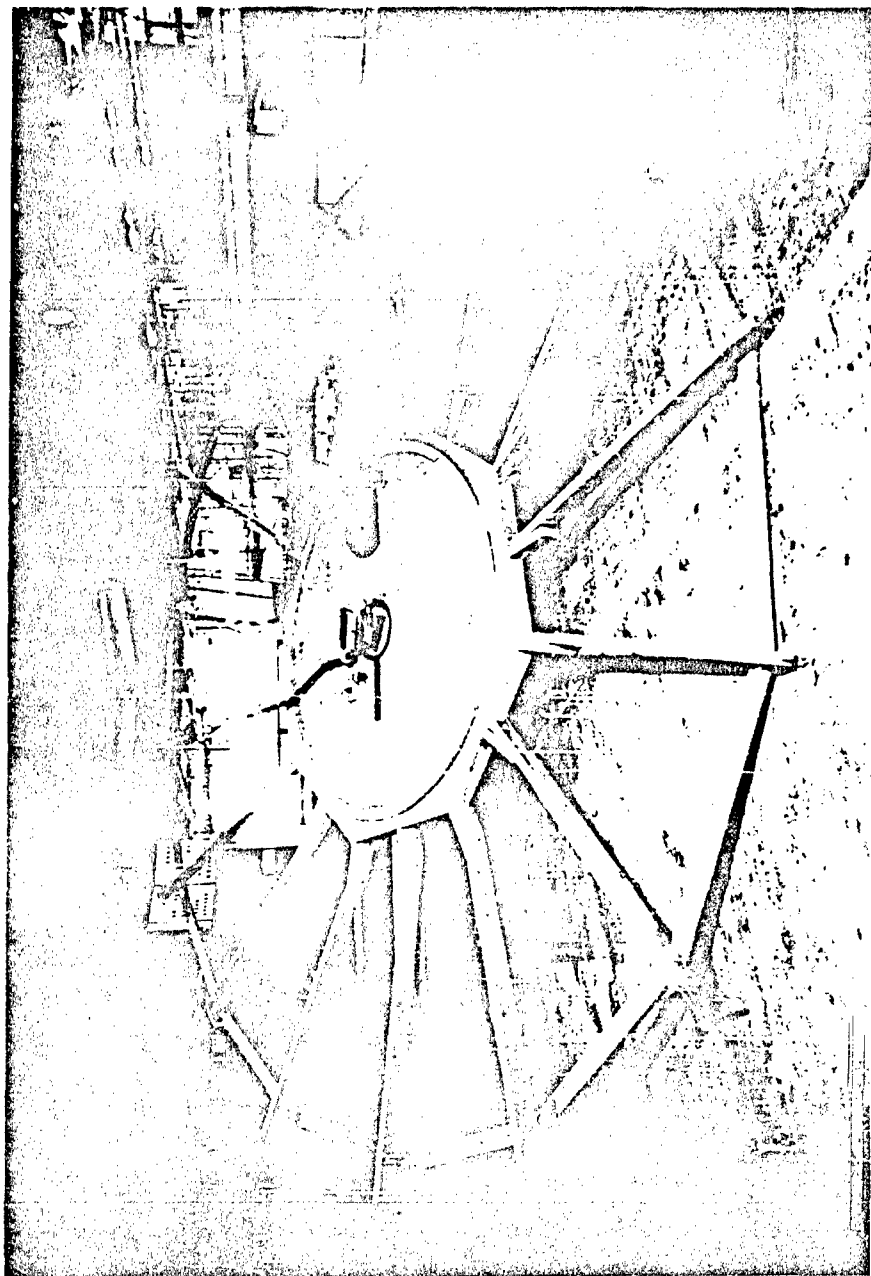


Figure 33. Scale Model Base Assembly

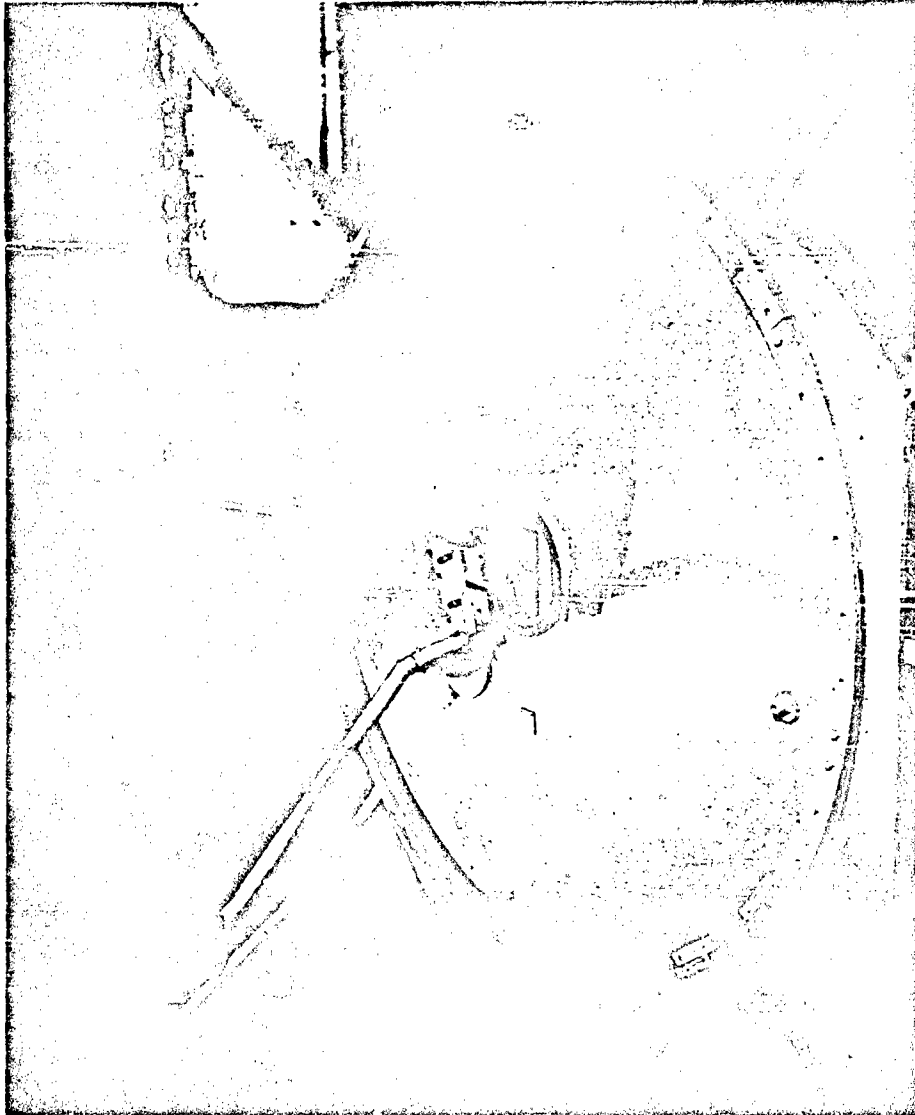


Figure 34. Base Assembly with Feed and Feed Adjustment Mounted

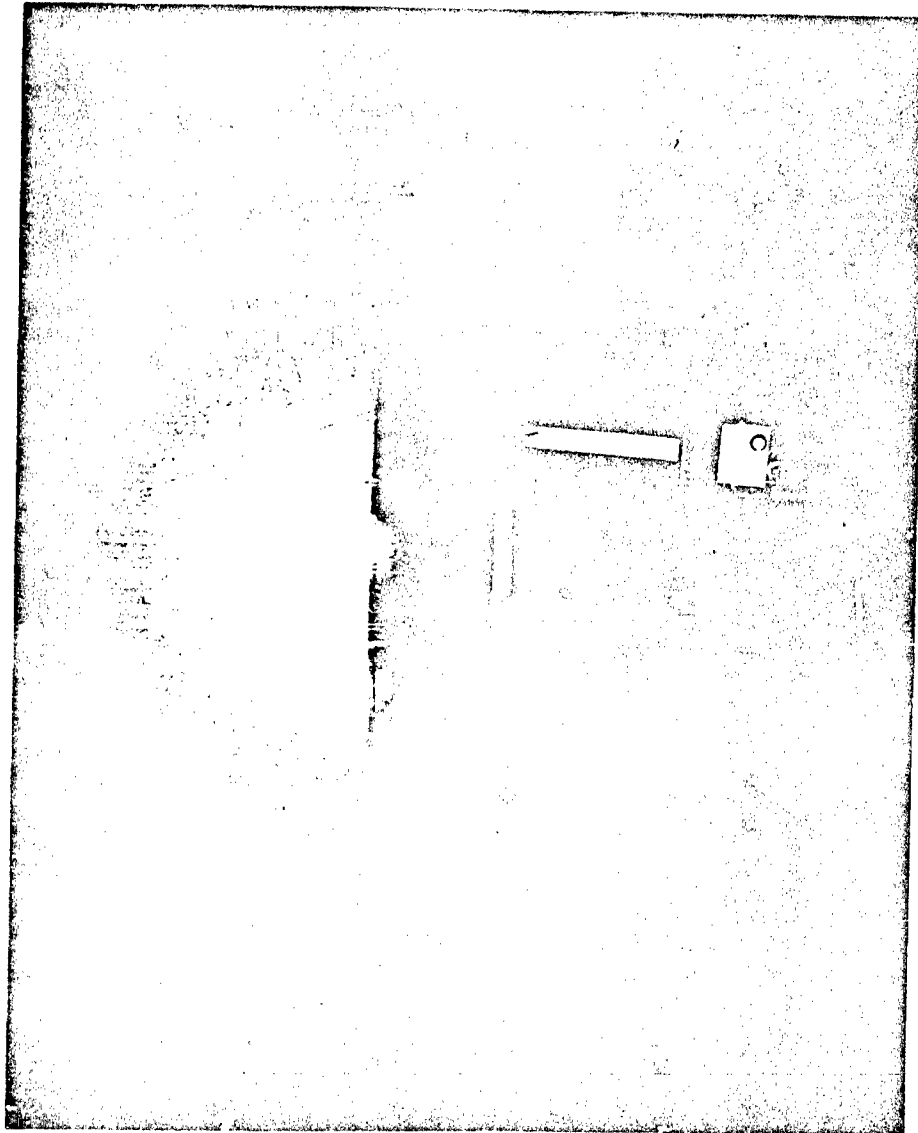


Figure 35. Scale Model with Entrance Air Lock Attached

the inflatable reflector surface, using the same feed and ground plane. The solid reflector, which is referred to as the standard dish, has an aperture equivalent to the portion of the inflatable reflector, which is illuminated with a taper greater than -14 db.

The standard dish horizontal and vertical contour was made from a special tool. The tool was fabricated from wood and plaster and accurately swept with a template cut to the contour of the universal dish. The standard dish was fabricated on the tool by laying up a reinforced laminate of fiberglass. After curing, the fiberglass was metal sprayed with zinc to obtain a reflective surface (see Figure 36). The standard dish was installed on the scale model base assembly in the same relative position that the inflatable structure reflector was in when inflated. The complete assembly was transferred to GAC's Wingfoot Lake Antenna Test Facility and installed on the silo test tower (see Figure 37).

The antenna pattern measurements were determined using a 960-foot antenna test range, with the transmitter and test antenna located 40 feet above ground level. The feed position was adjusted to obtain the best trade-off between azimuth and elevation patterns. Figure 38 shows the final feed position with respect to the contour coordinants. Figures 39 and 40 show the corresponding elevation and azimuth patterns at the center design frequency. The gain of the antenna was determined using a standard gain horn. The following electrical characteristics were determined:

Gain (G) = 31.35 db at $f_0 = 9.08$ gc.

Half power azimuth beamwidth (α) = 2 degrees at $f_0 = 9.08$ gc.

Side lobe level = -19 db at $f_0 = 9.08$ gc at elevation angle of maximum radiation intensity.

Elevation pattern: $\text{csc}^2 \theta$ from 9 to 30 degrees within ± 2 db at $f_0 = 9.08$ gc.

Table 9 gives side lobe levels and beamwidths (α) at the peak of the elevation pattern; deviations from the theoretical $\text{csc}^2 \theta$ elevation pattern between 0 and 30 degrees; and gain figures at the test frequencies 9.08, 8.72, and 9.44 gc.

TABLE 9.
Standard Dish Test Results

Frequency (gc)	Gain (db)	Azimuth Beamwidth at Peak of Elevation Pattern (Degrees)	Sidelobe Level (db)	Deviation From $\text{csc}^2 \theta$ Elevation Pattern (db)
9.08	31.35	2.0	-19.0	± 2.0
9.44	30.45	2.0	-19.25	± 2.0
8.72	32.50	2.0	-19.0	± 2.0

It should be noted that the elevation patterns exhibit an unusually high secondary lobe at an elevation angle of 13 degrees. The deviation of ± 2 db from the $\text{csc}^2 \theta$ curve was attributed to this lobe.

The deviation from the $\text{csc}^2 \theta$ curve was considerably less than ± 2 db in the region from $\theta = 13$ degrees to $\theta = 30$ degrees.

The results did not quite meet the desired design objective, but the data can be compared to the scale model Radoflector to prove the feasibility of the Radoflector concept.

The test results were less than the desired objectives because of the following factors: There was some warpage of the standard dish, particularly in the area of the upper two corners. The corners warped inward either during cure or metal spraying or both. This resulted in some deviation from the desired vertical contour, particularly in the area of the outer edges near the upper corners where the deviation was approximately 1/4 inch. Also this warpage causes the

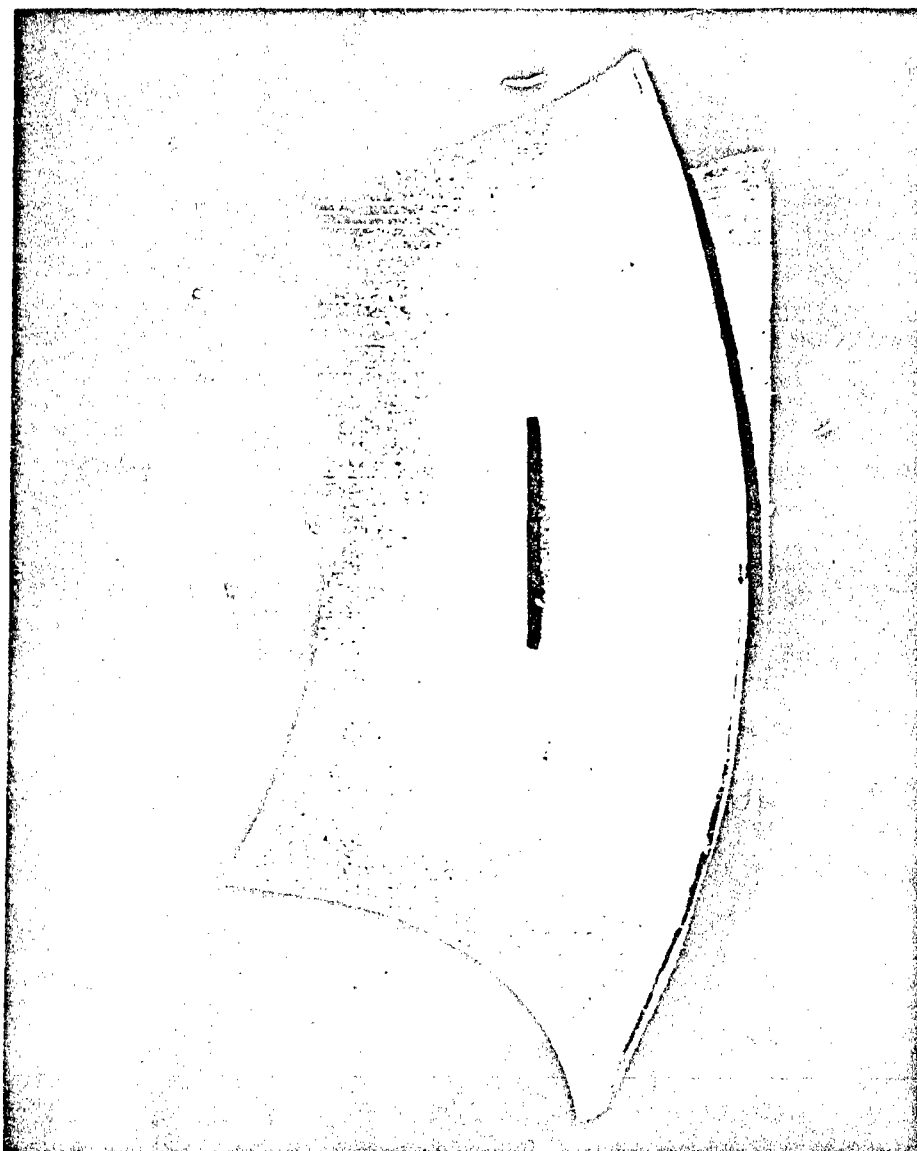


Figure 36. Standard Dish

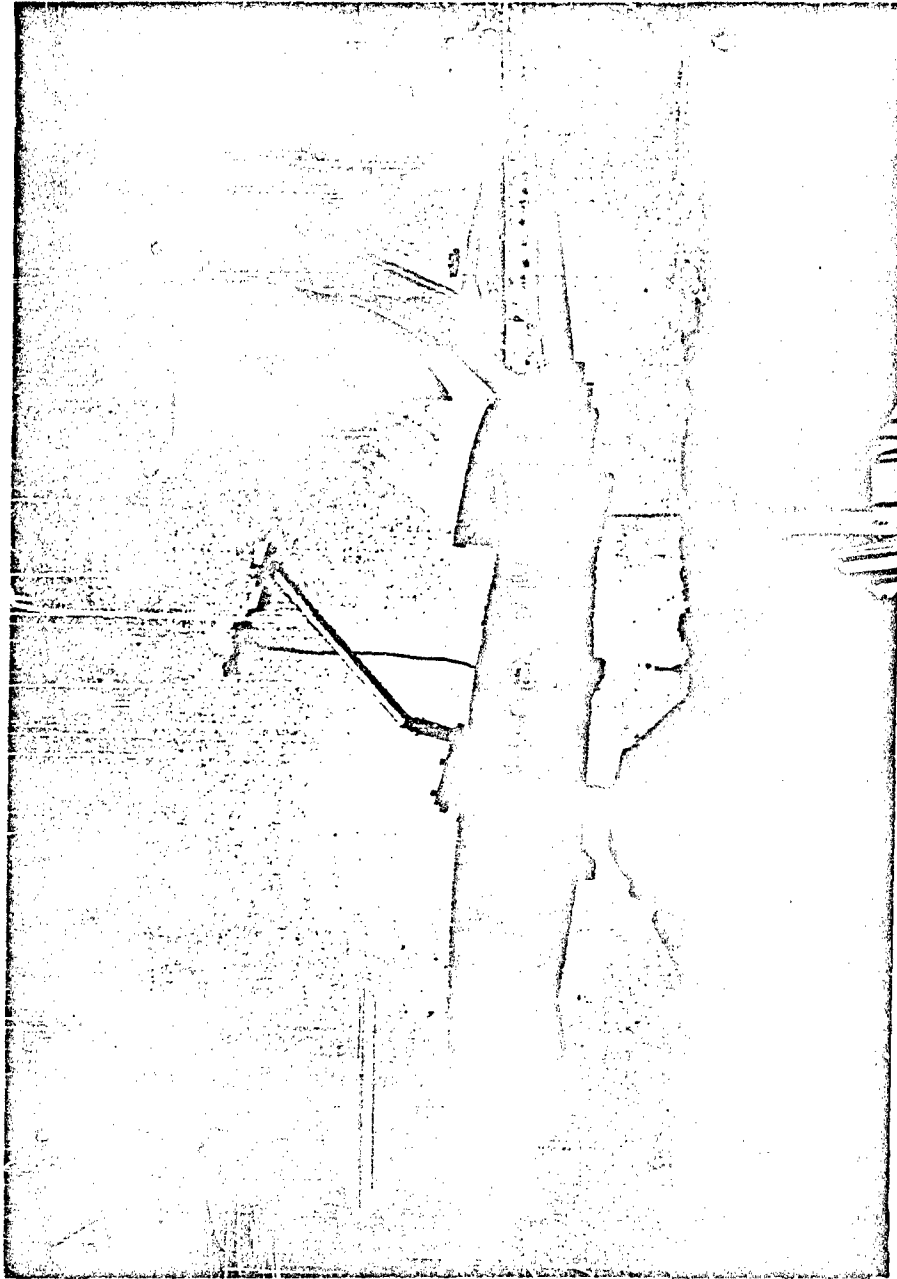


Figure 37. Standard Dish Mounted on Radaflector Support Base on Test Range

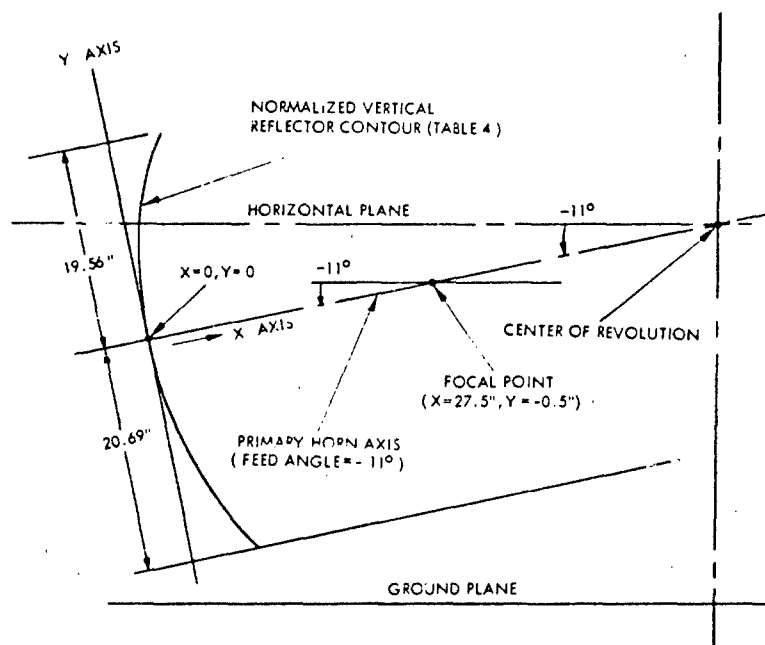


Figure 38. Feed Position Parameters Determined for Standard Dish Tests

horizontal radii to be sharper than desired near the upper edge where the corners were warped inward approximately $3/32$ inch.

The variation from the established vertical contour contributes to the vertical pattern deviation. The high secondary lobe at 13 degrees probably results from this condition. Also the change in horizontal curvature, due to the warpage, tends to cause the horizontal and vertical focal points to be separated from each other farther than anticipated. The feed position was adjusted to yield the best compromise between the horizontal and vertical patterns; however, the results were not as satisfactory as would have been expected if the horizontal and vertical focal points had been more nearly coincident.

3. Scale Model Tests

The standard dish that was used in the test previously described was replaced with the scale model Radoflector. The same feed and support structure were used in both tests. Figure 41 shows the inflated Radoflector mounted on the antenna test tower. The feed position was adjusted slightly (from the position determined from the standard dish tests) to achieve the best possible elevation and azimuth patterns. Figure 42 shows the final feed position with respect to the contour coordinates. Figures 43 and 44 show the corresponding elevation and azimuth patterns at the center design frequency. The gain of the antenna was determined in the same manner as in the standard dish tests, using a standard gain horn. The following electrical characteristics were determined:

Gain (G) = 30.9 db at $f_0 = 9.08$ gc.

Half-power azimuth beamwidth (α) = 2.1 degrees at $f_0 = 9.08$ gc.

Side lobe level = -15 db at $f_0 = 9.08$ gc at elevation angle of maximum radiation intensity.

Elevation pattern: csc^2 from 9 degrees to 30 degrees within ± 1.5 db at $f_0 = 9.08$ gc.

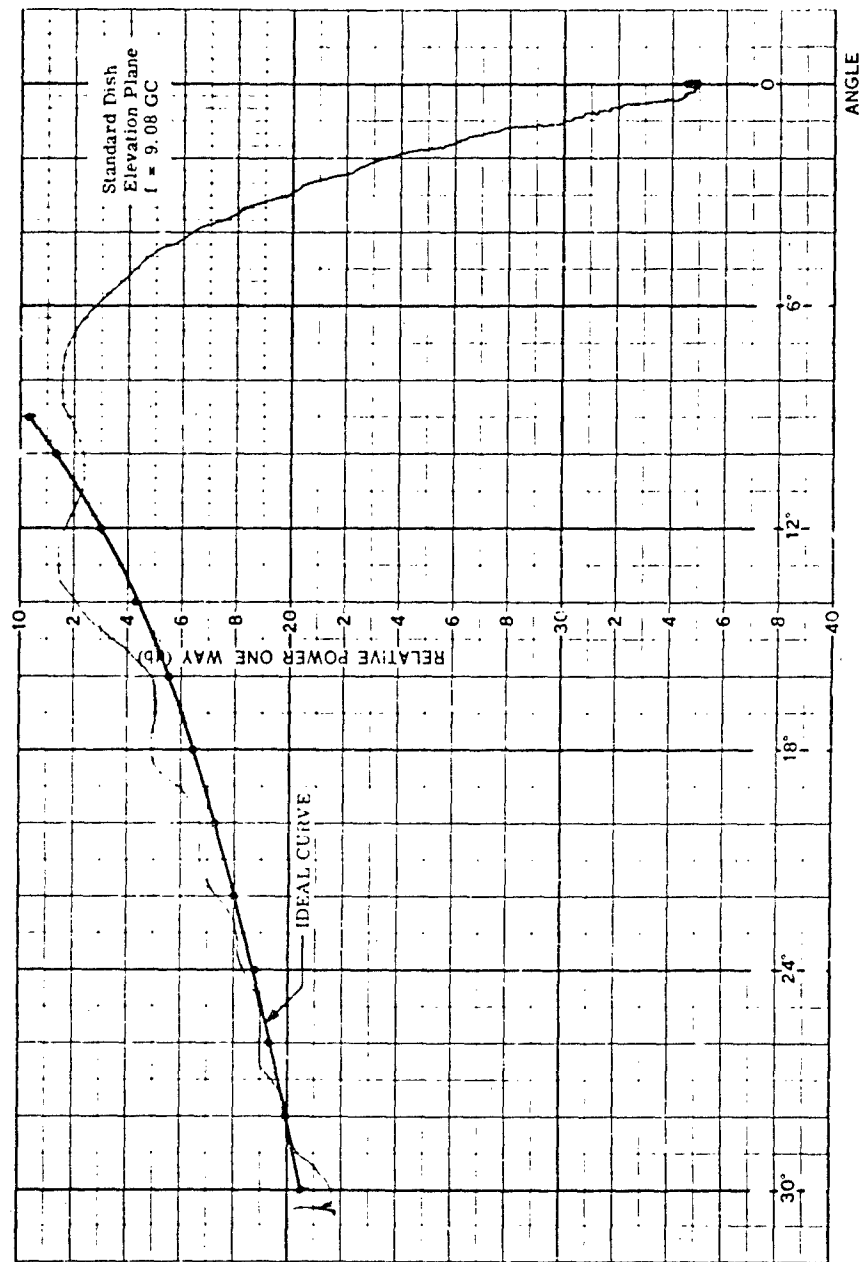


Figure 39. Standard Dish Elevation Pattern at Center Frequency

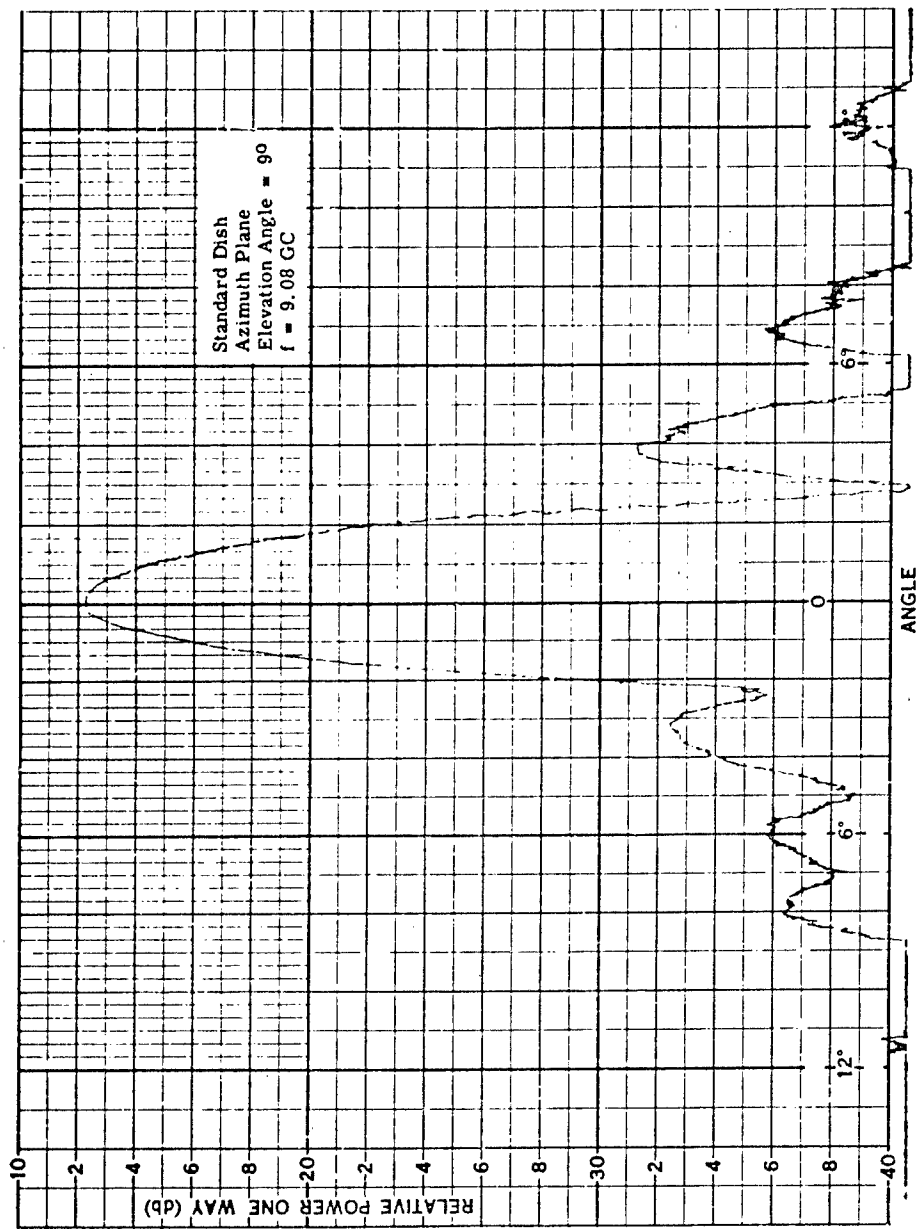


Figure 40. Standard Dish Azimuth Pattern at Center Frequency (Elevation Angle = 9 Degrees)

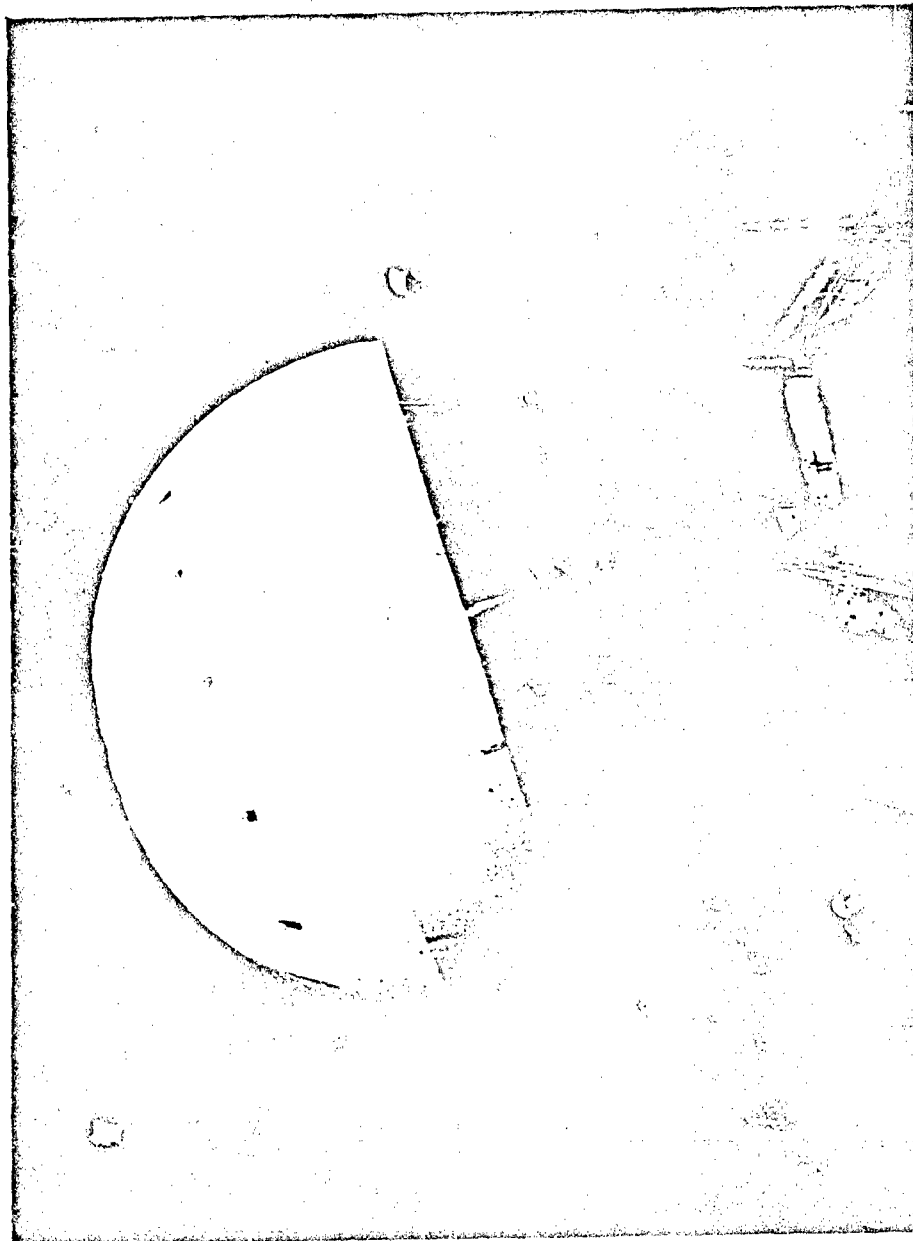


Figure 41. Scale Model Radoflector on Test Site

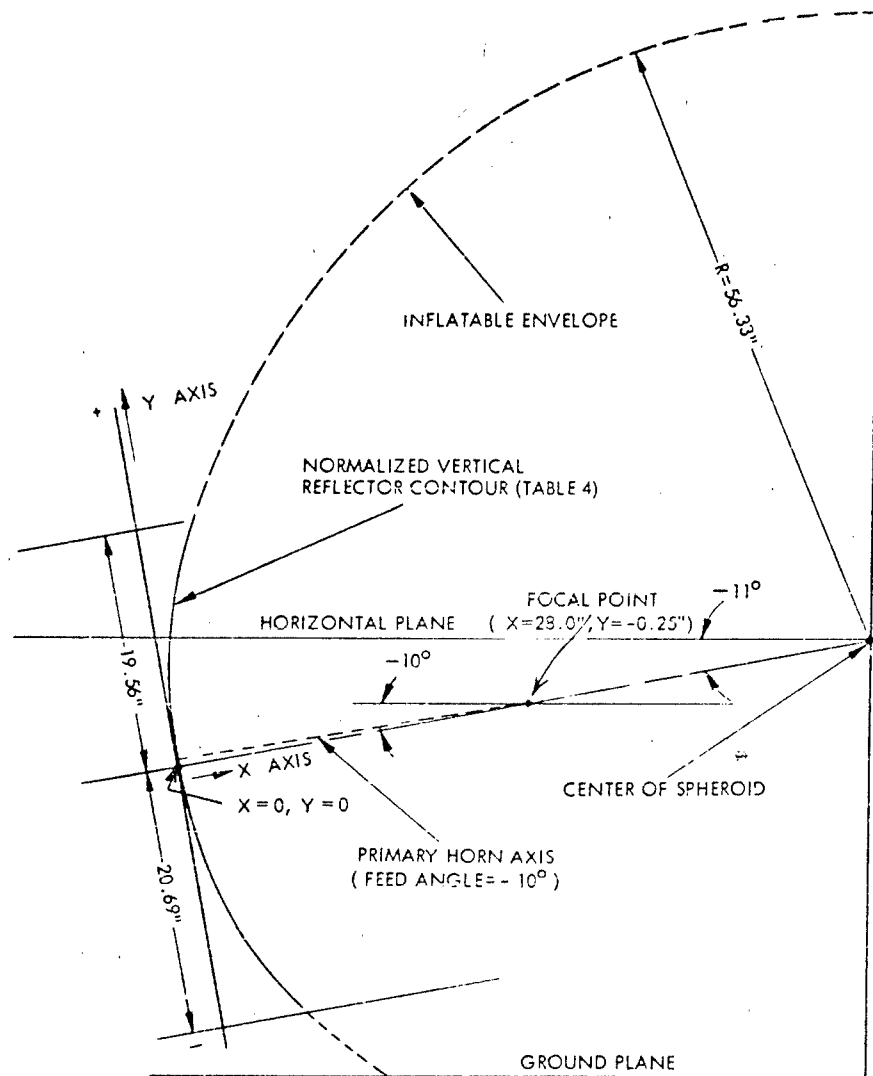


Figure 42. Feed Position Parameters Determined from Scale Model Radoflector Tests

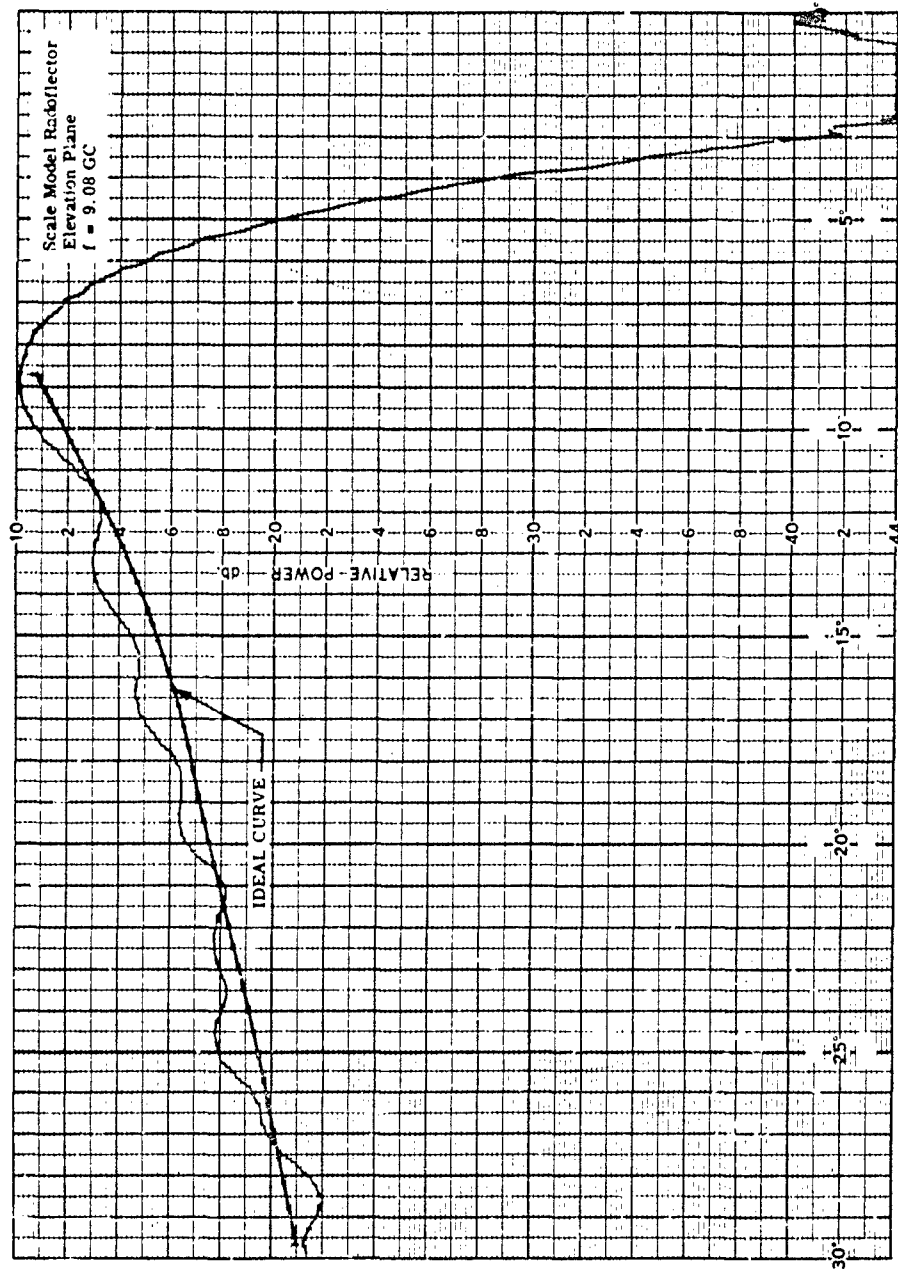


Figure 43. Scale Model Radreflector Elevation Pattern at Center Frequency

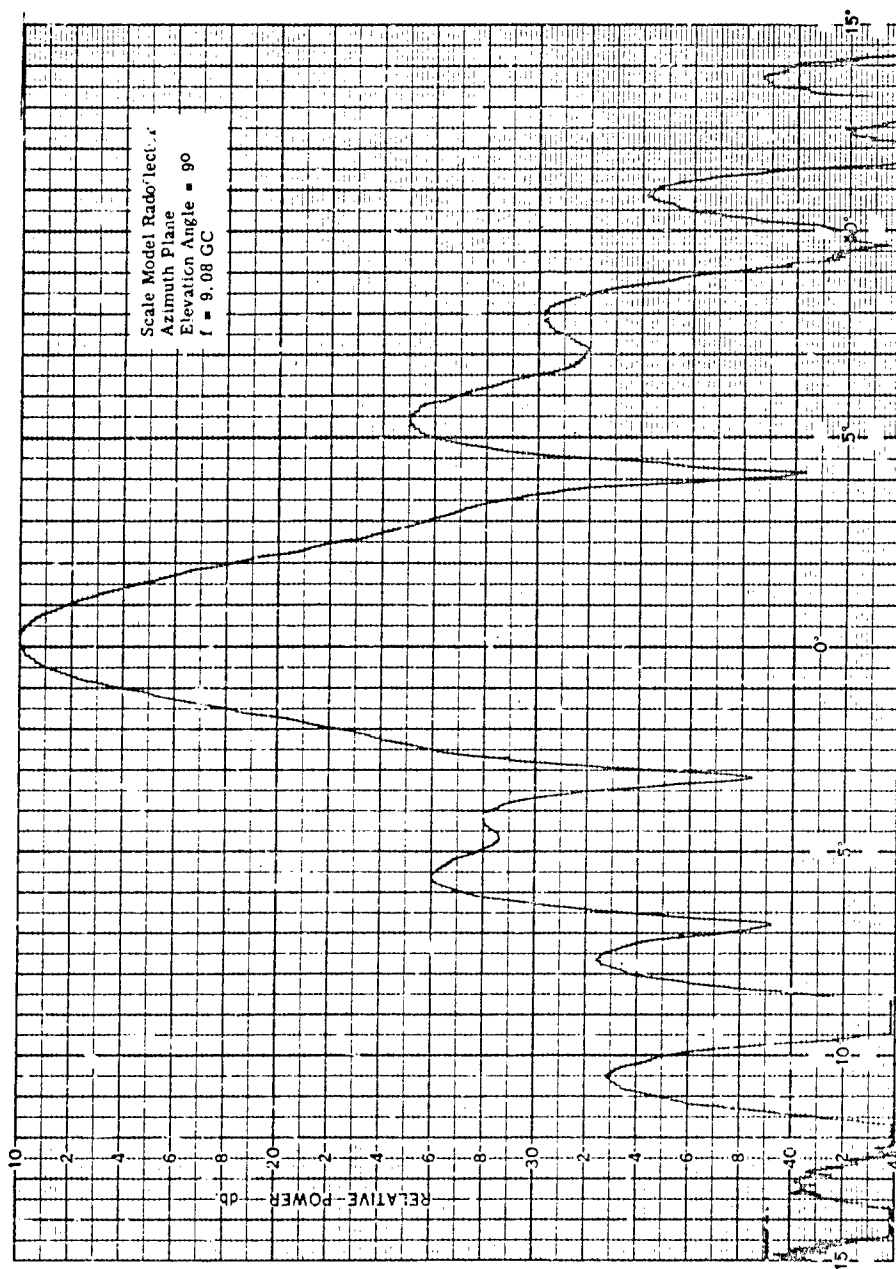


Figure 44. Scale Model Radoflector Azimuth Pattern at Center Frequency (Elevation Angle = 9 Degrees)

Table 10 gives the deviations from the theoretical $\csc^2 \theta$ elevation pattern between 0 and 30 degrees, side lobe levels, gain, and beamwidths (α) at the peak of the elevation pattern at test frequencies 9.08, 8.72, and 9.44 gc.

TABLE 10.
Scale Model Radoflector Test Results

Frequency (gc)	Gain (db)	Azimuth Beamwidth at Peak of Elevation Pattern (Degrees)	Sidelobe Level (db)	Deviation From $\csc^2 \theta$ Elevation Pattern (db)
9.08	30.9	2.1	-15.0	+1.5
9.44	-	2.1	-14.8	± 1.8
8.72	-	2.2	-15.0	± 1.8

It is interesting to note that the unusually high secondary lobe, which occurred at an elevation angle of 13 degrees in the standard dish test, diminished. It seems apparent that the inherent vertical curvature characteristics of the inflatable surface has eliminated the appearance of a warped surface, which was the case using the standard dish.

The uniformity of the reflector surface was determined by taking elevation and azimuth patterns with the feed position changed in azimuth in increments of 45 degrees. In this manner, various segments of the reflector surface were illuminated, and the variance in resultant patterns was observed. Table 11 gives the resultant azimuth beamwidth and side lobe characteristics as the feed position is rotated in azimuth.

TABLE 11.
Variation of Electrical Characteristics of Scale Model Radoflector as
Feed Position Is Varied in Azimuth ($f = 9.08$ GC)

Feed Position Variation in Azimuth (Degrees CW)	Azimuth Beamwidth at Peak of Elevation Pattern (Degrees)	Sidelobe Level (db)
0	2.1	-15.0
45	1.9	-11.8
90	2.0	-14.4
135	1.8	-10.6
180	2.5	-14.6
225	2.1	-12.0*
270	2.3	-12.4
315	1.9	-14.0

*A severe coma lobe appears in the main lobe with a value of -6.3 db at the 225-degree feed position.

4. Vertical Contour Evaluation

A template was used to check the Radoflector vertical contour. The template was fabricated to the theoretically calculated vertical contour and was mounted on a support that provided vertical, horizontal, and tilt adjustment.

Certain checks of the Radoflector contour were made prior to far field rf tests; however, after completion of the rf tests a more detailed evaluation of the scale model was made. The data obtained during this evaluation is given in Table 12.

To measure the contour deviation the template was mounted as shown in Figure 45 at one of the even numbered outrigger arms or station numbers shown in Figure 46. The template was adjusted until the upper and lower edges of the template were 0.50 inch from, and in line with, the upper and lower limits of the Radoflector reflective surface. (In Table 12 the dimensions +19.56 inches and -20.69 inches define the upper and lower limits, from $Y = 0$, of the reflector surface respectively.)

Measurements that define the Radoflector deviation from the template contour were then taken at $Y = +10$ inches, $Y = 0$, and $Y = -10$ inches. To supplement these measurements additional measurements were taken. These include the angular position of the template, the radial position of the template, and the gore seam indentation of the top, center, and bottom of the reflective surface.

The measurements defined above were made and recorded at every even numbered station around the complete circumference of the Radoflector.

An analysis of the data in Table 12 reveals that, even though the gore seaming problem outlined in Section 4, paragraph C-5, caused a scalloping of the inflatable structure, the deviations from the maximum surface tolerance of ± 0.081 inch is generally not severe over most of the gore sections. Because a solution to the gore seam problem has already been determined and tested on sample sections, it is believed that for future units the contour tolerance of $\lambda/16$ can be held over the entire surface.

An observation of the deviations of the bottom edge of the template horizontal position from the theoretical position of 44.00 inches shows that the inflatable structure diameter is undersize at this point by 1.25 inches. (The figure of 1.25 inches is an average of the deviations shown in Table 12.) This undersize condition is attributed primarily to the gore seam scalloping effect and would not be appreciable in future units.

5. Analysis of the Far Field Test Results

The results of the test program demonstrate that the Radoflector principle is capable of closely matching the performance of a solid reflector antenna. Comparisons between the scale model and the standard dish are as follows (refer to Tables 9 and 10):

- (1) The scale model Radoflector achieved the desired $\text{csc}^2 \theta$ elevation pattern from 9 to 30 degrees within ± 1.5 db. The standard dish did not quite achieve ± 1.5 db, but rather achieved +2.0 db because of warpage at the corners of the reflector.
- (2) At center frequency (9.08 gc) the difference in measured gain between the scale model and the standard dish was less than 0.5 db. Both reflectors exceeded the goal of 30-db gain by approximately 1 db.
- (3) The measured side lobe levels of the scale model were higher than those of the standard dish. At the elevation angle of peak radiation intensity, the scale model side lobe level was -15 db and the standard dish side lobe level was -19 db, or -4 db lower than the scale model. Neither reflector achieved the goal side lobe level of -25 db.

The uniformity tests conducted on the reflecting surface indicated that the principal effect of non-uniformity is an increase in side lobe level and degradation of azimuth pattern. The elevation pattern was affected, but to a lesser degree by the non-uniform surface. The respective elevation and azimuth patterns are contained in Appendix A.

With the exception of side lobe characteristics, the feasibility of efficiently producing a desired shaped beam radiation pattern using the inflatable Radoflector concept has been shown. The excessive side lobe levels have been attributed mainly to the horizontal contour deviations that occurred because of the gore seam indentation effect and aperture blockage due to the feed support.

The test results of the scale model have indicated areas in which electrical performance can be improved by moderate design modifications. For example, by reducing the 10-db beamwidth of the primary horn from 82 to 73 degrees, a reduction in side lobe level can be realized and has been

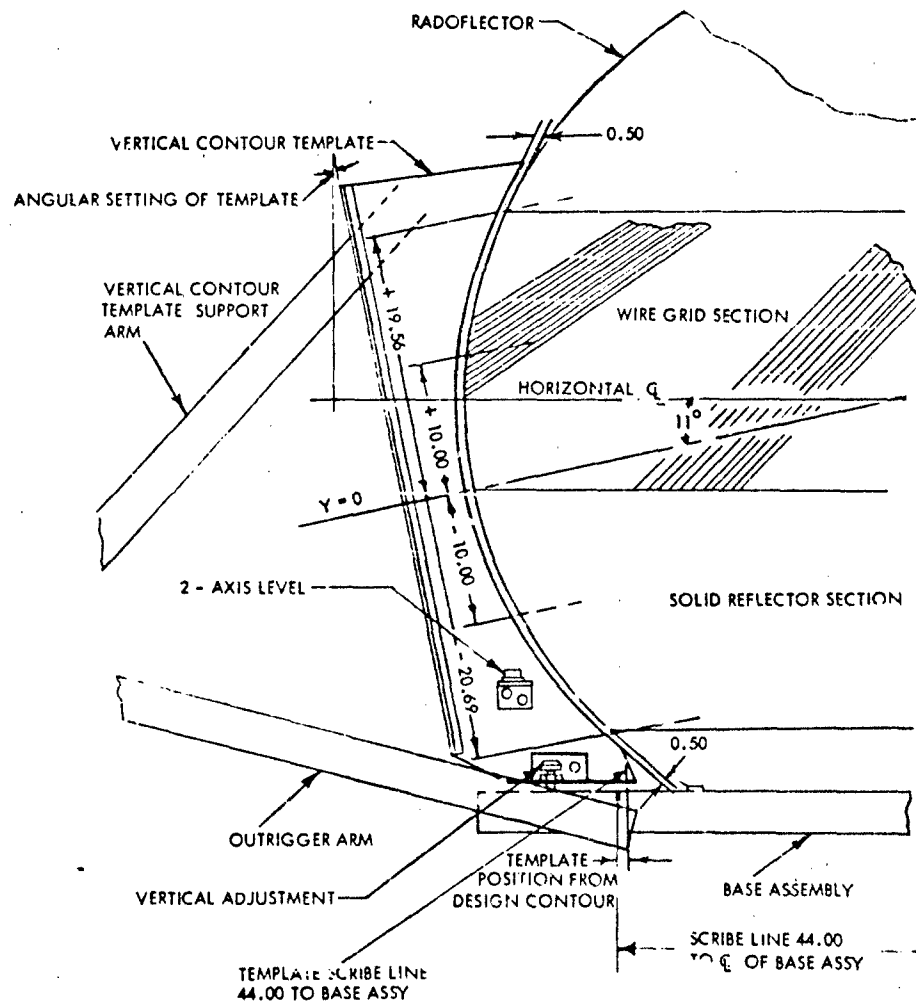


Figure 45. Scale Model Contour Template Mounting

TABLE 12.
Scale Model Radreflector Contour Measurements

Vertical Template Location		Core Seam Indentation			Vertical Contour Template Angle**	Inflation Pressure	Deviation of Bottom Edge of Template from 44.00 Inch Radius	Measurement Location along Vertical Edge of Contour Template	Deviation from Contour Template
Sta No. *	Core No. *	Position	Seam (in.)	Seam (in.)					
2	Between Core Seams No. 1 and 2	Y = +19.56 in.	1	2	11.5 degrees	7.2 in. of H ₂ O	-0.50 in.	Y = +19.56 in.	0
		Y = 0	0.064	0.032				Y = +13.00 in.	+0.064 in.
		Y = -20.69 in.	0.064	0.064				Y = 0	+0.064 in.
4	On Core Seam No. 3	Y = +19.56 in.	3		11.5 degrees	7.2 in. of H ₂ O	-0.50 in.	Y = +19.56 in.	0
		Y = 0	0.064					Y = +10.00 in.	0
		Y = -20.69 in.	0.032					Y = 0	+0.032 in.
6	Between Core Seams No. 4 and 5	Y = +19.56 in.	4	5	11.0 degrees	7.2 in. of H ₂ O	-0.62 in.	Y = +19.56 in.	0
		Y = 0	0.096	0.096				Y = +10.00 in.	+0.064 in.
		Y = -20.69 in.	0	0.064				Y = 0	+0.064 in.
8	On Core Seam No. 6 (A Closing Seam)	Y = +19.56 in.	6		11.0 degrees	7.2 in. of H ₂ O	-0.75 in.	Y = +19.56 in.	0
		Y = 0	0.064					Y = +10.00 in.	+0.125 in.
		Y = -20.69 in.	0.064					Y = 0	+0.156 in.
10	Between Core Seams No. 7 and 8	Y = +19.56 in.	7	8	11.0 degrees	7.2 in. of H ₂ O	-0.50 in.	Y = +19.56 in.	0
		Y = 0	0.064	0.064				Y = +10.00 in.	+0.125 in.
		Y = -20.69 in.	0.032	0.125				Y = 0	+0.125 in.

* See Figure 15

** See Figure 13

TABLE 12.
Scale Model Radoflector Contour Measurements (Continued)

Sta No. *	Vertical Template Location	Gore No. *	Gore Seam Indentation			Vertical Contour Template Angle**	Inflation Pressure H_2O	Deviation of Bottom Edge of Template from 44.00 Inch Radius	Measurement Location along Vertical Edge of Contour Template	Deviation from Contour Template
			Position	Seam (in.)	Seam (in.)					
12	On Gore	9	Y = +19.56 in. Y = 0 Y = -20.69 in.	0.064 0.064 0.096	9	11.0 degrees	7.2 in. of H_2O	-0.62 in.	Y = +19.56 in. Y = +10.00 in. Y = 0 Y = -10.00 in. Y = -20.69 in.	0 0 +0.032 in. +0.032 in. 0
14	Between Gore Seams No. 10 and 11		Y = +19.56 in. Y = 0 Y = -20.69 in.	0.094 0.125 0.218	10 11 12.5	12.0 degrees	7.2 in. of H_2O	-0.75 in.	Y = +19.56 in. Y = +10.00 in. Y = 0 Y = -10.00 in. Y = -20.69 in.	0 +0.060 in. +0.125 in. +0.090 in. 0
16	On Gore Seam No. 12 (A Closing Seam)		Y = +19.56 in. Y = 0 Y = -20.69 in.	0.069 0.069 0.069	12	12.0 degrees	7.2 in. of H_2O	-0.68 in.	Y = +19.56 in. Y = +10.00 in. Y = 0 Y = -10.00 in. Y = -20.69 in.	0 +0.032 in. 0 +0.150 in. 0

* See Figure 46.

** See Figure 45.

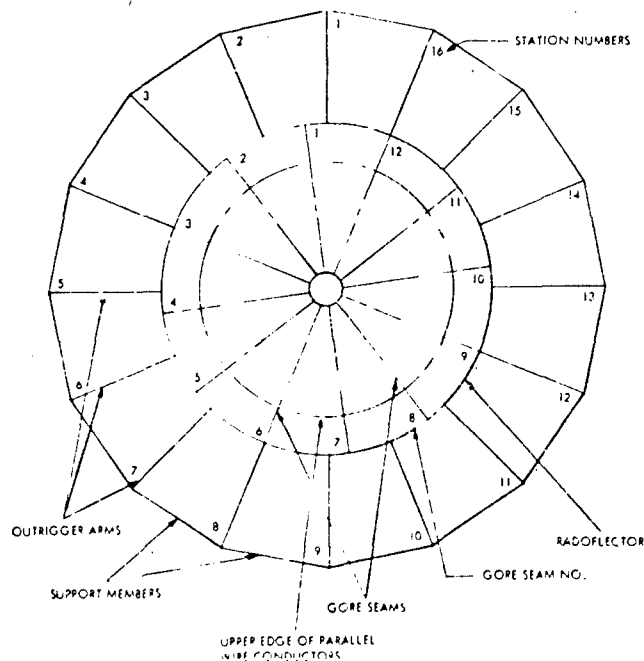


Figure 46. Scale Model Contour Measurement Locations

incorporated in the finalized full-scale design. In addition a more significant reduction in side lobe level can be realized by reducing the aperture blockage of the antenna system.

It was stated in paragraph H-4 that for future units it is believed that the fabrication contour tolerance of $\lambda/16$ can be held over the entire surface. As a result a significant azimuth pattern improvement should be realized with side lobes in the order of -19 db. The elevation and azimuth patterns should also be relatively independent of the rotational position of the feed.

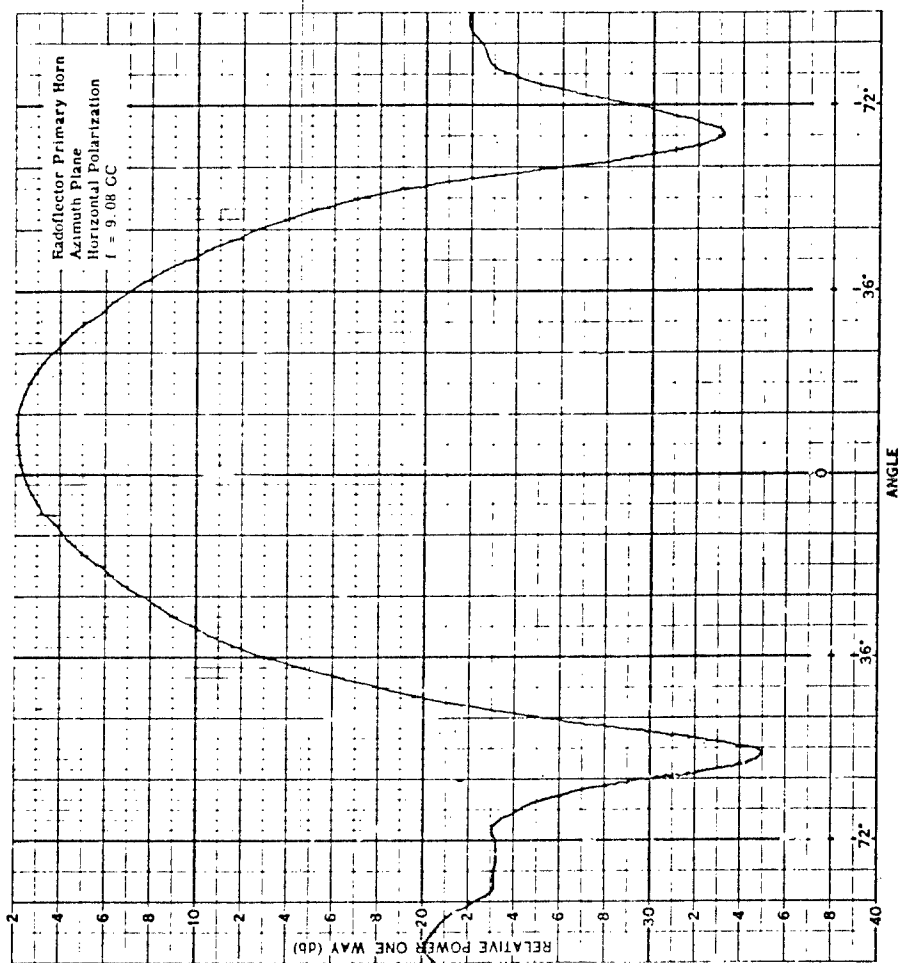
5. CONCLUSIONS AND RECOMMENDATIONS

The results of the engineering study and scale model testing have demonstrated that an inflatable structure can be fabricated to a specific contour and maintain this contour after inflation, that an inflatable structure can be surfaced with a grid of closely spaced parallel conductors or dipoles to form a reflector that does achieve specified radiation parameters, and that this completed inflatable structure (Radoflector) can be installed in a practical hardened enclosure to answer the military need for a survivable emergency antenna system.

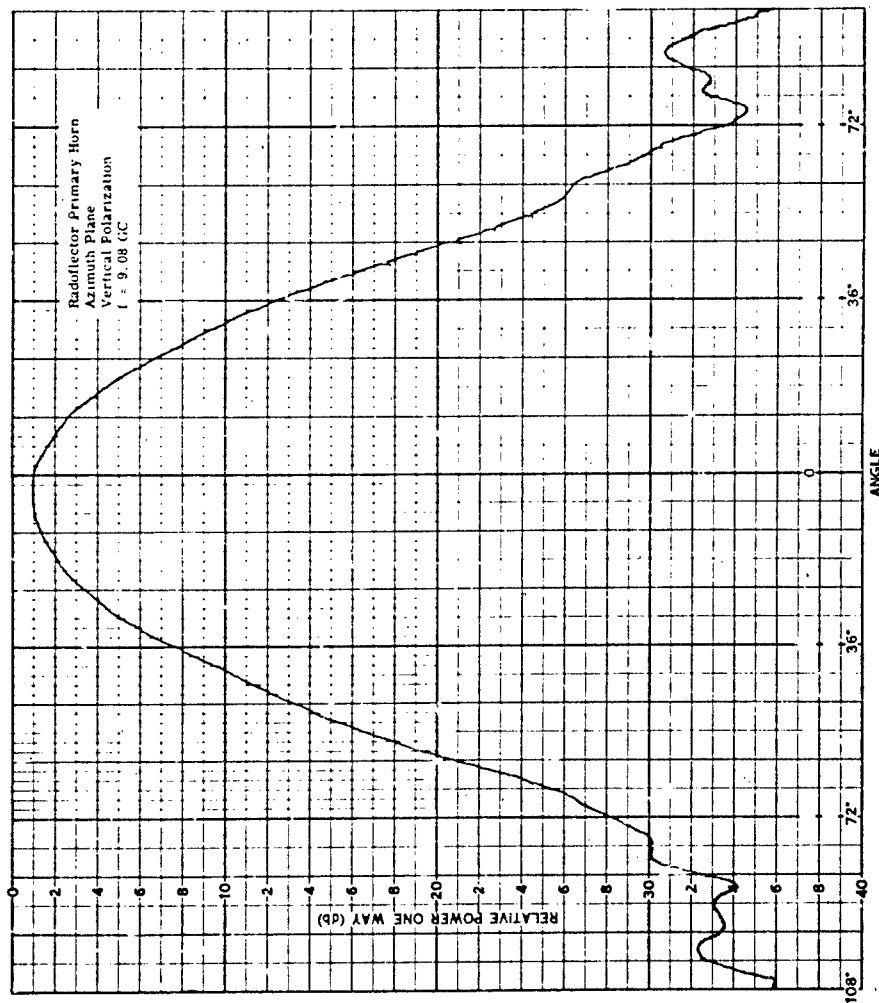
Installed as a ground control intercept or return to base communications antenna, in the environs of a missile silo complex as an emergency communications (troposcatter or microwave) system, or as an emergency search radar system in the aircraft air defense environment, it will be capable of erection and operation without external resources immediately following a devastating nuclear blast.

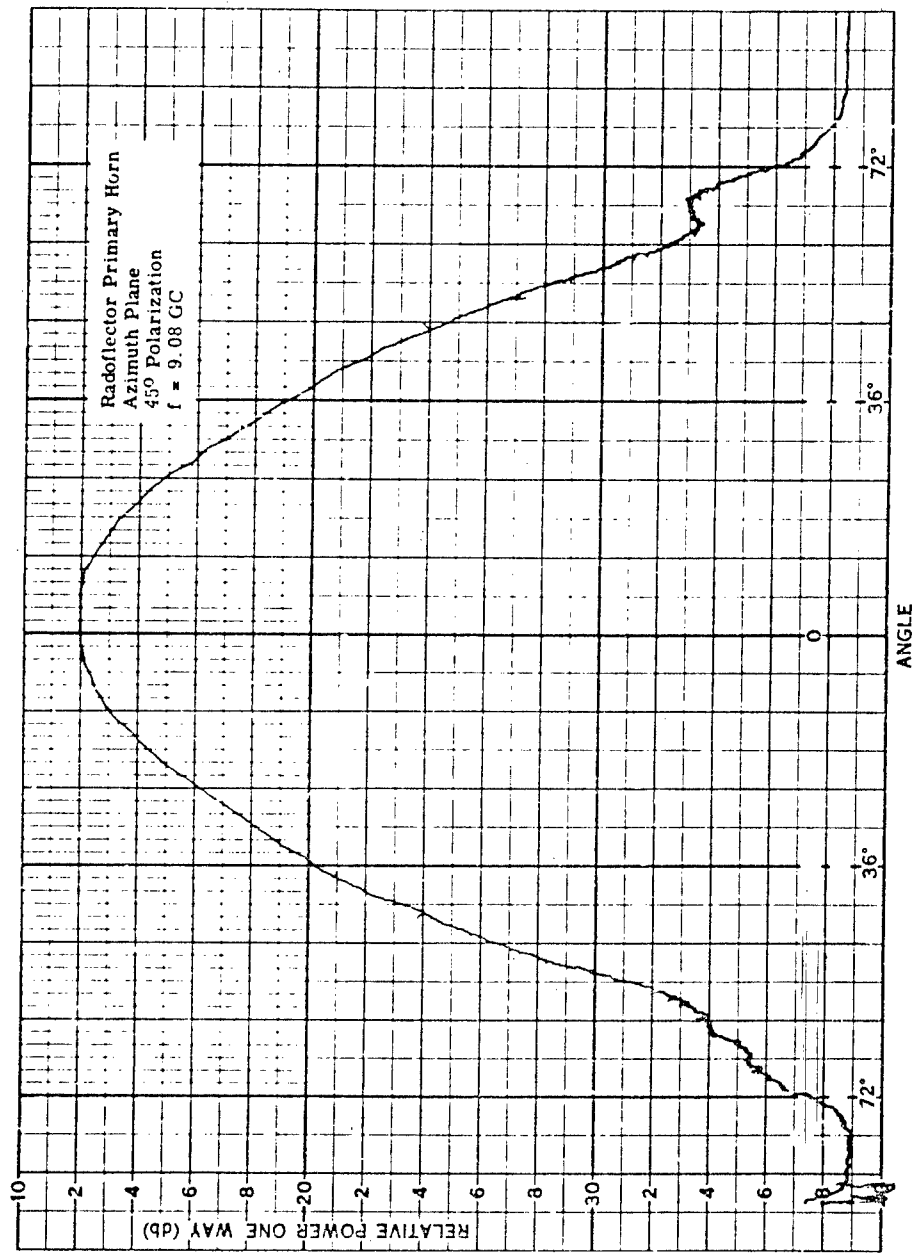
It is recommended that the Air Force proceed with the design and fabrication of an engineering service test model of the post-attack antenna system described herein and also included in the prototype design data (Reference 5). Particularly, it is recommended that immediate effort be applied to the materials test program outlined in Section 3 to select the best combination of high strength, lightweight, inflatable materials.

APPENDIX A
ANTENNA TEST PATTERNS

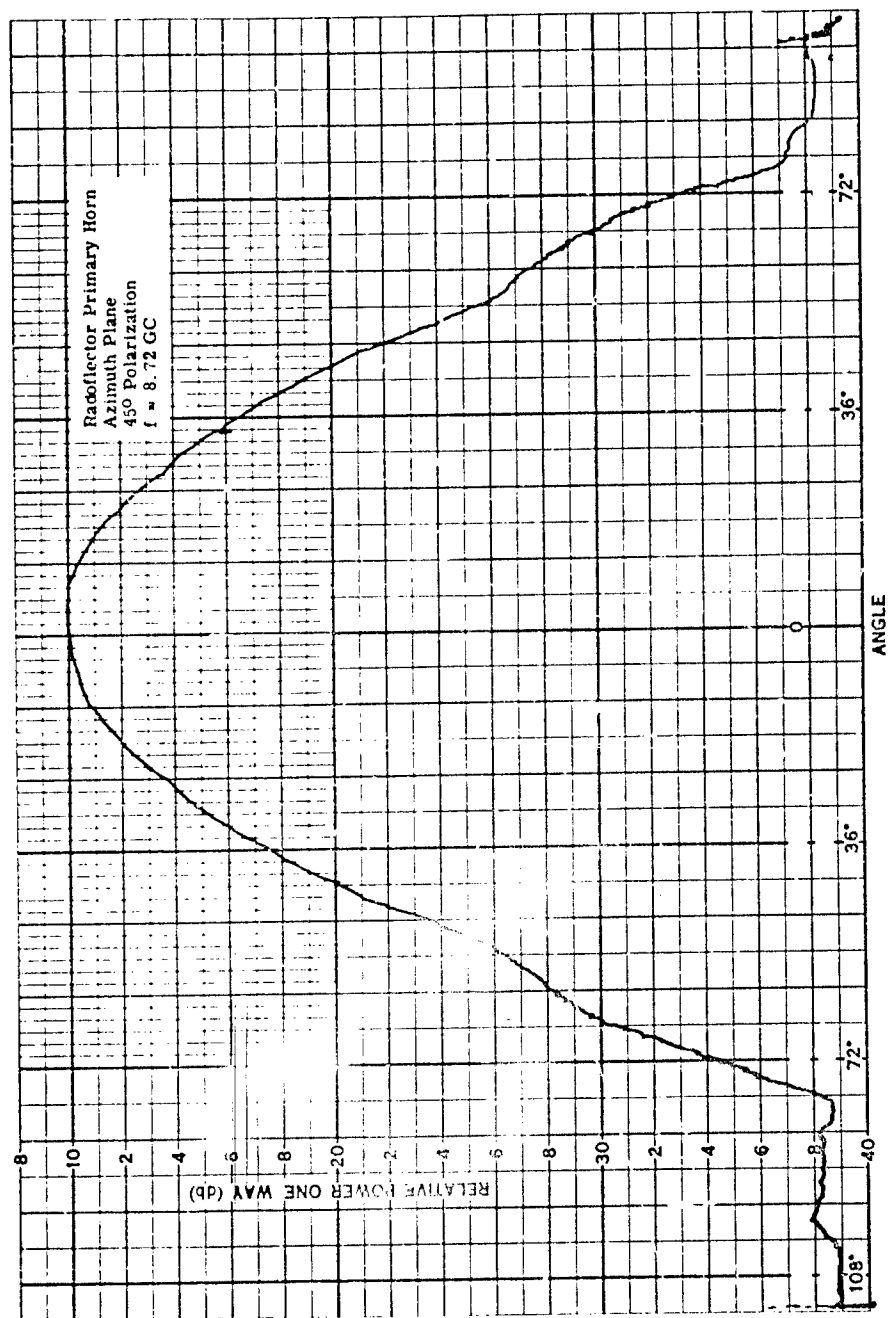


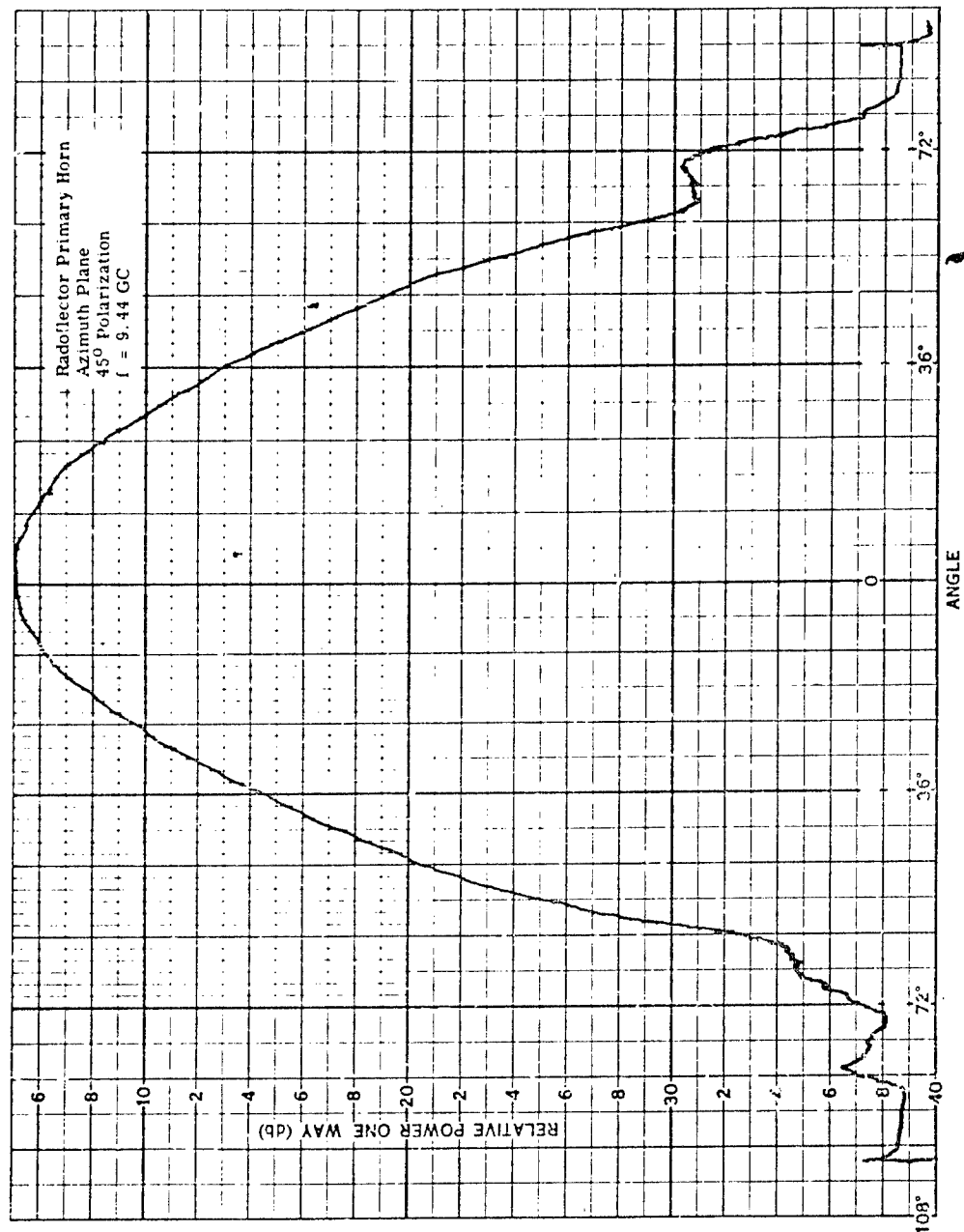
A-2

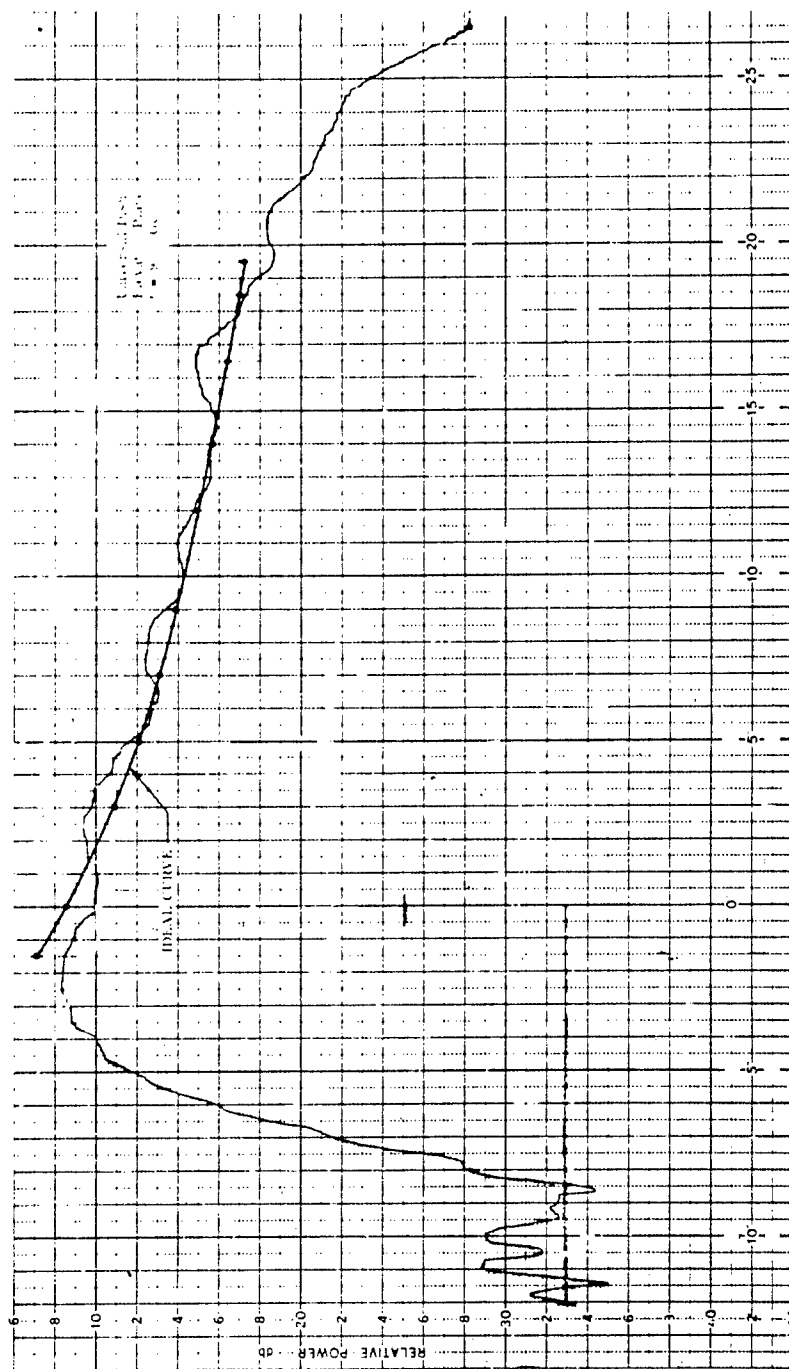


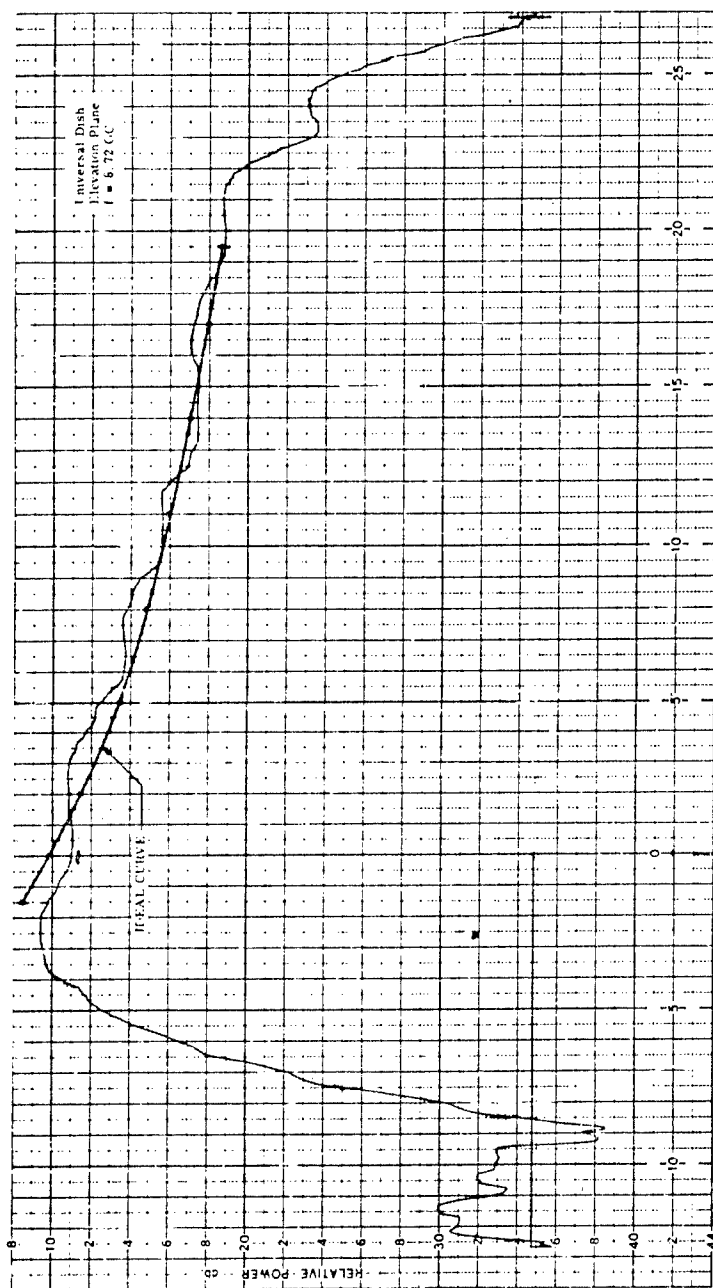


A.4

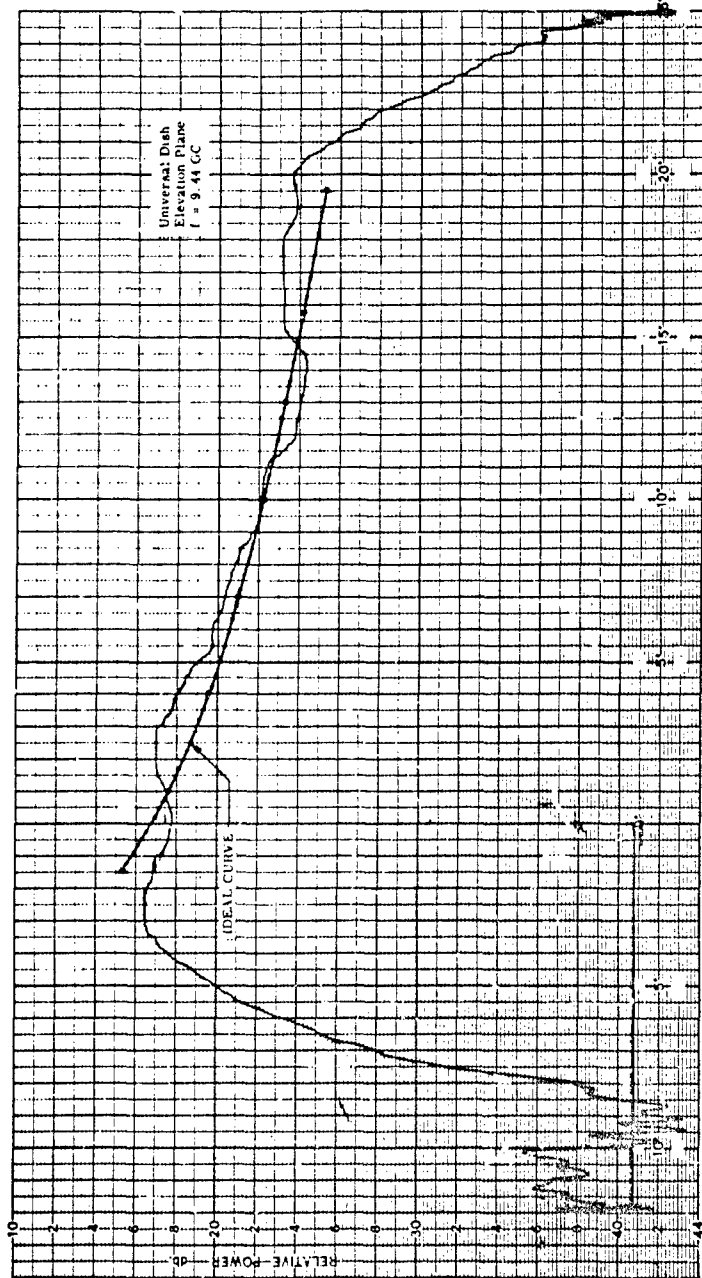


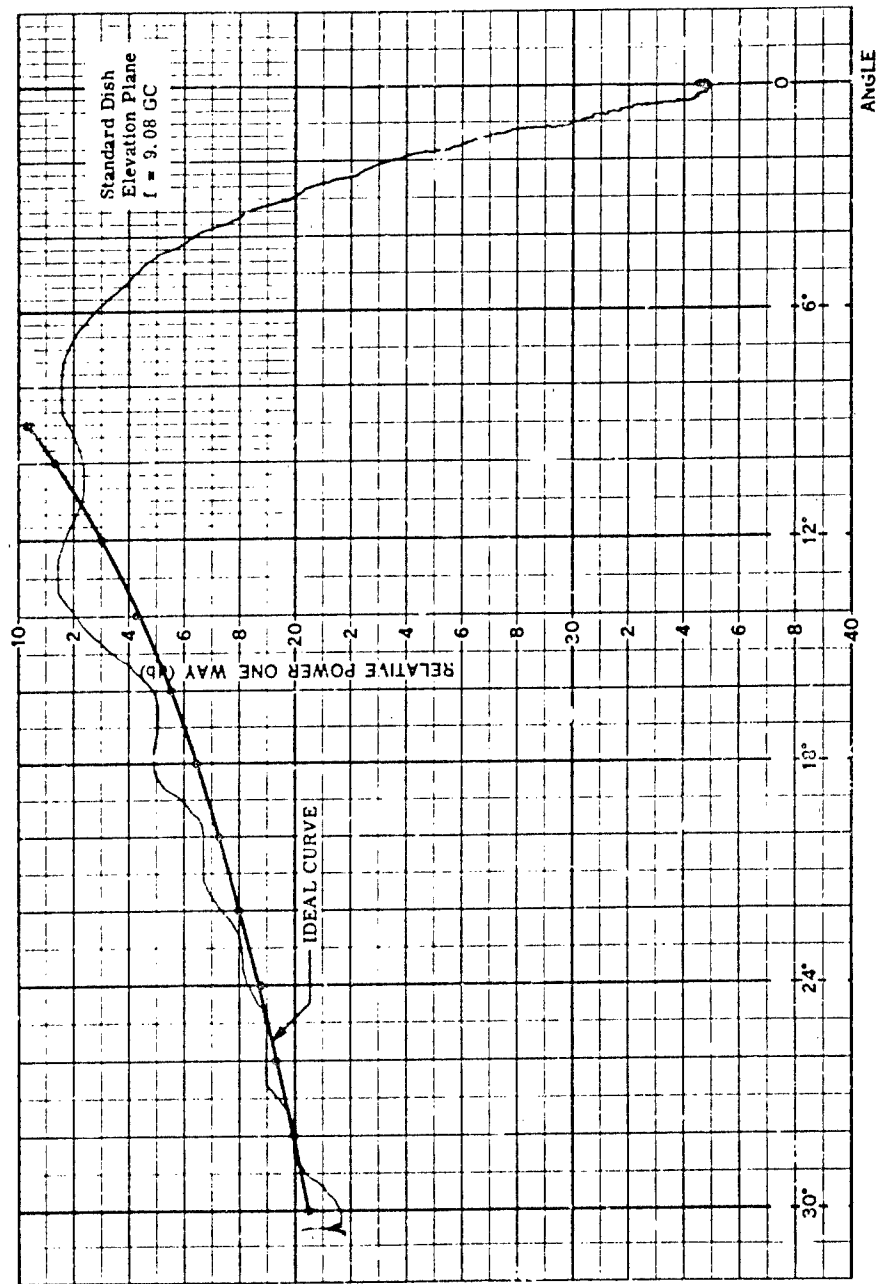




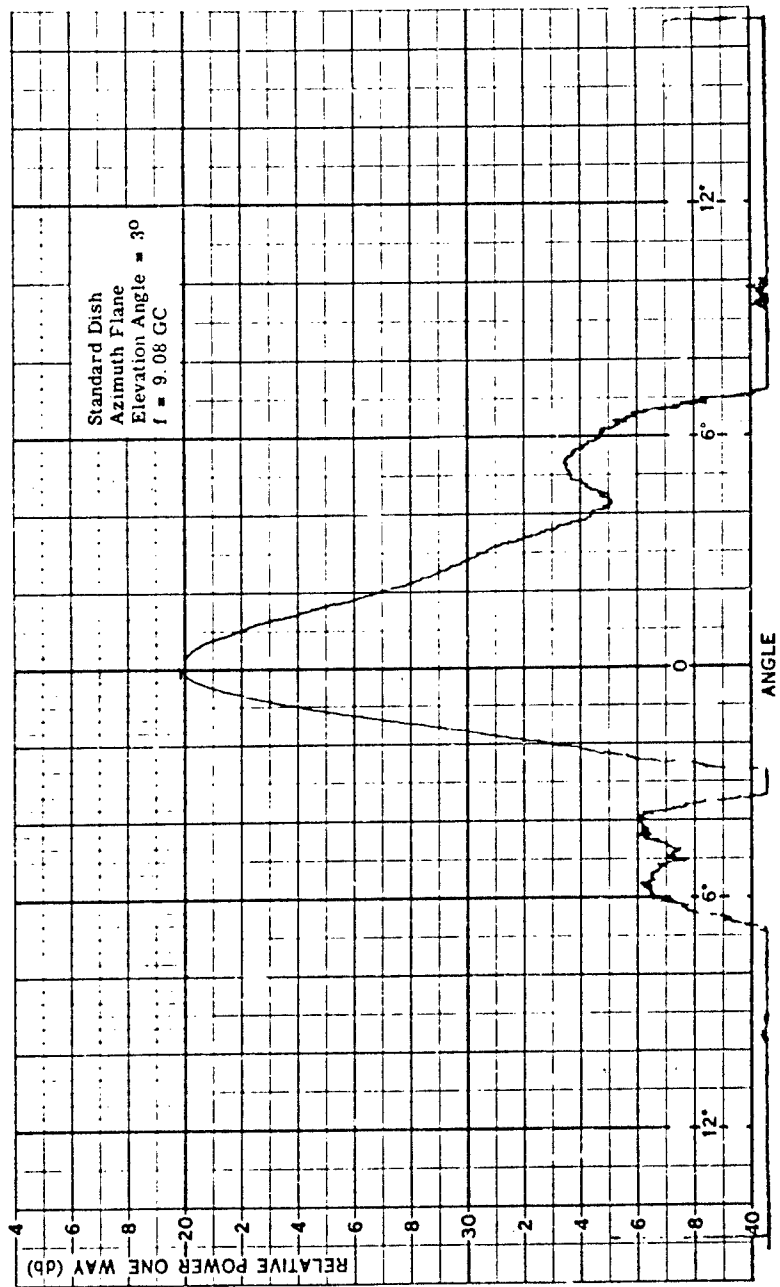


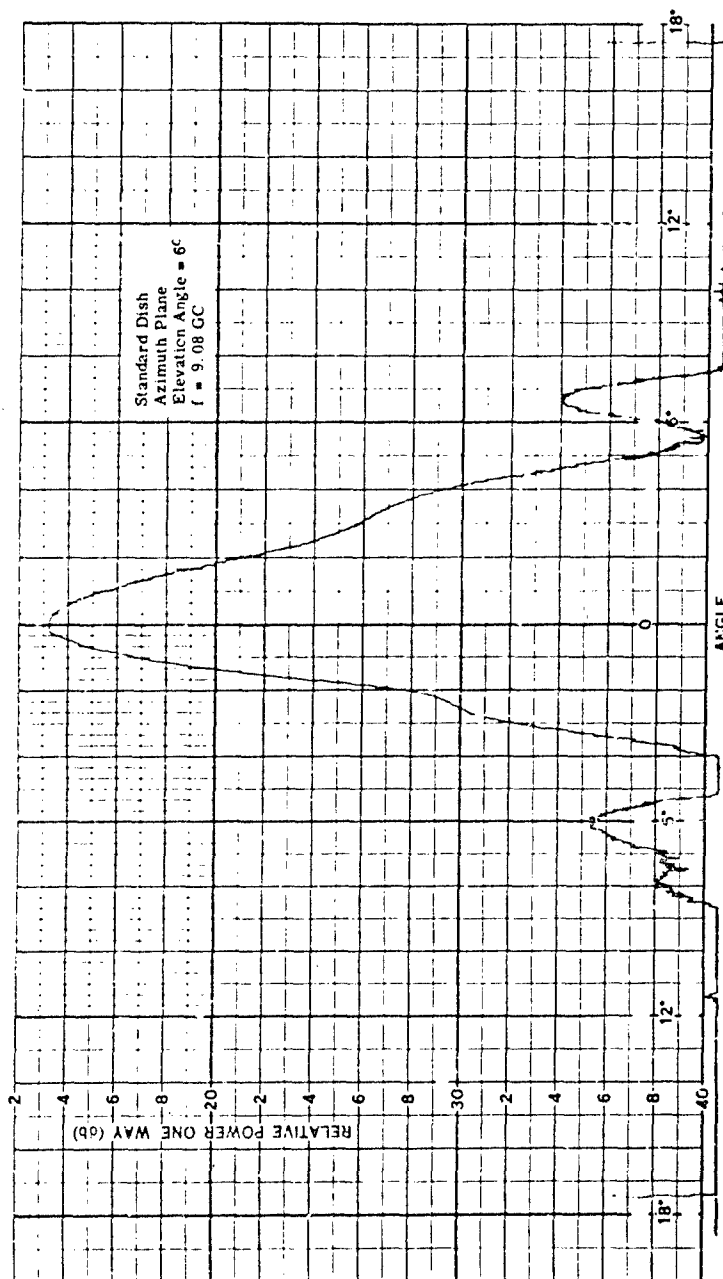
A-8



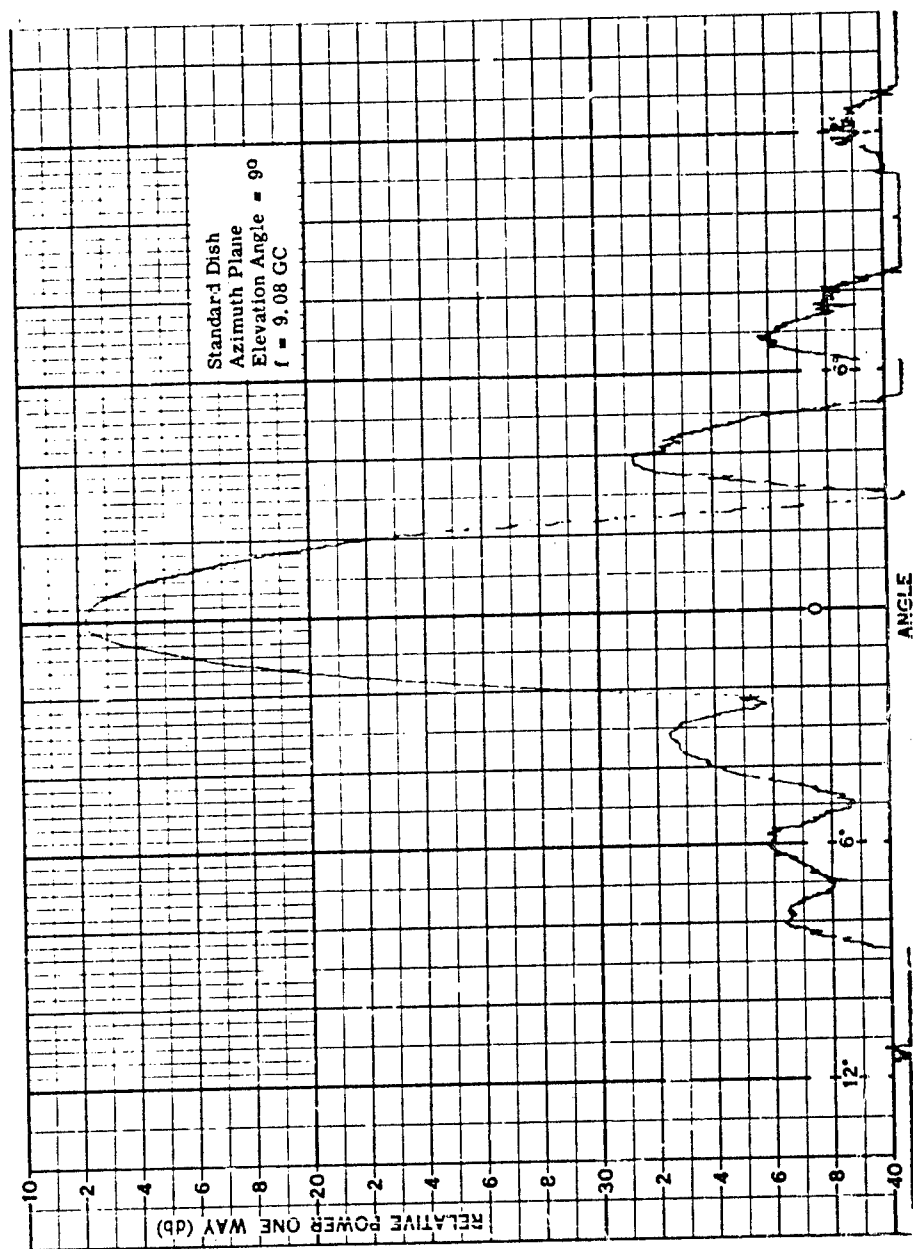


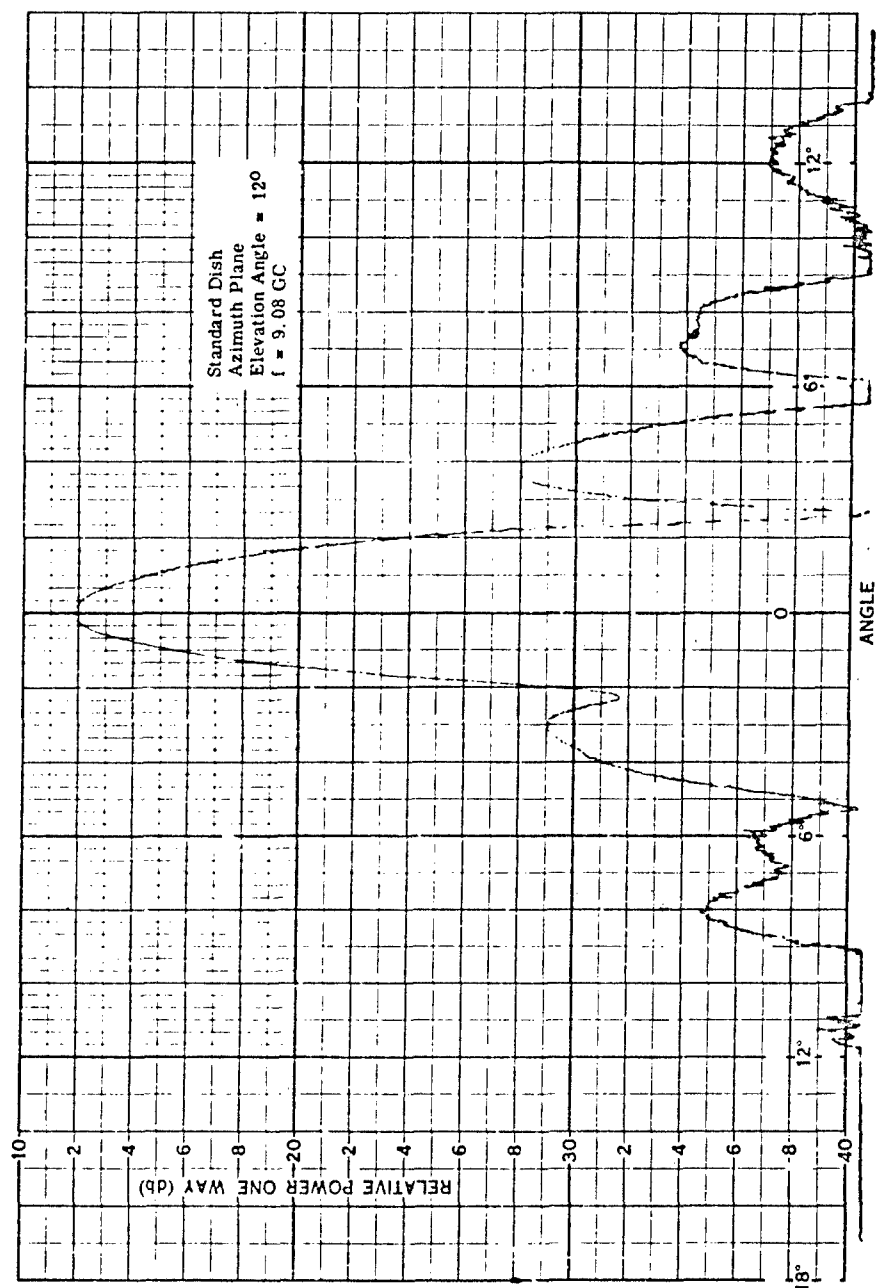
A-10



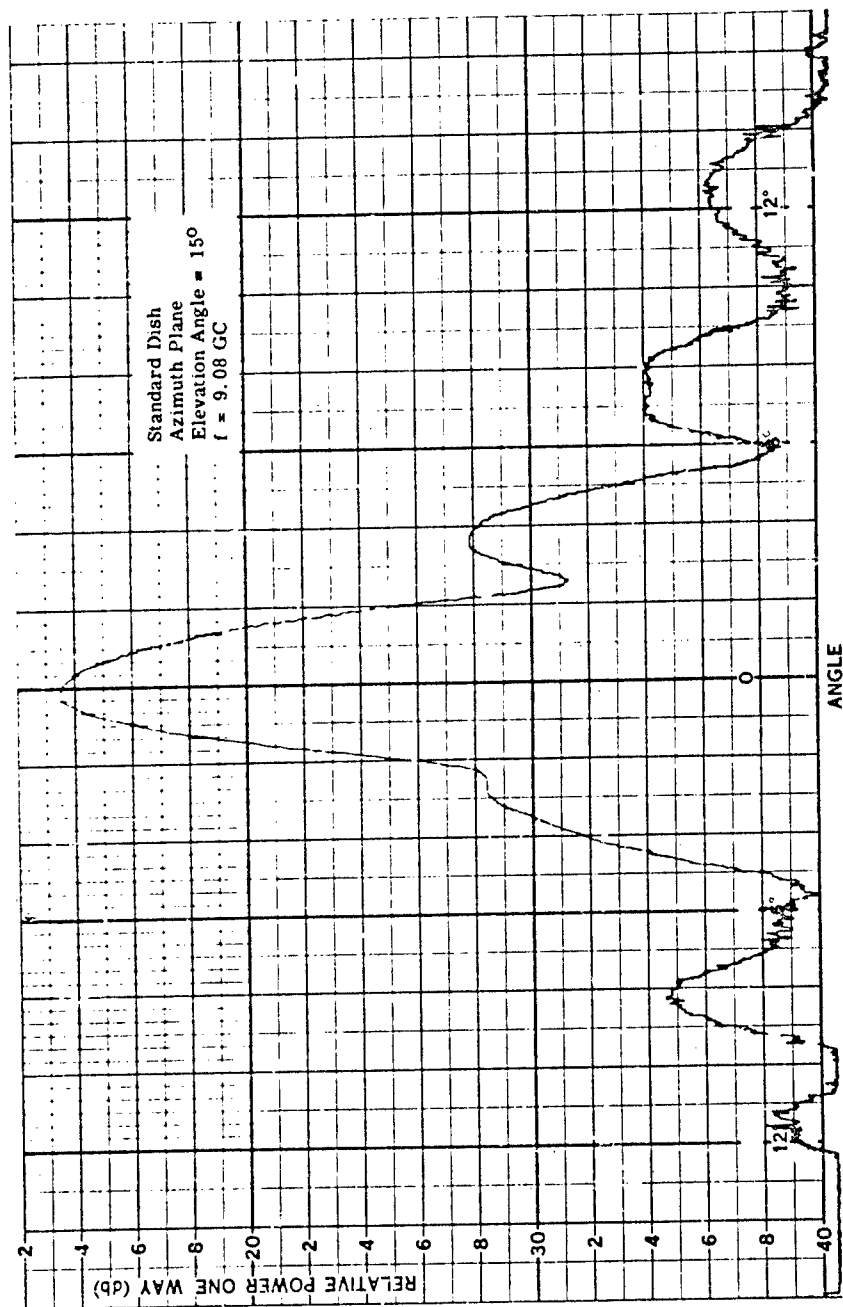


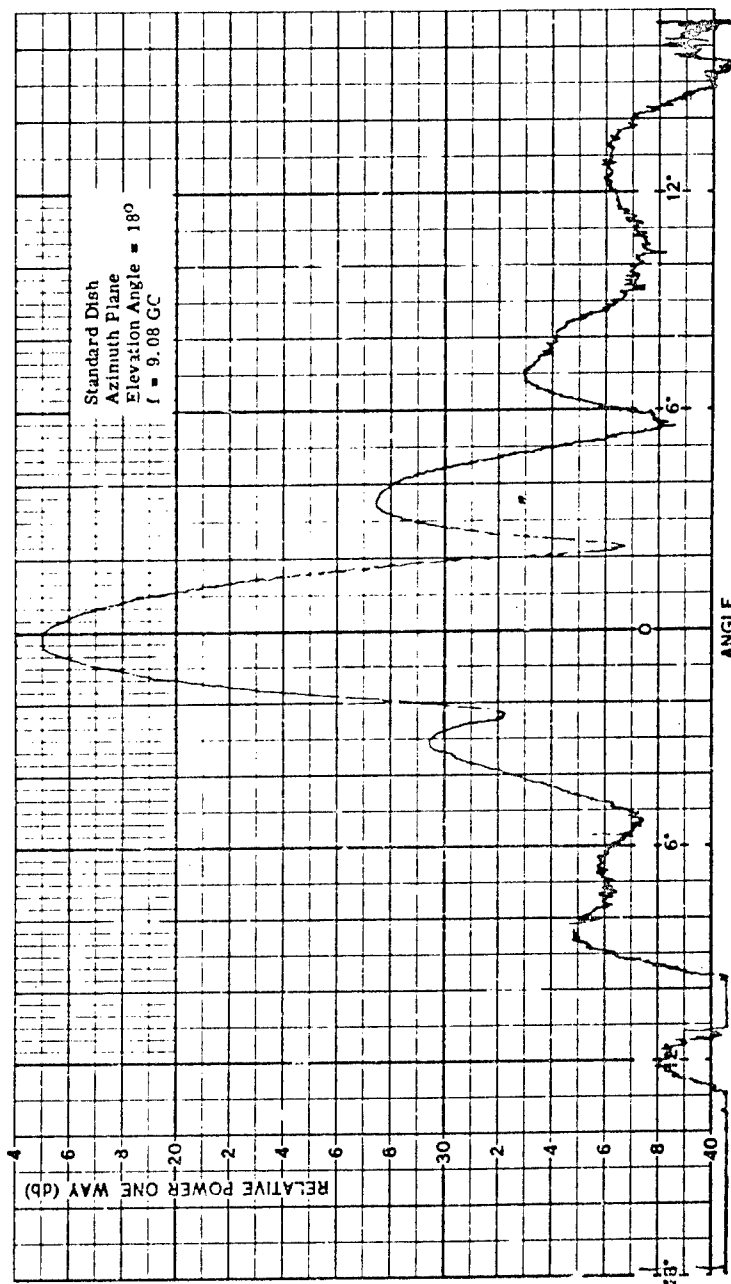
A-12



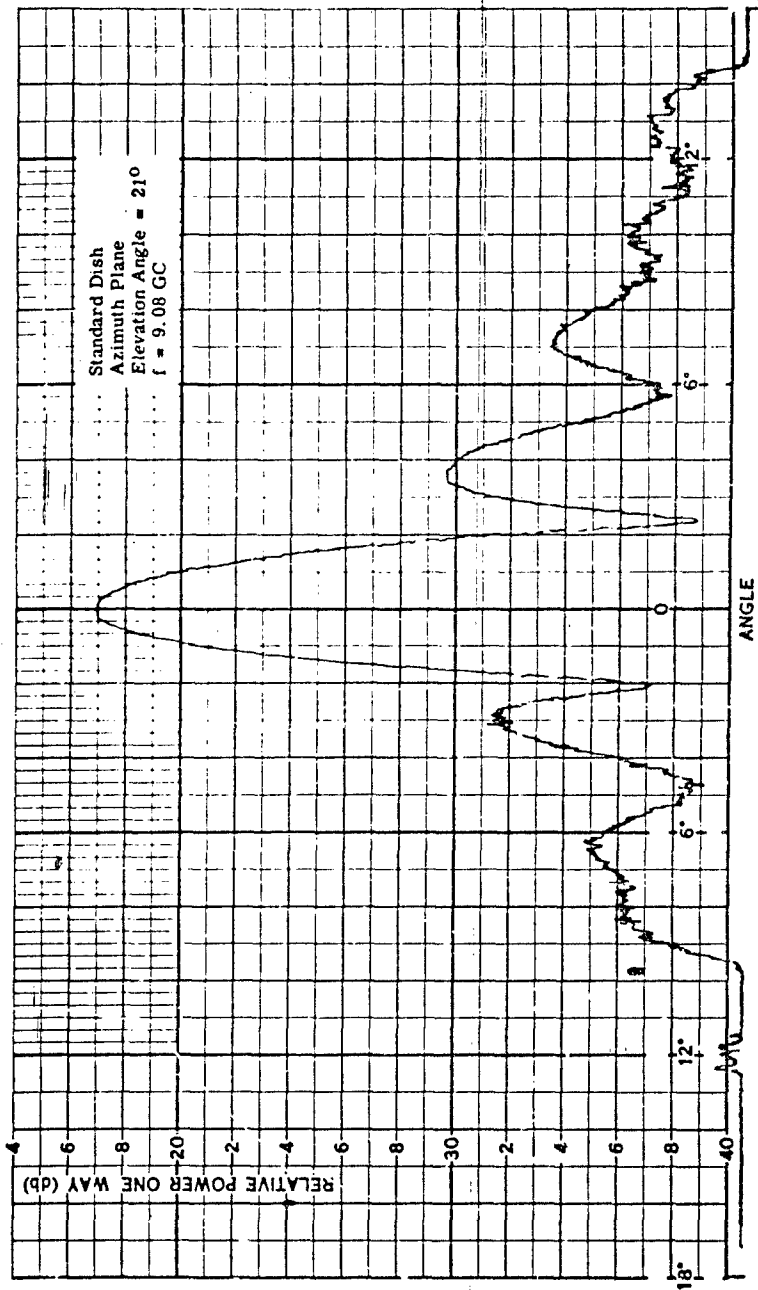


A-14

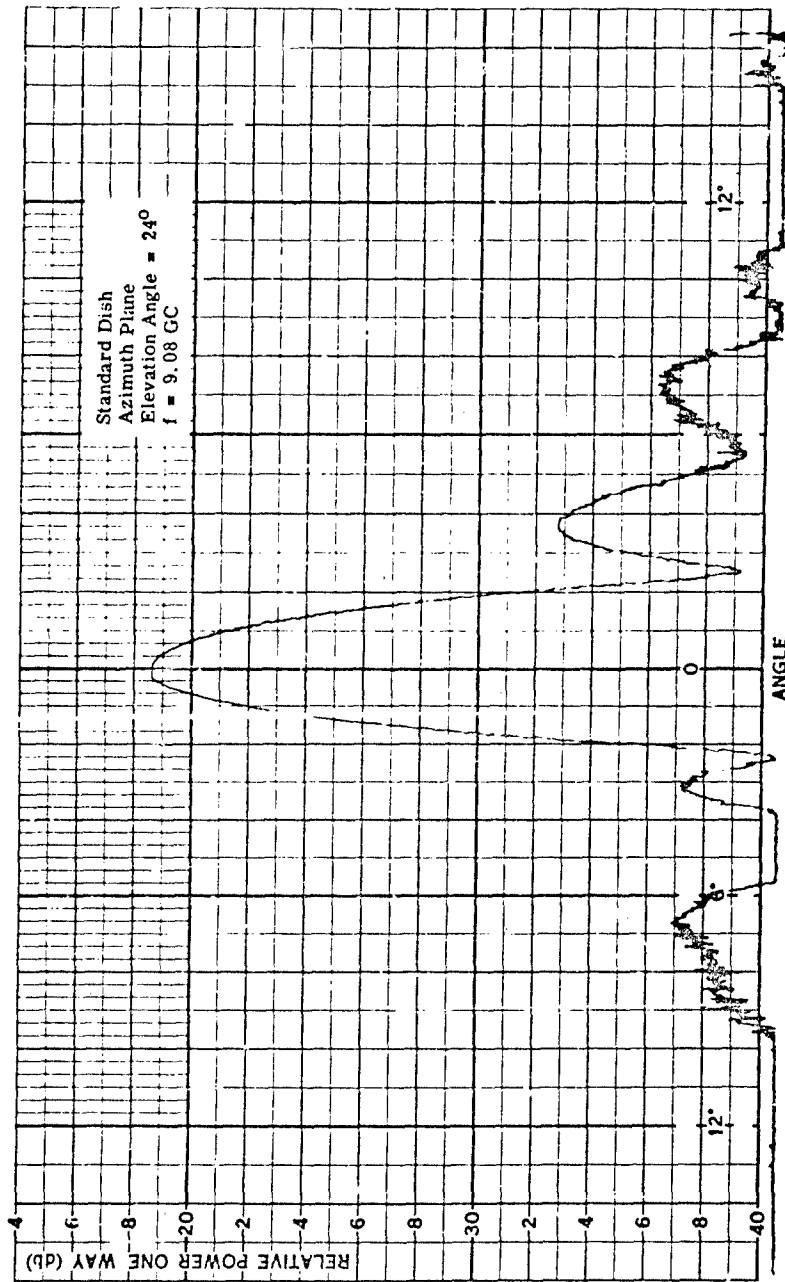




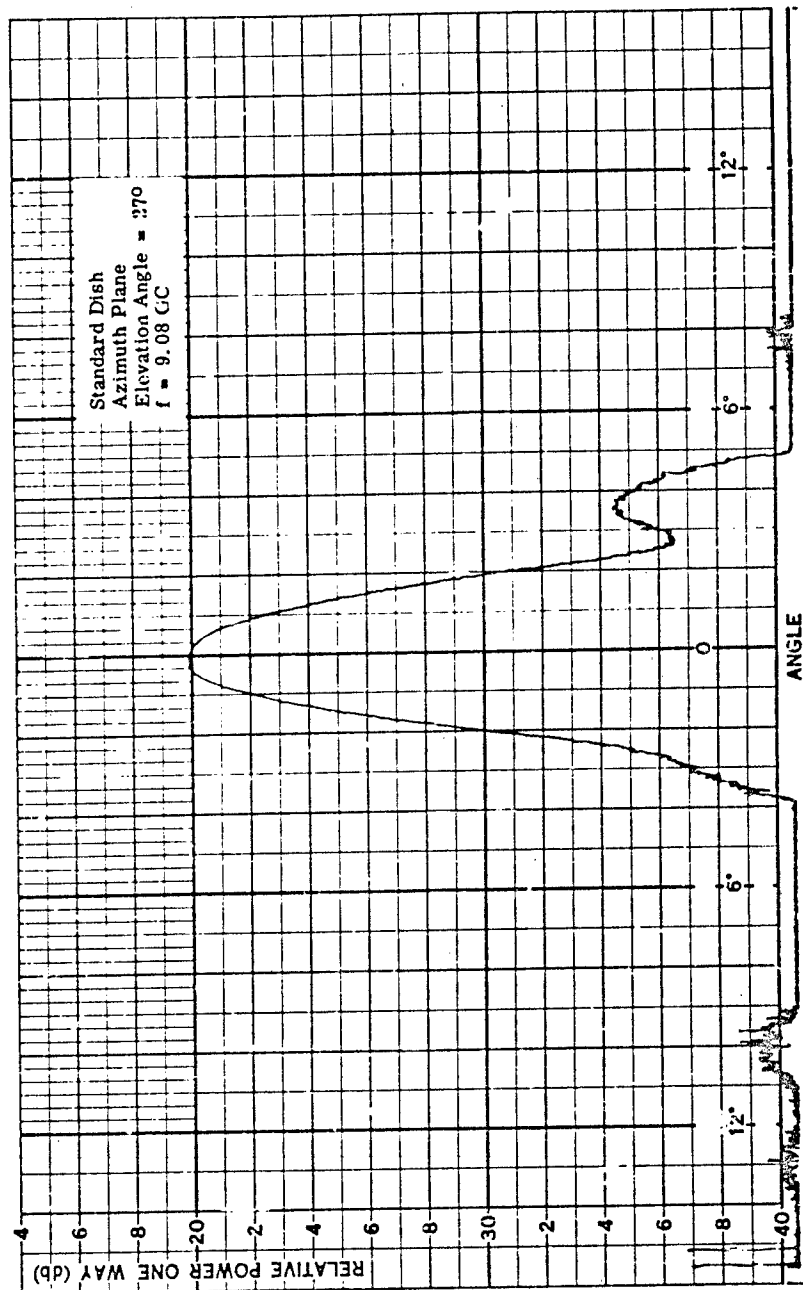
A-16

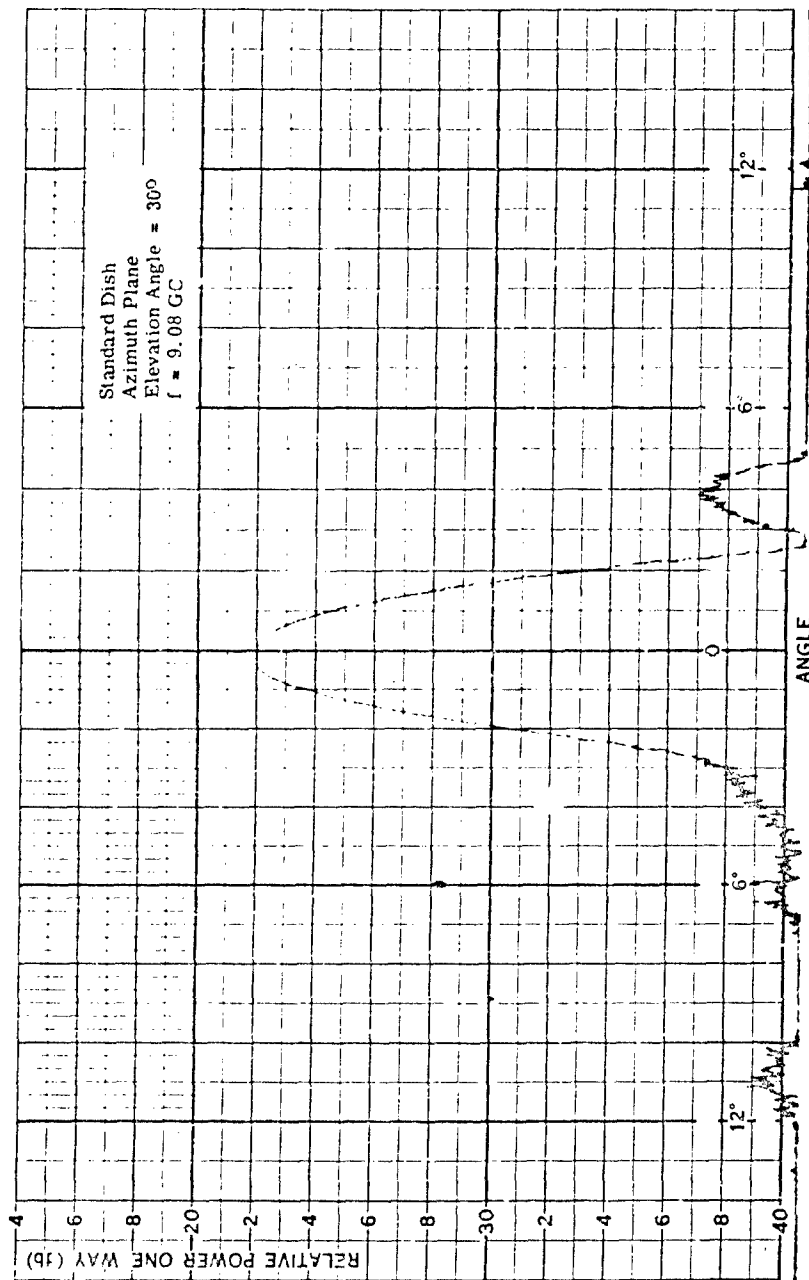


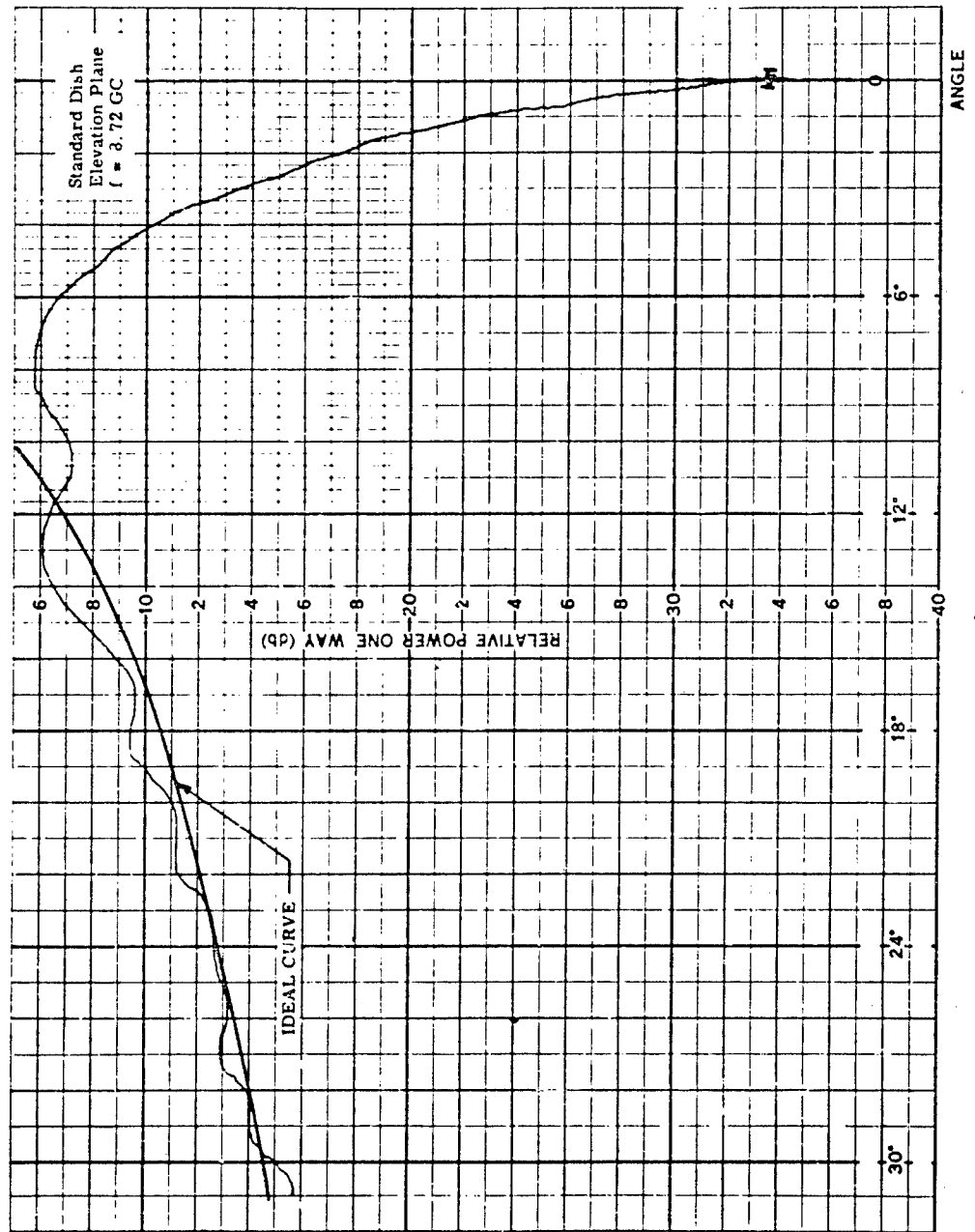
A-17

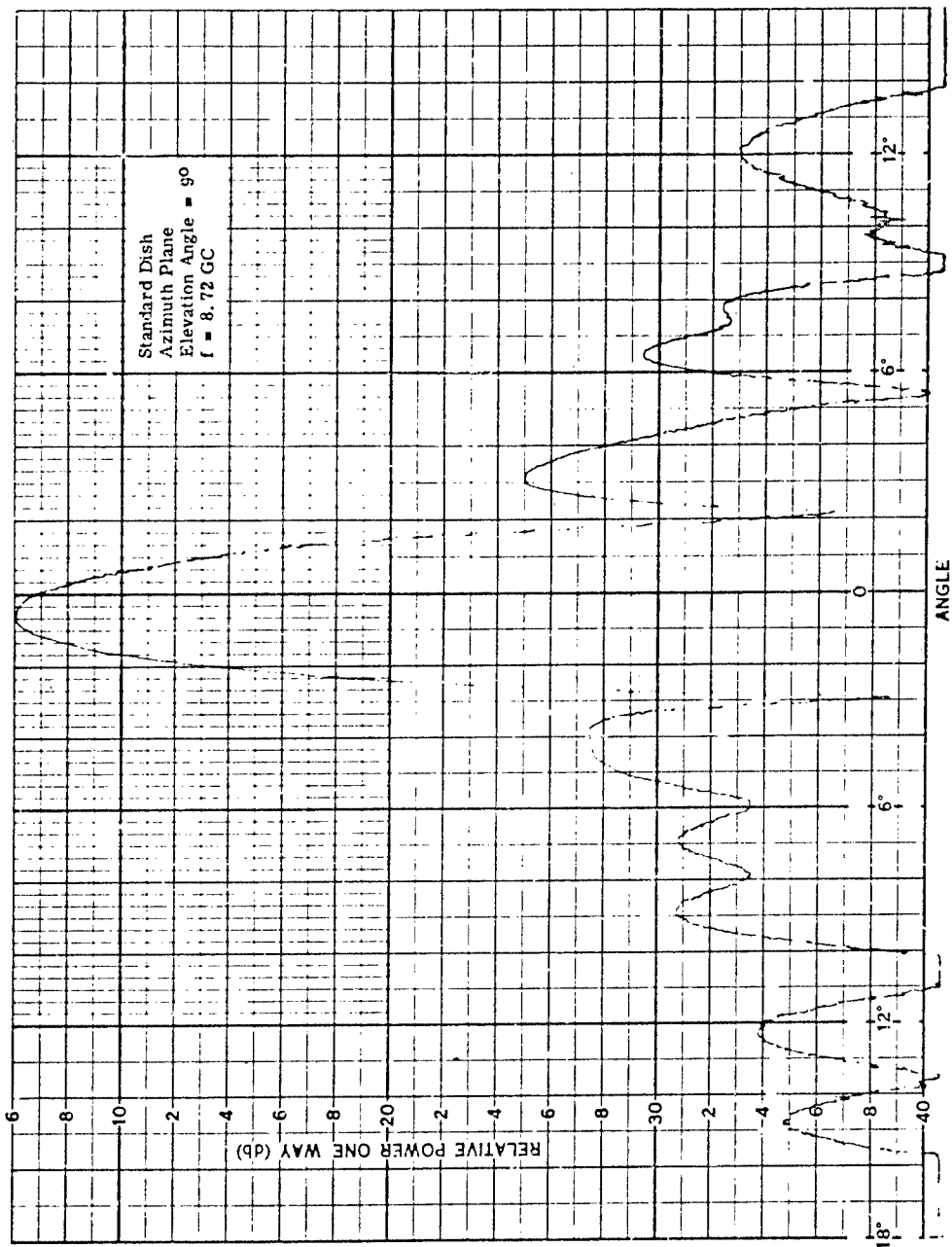


A-18

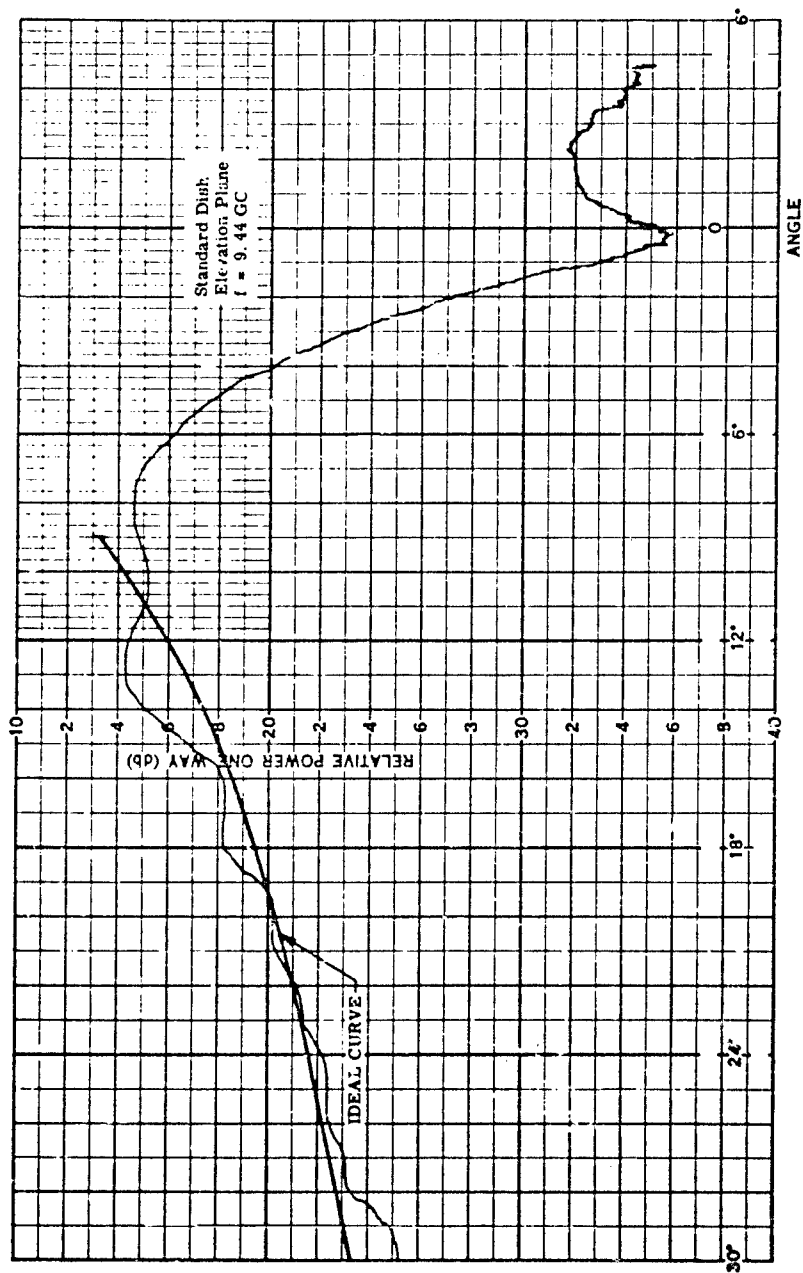


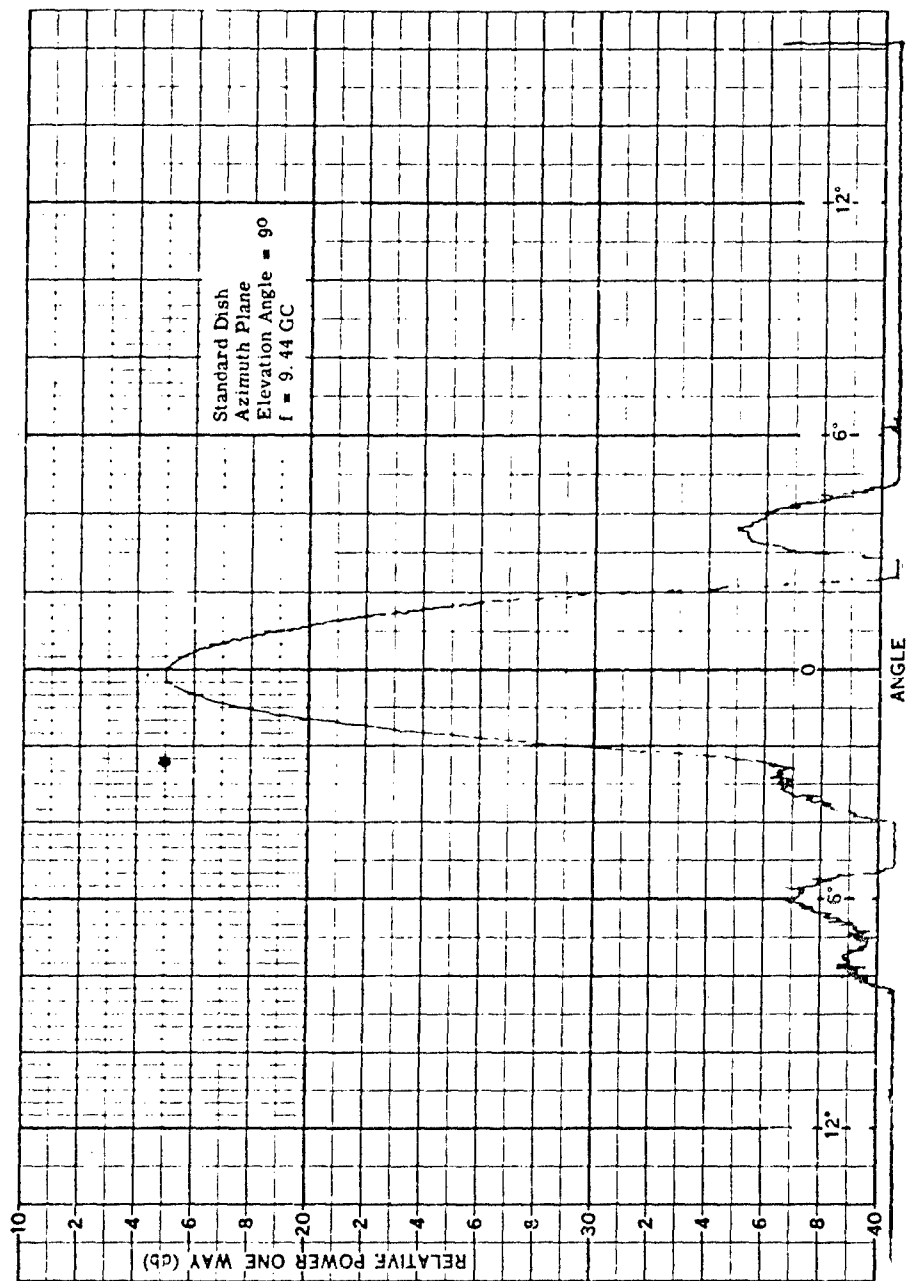




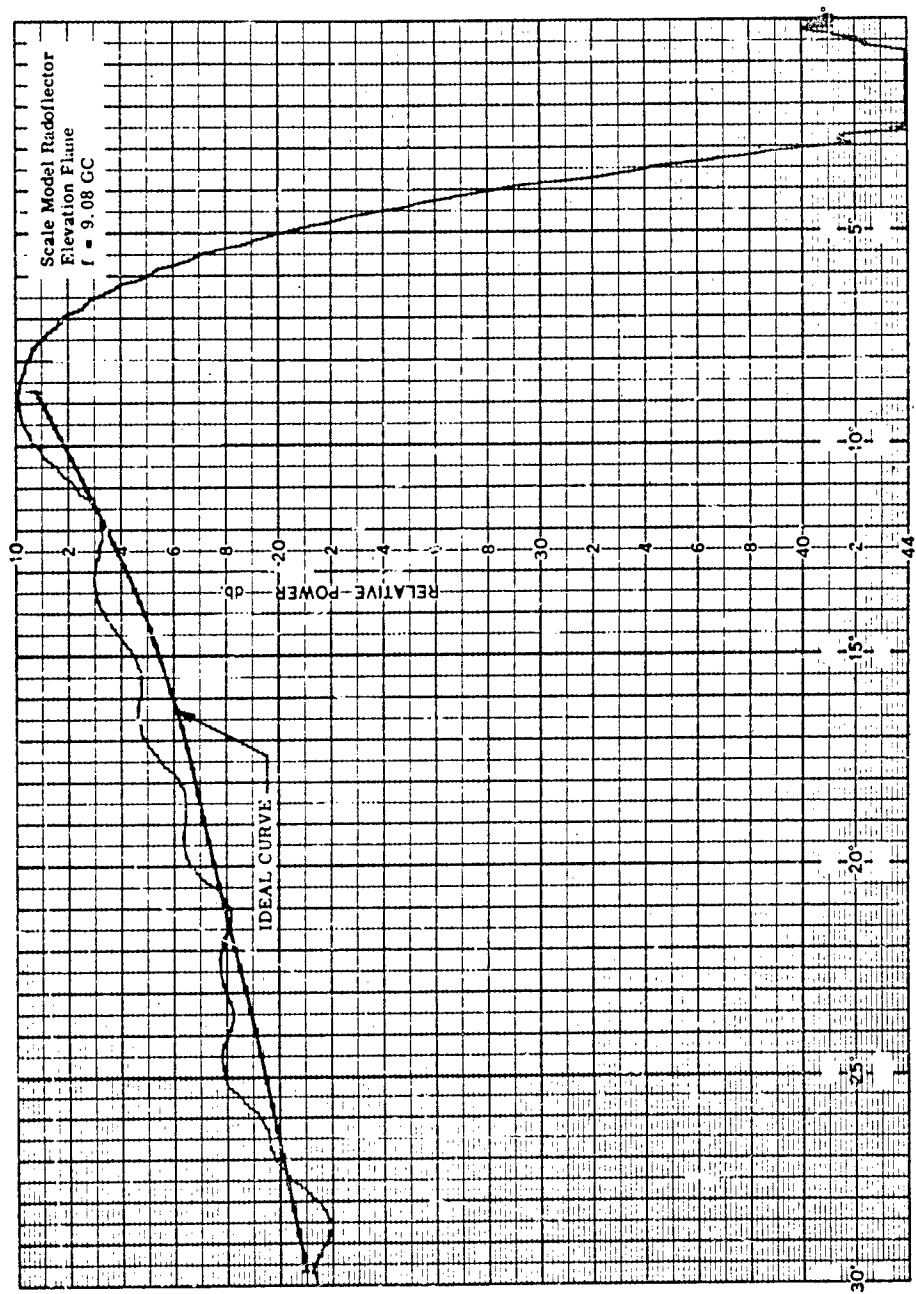


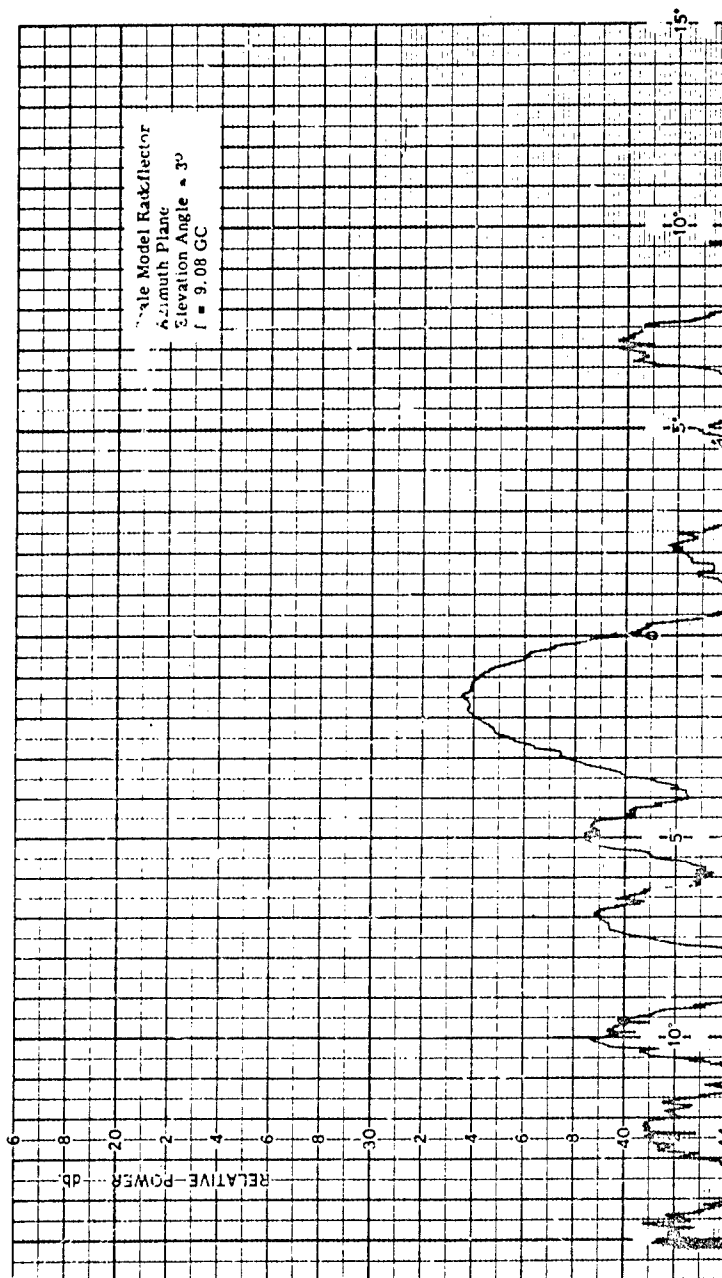
A-22



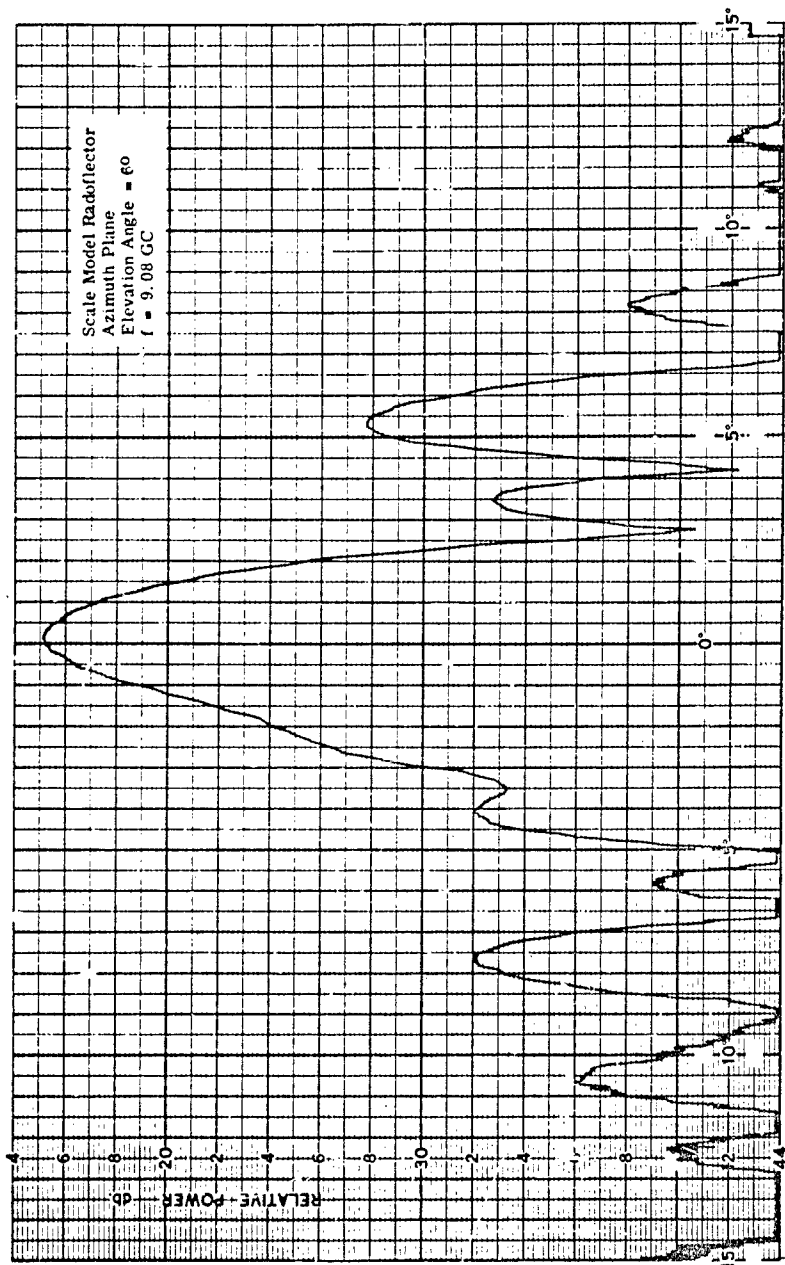


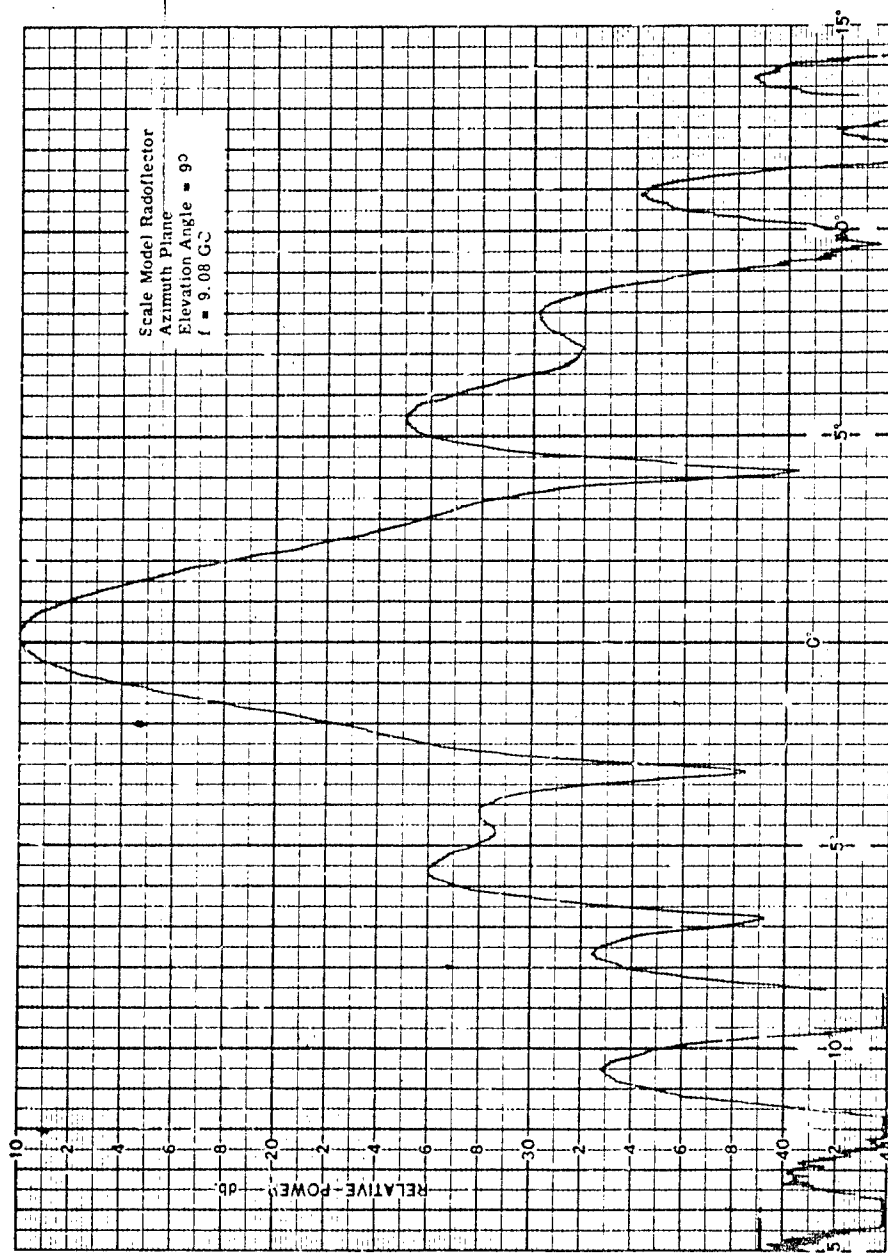
A-24

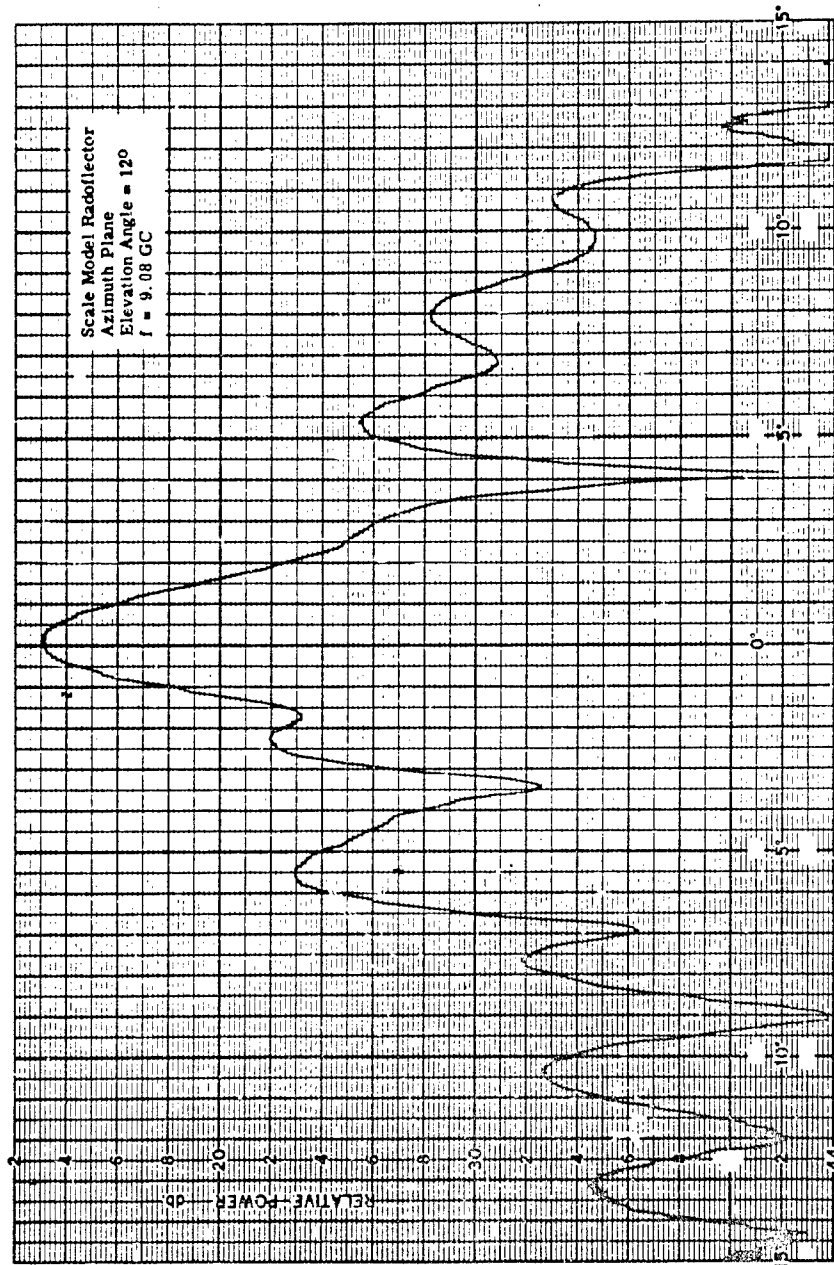


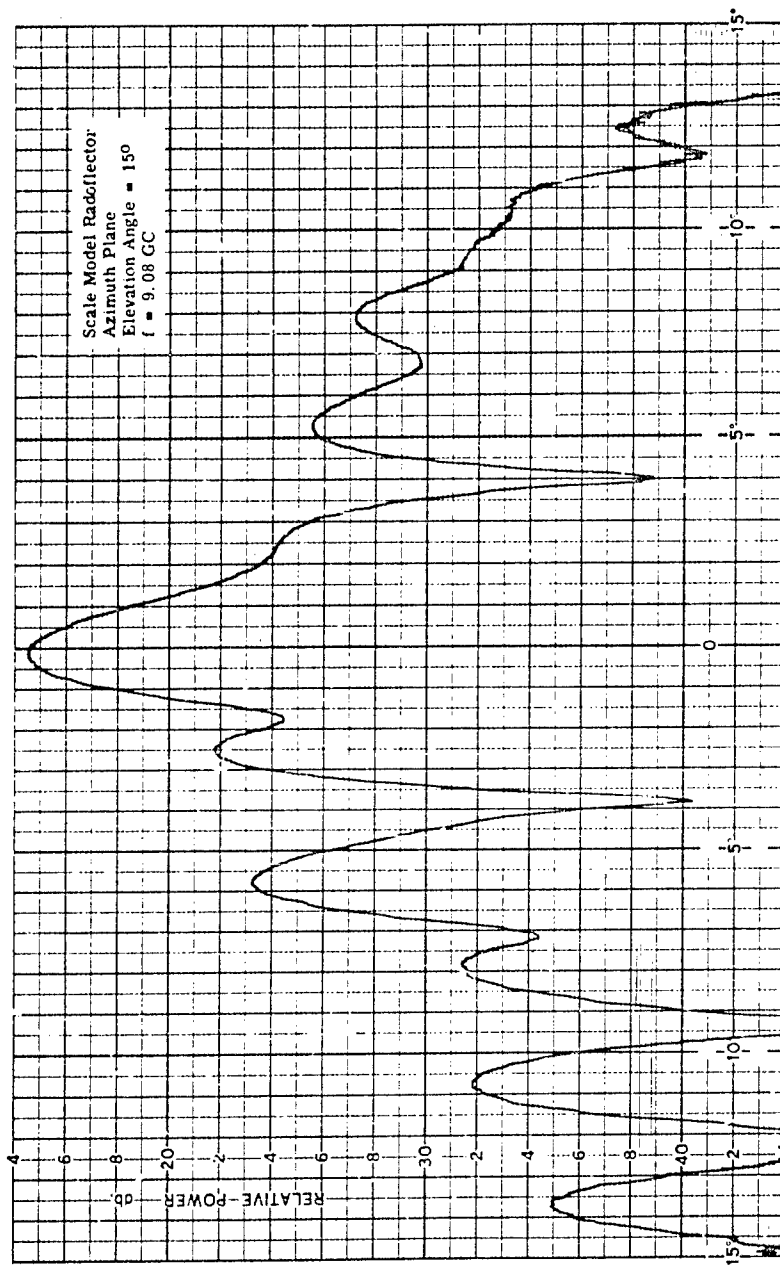


A-26

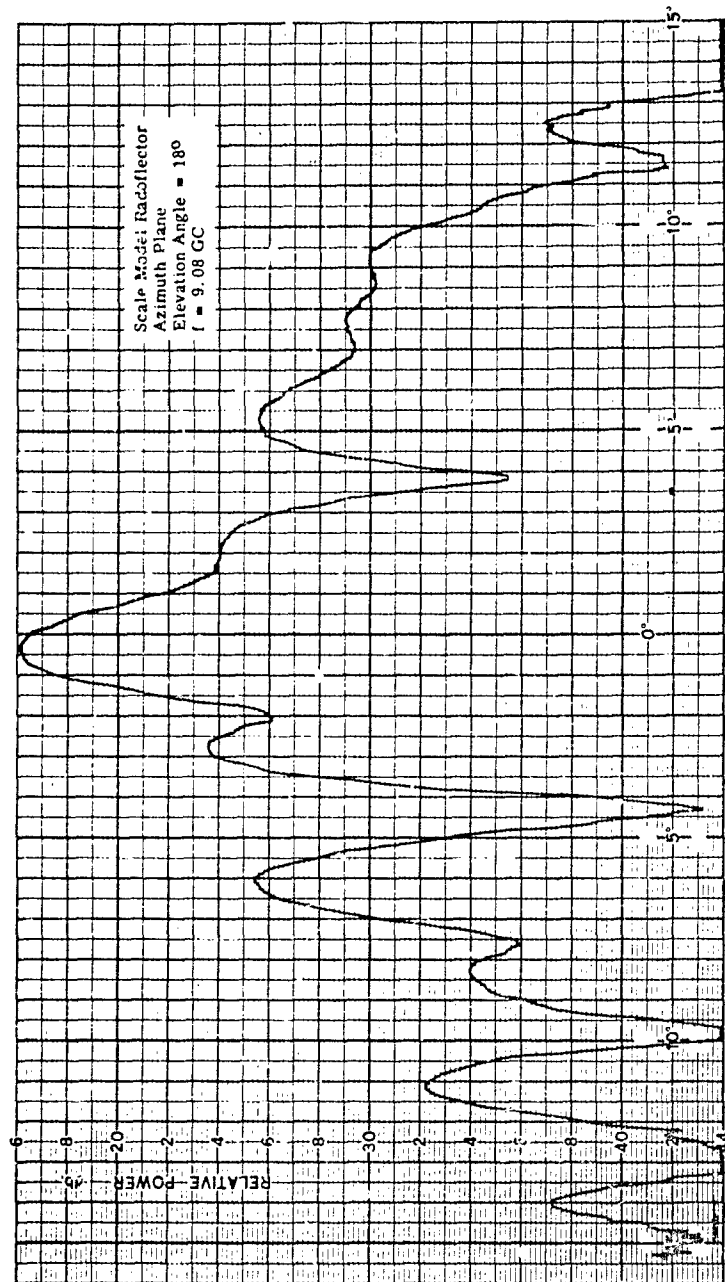


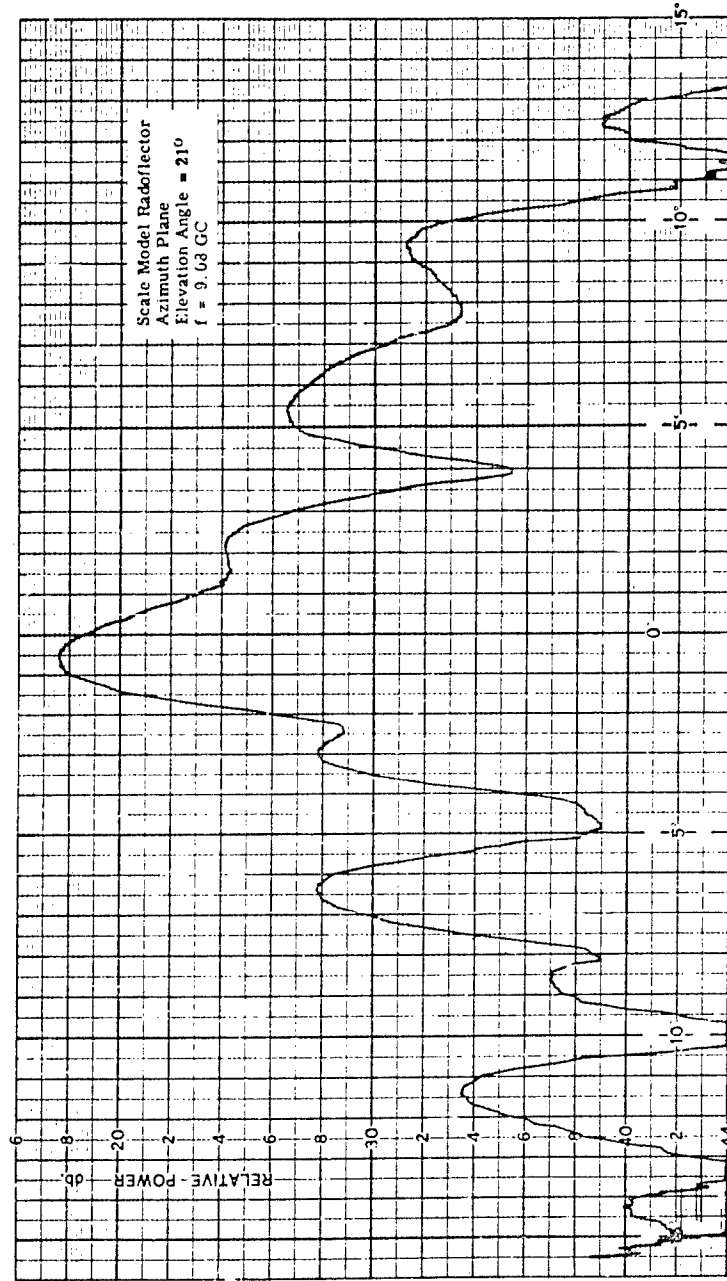




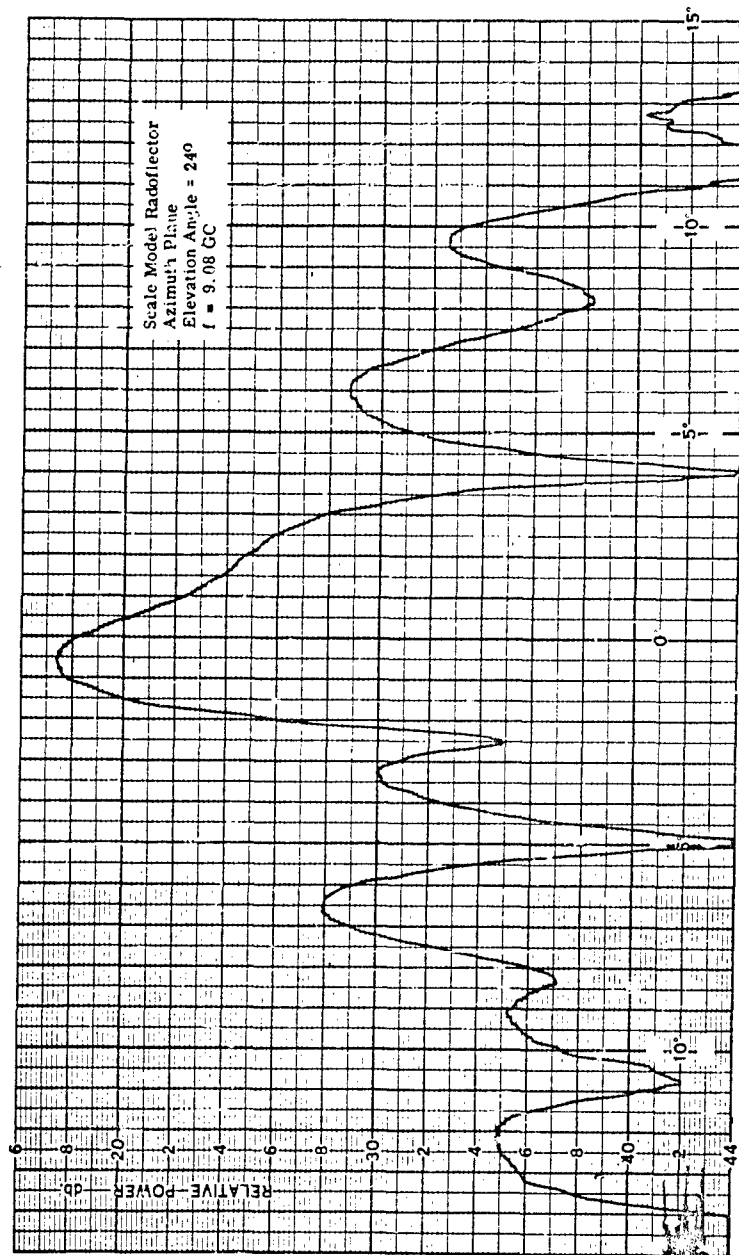


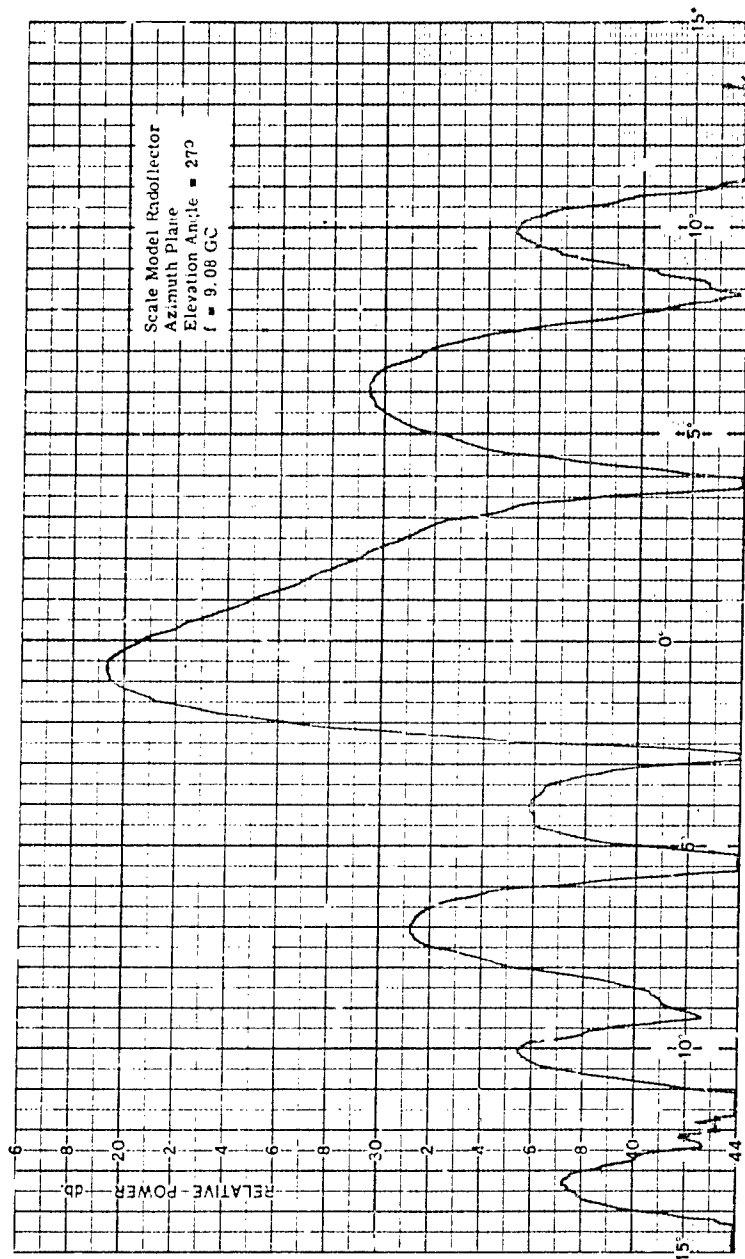
A-30



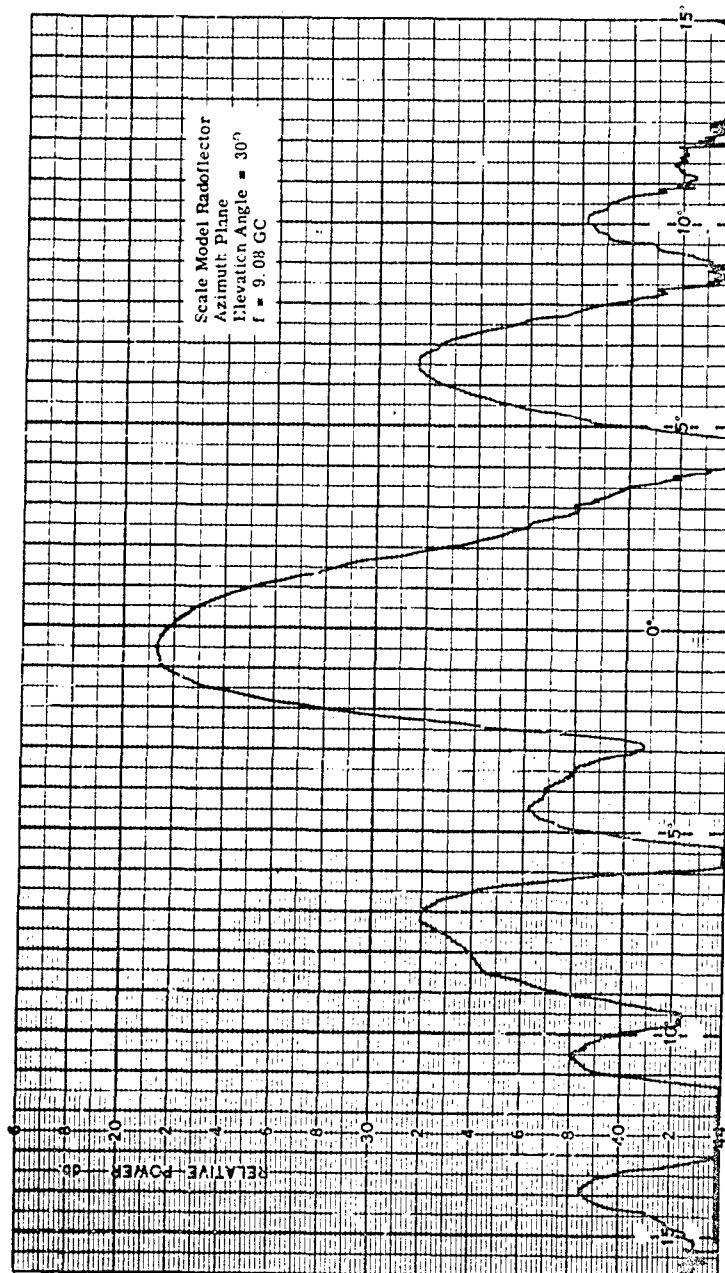


A-32

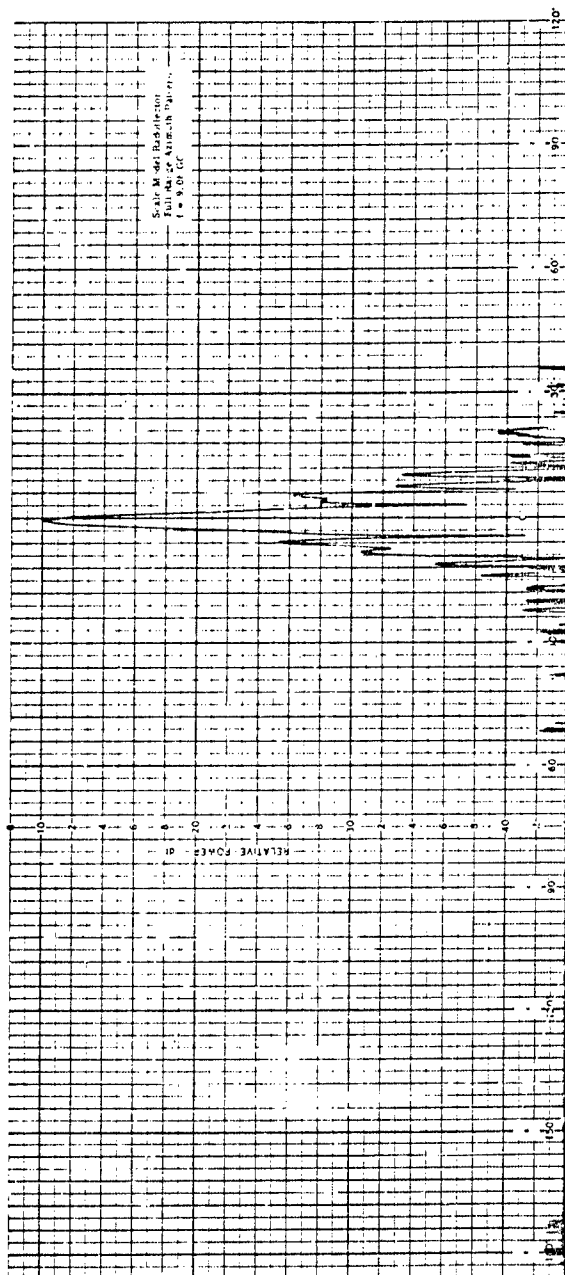




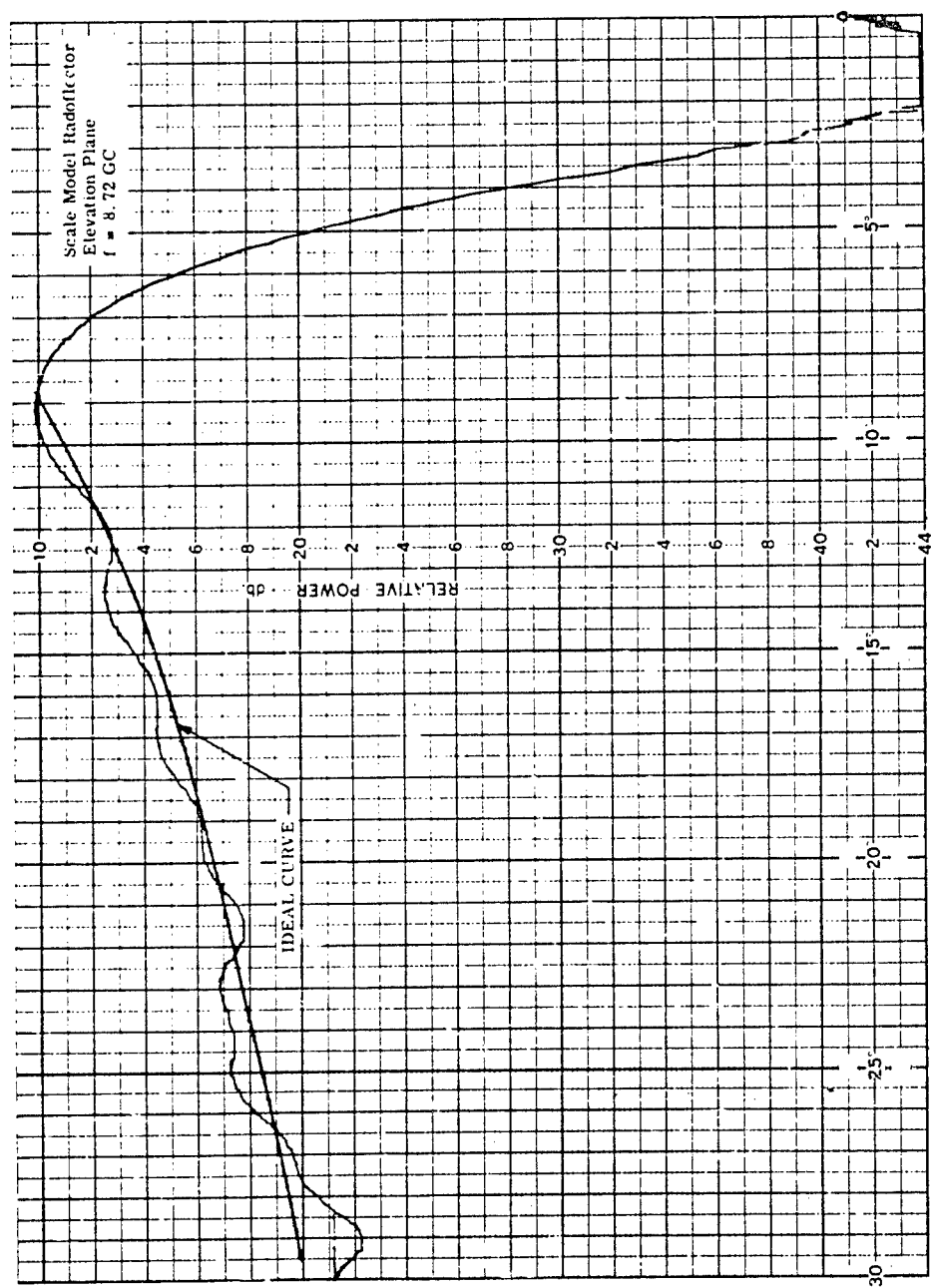
A-34

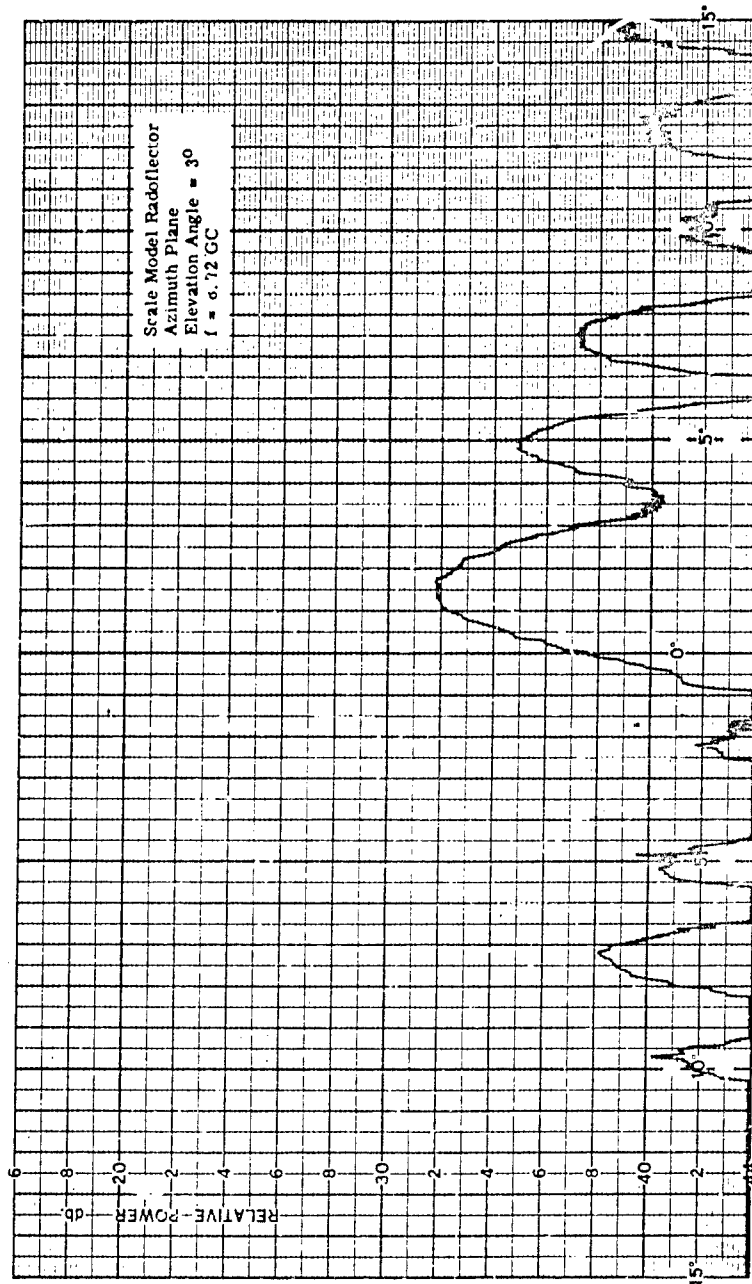


A-35

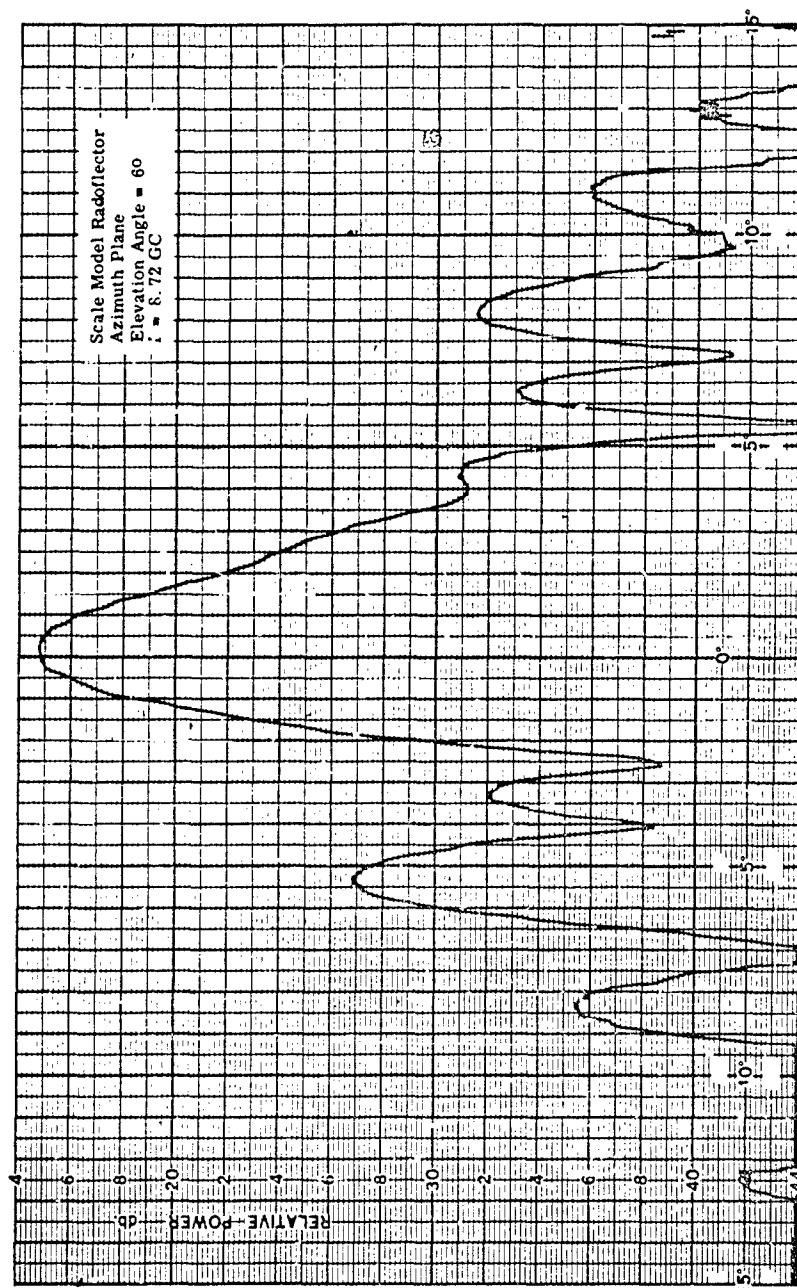


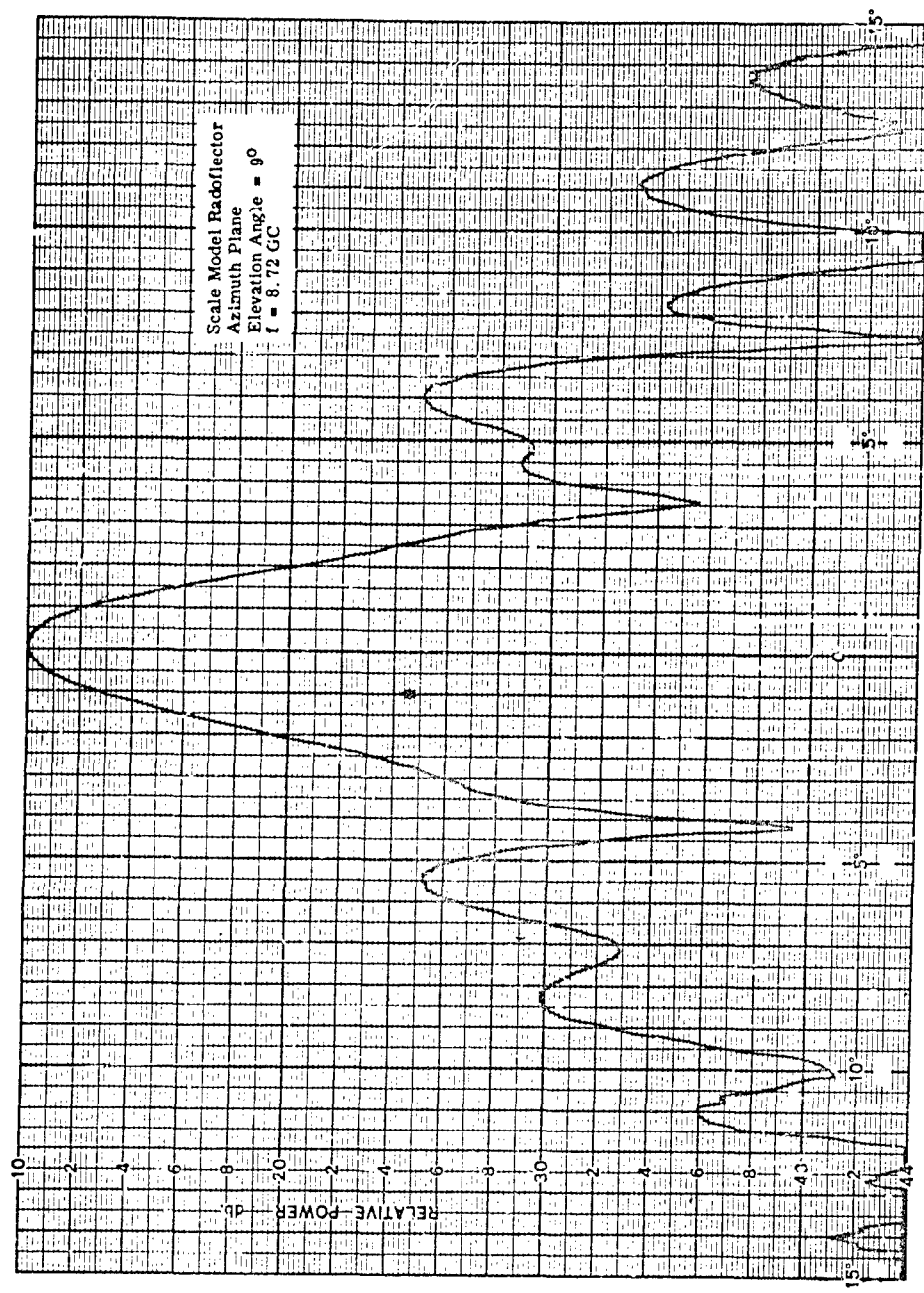
A-36



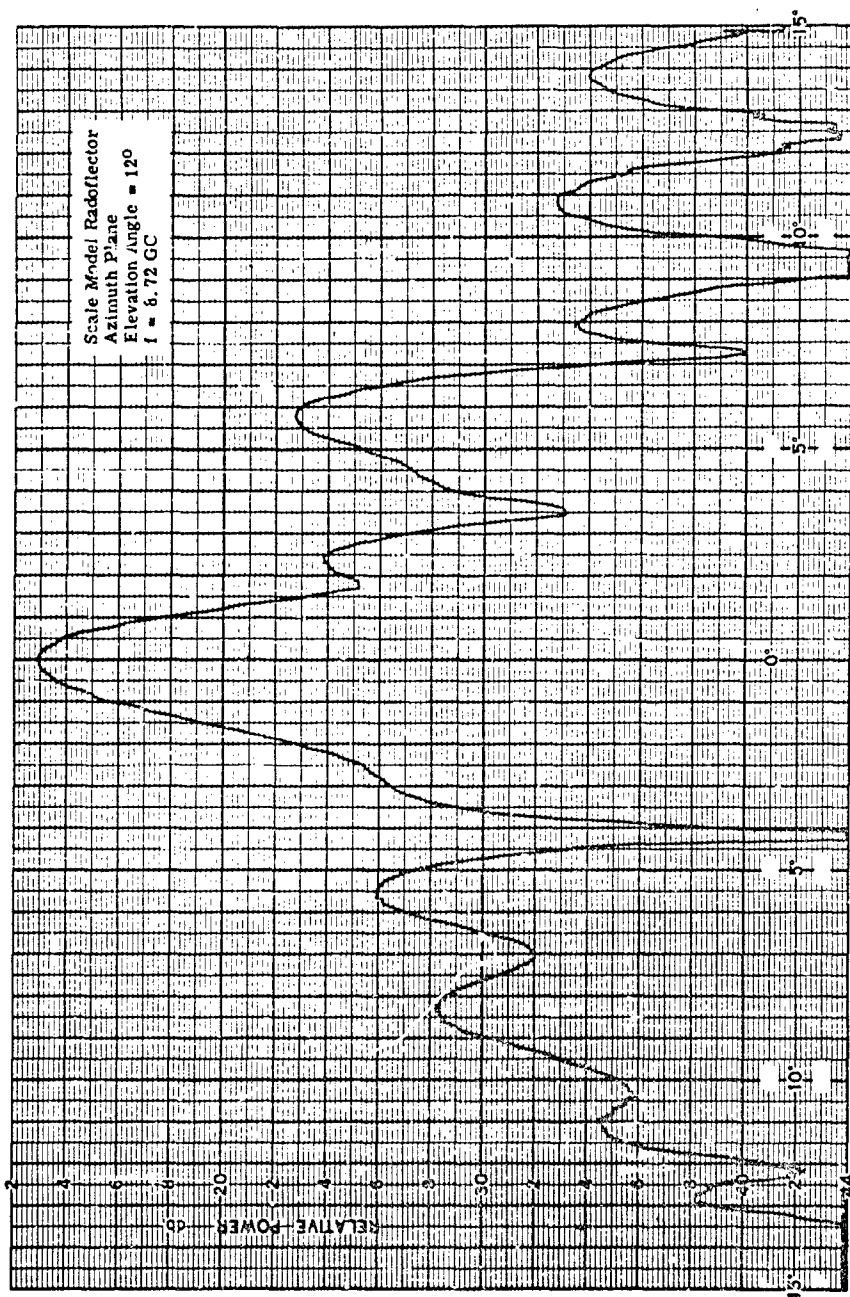


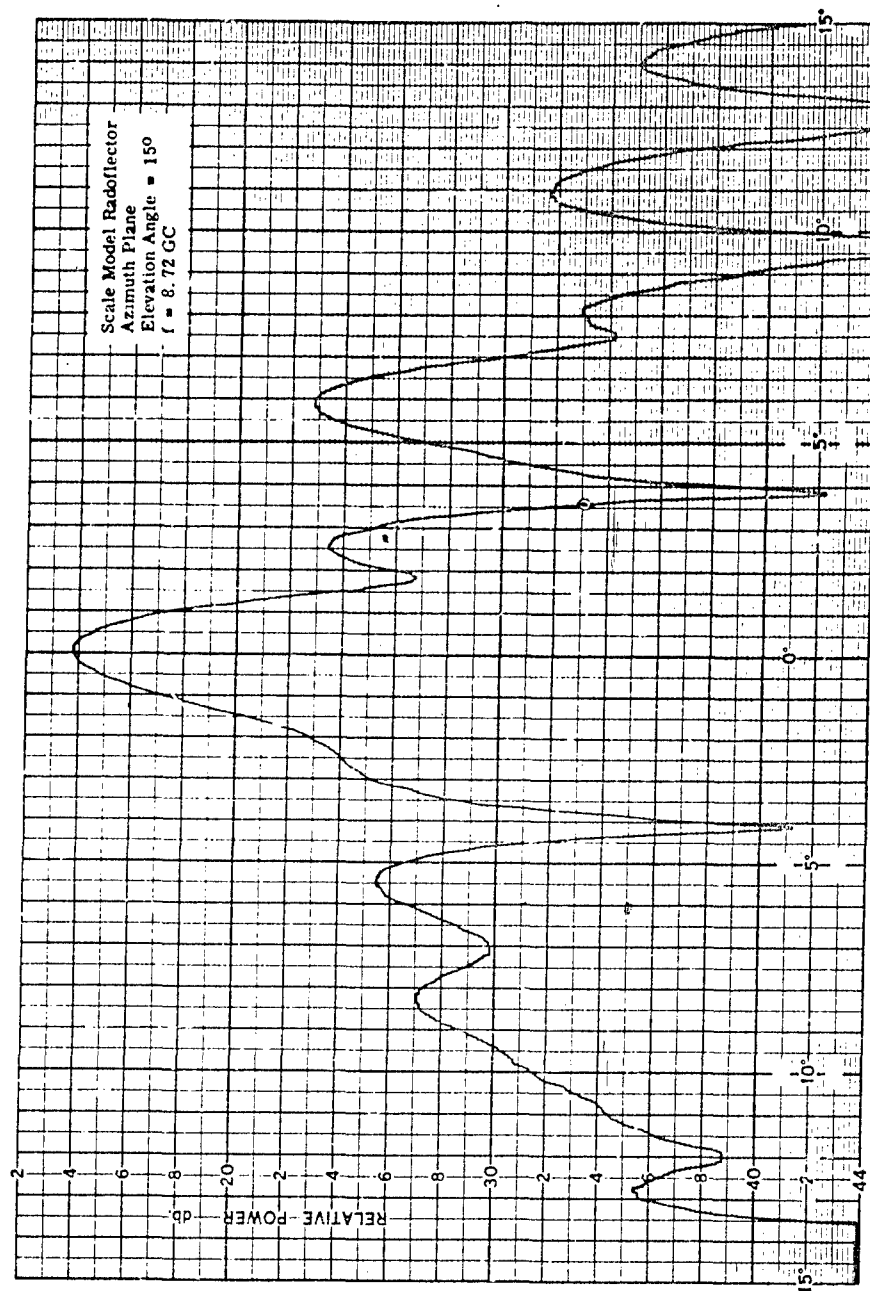
A-38



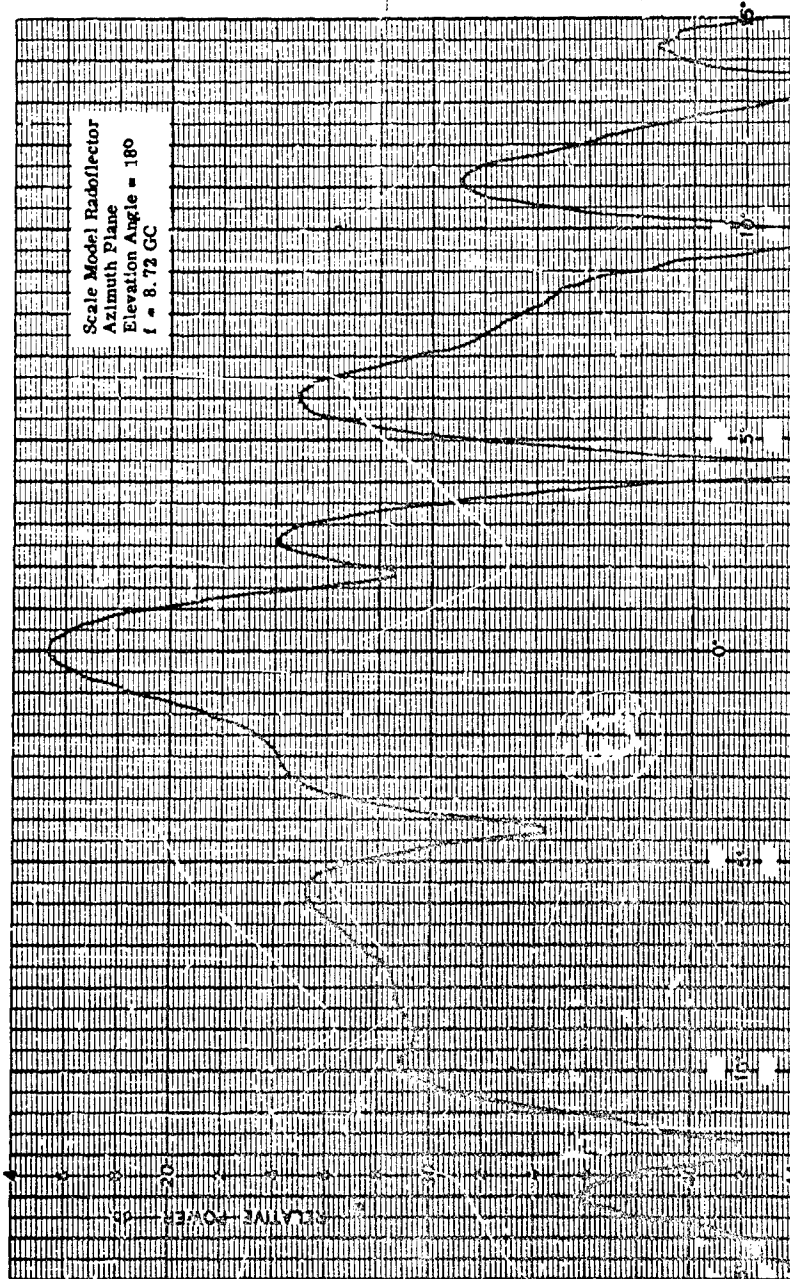


A-40

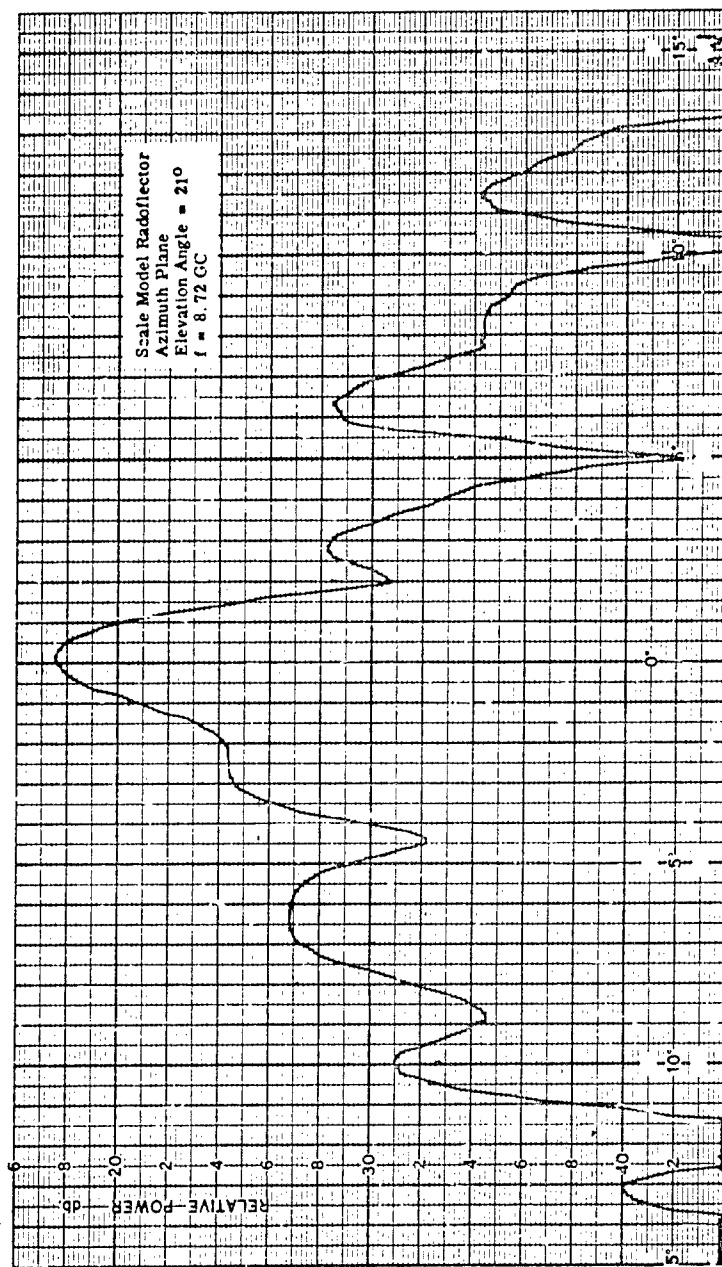




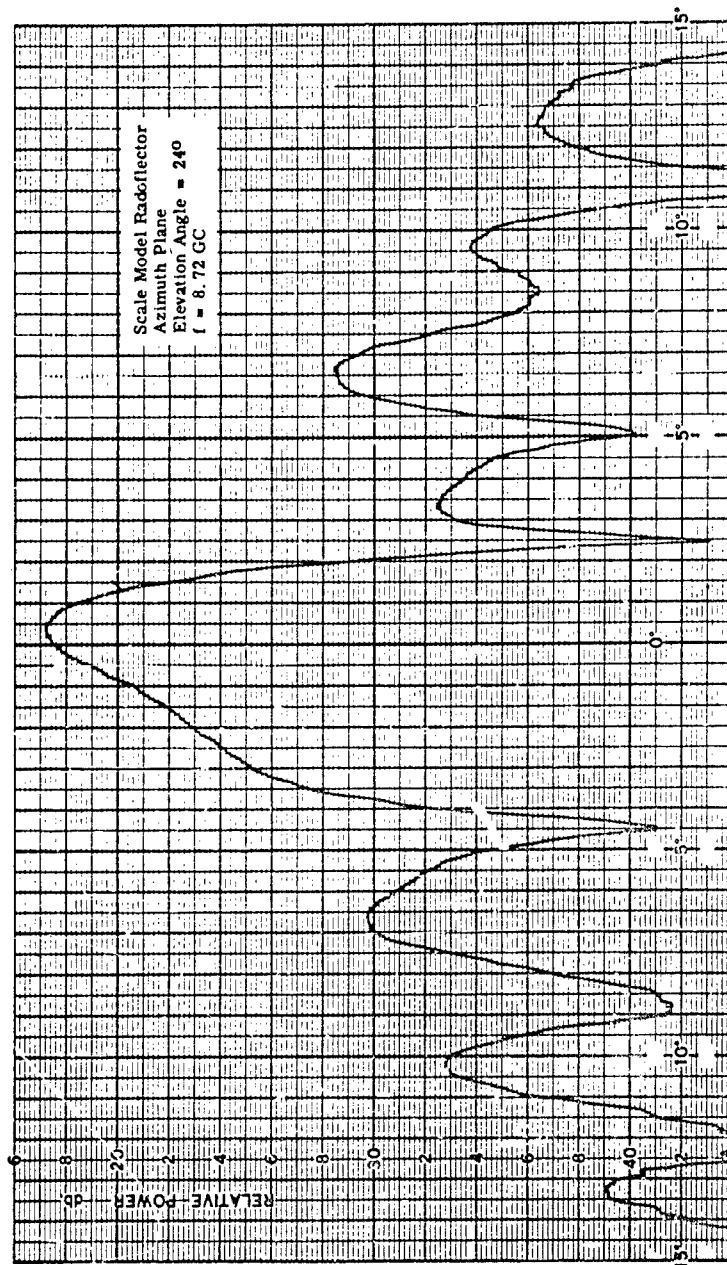
A-42

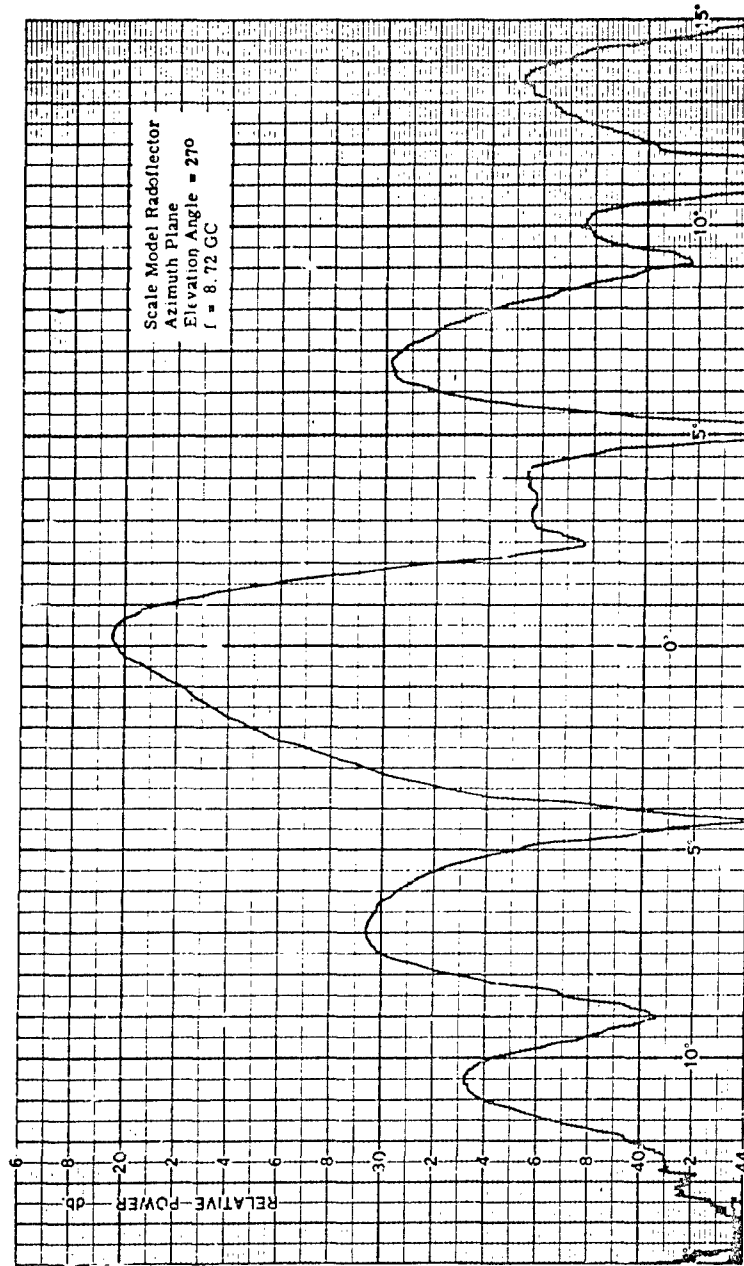


A-43

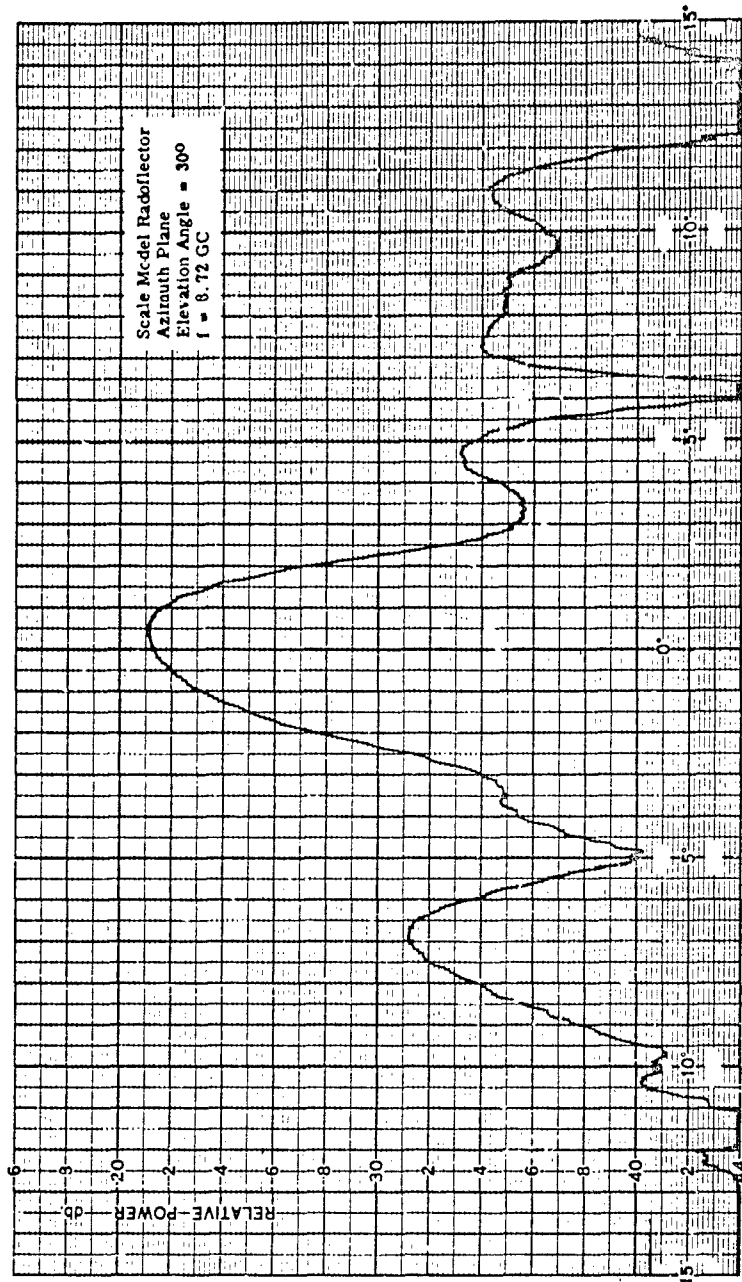


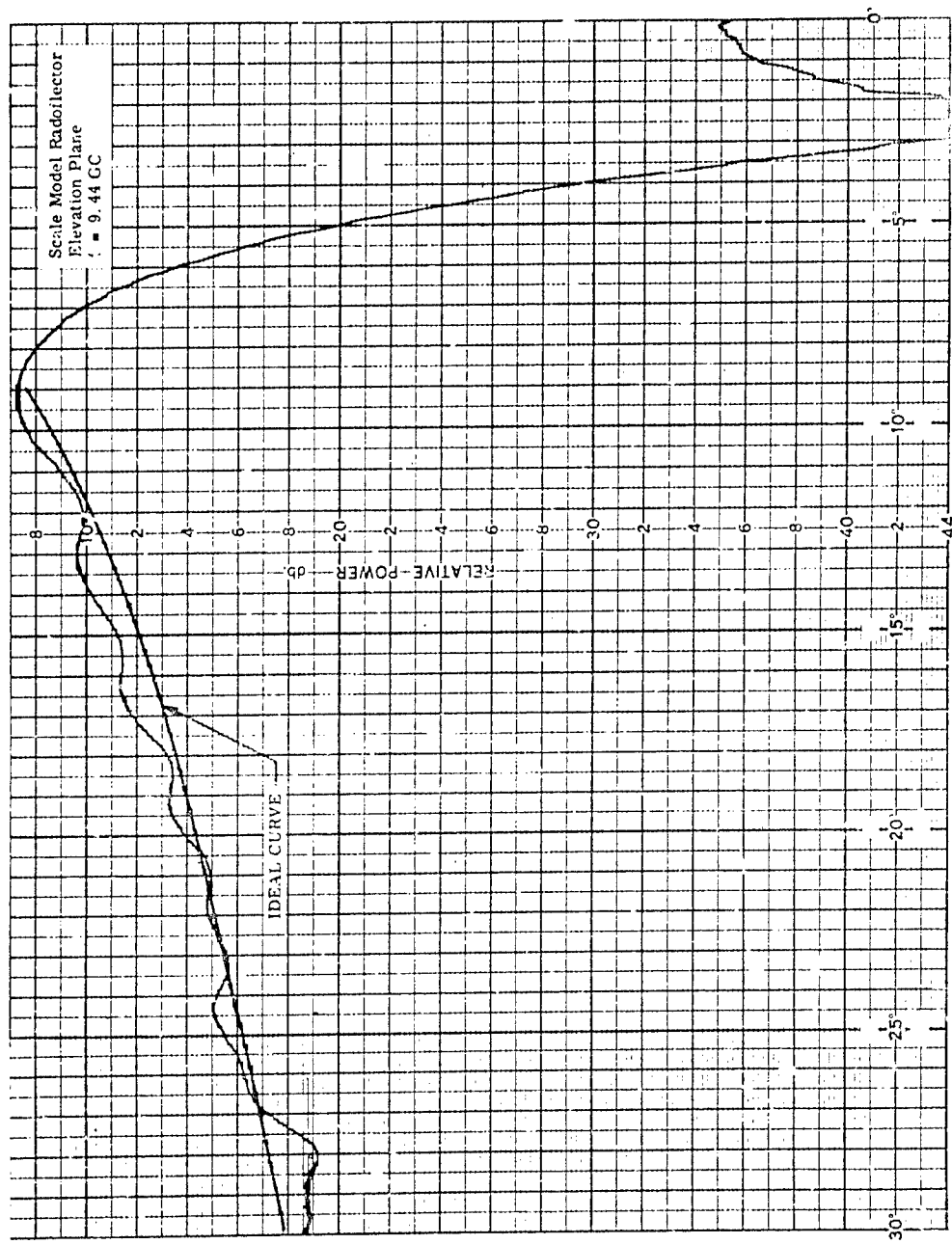
A-44



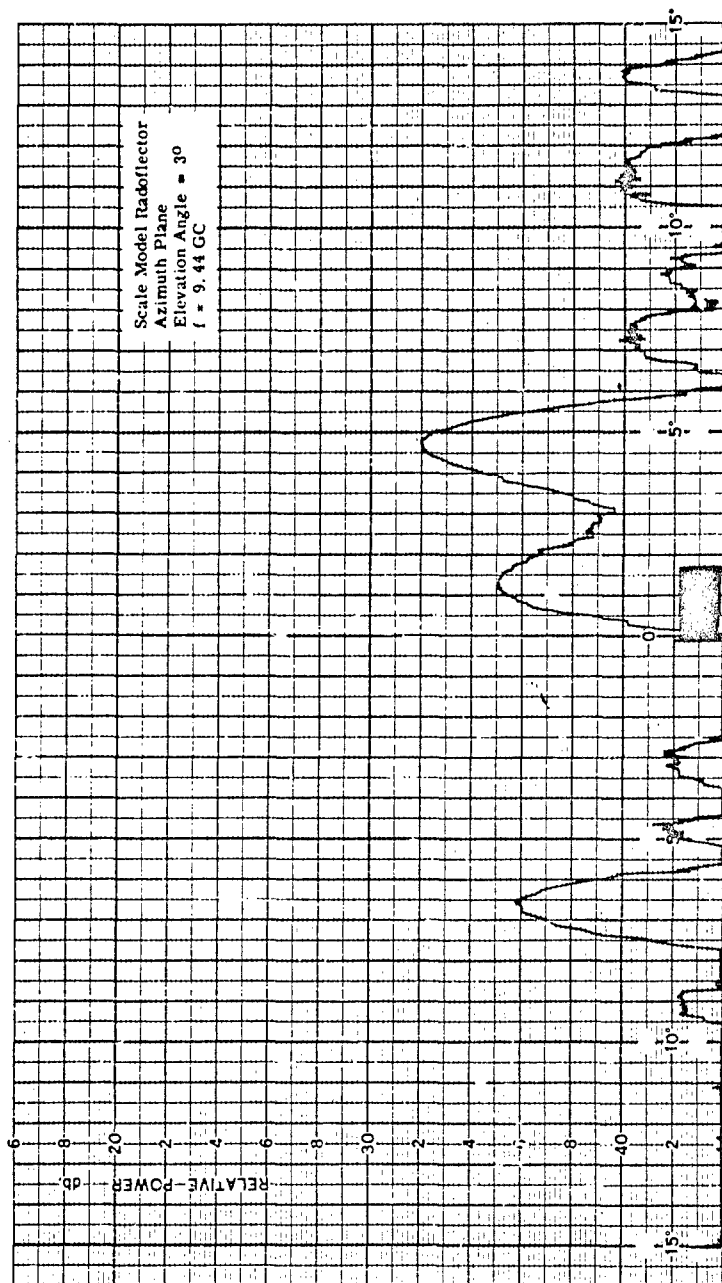


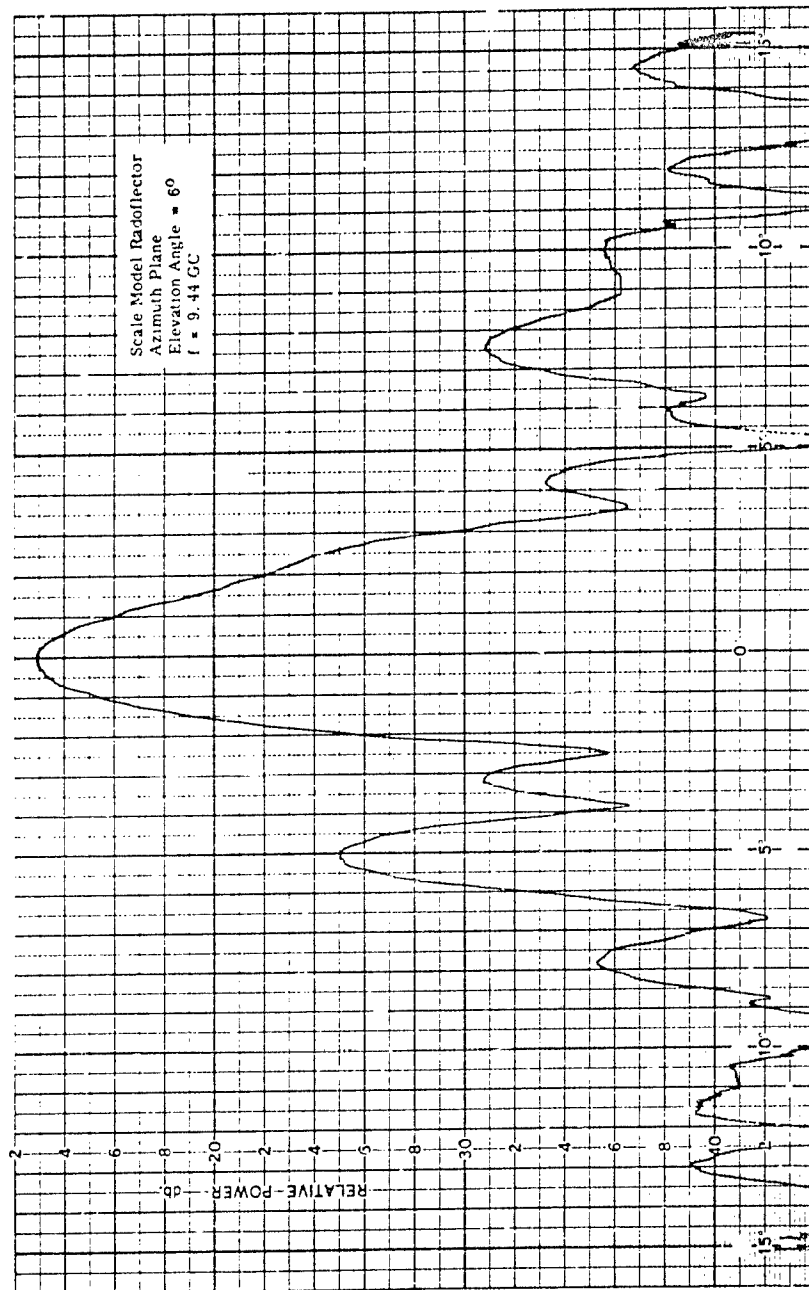
A-46



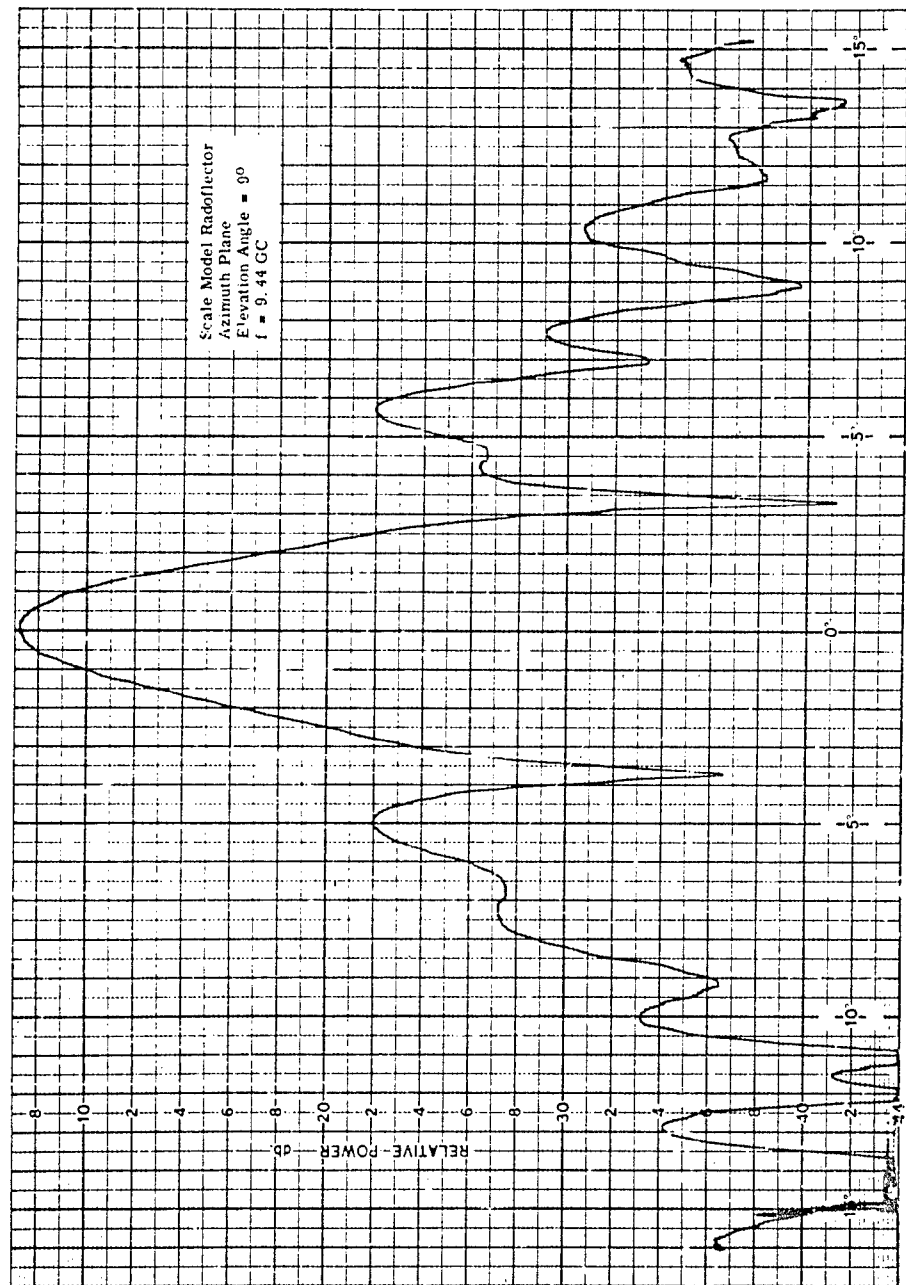


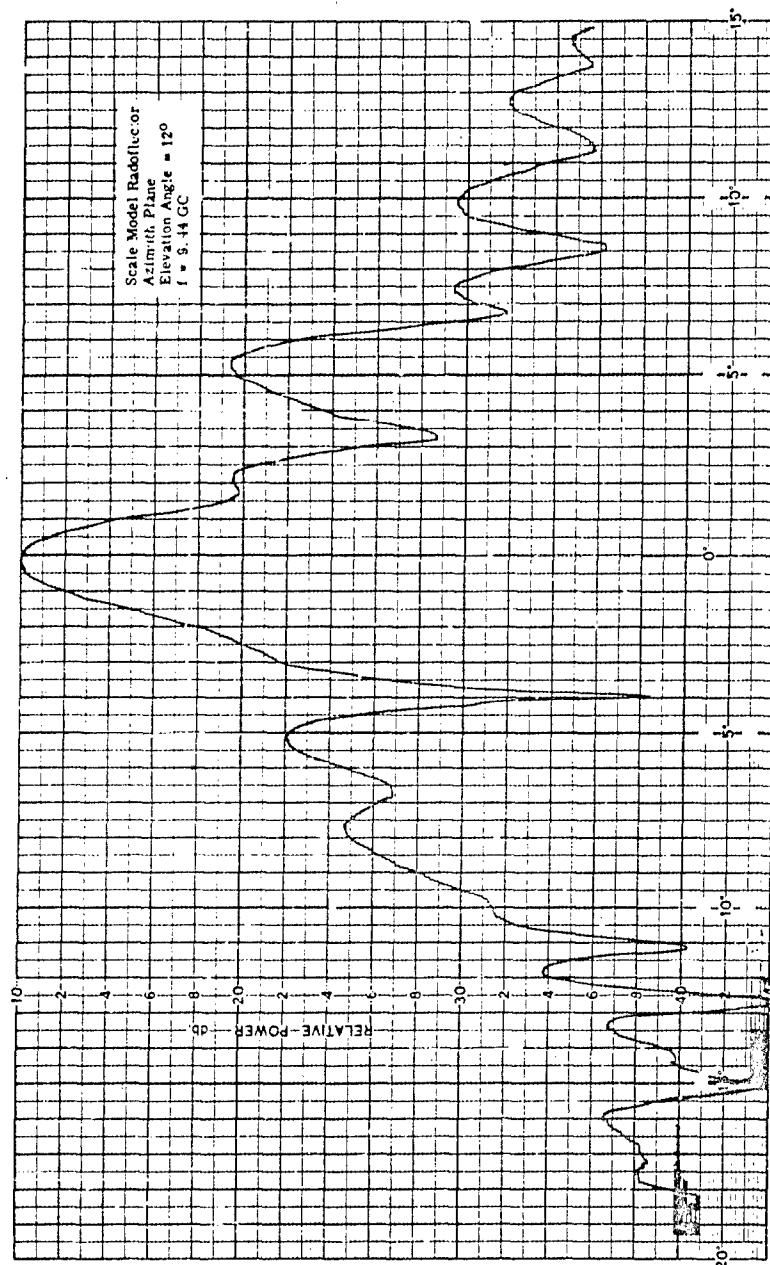
A-48



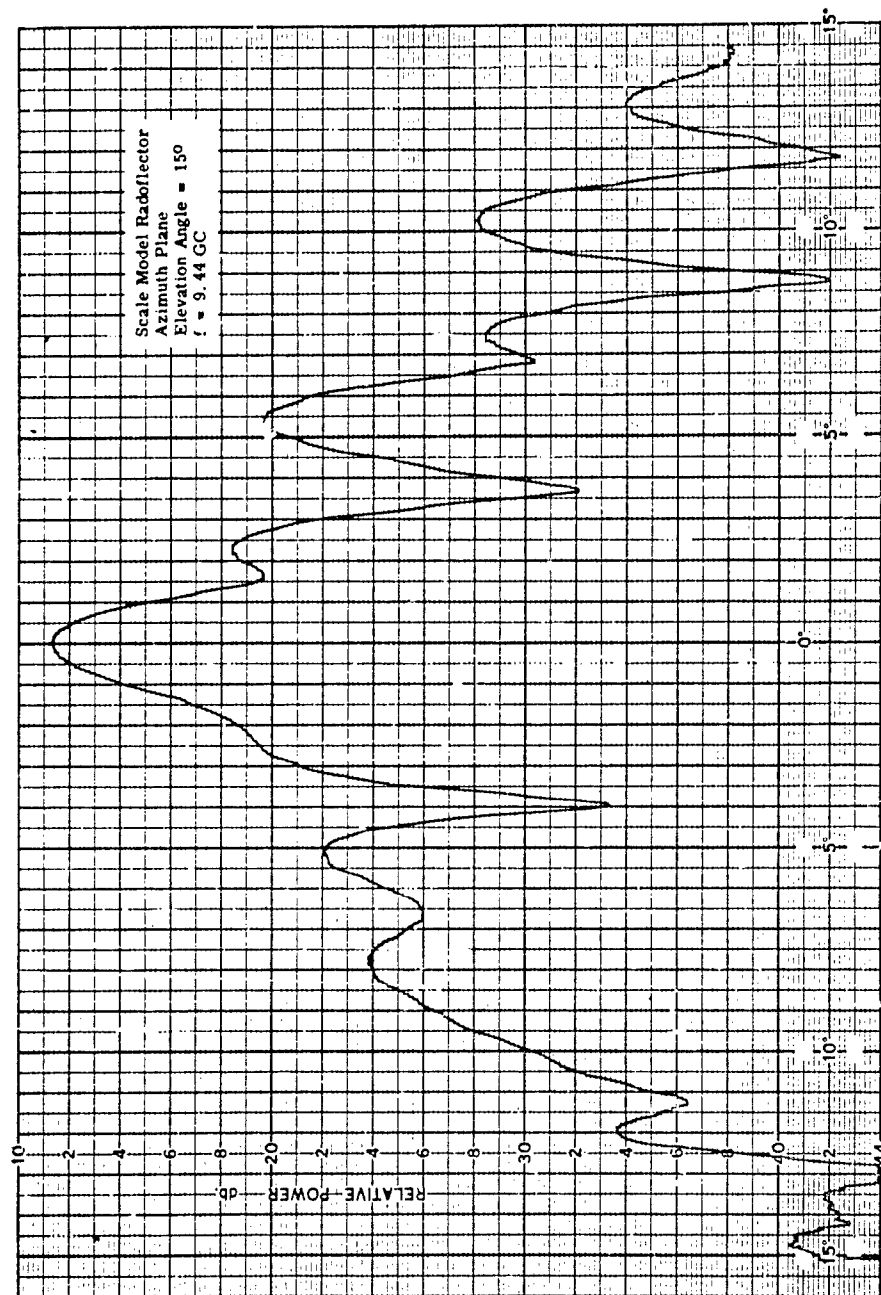


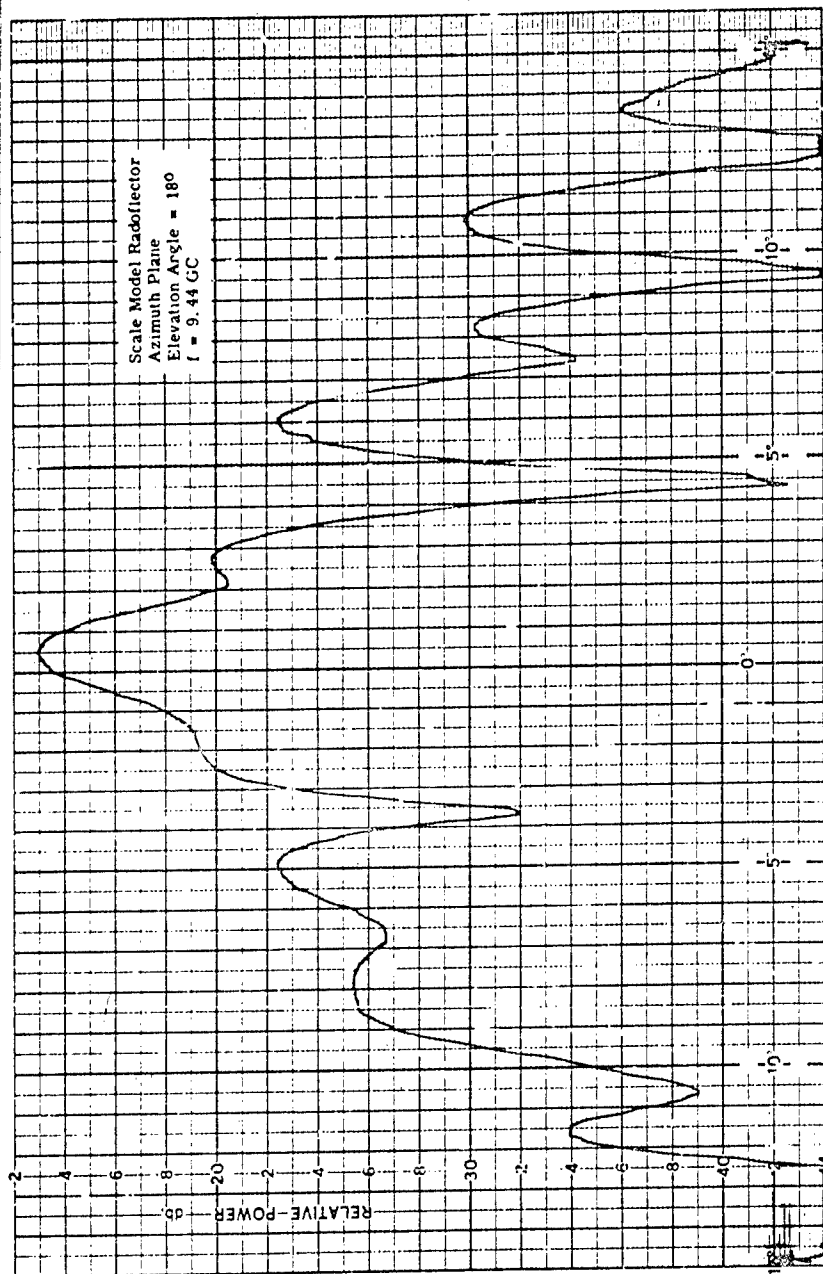
A-50



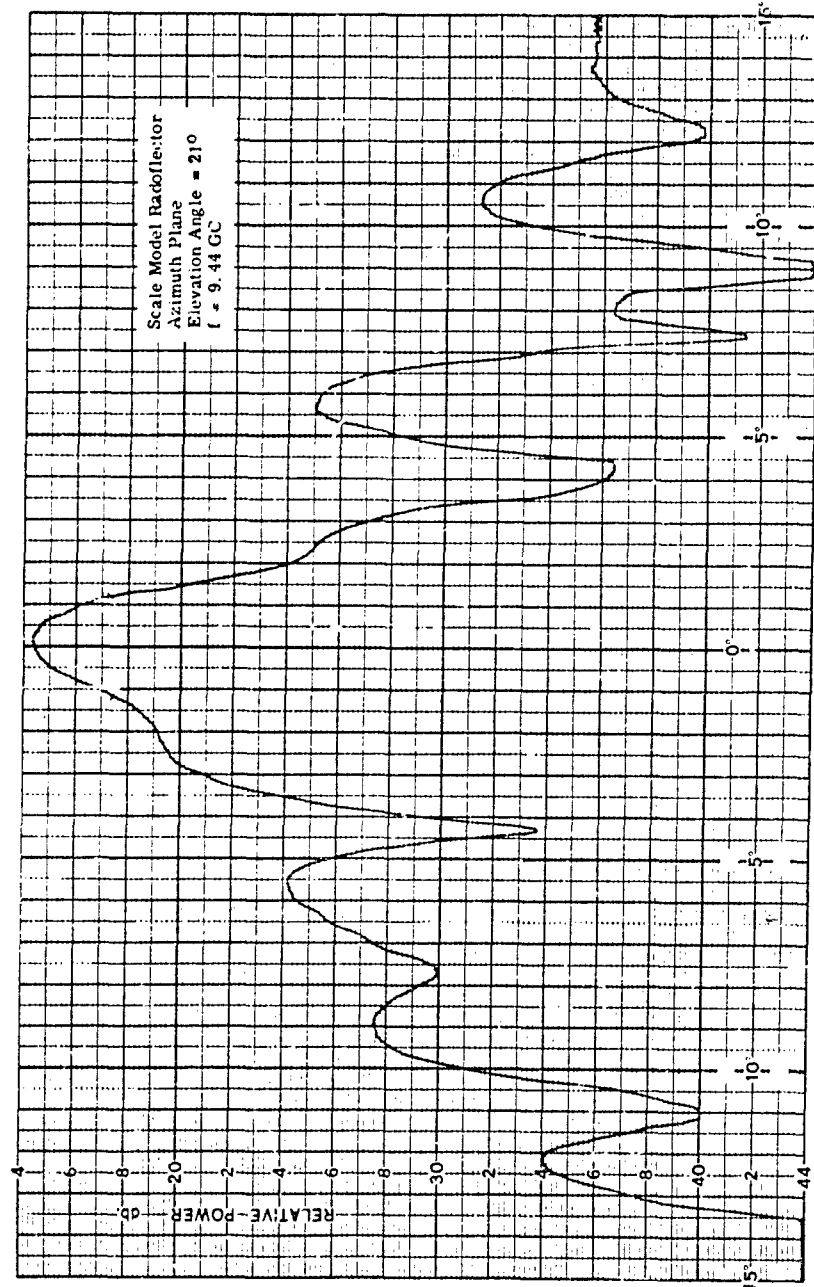


A-52

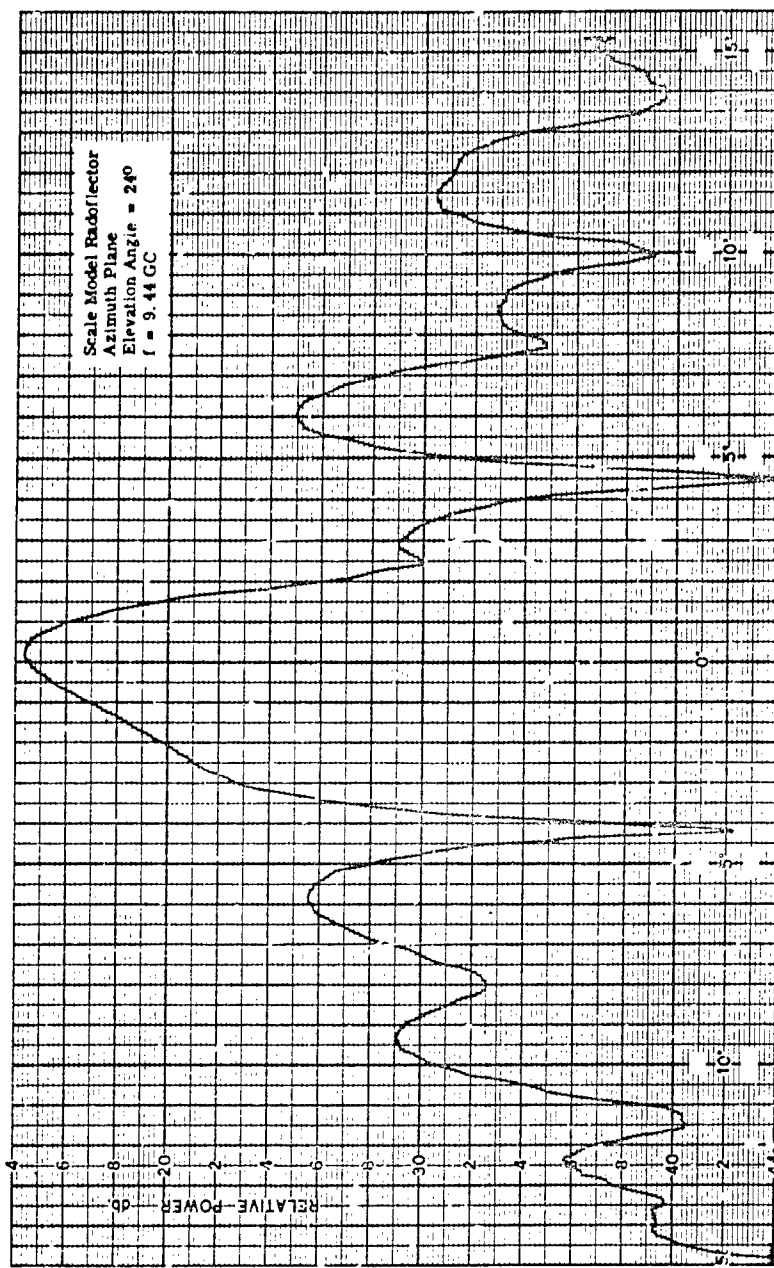




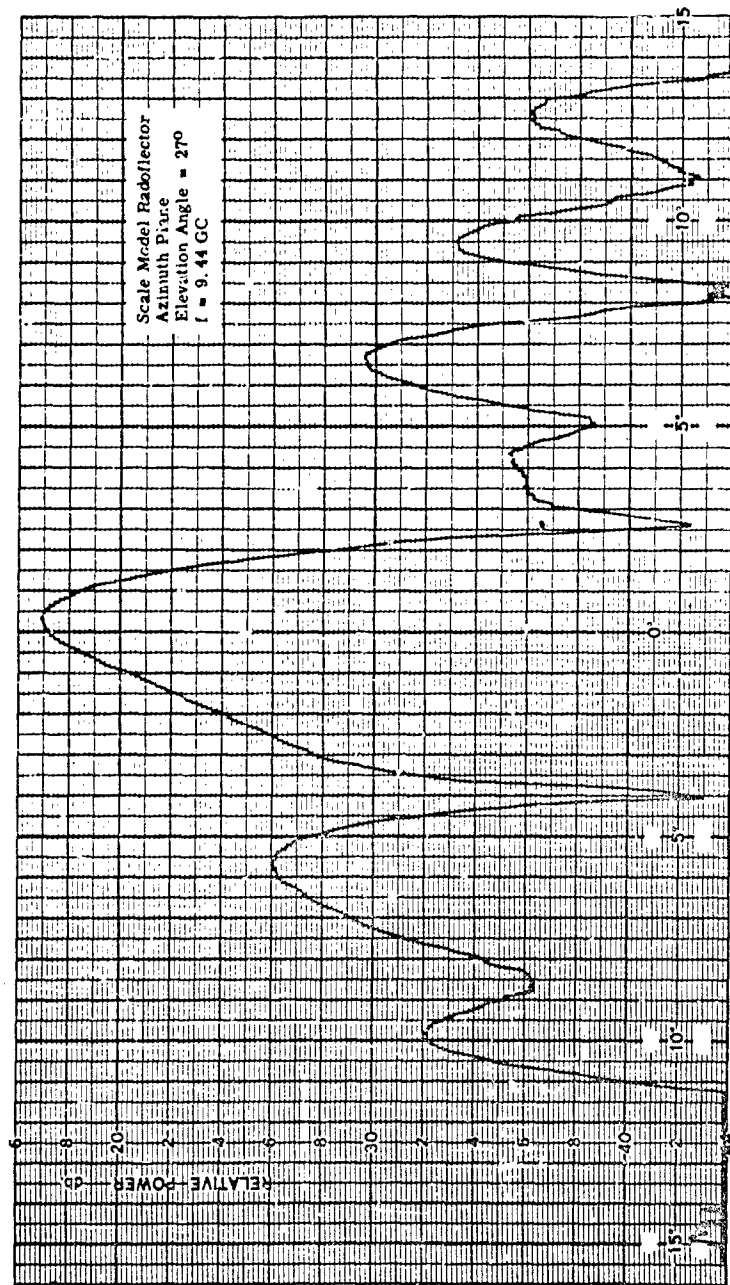
A-54



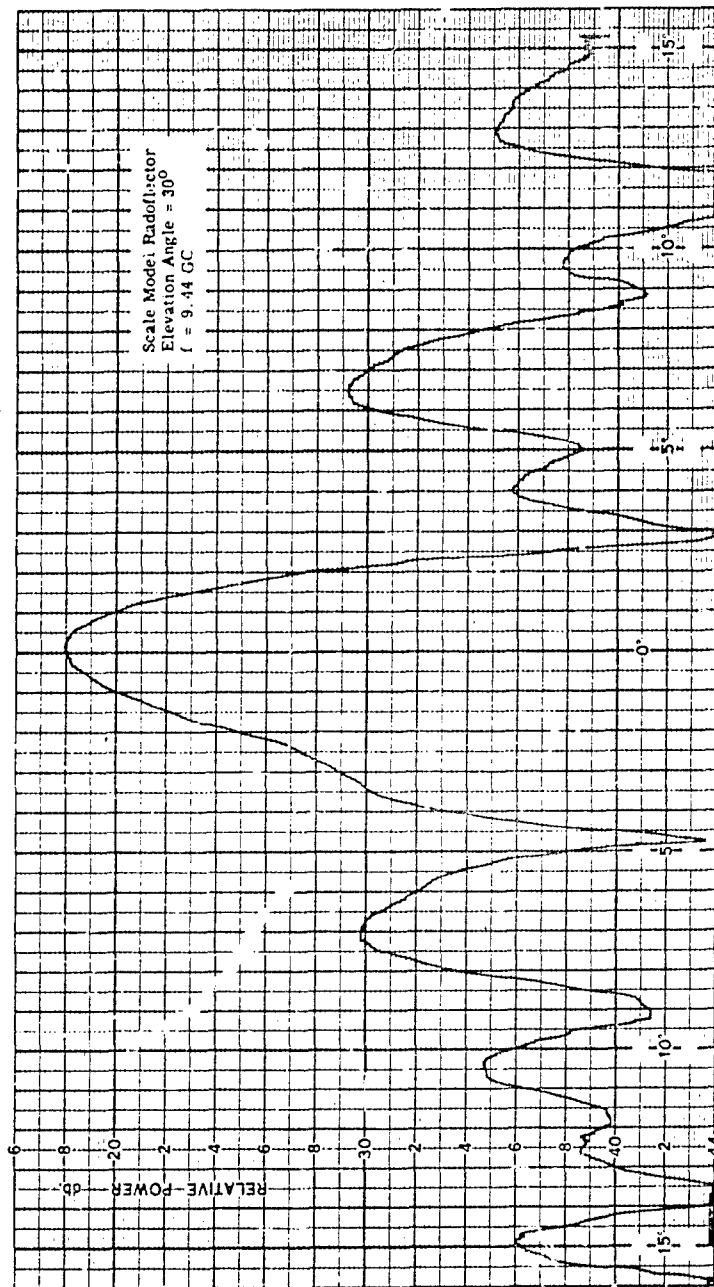
A-55



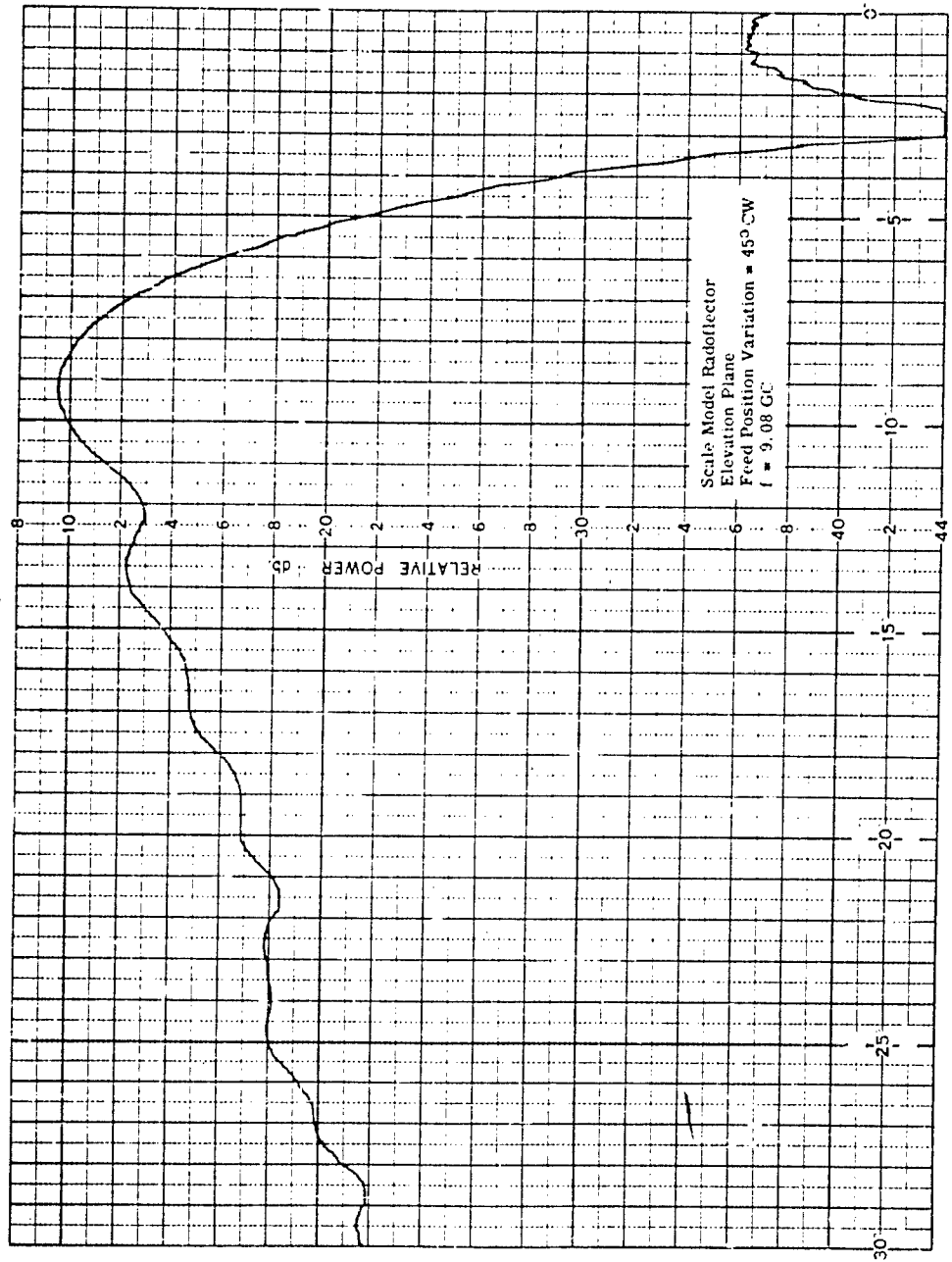
A-56

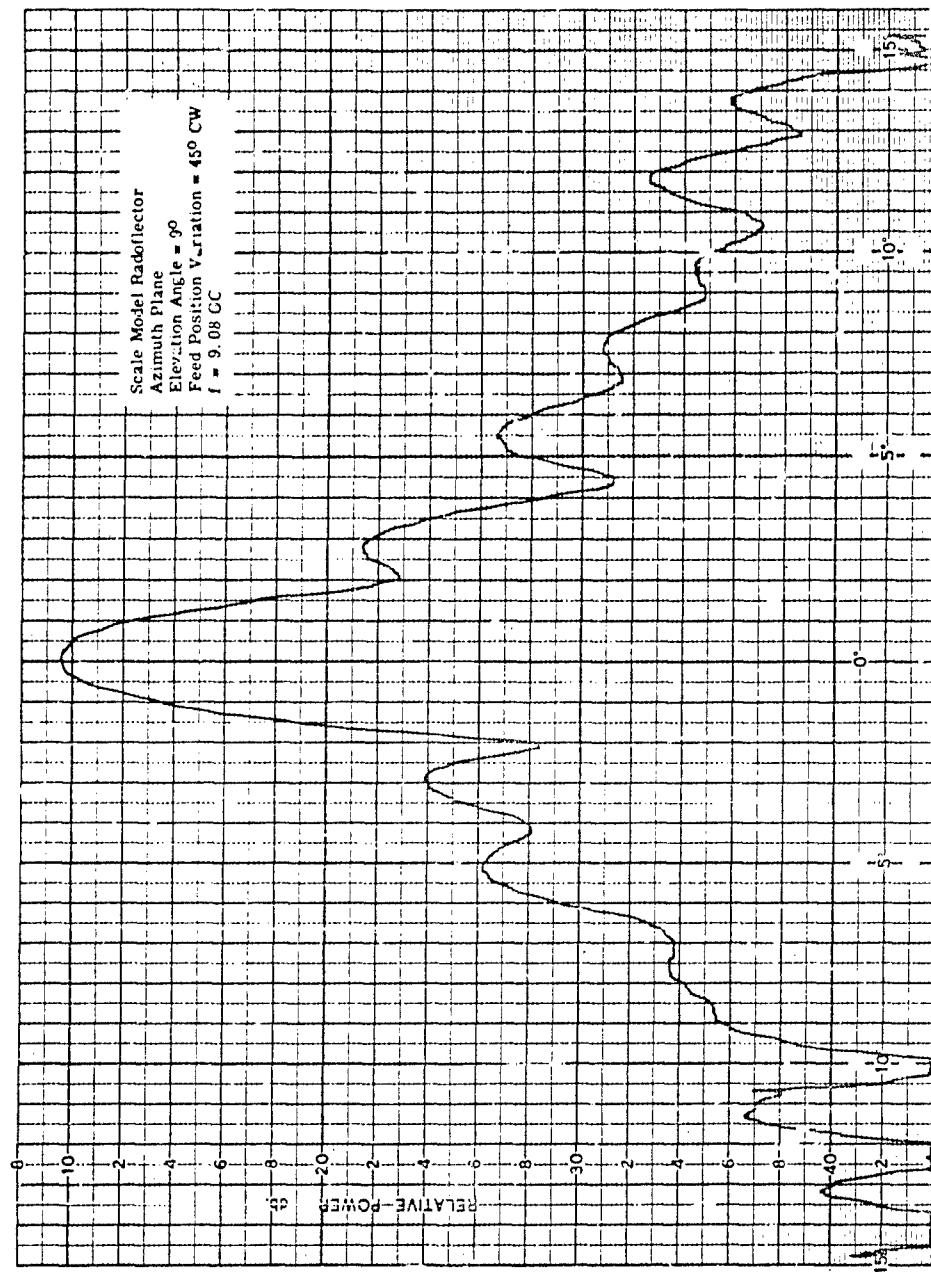


A-57

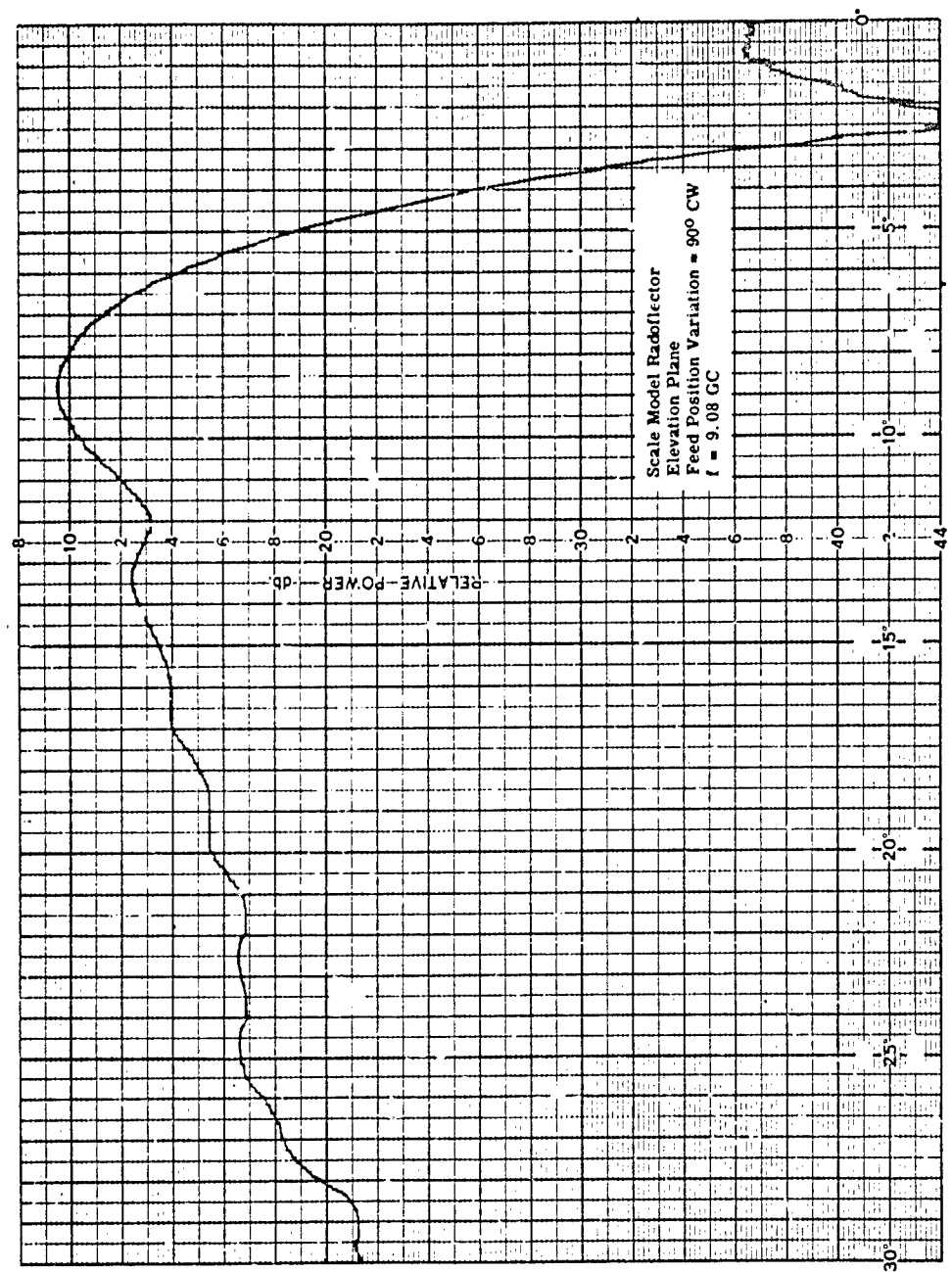


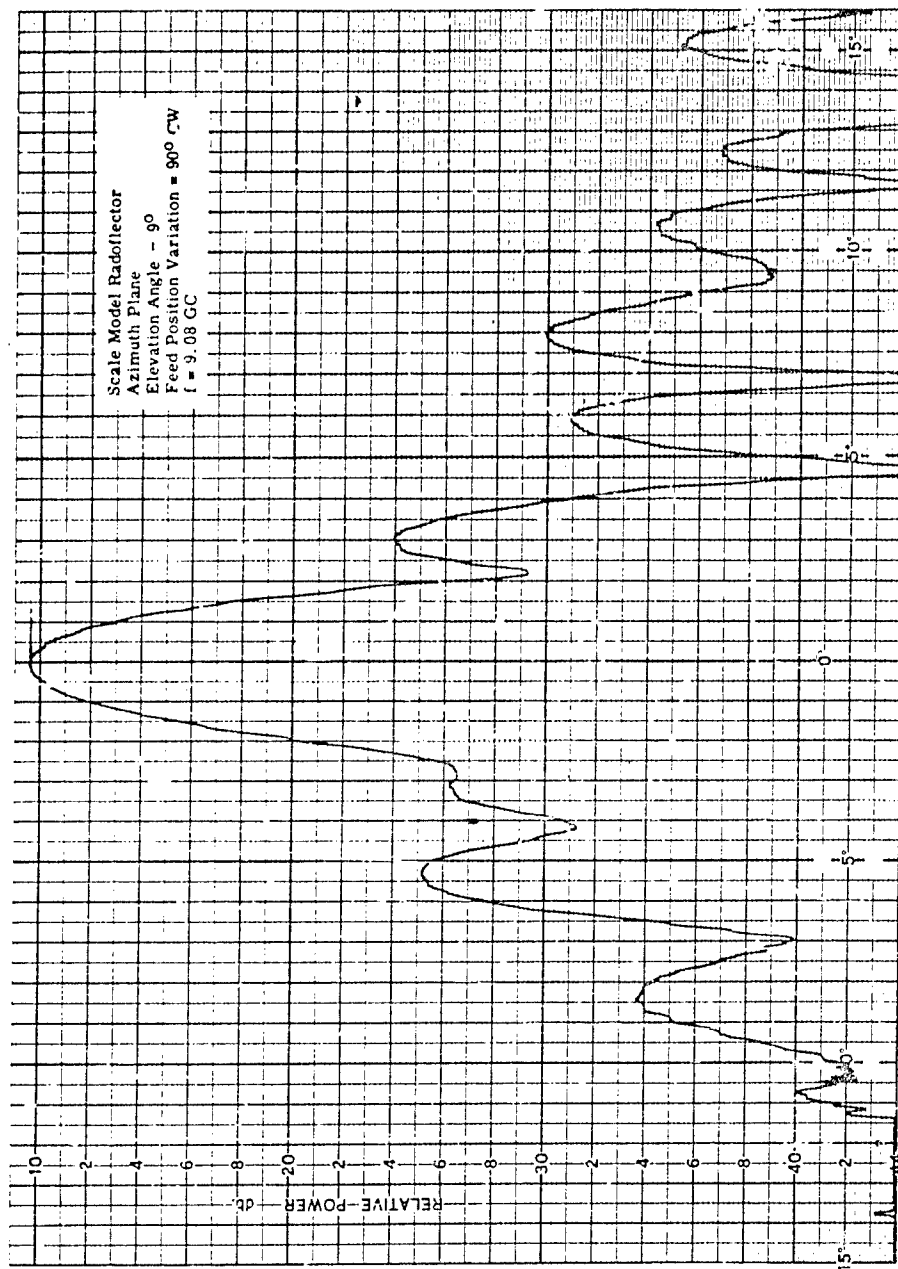
A-58



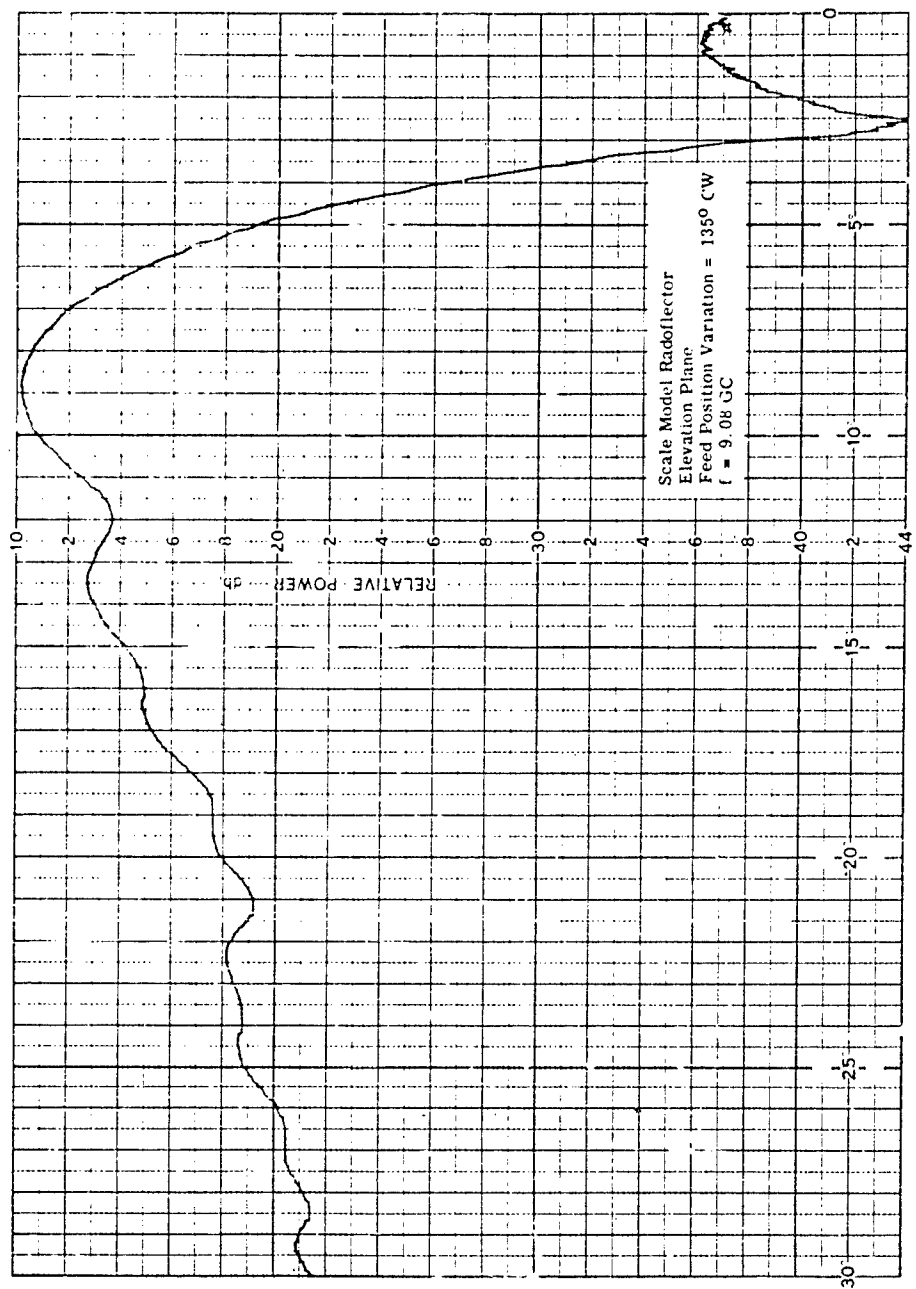


A-60

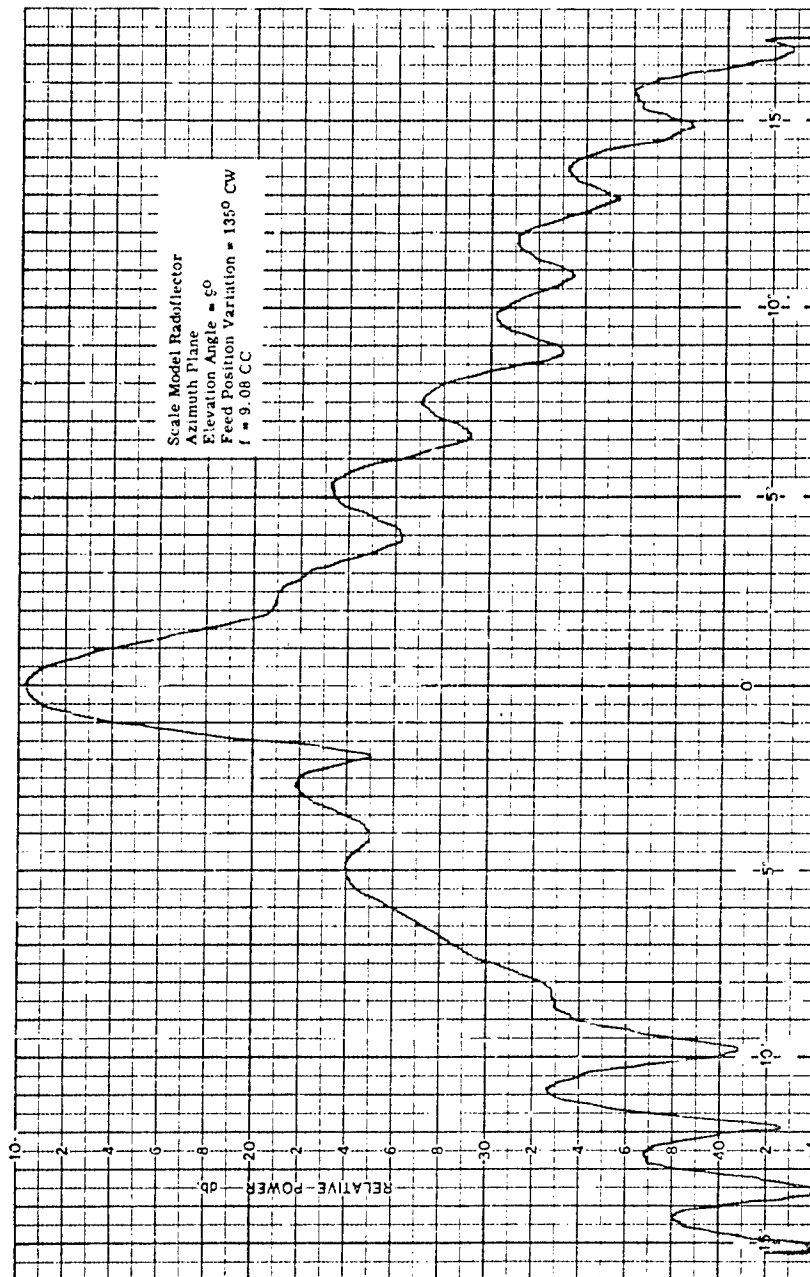




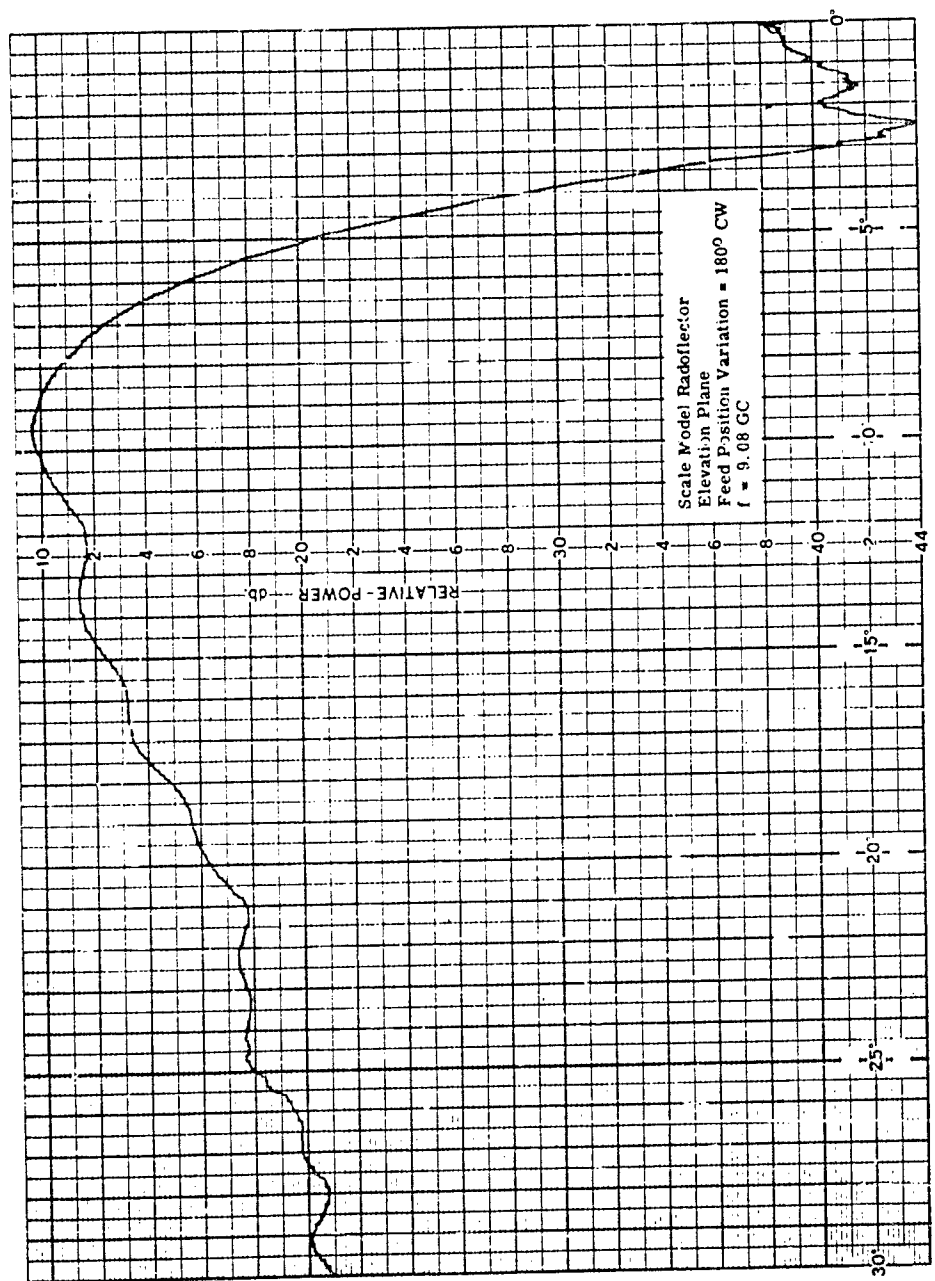
A-62



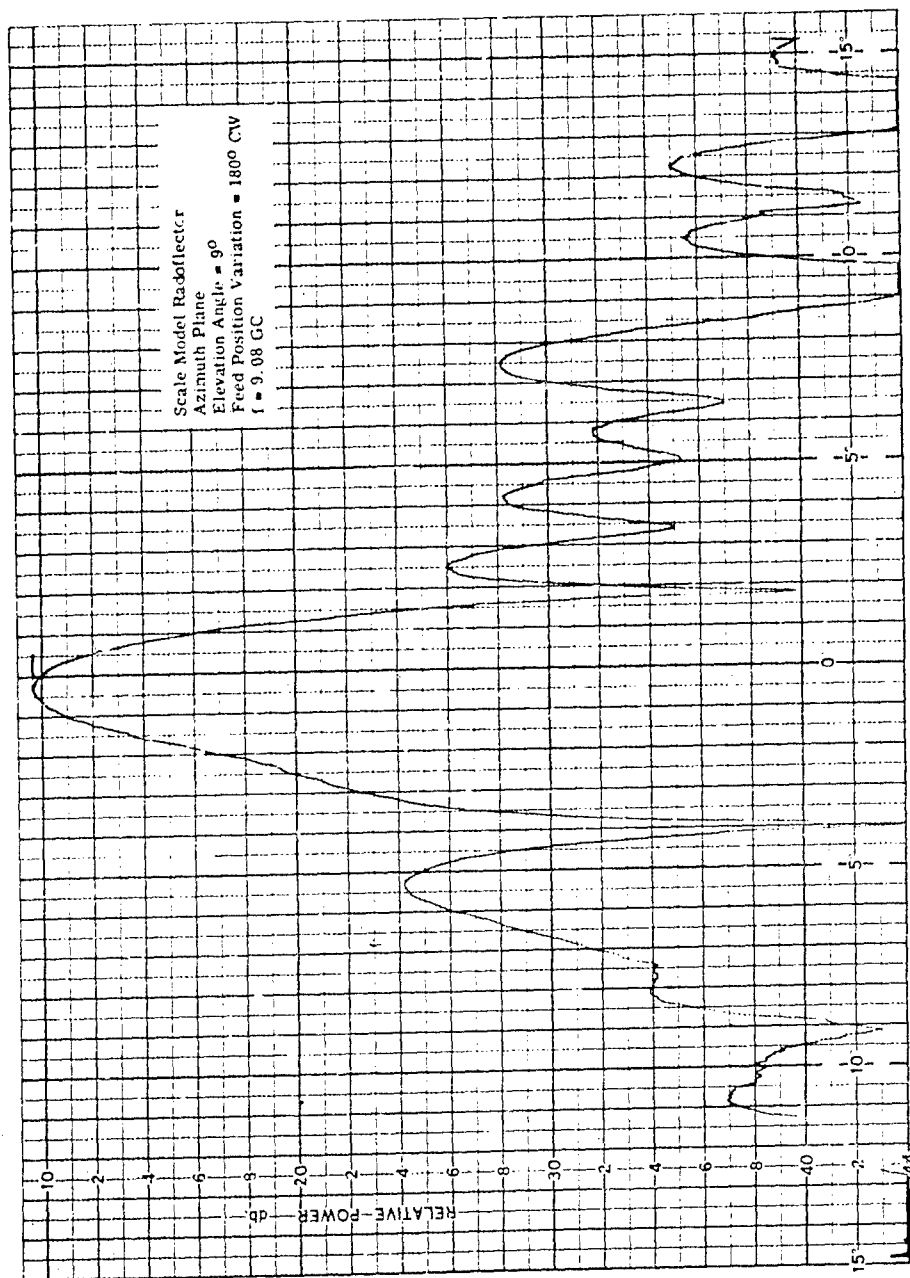
A-63



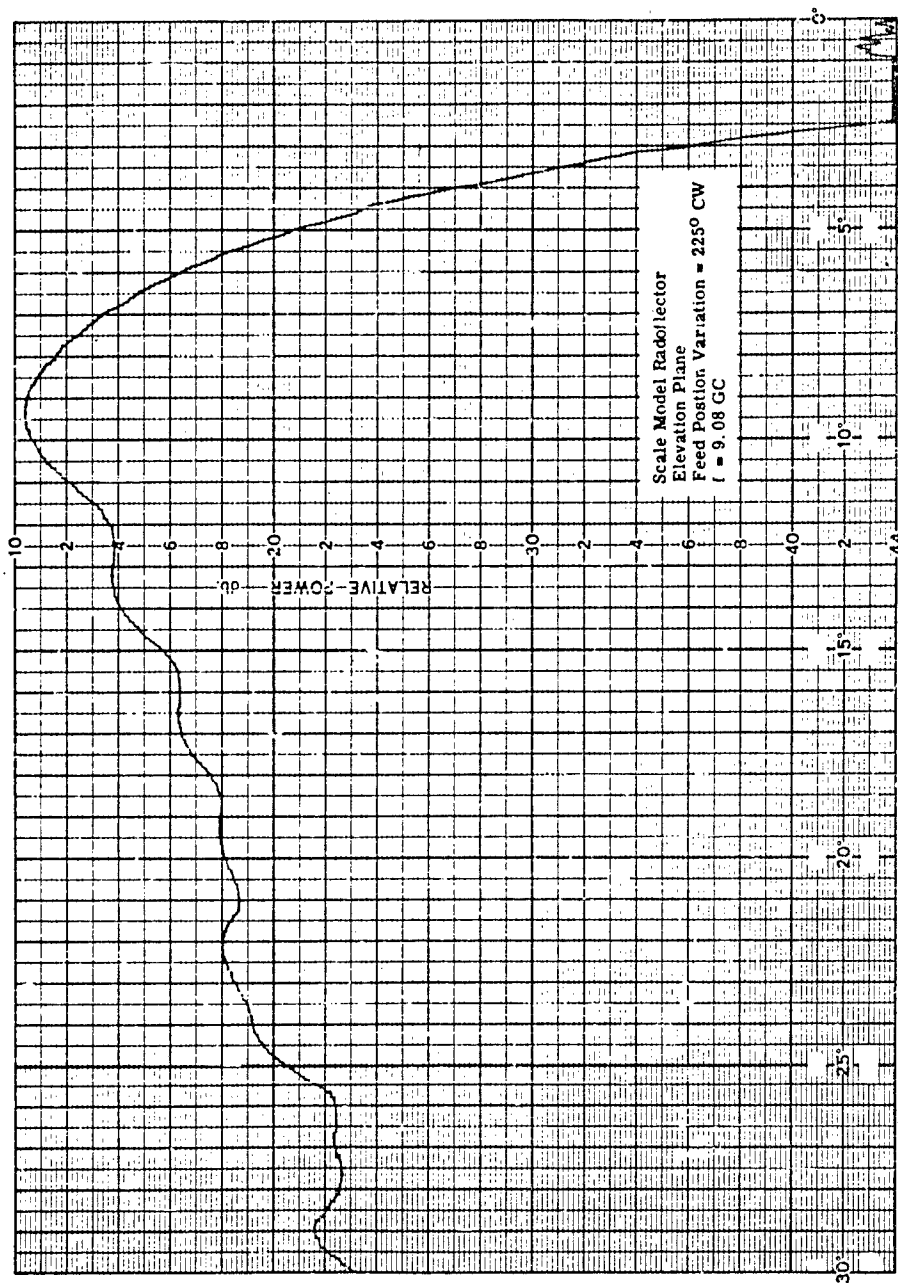
A-64



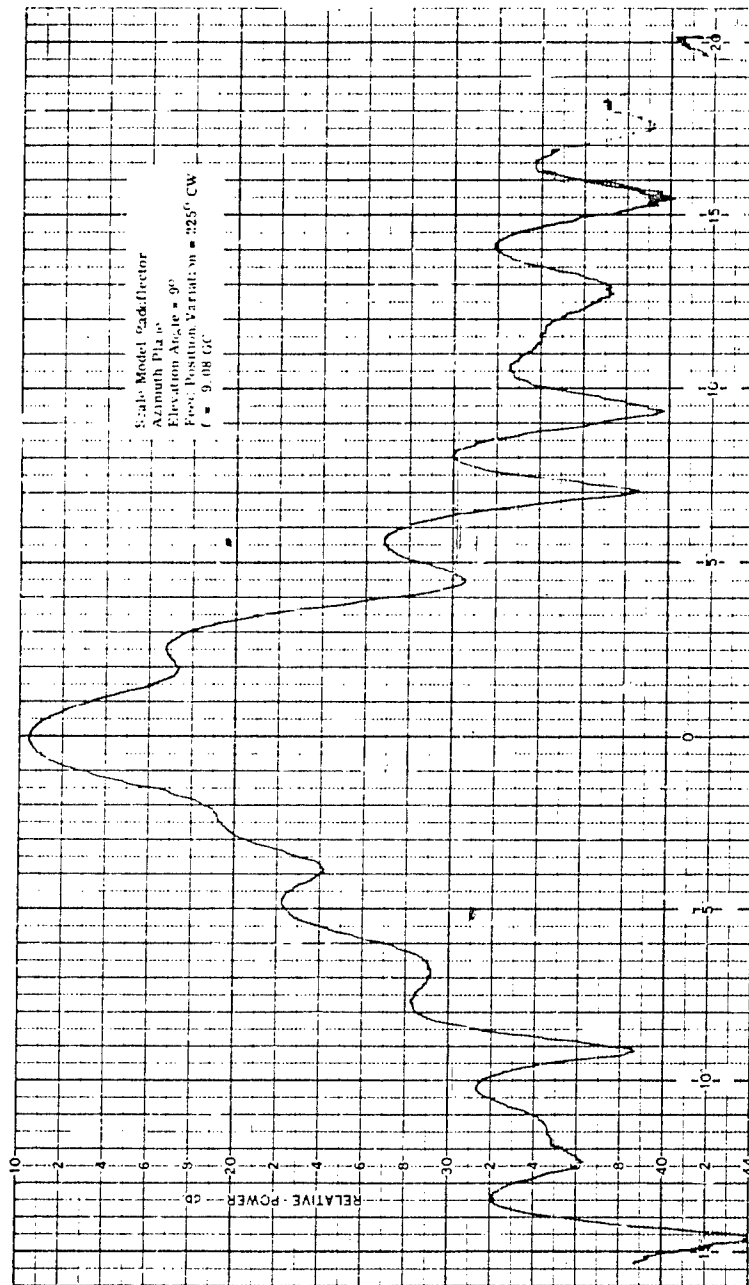
A-65



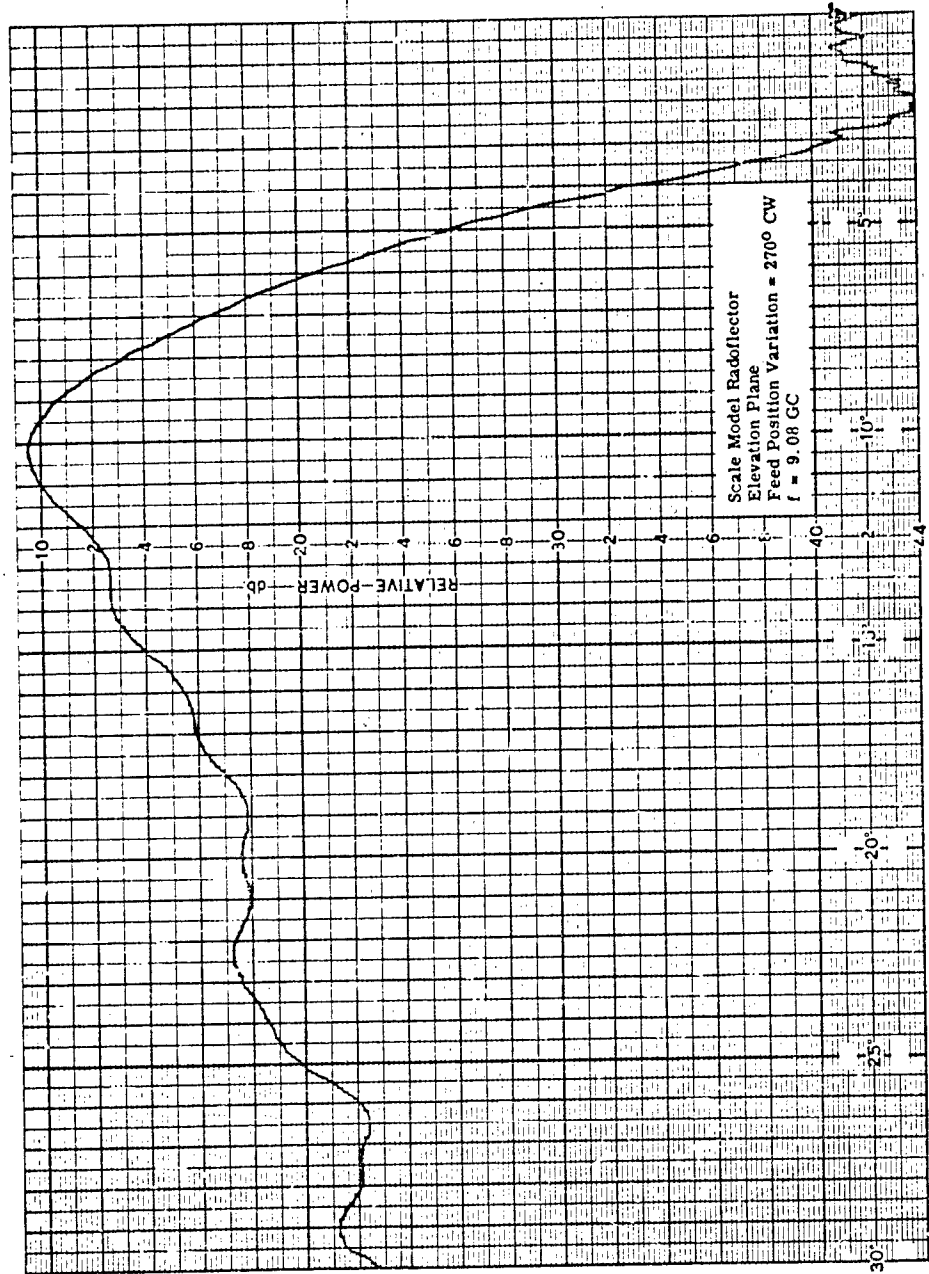
A-66

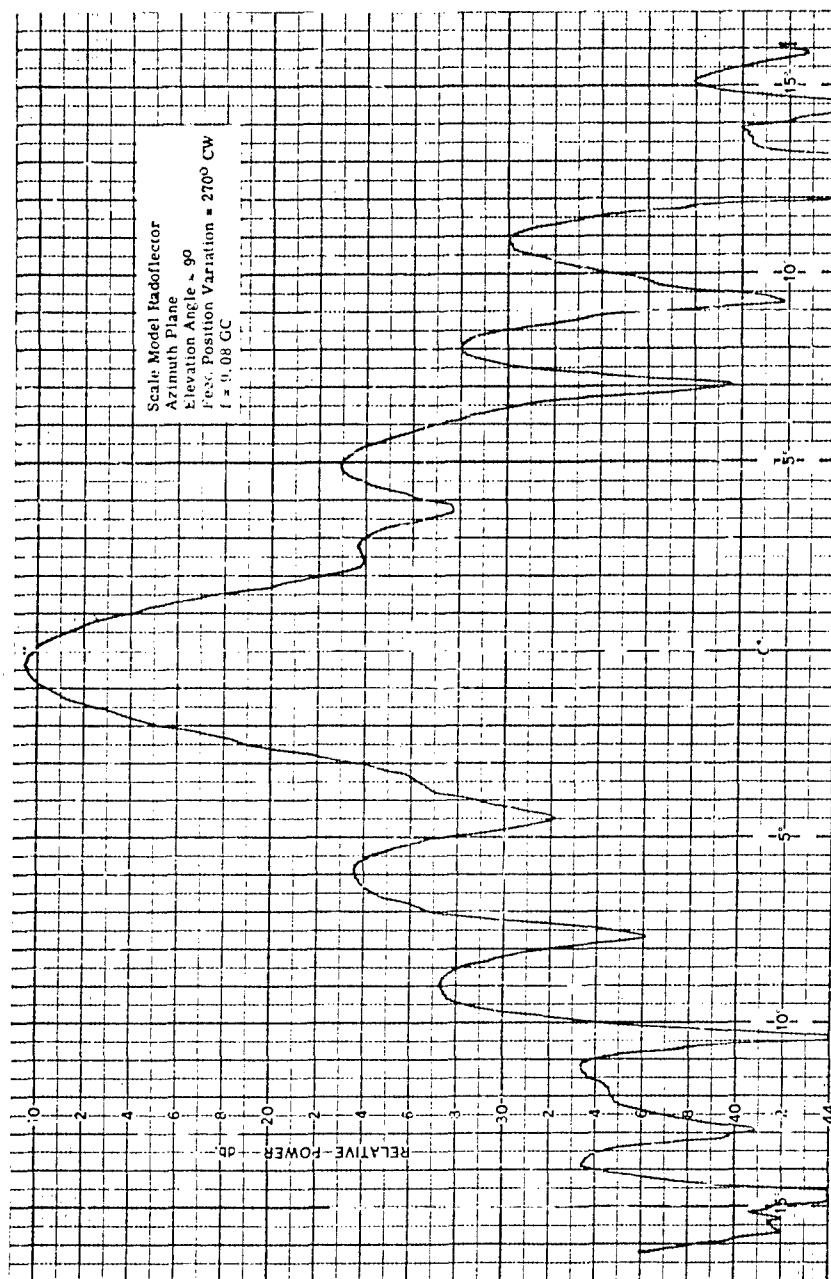


A-67

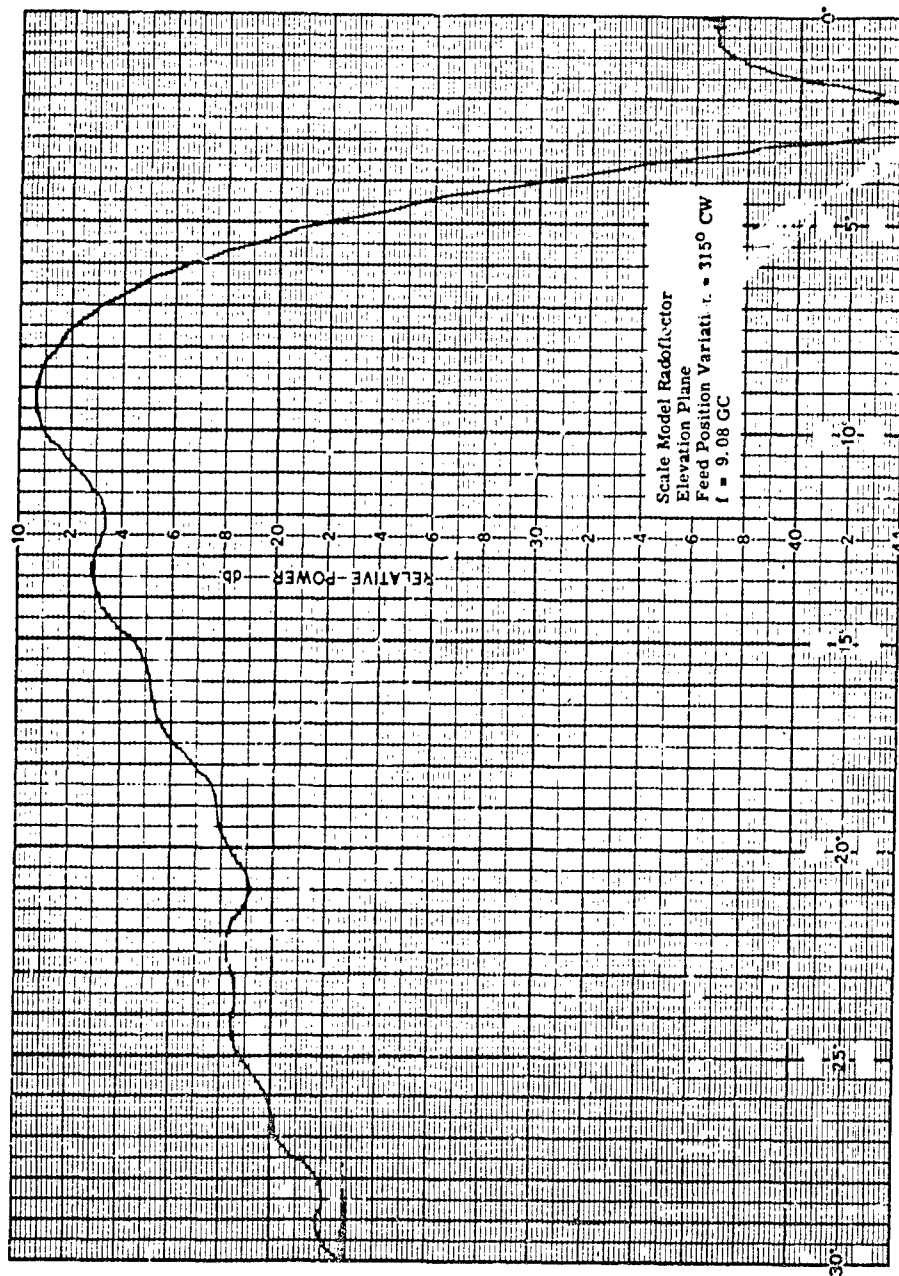


A-68

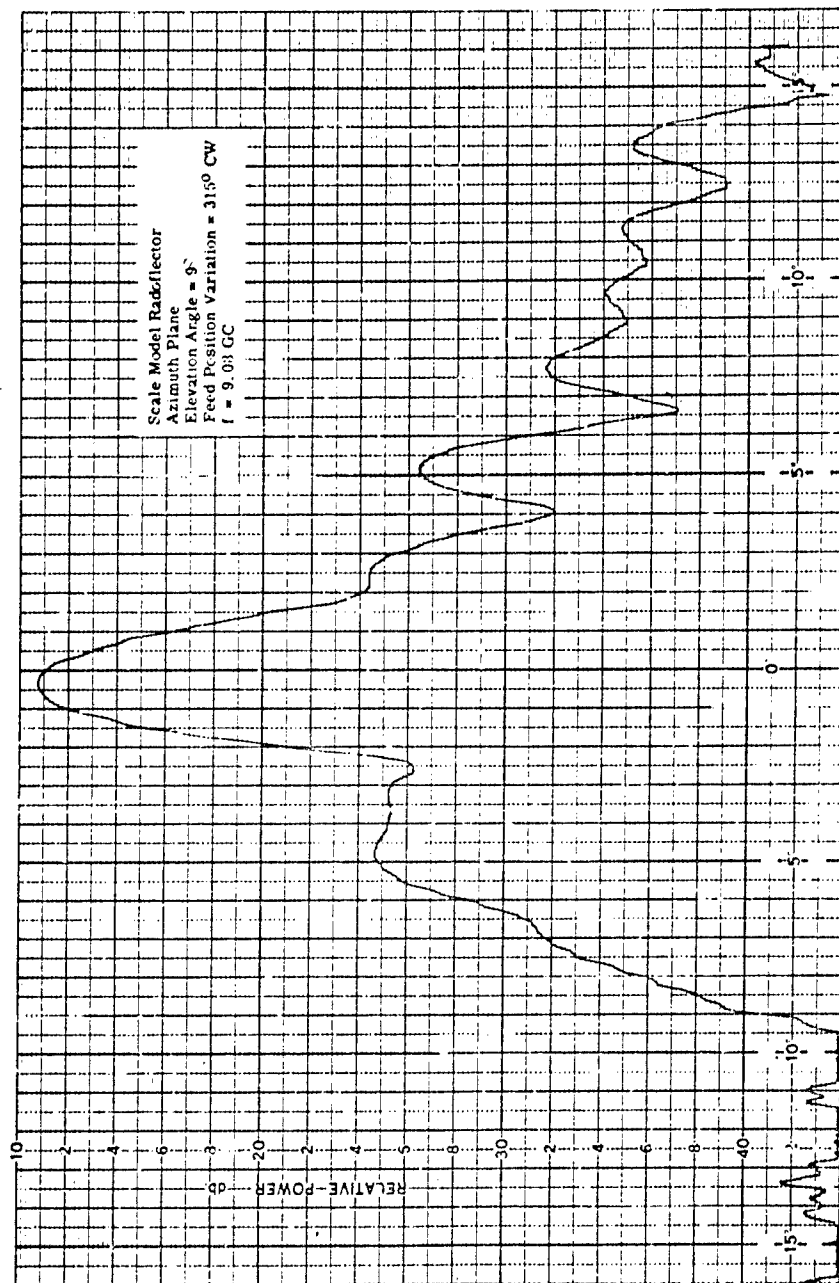




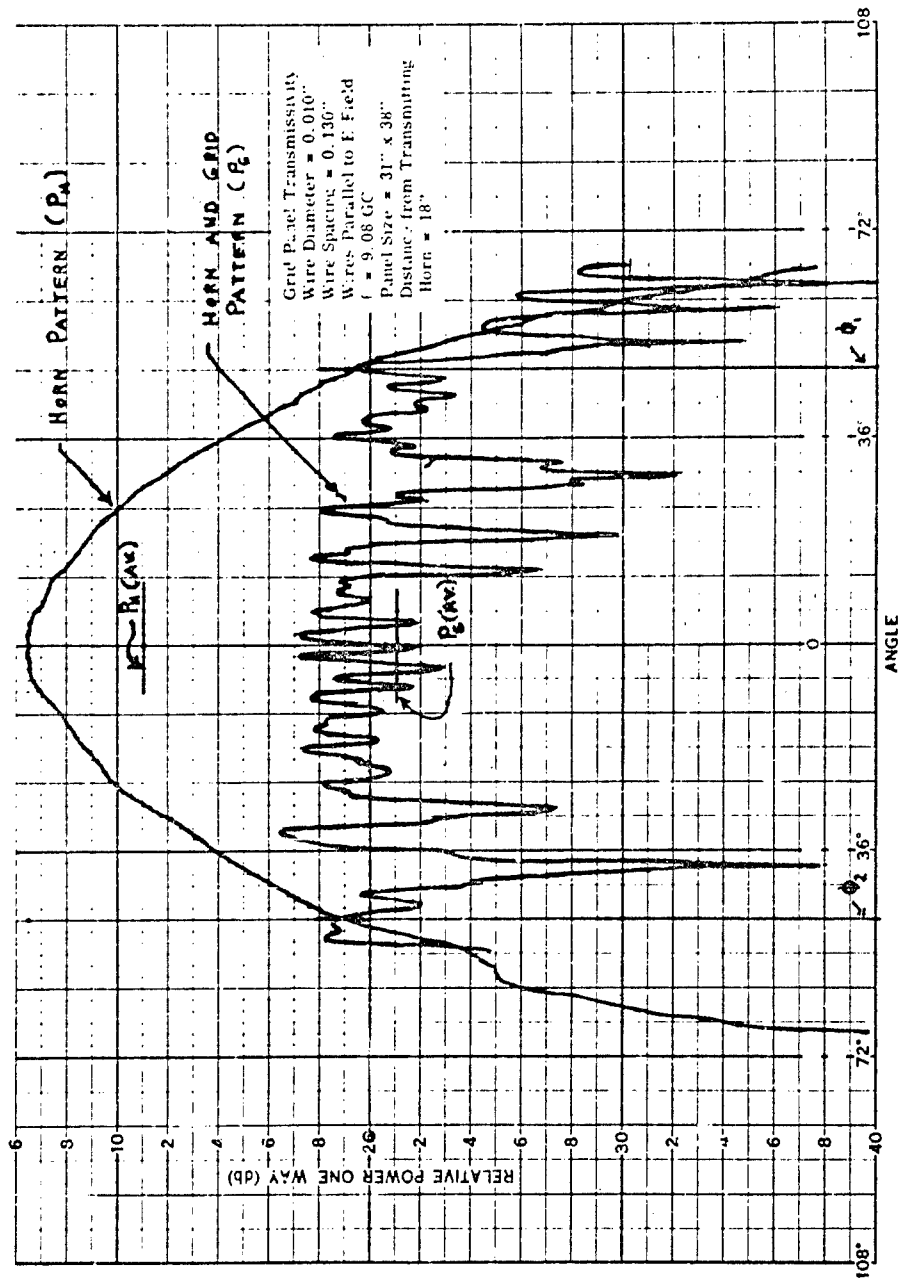
A-70



A-71



A-72



Appendix B

REFERENCES

1. Jasik, H., *Antenna Engineering Handbook*, Page 12 - 12, McGraw-Hill, New York, 1961.
2. Jasik, H., *Antenna Engineering Handbook*, Page 12 - 23, McGraw-Hill, New York, 1961.
3. Tingye Li, *Study of Spherical Reflectors*, IRE Trans, AP-7, July 1959.
4. Rad Lab Series Volume 10 Section 5, McGraw-Hill, New York, 1949.
5. Collins, D. D. and Congdon, G. W., *Pseudo-Hardened Emergency Antenna Installation, Prototype Design Data*, Goodyear Aircraft Corporation, GER-10884, 1 November 1962.
6. *Pseudo-Hardened Emergency Antenna Installation Specification*, Goodyear Aircraft Corporation, GER-10843, 30 October 1962.
7. Bezbatchenko, J. W., *A Study of Aerodynamic Loads on Large Spherical Radomes for Ground Installation*, Goodyear Aircraft Corporation, GER-8917, 13 August 1958.
8. Foerster, A. F., *Theory of Spherical Ground Radome*, Goodyear Aircraft Corporation, GER-0224, 1 May 1958.
9. Timoshenko, S., *Theory of Plates and Shells*, McGraw-Hill, Inc., New York, 1940.

Appendix C

ADDENDUM 1 TO RADC-TDR-63-64

It has been established that there was a difference of interpretation of the vertical pattern specification on the program reported herein. In essence, the interpretation made by Goodyear Aircraft Corporation (GAC) is that the pattern is defined from $\theta = 9^\circ$ to 30° elevation angle and shall follow a pattern $\csc^2 \theta$ between these limits. Rome Air Development Center (RADC) desired a pattern that is defined from 0° to 30° having a 9° beamwidth and then \csc^2 to 30° .

It is the opinion of GAC that either pattern can be achieved using the Radoflector. As will be listed below, the differences in the configuration to meet the alternate pattern requirements are small. Hence, the feasibility demonstrated in this TDR is applicable to both pattern requirements.

DESIGN OF VERTICAL APERTURE

A peculiarity of the Radoflector design is that the use of a single, simple feed horn requires that the vertical aperture be equal to the horizontal aperture. This fact is derived from the required use of a horn polarized at 45° and the undesirability of a canted elliptical illumination of the reflecting surface. Since the specified patterns can be met with a horizontally oriented elliptic reflector, a larger than necessary aperture must be used.

In the previous design, the excess aperture imposed no problem. With the pattern defined from 9° to 30° , the "tumblehome," or drop-off in energy outside these angles, could be as sharp as desired. Hence, extra height was used to sharpen the "tumblehome" in the angular range from 5° to 9° . This was accomplished by scaling the vertical aperture while maintaining the ratio of the parabolic to shaped apertures.

However, since the pattern desired by RADC is defined from 0° to 30° , the approach used previously is no longer entirely correct. A suitable alternate approach, though, lies in the use of a beam consisting of \csc^2 shaping from 9° to 30° and the modified shaping required from 0° to 9° . In this way, the "tumblehome" resulting from too large an aperture is "filled in" by a section of the reflector at the top of the aperture. The computational effort to define this contour is not appreciably different from that used on the previous simpler design.

A cursory computation of the probable contour based on relative energy considerations has been made. A plot of this contour is shown in Figure 19A, which gives the previous contour for comparison. To accentuate the extent of the differences, the bottom point of each contour is made the same. A plot of the elevation pattern obtained with the original contour compared with the predicted elevation pattern for the modified contour is shown in Figure 19B.

As is evident, both contours led to essentially the same configuration. The most noticeable differences lie in the relative widths of the bands of solid reflector and parallel wire reflectors. This variation, however, has an almost negligible effect on the electrical performance, resulting as it does in a small loss in gain. As is noted in this TDR, the gain specification is exceeded.

MECHANICAL AND STRUCTURAL DESIGN

In considering the effects of the modified reflector contour from a mechanical and structural design standpoint, no change has resulted that would affect the feasibility of the Radoflector concept. The mechanical characteristics of the initial reflector contour, developed and tested during the Radoflector program, will be basically the same for the modified reflector contour. As can be noted in Figure 19A, two basic changes would occur in the mechanical design as a result of the modified reflector contour:

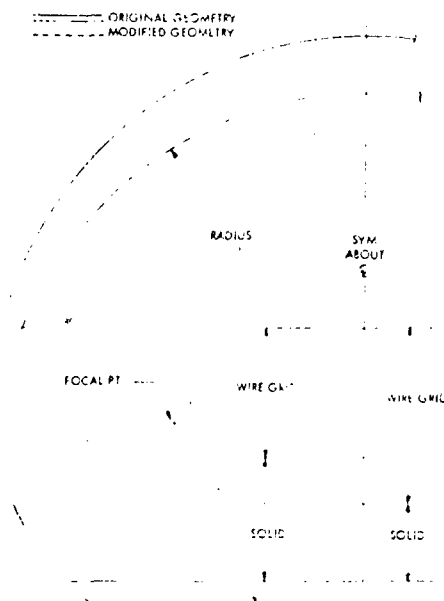


Figure 19A. Modified versus Original Geometry

- (1) The over-all Radoflector size is smaller.
- (2) A larger percentage of the reflector surface is a parallel wire grid rather than a solid reflector.

The smaller Radoflector size presents no design or fabrication problems. If anything, the reduction in size improves the structural performance somewhat, since it reduces deflections caused by the wind loading on the structure.

SUMMARY

The novelty of the proposed design results strictly from the rarity of a problem involving too much aperture. The concept is practical, straight-forward, and relatively simple. The resultant design varies in only minor details from that previously achieved and in no way casts doubt on the proof of feasibility. Inasmuch as the design variation is insignificant, there is no change in the budgetary estimate for the full-scale engineering service test model.

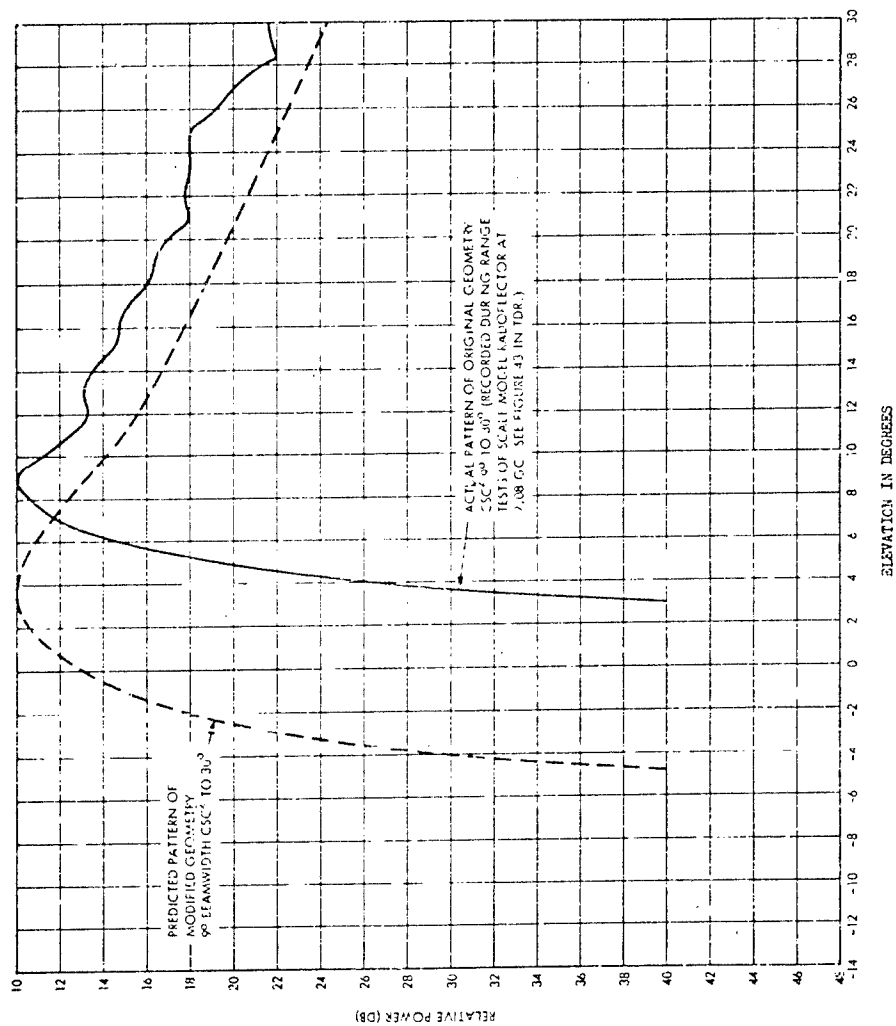


Figure 198. Comparison of Modified versus Original Elevation Pattern

CATALOGUE FILE CARD

<p>Rome Air Development Center, Griffins AF Base, NY Rpt No. RADG-TDR-63-64, AN ENGINEERING STUDY OF A POST-ATTACK ANTENNA SYSTEM. Final Rpt. Dec 62, 90p, illus, tables, 9 refs. Unclassified Report</p> <p>Describes results of a study program for a post-attack antenna installation. The purpose was to determine the feasibility of an air supported, integrated, radome-antenna configuration that can be packaged and stored in a hardened enclosure. Theoretical computations to establish aperture parameters and confirming test results are shown. Preliminary stress analysis and design configuration are shown. Materials and manufacturing techniques are discussed. A preliminary concept is presented for a hardened enclosure, feed erection and rotation mechanisms, and inflation system. A scale model was designed, fabricated and tested. Test results are shown and analysed. Program</p>	<p>1. Radar Antennas, parabolic, inflatable 2. Radomes, inflatable 3. Antennas radiation patterns I. AFSC Project 5579 Task 557901 II. Contract AF30(602)-2753 Goodyear Aircraft Corp. Akron 15, Ohio IV. Collins, D.D. and Congdon, G.W. V. Secondary Rpt No. GER-10670 VI. Not in DDC collection</p>	<p>Rome Air Development Center, Griffins AF Base, NY Rpt No. RADG-TDR-63-64, AN ENGINEERING STUDY OF A POST-ATTACK ANTENNA SYSTEM. Final Rpt. Dec 62, 90p, illus, tables, 9 refs. Unclassified Report</p> <p>Describes results of a study program for a post-attack antenna installation. The purpose was to determine the feasibility of an air supported, integrated, radome-antenna configuration that can be packaged and stored in a hardened enclosure. Theoretical computations to establish aperture parameters and confirming test results are shown. Preliminary stress analysis and design configuration are shown. Materials and manufacturing techniques are discussed. A preliminary concept is presented for a hardened enclosure, feed erection and rotation mechanisms, and inflation system. A scale model was designed, fabricated and tested. Test results are shown and analysed. Program</p>	<p>1. Radar Antennas, parabolic, inflatable 2. Radomes, inflatable 3. Antennas radiation patterns I. AFSC Project 5579 Task 557901 II. Contract AF30(602)-2753 Goodyear Aircraft Corp. Akron 15, Ohio IV. Collins, D.D. and Congdon, G.W. V. Secondary Rpt No. GER-10670 VI. Not in DDC collection</p>	<p>Rome Air Development Center, Griffins AF Base, NY Rpt No. RADG-TDR-63-64, AN ENGINEERING STUDY OF A POST-ATTACK ANTENNA SYSTEM. Final Rpt. Dec 62, 90p, illus, tables, 9 refs. Unclassified Report</p> <p>Describes results of a study program for a post-attack antenna installation. The purpose was to determine the feasibility of an air supported, integrated, radome-antenna configuration that can be packaged and stored in a hardened enclosure. Theoretical computations to establish aperture parameters and confirming test results are shown. Preliminary stress analysis and design configuration are shown. Materials and manufacturing techniques are discussed. A preliminary concept is presented for a hardened enclosure, feed erection and rotation mechanisms, and inflation system. A scale model was designed, fabricated and tested. Test results are shown and analysed. Program</p>	<p>1. Radar Antennas, parabolic, inflatable 2. Radomes, inflatable 3. Antennas radiation patterns I. AFSC Project 5579 Task 557901 II. Contract AF30(602)-2753 Goodyear Aircraft Corp. Akron 15, Ohio IV. Collins, D.D. and Congdon, G.W. V. Secondary Rpt No. GER-10670 VI. Not in DDC collection</p>
<p>Rome Air Development Center, Griffins AF Base, NY Rpt No. RADG-TDR-63-64, AN ENGINEERING STUDY OF A POST-ATTACK ANTENNA SYSTEM. Final Rpt. Dec 62, 90p, illus, tables, 9 refs. Unclassified Report</p> <p>Describes results of a study program for a post-attack antenna installation. The purpose was to determine the feasibility of an air supported, integrated, radome-antenna configuration that can be packaged and stored in a hardened enclosure. Theoretical computations to establish aperture parameters and confirming test results are shown. Preliminary stress analysis and design configuration are shown. Materials and manufacturing techniques are discussed. A preliminary concept is presented for a hardened enclosure, feed erection and rotation mechanisms, and inflation system. A scale model was designed, fabricated and tested. Test results are shown and analysed. Program</p>	<p>1. Radar Antennas, parabolic, inflatable 2. Radomes, inflatable 3. Antennas radiation patterns I. AFSC Project 5579 Task 557901 II. Contract AF30(602)-2753 Goodyear Aircraft Corp. Akron 15, Ohio IV. Collins, D.D. and Congdon, G.W. V. Secondary Rpt No. GER-10670 VI. Not in DDC collection</p>	<p>Rome Air Development Center, Griffins AF Base, NY Rpt No. RADG-TDR-63-64, AN ENGINEERING STUDY OF A POST-ATTACK ANTENNA SYSTEM. Final Rpt. Dec 62, 90p, illus, tables, 9 refs. Unclassified Report</p> <p>Describes results of a study program for a post-attack antenna installation. The purpose was to determine the feasibility of an air supported, integrated, radome-antenna configuration that can be packaged and stored in a hardened enclosure. Theoretical computations to establish aperture parameters and confirming test results are shown. Preliminary stress analysis and design configuration are shown. Materials and manufacturing techniques are discussed. A preliminary concept is presented for a hardened enclosure, feed erection and rotation mechanisms, and inflation system. A scale model was designed, fabricated and tested. Test results are shown and analysed. Program</p>	<p>1. Radar Antennas, parabolic, inflatable 2. Radomes, inflatable 3. Antennas radiation patterns I. AFSC Project 5579 Task 557901 II. Contract AF30(602)-2753 Goodyear Aircraft Corp. Akron 15, Ohio IV. Collins, D.D. and Congdon, G.W. V. Secondary Rpt No. GER-10670 VI. Not in DDC collection</p>	<p>Rome Air Development Center, Griffins AF Base, NY Rpt No. RADG-TDR-63-64, AN ENGINEERING STUDY OF A POST-ATTACK ANTENNA SYSTEM. Final Rpt. Dec 62, 90p, illus, tables, 9 refs. Unclassified Report</p> <p>Describes results of a study program for a post-attack antenna installation. The purpose was to determine the feasibility of an air supported, integrated, radome-antenna configuration that can be packaged and stored in a hardened enclosure. Theoretical computations to establish aperture parameters and confirming test results are shown. Preliminary stress analysis and design configuration are shown. Materials and manufacturing techniques are discussed. A preliminary concept is presented for a hardened enclosure, feed erection and rotation mechanisms, and inflation system. A scale model was designed, fabricated and tested. Test results are shown and analysed. Program</p>	<p>1. Radar Antennas, parabolic, inflatable 2. Radomes, inflatable 3. Antennas radiation patterns I. AFSC Project 5579 Task 557901 II. Contract AF30(602)-2753 Goodyear Aircraft Corp. Akron 15, Ohio IV. Collins, D.D. and Congdon, G.W. V. Secondary Rpt No. GER-10670 VI. Not in DDC collection</p>